A GEOLOGICAL FRAMEWORK FOR TEMPORAL SEDIMENTARY DYNAMICS IN A SMALL TEMPERATE PARAGLACIAL TURBID OUTWASH FJORD: SIMPSON BAY, PRINCE WILLIAM SOUND, ALASKA

A Dissertation

by

CHRISTIAN JOHN NOLL IV

Submitted to the Office of Graduate Studies of
Texas A&M University
in partial fulfillment of the requirements for the degree of

DOCTOR OF PHILOSOPHY

December 2008

Major Subject: Oceanography

A GEOLOGICAL FRAMEWORK FOR TEMPORAL SEDIMENTARY DYNAMICS IN A SMALL TEMPERATE PARAGLACIAL TURBID OUTWASH FJORD: SIMPSON BAY, PRINCE WILLIAM SOUND, ALASKA

A Dissertation

by

CHRISTIAN JOHN NOLL IV

Submitted to the Office of Graduate Studies of
Texas A&M University
in partial fulfillment of the requirements for the degree of

DOCTOR OF PHILOSOPHY

Approved by:

Chair of Committee,	Timothy Dellapenna
Committee Members,	William Bryant
	James Kaihatu
	William Sager
Head of Department,	Piers Chapman

December 2008

Major Subject: Oceanography

ABSTRACT

A Geological Framework for Temporal Sedimentary Dynamics
in a Small Temperate Paraglacial Turbid Outwash Fjord:
Simpson Bay, Prince William Sound, Alaska. (December 2008)
Christian John Noll IV, B.S., Texas A&M University at Galveston;
M.S., Texas A&M University
Chair of Advisory Committee: Dr. Timothy M. Dellapenna

Geophysical, geochemical and geotechnical methods were used to investigate the spatial and temporal aspects of sediment distribution, accumulation, post-depositional alterations, and seafloor response and recovery to major events in a temperate, paraglacial, turbid outwash fjord. The goals of this study are to generate a complete geological model and compare the results to the global distribution of fjords. The over arching theme of this study is that the ratio of the area of the watershed to the area of the receiving basin can provide a first order indicator of many factors including glacial mass; the timing of glacial retreat; sediment input, accumulation, and preservation; and other factors. Temporal observations reveal the change of this fjord from a glaciated basin to and estuarine environment. These observations become important when viewed in the context of global climate change and the continued loss of ice. Preserved strata provide a 2800 yr record of changing modes of sedimentation as the system evolved from a glaciated basin to a non-glaciated fjord revealing a detailed chronology of change between end-member systems which can be used to infer changes as glaciers retreat from other fjords. Short lived radio isotopes were used to investigate post-depositional alteration of modern sediments. Without an understanding of how biological and physical processes work to modify sedimentary fabric during preservation, changes seen in sediment and rock core data cannot be accurately resolved. Physical processes can cause erosion and lateral transport; winnowing and armoring; and instantaneous sedimentation, all of which may be preserved. Biological processes can modulate the preservation of strata by destroying sedimentary fabric and integrating signals. The final fundamental need is to investigate the seafloor response and recovery to

these events. Massive earthquakes are frequent in the study area and cause perturbations to sediment input and preservation. By understanding how lakes and deltas modulate sediment discharge after the event; how shorelines are modified after the event; and where sediment is deposited we can determine the influence these changes have on the environment and on humans.

DEDICATION

To the multitude that made this work possible, I cannot thank you enough.

ACKNOWLEDGMENTS

Funding for this project was made possible through grants from the Earthwatch Foundation, the Department of Marine Sciences at Texas A&M University at Galveston, the Oceanography Graduate Council at Texas A&M University, and the Office of Naval Research. The work could not have been completed with out generous loans of equipment and time from Keith Vickery with GeoAcoustics, Shorty Shipp with C&C Technologies, Mead Allison and Charles Nittrouer for the donation of their kasten cores to the seafloor, and GERG.

Thanks go out to Bryan Fielder, Robert Webster, Alan Thompson, Cliff Nunnally and the crew of the F/V *Miss Kayle* for their assistance taking and processing the box cores. It was a demanding job and I could not have done it without them.

Frederick Weltz deserves special recognition for his tireless and selfless support of this project. His time and energy not only made this project possible, but also contributed to its success. The use of his boat, the F/V Dancing Bear, and his local knowledge of the area were instrumental in the survey and I can never thank him enough.

Thanks to the other members of the Coastal Geology for their help, especially Julie Manuel and Erin Weaver.

Special thanks go out to Christi Pondell. Her tireless work with the radioisotope and geochemical data were an invaluable contribution to this project. She deserves more credit than I can provide here.

I would like to thank my family and especially my wife for their tireless support throughout this lengthy process. My wife's patience and understanding through difficult times has made all the difference. I appreciate the support of Chris and Cindi. Every time I passed through Anchorage they were there with open arms and their persistent prodding helped keep me on track.

I would like to thank my committee members, Dr. Sager, Dr. Bryant, and Dr. Davis and especially my committee chair, Dr. Dellapenna. There was never a thing I asked for that he did not beg, borrow, and steal for to help me finish this project.

TABLE OF CONTENTS

CHAPTER Page

Page

LIST OF FIGURES

FIGURE Page

FIGURE Page

FIGURE Page

CHAPTER I

INTRODUCTION

This investigation of Simpson Bay is an attempt to develop a geological framework of sedimentary processes for a deglaciated, temperate fjord and to apply the lessons learned to the global distribution of fjords. This study of the temporal aspects of fjord sedimentation builds on previous work investigating the spatial aspects of sediment distribution in Simpson Bay by Noll et al. (2008). The work is also an integral part of a multi-disciplinary effort to generate a complete scientific framework of the physical, chemical, geological and biological oceanographic aspects of this site in order to apply the knowledge gained here to world wide fjord environments. This approach becomes more important in the face of increasing rates of glacial and sea ice loss. Understanding the evolution and modern processes of fjords provides an opportunity to understand the environments that will open up as a consequence of disappearing ice.

Simpson Bay is a turbid outwash fjord located within this environment that provides a natural laboratory to investigate the record of sedimentary processes during deglaciation in a highly dynamic fjord. Simpson Bay's position away from industrialized areas leave it free from the affects of mining, deforestation and other anthropogenic contributions to sediment input. By choosing a relatively pristine, dynamic system, we can investigate the many possibilities nature presents without having to account for the factors applied by anthropogenic forcing.

The goals of the temporal aspects of this study are to develop a chronological succession of deglaciation specific to Simpson Bay, to investigate the factors that controlled the sedimentary record produced during glacial retreat, and to compare this record to worldwide glacial fluctuations. Fjords act as sediment sinks during interglacial periods, during which they capture and preserve a high resolution record of paleoclimatic, paleoceanographic and paleodepositional environments (Aarseth 1997; Andrews and Syvitski 1994; Syvitski and Shaw 1995; Vorren et al. 1989). The stratragraphic record in Simpson Bay

---

This dissertation follows the style of *Geo-Marine Letters*.

affords the opportunity to investigate local-to-regional scale variations in climate, sea level, sediment input and seismic activity. Other important issues addressed are the relationships between the stratagraphic record from Simpson Bay and other records of glacial fluctuation from the region (moraine dating, etc...). The investigation of this system has allowed the development of a fine scale chronology and has examined the small fluctuations that drive the high frequency local fluctuations that cannot be resolved in the worldwide record. This study focused on seismic data to investigate the complex spatial and temporal distribution of sedimentary strata and its relationship to local climate, worldwide glacial activity, and basin morphology. Simpson Bay is partitioned into discrete units with individual properties that vary in their contribution to the overall sedimentary environment. By breaking apart the sub-basins in Simpson Bay and focusing on each individually, it is apparent that the timing, rate and extent of deglaciation within the system are controlled by factors specific to each basin. These factors show the fickle nature of deglaciation and this conceptual model helps explain the differences in glacial activity on a regional scale. This was accomplished by conducting a high resolution geophysical survey using side scan sonar, bathymetry, and seismic data, as well as core data for the purposes of determining modern sediment accumulation rates.

The factors governing modern sediment deposition and preservation are key components to provide linkages to understand the environments under which material preserved in the rock record were deposited. Physical, biological, and chemical processes combine to alter deposited sediment and can cause misinterpretation when investigating the origin and depositional environments of preserved strata. Only when these processes are understood and can be accounted for, can we make an accurate assessment of preserved material. A part of this study addresses the relationships between physical and biological processes, post depositional alteration of sediment, and preserved strata. These environments range from physically dominated delta fronts to biologically dominated deepwater environments to biologically and physically modified relict glacial deposits. By choosing a relatively pristine, dynamic system, we can investigate the many possibilities nature presents without having to account for the factors applied by anthropogenic forcing. Simpson Bay has been deglaciated for ~2800 years, so it reflects long term sedimentary properties of a non-glaciated temperate fjord. Geochemical and geotechnical analysis of

cores using radioisotopes, sedimentological properties, and qualitative analysis of x-rays will be used to asses the degree to which sediment is preserved. Cores of different lengths and tracers that work on different time scales will allow assessment of processes that work on decadal to centennial intervals.

The final part of this study is to identify the seafloor response and recovery to large seismic events. Large earthquakes are common in Alaska (five M_s 7.0 or greater earthquakes have been recorded since 1979); (Jaeger et. al 1998; Johnson et. al 1996; Nishenko and Jacob 1990) and include the second largest earthquake ever recorded, the Great Alaskan Earthquake March 27, 1964 (M_s 9.2). These earthquakes have shown the potential to cause catastrophic aerial, intertidal, and subtidal failures. This study gives an example of an Alaskan fjord near the epicenter of the earthquake (~110 km southeast of the epicenter) that did not undergo catastrophic subtidal seafloor changes, but did show specific geochemical responses to the earthquake and has experienced basin specific changes during the time following the earthquake. Hopefully this aspect of the study will bring to light the occurrence of these small events and emphasize their importance on benthic community health, preservation of strata, and the effects on stratagraphic incompleteness.

CHAPTER II

THE HISTORY OF GLACIAL RETREAT IN A PARAGLACIAL TURBID OUTWASH FJORD: SIMPSON BAY, PRINCE WILLIAM SOUND, ALASKA

OVERVIEW

Seismic profiles and sediment cores have been used to investigate at the distribution of sedimentary strata and to develop a chronology of glacial retreat in a small turbid outwash fjord, Simpson Bay, Alaska. An approximately 2800 yr record of punctuated changes in strata are evidence of changing modes of sedimentation as the system evolved from a glaciated basin to a non-glaciated fjord. Within stratal units, reflectors are found indicative of short term changes in sediment distribution. In Simpson Bay, immediately above a basal surface of glacial diamicton is a unit of thick high amplitude parallel to sub-parallel continuous and discontinuous reflectors. Transparent and chaotic units as well as truncated reflectors within this layer indicate debris flows in the proglacial environment. This unit marks the beginning of glacial retreat in Simpson Bay about 2800 years before present (ybp). Sedimentation rates during this stage were rapid due to large input of sediment from the glacier. The next unit is composed of ponded sediment, atop the previous layer, indicative of a phase of glacial retreat where glaciers are grounded in the drainage basin. Coarse grain material is entrained in the drainage basin, rivers, and fjord head deltas and sedimentation rates decrease. This unit is largely transparent with occasional reflectors and side echoes from bedrock features. A unit of fine scale low amplitude reflectors is found at the top of the sequence. This unit is indicative of neoglacial changes of glaciers in the watershed that affect sediment discharge and has captured approximately the last 1100 yrs of sediment deposition. Modern sedimentation rates were extrapolated to calculate ages of reflectors to correlate the changes in strata type to regional to global scale climate changes. In general calculated dates correlate well to global events, but the presence of additional layers points to the effectiveness of fjords at preserving fine scale sedimentary records and the importance of small local scale shifts in basin evolution.

INTRODUCTION

Fjords act as sediment sinks during interglacial periods, which capture and preserve a high resolution record of paleoclimatic, paleoceanographic and paleodepositional environments (Aarseth 1997; Andrews and Syvitski 1984; Syvitski and Shaw 1995; Vorren et al. 1989). The south central coast of Alaska is a fjord dominated coastline with high precipitation, high coastal mountains, easily eroded geology, and frequent seismic perturbations. Simpson Bay is a turbid outwash fjord located within this environment which provides a natural laboratory to investigate the record of sedimentary processes during deglaciation in a highly dynamic fjord (Fig. 1). The stratragraphic record in Simpson Bay affords the opportunity to investigate local-to-regional scale variations in climate, sea level, sediment input and seismic activity. Simpson Bay has a comparatively small volume of sediment fill, which by comparison, suggests recent deglaciation (Cai et al. 1997; Lysa et al. 2004) and is partitioned into discrete units with individual properties that vary in their contribution to the overall sedimentary environment. By breaking apart the sub-basins in Simpson Bay and focusing on each individually, it is apparent that the timing, rate and extent of deglaciation within the system are controlled by factors specific to each basin. These factors show the fickle nature of deglaciation and this conceptual model helps explain the differences in glacial activity on a regional scale.

This investigation is part of a larger effort to unravel the past and present sedimentary processes in a pristine Alaskan fjord. Simpson Bay's position away from industrialized areas leave it free from the affects of mining, deforestation and other anthropogenic contributions to sediment input. The goal of this study is to develop a chronological succession of deglaciation specific to Simpson Bay, investigate the factors which controlled the sedimentary record produced during glacial retreat, and compare this record to worldwide glacial fluctuations. Another important issue addressed is the discrepancy between the stratagraphic record from Simpson Bay and other records of glacial fluctuation from the region (moraine dating, lichenology, etc...). The investigation of this system has allowed the development of a fine scale chronology and has examined the small fluctuations that drive the high frequency local fluctuations that cannot be resolved in the worldwide record. This was accomplished by conducting a high resolution geophysical survey using side scan sonar, bathymetry, and seismic data, as well as cursory core data for

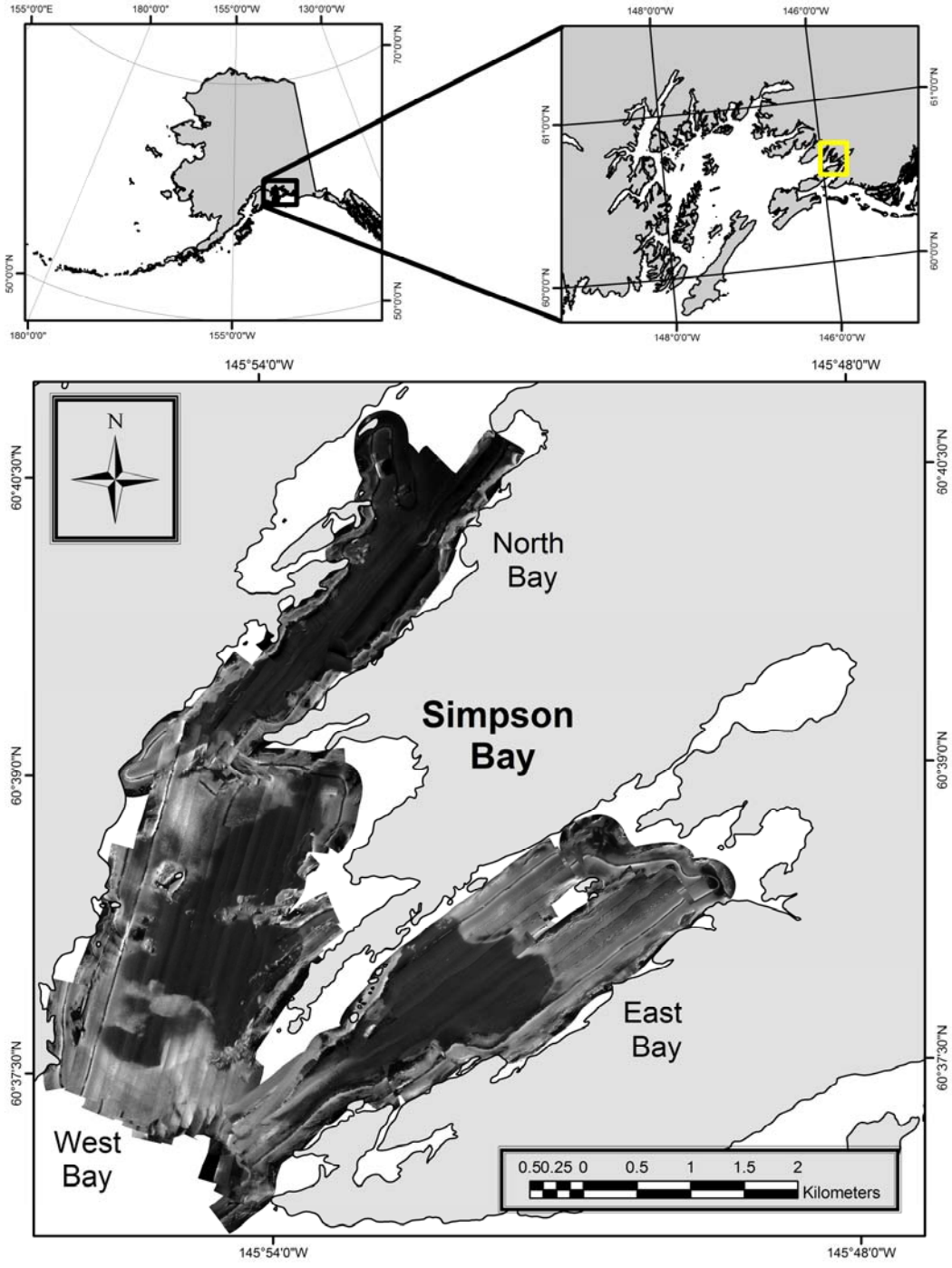

Fig.1 Simpson Bay located in Prince William Sound on the south-central coast of Alaska. Simpson Bay is divided into three morphologically distinct units: West Bay, North Bay, and East Bay. Light tones on the side scan sonar mosaic indicate coarse grain material, bedrock and shorelines, while dark tones indicate estuarine mud deposits

the purposes of determining modern sediment accumulation rates. This study focused on seismic data to investigate the complex spatial and temporal distribution of sedimentary strata and its relationship to local climate, worldwide glacial activity, and basin morphology. The seismic data are also correlated to surface features identified in the side scan sonar mosaics as a way of further enhancing the understanding of the underlying basin morphology and determine the specific geologic features that divide Simpson Bay into distinct sub-basins.

BACKGROUND

Simpson Bay is a small macrotidal (>5 m) fjord located in Prince William Sound (PWS on the south central coast of Alaska (Fig. 1). Because of its morphology and hydrographic conditions, it is classified as a partially mixed, shallow fjord (Gay and Vaughn 2001). Simpson Bay is Y-shaped with distinct morphological features partitioning the system into three discrete basins. The western and eastern arms exchange directly with PWS and a northern arm feeds into the head of the western arm. In Simpson Bay, freshwater originates as precipitation (355-460 cm yr^{-1}; Fig. 2); (AGDC 1998) in the large watershed of Simpson Bay (Fig. 3) and from the melt water of high alpine glaciers in the northern and eastern arms (Fig. 4); (AGDC 1998; Gay and Vaughn 2001). Fresh water input delivers sediment to the heads of each bay through bayhead deltas and along the shoreline through small creeks. The presence of glaciers and the comparatively large watershed:basin surface area ratio (8:1) suggest a high sediment load may be introduced to Simpson Bay. The drainage basin morphology of Simpson Bay creates large differences in the watershed:basin surface area ratio of each arm. The western arm, with the largest surface area, has by far the smallest drainage basin. In contrast, the small northern arm has a drainage basin 15 times larger than the western arm. This data has great implications in the source, distribution and fate of sediment in Simpson Bay (Noll et al. 2008).

Side scan sonar and bathymetry surveys of Simpson Bay (Figs. 1 and 5; Noll et al. 2008) have classified bottom types and described basin morphology. West Bay is the western arm of Simpson Bay (Fig. 1). This arm has the largest surface area (7.5 km^2), but has a small drainage basin (7.5 km^2) giving it an approximately 1:1 watershed:basin surface area ratio (Fig. 3). This arm is approximately 4 km long

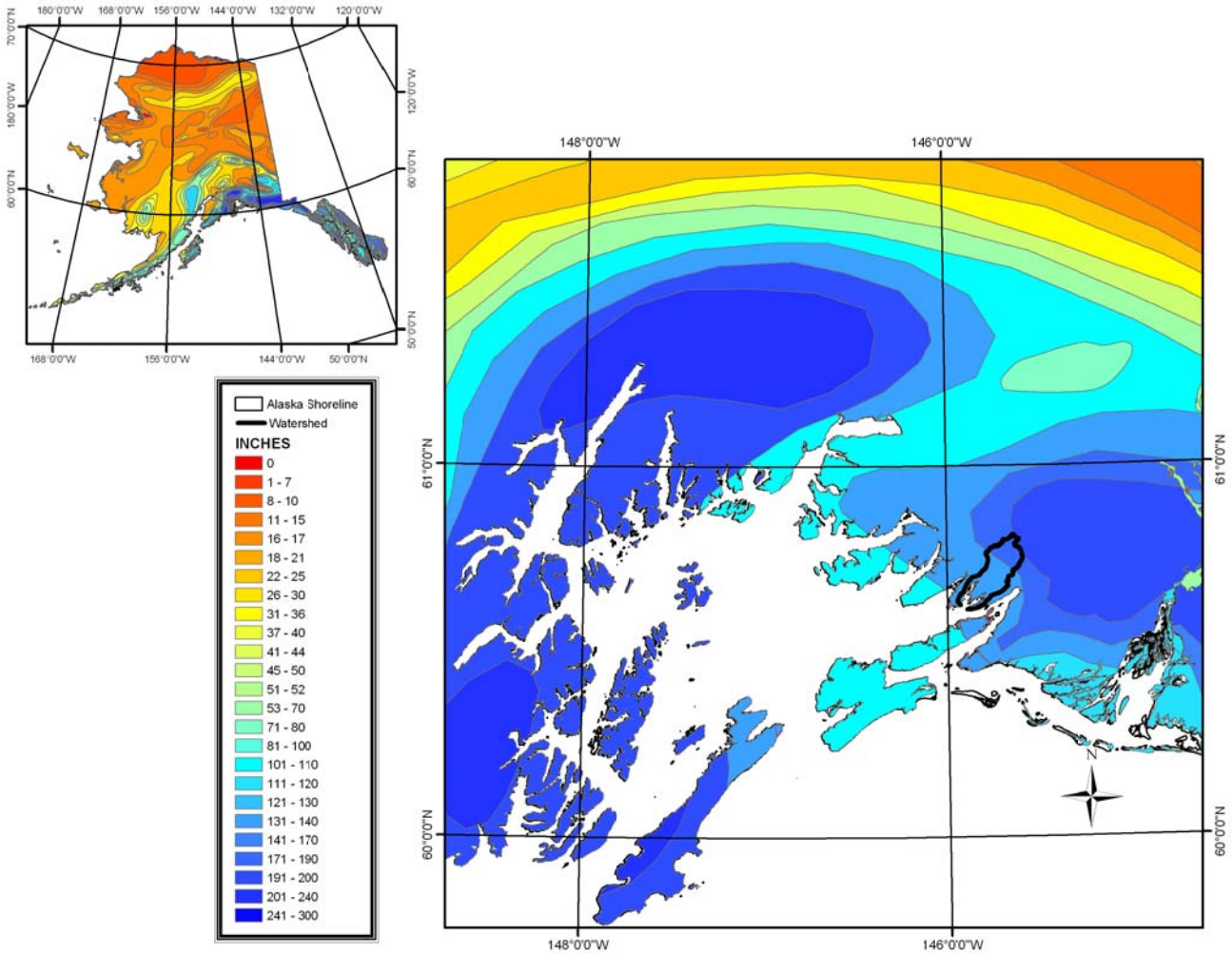

Fig. 2 Local and regional precipitation patterns in Alaska. Simpson Bay receives approximately 355-460 cm yr^{-1} of precipitation (Map generated with information from the AGDC, 1998; Data shown in inches of precipitation per year)

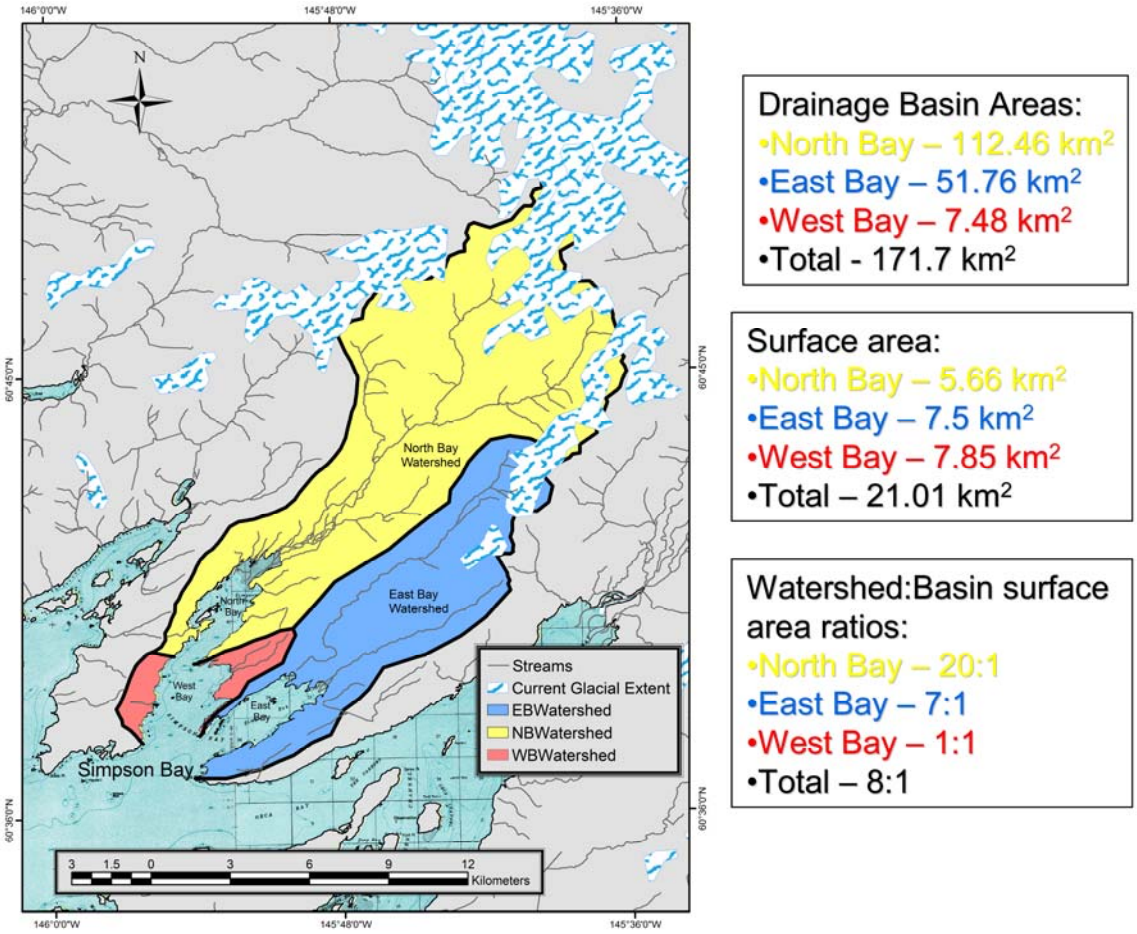

Fig. 3 Simpson Bay watershed, streams, and glaciers. The North Bay has the largest watershed and the largest watershed:basin surface area ratio (20:1). North Bay drains high altitude glaciers and has a large network of streams. West Bay has the smallest watershed and a watershed:basin surface area ratio (1:1). East Bay has an intermediate watershed:basin surface area ratio (7:1) and drains some high altitude glaciers. (Map generated with data from the AGDC, ADNR and the USDA)

and 2 km wide and opens directly into PWS. West Bay is morphologically the most dynamic portion of Simpson Bay. On average, it is the shallowest (25 to 55 m; Fig. 5), and the bottom is irregular. Fine grain sediment is found ponded in bathymetric lows while high backscatter diamicton and bedrock deposits form bathymetric highs (Fig. 1). This portion of Simpson Bay is bounded to the north by the shoreline and the bedrock moraine morainal bank that separates North Bay and West Bay and to the south by a low

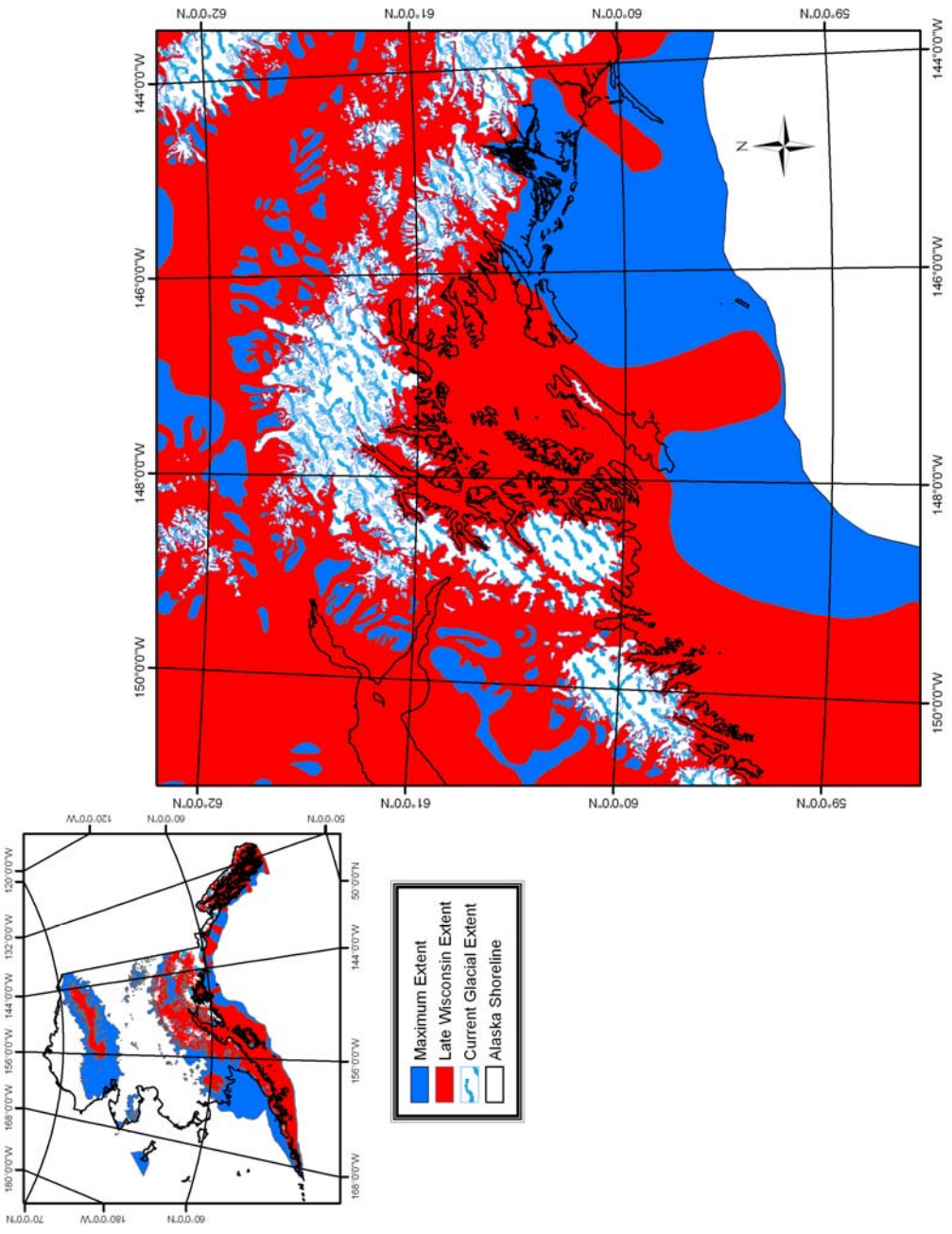

Fig.4 Summary of Alaskan paleoglaciers. The blue is the extent of maximum glaciation in Alaska and the red is the late Wisconsin extent. The white areas are positions of current glaciers. (Map generated with data from ADNR, 1998; Manley and Kaufman, 2002)

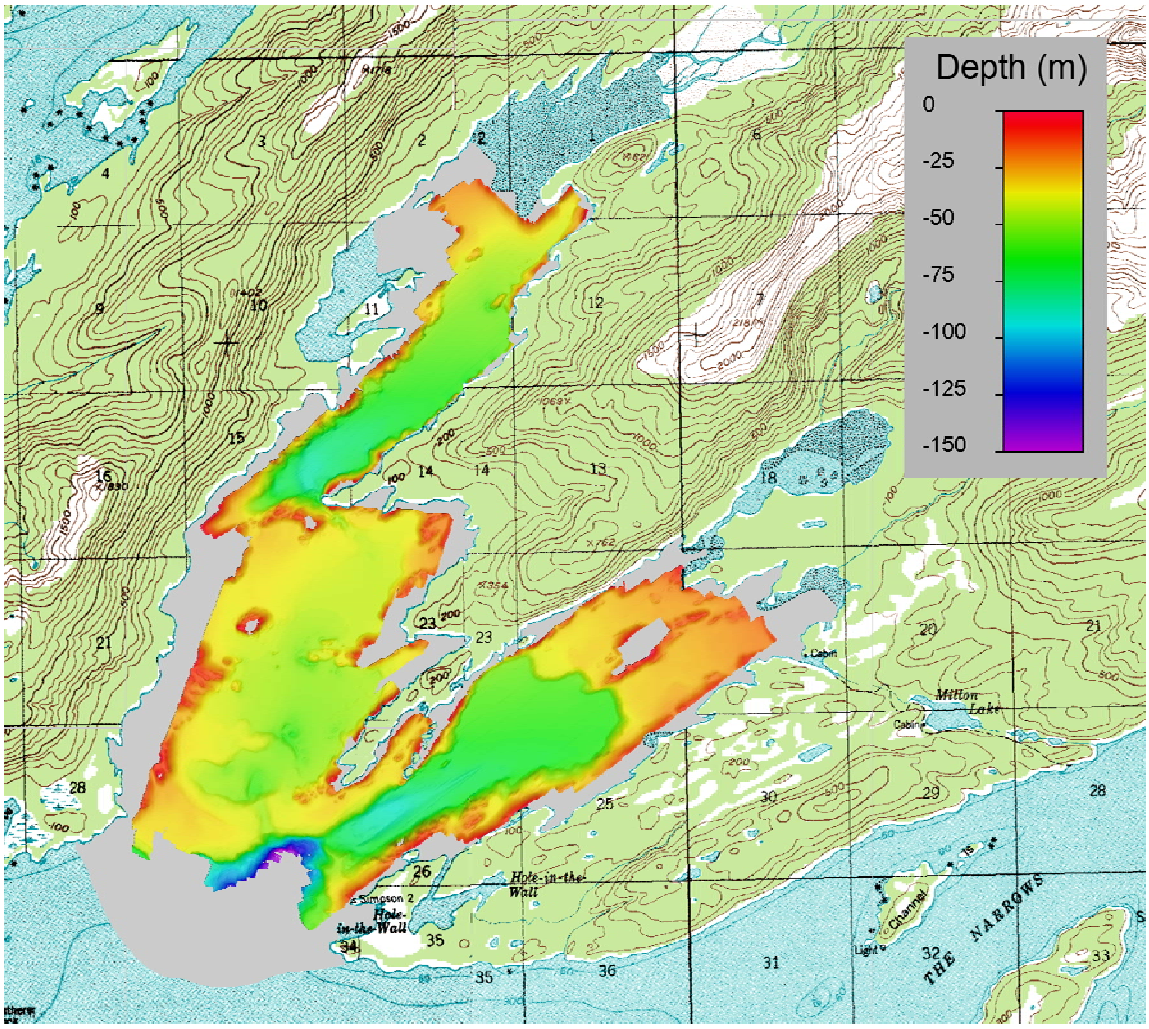

Fig. 5 Swath bathymetry map of Simpson Bay collected using a GeoAcoustic Geoswath inferometric bathymetry system and processing software

relief morainal bank and PWS. East Bay is the eastern arm of Simpson Bay (Fig. 1). This northeast/southwest oriented basin is long (4 km) and narrow, thinning from 2 km at the head to 1 km at the mouth with depths ranging from 10-80 m (Fig. 5). East Bay has almost the same surface area (7 km^2) as West Bay, but its drainage basin is much larger (52 km^2), giving it a 7:1 watershed:basin surface area ratio (Fig. 3). The mouth of East Bay is at the southern end of Simpson Bay, and unlike North Bay, water

masses exchange directly with PWS. There is no sill at the mouth that restricts circulation, but there is a low relief (~15 m), high backscatter diamicton morainal bank that separates East Bay from the rest of Simpson Bay (Figs. 1 and 5). The deep area of East Bay is composed of low backscatter fine grain estuarine mud that transitions to rocky shoreline along the periphery. At the head of the bay, depths decrease sharply to a high backscatter, shallow plateau composed mainly of coarse grain material with a thin veneer of estuarine mud on top. North Bay is the long (4 km) and narrow (0.7 - 1.3 km) northern arm of Simpson Bay (Fig. 1). Depths range from 5 - 80 m (Fig. 5), and this arm has steep sides (5° to 25°) composed of diamicton and bedrock that transition to shoreline. In some areas, bathymetry data show sheer rock faces that descend from above the water to the bottom of the fjord. North Bay is the smallest arm of Simpson Bay (5.5 km^2), but has the largest drainage basin (112 km^2) resulting in a 20:1 watershed:basin surface area ratio (Fig. 3). Bedrock is exposed at the morainal bank complex at the mouth of North Bay making this the only portion of Simpson Bay that has a true restrictive sill (Figs. 1 and 5). The rest of the bay is composed of estuarine mud and rock shorelines except for the delta at the head of the bay. Aerial photography shows riverine input is constrained to North Bay by this sill.

While once entirely covered with ice, the coastline of Alaska has undergone dramatic changes on a short geologic timescale (Fig. 4); (Manly and Kaufman 2002). In the last ~20,000 yrs, ice sheets have retreated from the continental shelf to the point that only ~20% of the coastal area is glaciated and few tidewater glaciers exist (Jaeger et al. 1998; Lethcoe 1990). As glacial retreat began, rising sea level flooded the coastline, filling in the glacially carved U-shaped valleys, creating fjords and preserving depositional features including sills, moraines, turbidite deposits, and sedimentary sequences indicative of climate fluctuations.

Simpson Bay became de-glaciated late in the Holocene, and although tidewater glaciers have not been found in Simpson Bay in recorded history (Davidson 1904), the antecedent geology left as a result of glacial retreat is preserved. Glacial processes scour the landscape and erode massive amounts of sediment (Hallet et al. 1996; Jaeger et al. 2001; Milliman and Syvitski 1992), moving it down slope and depositing it at the terminus of the glacier. Modern and ancient depositional processes since deglaciation are evident in the sediment record as Quaternary sediment deposited on a glacially eroded surface (Barrie and Conway

1999; Carlson 1989; Dowdeswell et al. 2000; Hunter 1996; Syvitski et al. 1997). Many processes drive the spatial distribution of sediment in fjords including seismic perturbations, tidal currents, and fluctuations in sediment load (Syvitski 1989; Syvitski et al. 1987).

Seismic processes are important to understanding the distribution of sediments in Alaskan fjords. Earthquakes occur frequently in Alaska. Five M_s 7.0 or greater earthquakes have been recorded since 1979 and PWS is near the epicenter of the second largest earthquake in recorded history. In 1964, a magnitude 9.2 earthquake rocked the area creating vertical uplifts averaging 2 m and reaching a maximum of 11 m, while horizontal displacements were as high as 25 m (Fig. 6); (ADNR 1964; Jaeger et al. 1998; Johnson et al. 1996). These earthquakes trigger gravity driven sediment flows that erode and deposit large amounts of sediment very quickly. Gravity flows erode sediment from areas with high slope and deposit it in areas of low slope as both suspended and bed load. Sedimentary deposits left after these disturbances indicate the type of flow. Steep slopes along the shorelines and associated with morainal bank complexes are areas where gravity flows may originate.

The typical morphology of fjords creates basins with large tidal ranges. Tidal currents are very important in the spatial distribution of sediments. Hydrographic data collected in Simpson Bay by Gay and Vaughan (2001) show high spatial variability in surface and bottom currents. Bottom currents appear to be tide dominated, but generally weak (< 5 - 20 cm s^{-1} at 10 m; Gay and Vaughan, 2001). Stronger currents were found along shorelines and outcrops exhibiting erosion and lack of estuarine mud deposition. Sediment delivered to the mouth of the fjord is moved on a daily basis due to the ebb and flow of tides. The dynamic seafloor topography (Fig. 4) of this system controls tidal currents, affecting their direction and velocity. Large amounts of estuarine mud are found in the deep, open portions of the fjord where slower tidal currents are found, while shorelines, shoals, sills, and outcrops exhibit coarse surfaces (Noll et al. 2008).

Sediment input into Simpson Bay is driven by unique morphological features and hydrography. Orogeny in the south central coast of Alaska has created one of the highest coastal reliefs in the world. Simpson Bay is part of the Orca Group, a component of the Prince William lithotectonic terrane. The Orca Group is composed of a deep-sea fan complex of flyschoid greywacke and minor pelite interbedded

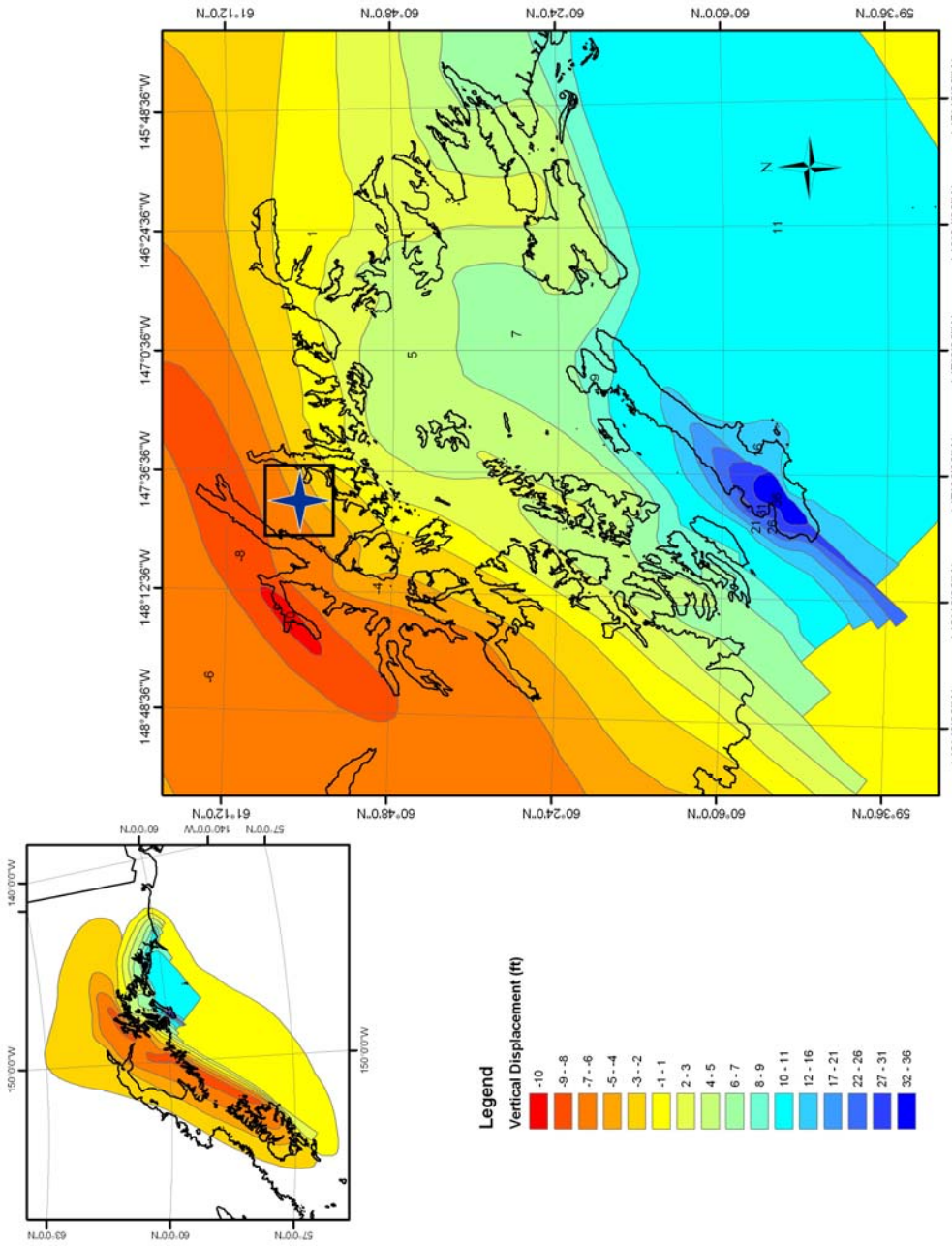

Fig. 6 Regional vertical displacements as a result of the 1964 earthquake. Displacement exceeded 9m on Montague Island and was approximately 1.5m in Simpson Bay. (Map generated using data from ADNR. 1996)

with subordinate oceanic volcanic rocks and minor pelagic sediment (Farmer et al. 1993). Fine grain sedimentary rock and conglomerates, often nearly vertically dipping, are found throughout Simpson Bay (Lethcoe 1990). PWS has shoreline mountains that reach 1000 m in elevation and is bordered to the north by the Chugach Mountains that reach heights in excess of 4000 m less than 60 km from the coast (Gay and Vaughn 2001). The Aleutian Low is a low pressure atmospheric system that dominates the weather patterns of Alaska's southern coast. The interaction of the Aleutian Low with this coastline produces meters of precipitation each year that supply snow to the high altitude ice fields that feed massive glaciers and rain/snow to low altitude temperate rainforests. These factors, coupled with a rapidly uplifting (several meters per 1000 yrs), easily erodable coastal mountain range, create a drainage system with some of the highest sedimentation rates in the world (Hallet et al. 1996; Jaeger et al. 1998; Powell and Molinia 1989). A high freshwater flow during the late summer maximum brings sediment into the Simpson Bay at the fjord head and along the shoreline. Rivers at the head of the two upper arms tap large drainage basins and bring sediment laden glacial water to the fjord. Coarse sediment is trapped in prograding fjord head deltas found at the heads of both arms of Simpson Bay. The northern arm drains a larger area and more glaciers than the eastern arm and consequently a larger delta has built at the head of the northern arm (Gay and Vaughn 2001).

METHODS

The site was surveyed using multiple tools over multiple summers. Side scan sonar and swath bathymetry surveys were conducted and are described in Noll et al. (2008). These surveys were the basis for building the seismic survey. The survey utilized two instruments to generate high resolution sub-bottom profiles, while still penetrating to bedrock. An Edgetech 216S CHIRP (2-16 kHz) towfish captured the fine strata in the upper layers, but was unable to penetrate to bedrock where fine grain sediment thicknesses exceeded 40 m or in areas of glacial diamicton. The Edgetech 512i CHIRP (0.5-12 kHz) towfish was able to penetrate to bedrock in many places and image gross strata, but was unable to image the fine scale stratigraphy in the shallow subsurface. The data sets for both instruments are displayed together to enhance interpretation.

Fieldwork was conducted in October of 2004 and July 2005 aboard the F/V Dancing Bear, a 14 m long lining boat associated with Alice Cove Research Station. Simpson Bay was surveyed in 2004 using an Edgetech SB-216S CHIRP sub-bottom profiler operating at 2 – 16 kHz with a resolution of 6 - 10 cm. A Trimble Ag132 differential GPS using a Coast Guard beacon was used for navigation in Hypack and for position in the seismic acquisition software. A survey grid was designed using previously collected bathymetric and side scan sonar data to maximize coverage in the fine grain depositional areas, while keeping the towfish as close to the sea floor as possible. Survey transects were run along and across the axis of the bay at 300 m line spacing at an average of 3 - 4 knots. Return intensities were recorded digitally and displayed using the Triton Elics software suite. Delph Seismic Plus was used to record raw data and SGIS was used for data analysis and image export. The data were georeferenced and filtered using an AGC Exponential filter. SGIS was also used for reflector picking and ship track output as well as image export in TIFF format. All profiles are displayed in figures as two-way travel time (TWT) and are discussed in the text as meters converted using an average acoustic velocity of 1500 m s^{-1}.

In 2005 the previous year's survey lines were rerun using an Edgetech 512i CHIRP sub-bottom profiler operating at 0.5 - 12 kHz with a resolution of 8 - 20 cm. The survey grid was expanded to cover the areas of glacial diamicton that were ignored with the previous system. Penetration in areas of fine grain sediment reached greater than 80 m, penetration over diamicton was up to 5 m, while penetration over bedrock was negligible.

Twenty-two box cores were taken throughout the bay in locations that are indicative of the bottom types imaged in the sidescan sonar data. The cores were analyzed for a number of sedimentological properties, but only the radioisotope analysis will be discussed in this study. Activity profiles of short lived (~100 yr) radioisotopes were used to determine sedimentation rates in the different sedimentary environments throughout Simpson Bay. Activities of ^{210}Pb ($t_{1/2}$ = 22.3 yr) in core samples were measured and plotted to determine sedimentation rates. ^{210}Pb activities were determined using the ^{210}Po method (Nittrouer et al. 1979; Santschi et al. 2001). Aliquots (1 g) of dried sample were prepared by complete digestion with HNO_3 and HF. A ^{209}Po tracer was added to the sample, after which ^{210}Po and ^{209}Po was chemically separated and spontaneously deposited onto Ag disks (Santschi et al. 2001).

Activities were measured using a surface barrier alpha detector. Sediment accumulation rates were determined by the equation:

$$S = (0.031(z_d - z_o))/(LN(A_d/A_o))$$

where S = sediment accumulation rate, z_d = final depth of the regression, z_o = depth of the beginning of the regression, A_d = activity at z_d, A_o = activity at z_o, and 0.031 yr^{-1} = radioisotope decay constant.

^{137}Cs ($t_{1/2}$ = 30 yr) was counted in a low-background, high efficiency, high-purity germanium (HPGe) planar detector coupled with a multi channel analyzer. Samples were dry packed and counted for approximately 24 hrs to determine the first occurrence of ^{137}Cs in the core. ^{137}Cs was produced by bomb fallout as a result of atmospheric nuclear bomb testing in the late 1950's and early 1960's. The depth of first appearance will coincide with the beginning of atmospheric bomb testing in 1954 (Krishnaswami et al. 1971).

Three short piston cores were taken near three of the box core locations to capture a longer record and to ground truth the seismic data. Cores were split, photographed, x-rayed, and subsampled. Water content and grain size were determined for all samples.

RESULTS

Geophysical

Seismic profiles throughout Simpson Bay contain four stratigraphic units, overlying a basal bedrock surface, which are separated by distinct reflectors. Shallow, biogenic gas caused gas wipeouts in parts of the system obscuring the underlying strata.

Bedrock Glacial Surface

The Bedrock (BR) surface is found exposed at the crests of ridges and occurs as a dark, high amplitude reflector, which is presumed to exist throughout the basin. This surface displays stark acoustic contrast where exposed, but is obscured where covered by glacial diamicton and other units. The BR surface is found most commonly as bedrock morainal banks and as subtidal extensions of terrestrial landforms.

Unit I

Unit I is characterized as sub-glacial diacmicton and comprises the morainal banks found at the mouths of the bay. Unit I lies on the bedrock surface and is overlain by Unit II. Unit I is identified by chaotic, high amplitude reflections found proximal to the bedrock surface. Grab samples and cores taken on the morainal banks show poorly sorted sediment ranging in size from clay to large cobbles and boulders. Due to attenuation by progressively thickening deposits in areas away from the exposed banks, this unit was not imaged throughout the bay with the 216S CHIRP system, but was clearly delineated with the 512i. Unit I obscures the bedrock layer except in places where bedrock outcrops at or near the surface.

Unit II

Unit II comprises ice-proximal deposits and was imaged in West Bay in the large basins incised into the bedrock and diamicton surfaces. In East Bay Unit II is found bayward of the entrance moraine, in areas not obscured by the presence of gas. Its complexly ponded stratigraphic style is discontinuous throughout the bay, found only in the deep depressions in the diamicton unit and bedrock surfaces separated by bathymetric highs. This unit is composed of parallel high amplitude reflectors with increasing onlap fill characteristics interbedded with transparent reflectors. Mass transport deposits are evident as transparent and/or chaotic packages that truncate reflectors and are bound by discontinuous high amplitude reflectors.

Unit III

Unit III was imaged in West and East Bay and is characterized as a transparent unit lying on Unit II. In West Bay this unit is found in depressions and in some cases covers diamicton and bedrock highs where they do not outcrop. This unit is bounded below by high amplitude discontinuous reflectors of Unit II and above by low amplitude fine scale reflectors of Unit IV. In some places low amplitude reflectors can be traced through the unit. In East Bay the majority of this unit is obscured by gas wipeout. It lays above Unit II and onlaps the morainal bank at the mouth of the bay. Near the mouth the unit may outcrop from beneath Unit IV, but is probably covered continuously by a thin layer of modern sediment.

Unit IV

Unit IV is composed of thin, continuous reflectors. The unit displays onlap fill characteristics

except where it abuts steep slopes where hydraulic jump erosion truncates the internal reflectors. This unit drapes over Unit III, but is not well defined in the small depressions on the diamicton surface at the mouth of West Bay. This is the thinnest unit identified, reaching a maximum thickness of approximately 5 m and pinching out towards the diamicton and bedrock surfaces. In East Bay the unit is thickest near the base of the slope leading off the plateau near the head of the bay. The unit thins to a point midway down the bay where it pinches out. Past this point there may be a thin layer of modern sediment, thinner than the resolution of the seismic system.

Gas

Biogenic gas deposits are found extensively in East Bay and in pockets in West Bay. Gas deposits throughout North Bay prohibited imaging almost exclusively in the bay. These deposits are found when sedimentation rates are high, causing rapid burial of organic carbon and a reduction in diagenesis and uptake by benthic organisms. These high rates are found in Unit III in West and East Bay and in Unit IV in North Bay.

West Bay

The head of West Bay is separated from the mouth of North Bay by a bedrock and diamicton morainal bank complex. This bank includes a broad, shallow plateau composed of outcropping Unit I and areas where a veneer of modern sediment sits on Unit I. The morainal bank complex is characterized by high amplitude surface reflection with little subsurface penetration (Fig. 7). Unit I outcrops here as a glacial diamict, composed of poorly sorted, unconsolidated sediment. The rocky, intertidal outcrops at the head of the bay and near the rocky promontories are part of the bedrock surface and are characterized by high reflection surface returns with no subsurface penetration. This surface defines the morphology and acoustic basement of the basin.

The mouth of the bay has a broad morainal bank composed of outcropping Unit I with approximately 20 m of relief that delineates the entrance to Simpson Bay. This morainal bank has irregularly shaped depressions which have been filled with material (Fig. 7). Unit II and III are found in these depressions indicated by the changes in strata. Although the thin reflectors in Unit IV sediments are

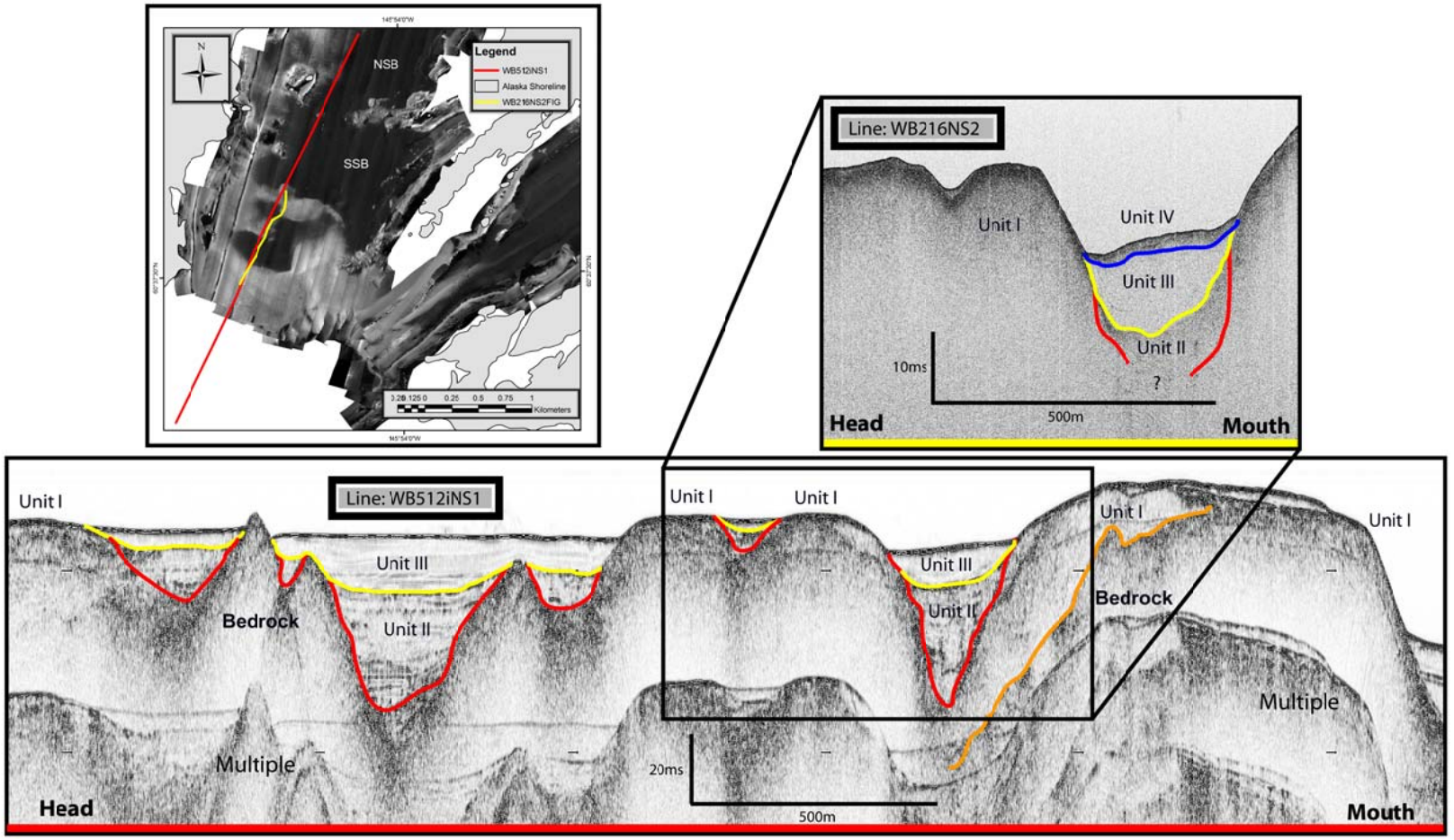

Fig. 7 Seismic profile WB512iNS1 with WB216NS2 (inset) run from the head of West Bay to the mouth. Tracklines are overlaid on the side scan sonar mosaic. Profile WB512iNS1 was collected with the Edgetech 512i system while profile WB216NS2 was collected with the Edgetech 216s

not visible, there is an abrupt shift to higher amplitude reflection demarcating the shift from Unit III to Unit IV (Fig. 7; see inset). Throughout the central portion of West Bay, all units are found deposited in deep depressions incised into the Bedrock surface (Fig. 8). The large fine grain (low reflection) sediment deposit, seen in the side scan sonar mosaic in the center of the bay (Fig. 1), is separated into sub-basins above and below the seafloor by a bedrock ridge that extends across the bay from the eastern shoreline as an extension of a rocky promontory (Figs. 5 and 8). The physical delineation of the two basins is more dramatic on the eastern side of Simpson Bay where the rocky promontory is exposed. The feature is buried mid way across the bay where the two basins merge. The ridge is exposed on the western shoreline as islands and shoreline outcrops.

The North Sub-Basin (NSB) is found in a deep basin, incised into the Bedrock surface, north of the promontory (Fig. 8). The basal glacial surface in NSB is asymmetrically shaped, with the southeastern portion deeper than the northwestern (Fig. 9). Unit I slopes upward to the plateau that occupies the north western portion of West Bay and is covered by a thinning veneer of fine grain sediment (Fig. 7). The bedrock surface that is the extension of the rocky promontory is easily distinguished where it outcrops, but is less defined as it is progressively buried by sediment (Fig. 7). Unit II was ponded rather than draped on Unit I and consequently is deepest in the eastern part (~56 m) and thins towards the western side of NSB (Figs. 8 and 9). Debris flow deposits are identified in Unit II indicated by chaotic units proximal to truncated reflectors (Figs. 8 and 9). Following deposition of Unit II, NSB was infilled with Unit III sediment. This unit is composed of low amplitude homogenous reflection with few low amplitude reflectors and can be up to 10 m thick (Figs. 7, 8, and 9). Unit IV is draped on Unit III and reaches a thickness of ~5 m before it pinches out toward Unit I and the bedrock surface near shorelines and other shoals. Near the steep shoals, reflectors in Unit IV narrow and truncate at the base of the slope due to erosion and lack of deposition from hydraulic jump currents (Fig. 8); (Noll et al. 2008). Unit IV is characterized by fine scale high amplitude parallel reflectors which are interbedded in sediment of medium amplitude reflection. Unit IV also drapes onto Unit I as it outcrops at the head of the bay. This veneer of sediment does not exhibit any internal reflectors, but is considered part of the modern Unit IV.

The South Sub-Basin (SSB) is found south of the promontory and north of the morainal bank at

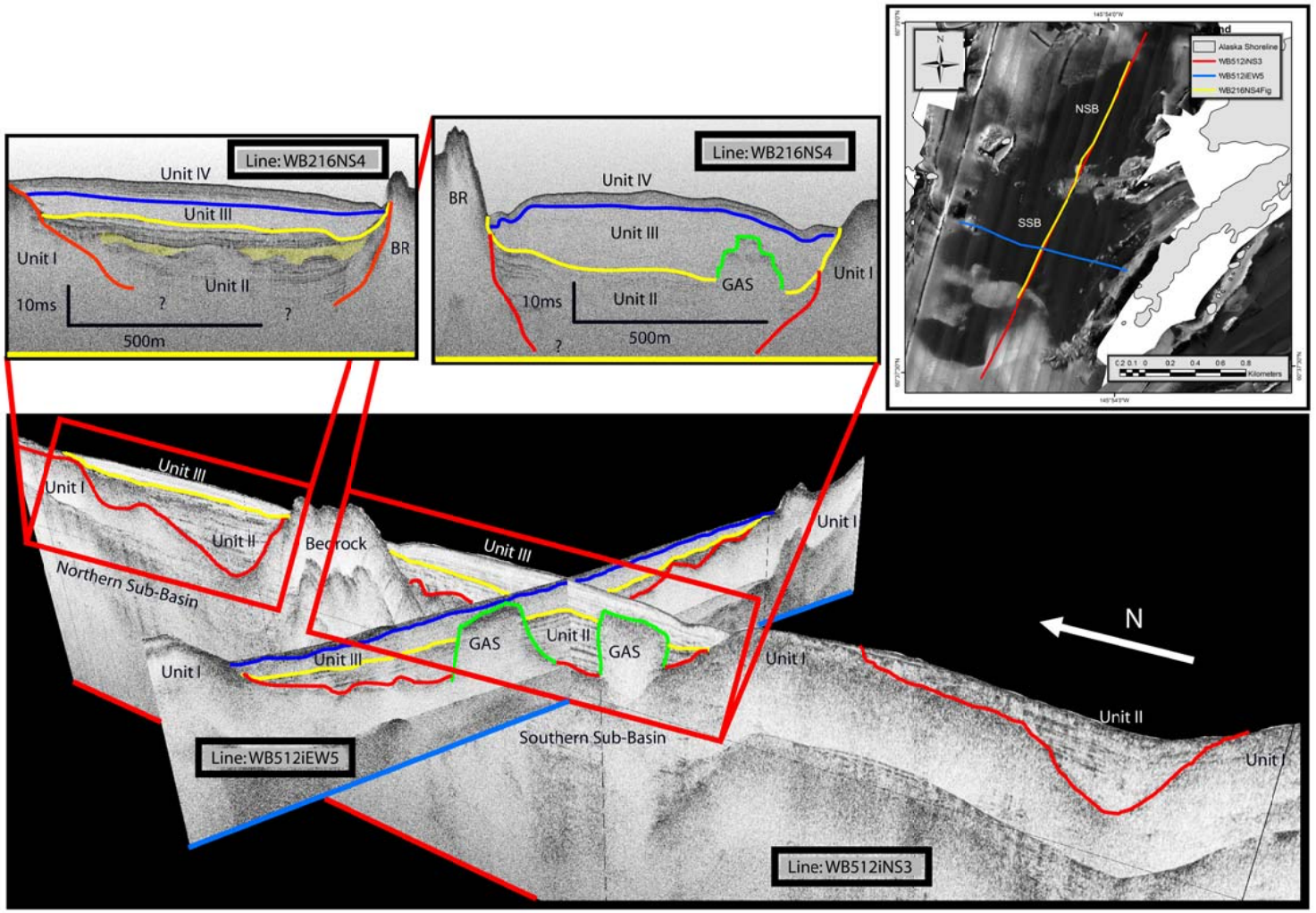

Fig. 8 Fence diagram of seismic profiles from West Bay. Tracklines are overlaid on the side scan sonar mosaic. Profiles WB512iNS3 and WB512iEW5 were collected with the Edgetech 512i system while profile WB216NS4 was collected with the Edgetech 216s

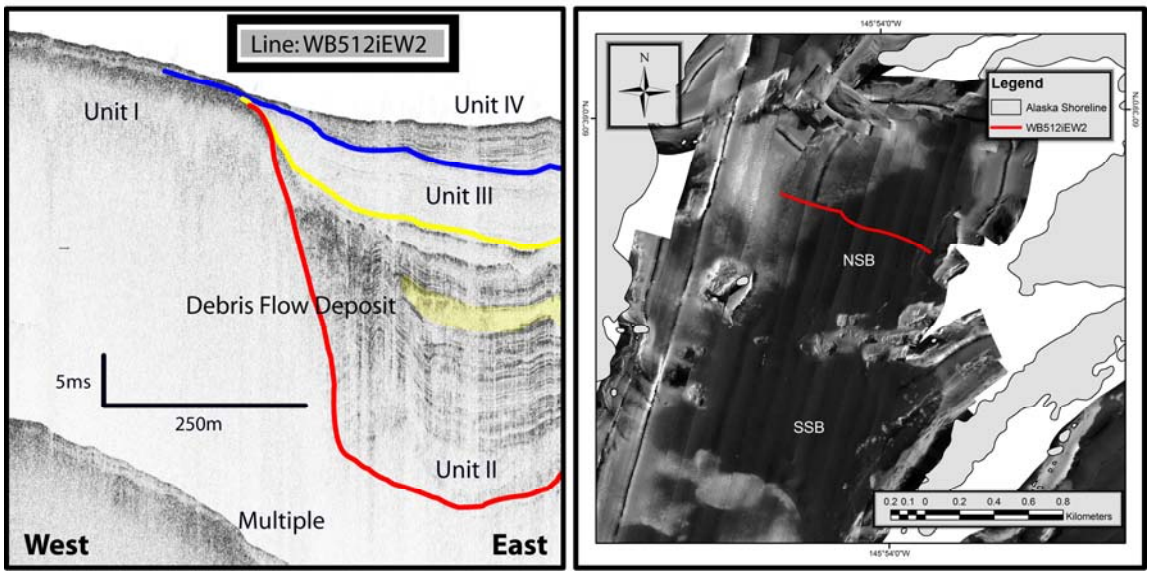

Fig. 9 Across axis (E-W transect) seismic profile from West Bay. Tracklines are overlaid on the side scan sonar mosaic. Profile WB512iEW2 was collected with the Edgetech 512i system

the mouth of Simpson Bay. It has many of the same characteristics as the NSB (Figs. 7 and 8). The Bedrock surface is poorly imaged continuously below the thicker units, but dips sharply from the morainal bank complex at the mouth of the bay and the promontory to form an irregularly shaped depression. A sequence of Unit II, slightly thinner than that found in NSB (~41 m), is found atop Unit I in SSB. Unit III is thickest in this basin (Fig. 8) reaching a maximum of ~18 m. The small amount of gas wipe out in West Bay is found in Unit III in the south eastern portion of SSB, north of the promontory that separates East and West Bay (Fig. 8). Unit IV is thinner than in NSB (< 3 m) and contains similar high amplitude, thin reflectors, although they are not as clearly delineated or numerous (Fig. 8). Sediment in this unit is distinguishable though, by the higher amplitude reflection.

East Bay

Sediment fill in East Bay is confined to one basin, delineated by the Unit I outcrop at the mouth and by a shallow, Unit I and Bedrock plateau at the head (Fig. 10). The Bedrock surface was not found in

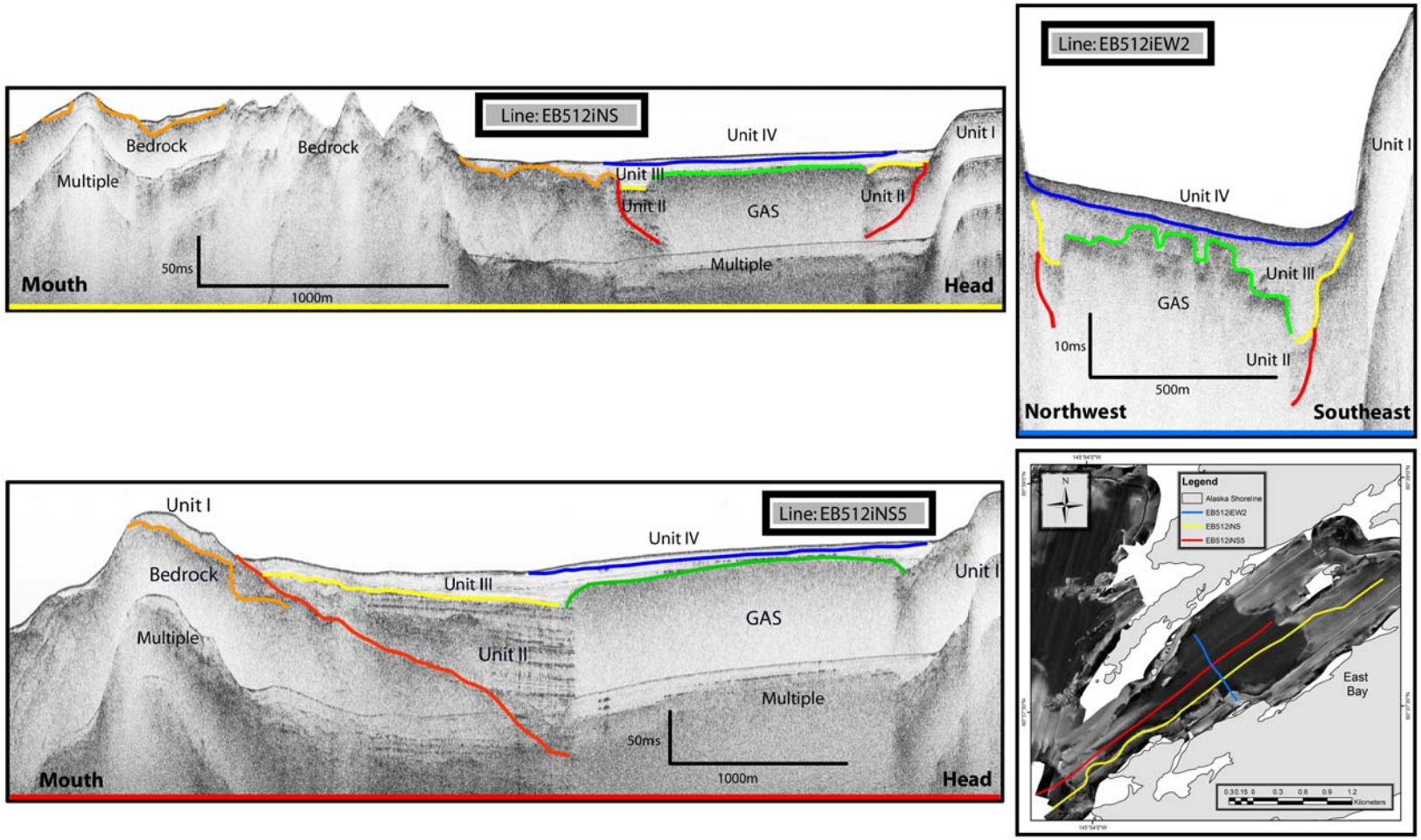

Fig. 10 Seismic profiles from East Bay. EB512iNS and EB512iNS5 run from the bay mouth to the head. EB512iEW3 runs from northwest to southeast in the main part of the bay. Tracklines are overlaid on the side scan sonar mosaic. Gas deposits are found in depositional areas near the head of the bay. All profiles in East Bay were collected with the Edgetech 512i system

the open portions of the bay, but was imaged directly and as side echoes where transects were run near shoreline bedrock outcrops (Fig. 10). Bedrock outcrops form the two small islands found in the middle of the plateau and are seen in side scan sonar images (Noll et al. 2008) and visual observation. Seismic profiles in the main portion of the basin (seaward of the plateau) show gas deposits in the northern half of the bay (Fig. 10). In areas where there is no gas, a complete sequence was imaged. The seaward half of the profile shows a thick sequence of Unit II (~75 m) that appears to be thickening towards the bay head where it contacts the gas wipeout. It shows the same coarse parallel reflectors found in West Bay. Unit III is thick here, reaching 18 m and lapping onto the morainal bank at the head of the bay. Gas prone areas in the seismic record are confined to Unit III in the northern portion of the bay. Unit IV thickens to ~4 m in East Bay before pinching out where the bay narrows near the morainal bank at the mouth of the bay. The bay floor is asymmetrically shaped in the main portion of the bay, sloping from northwest to southeast. Strata shows onlapping basin fill modified by coreolis circulation (Syvitski 1989). This is reflected in the seismic data as well (Fig. 10). The contact between Unit IV and III parallels this slope, but due to the gas deposits, the slope of the basal glacial layer is difficult to determine. At the mouth, deposition is modified by a paleo-channel (possibly a meltwater conduit left from the tidewater glacier) which enhance tidal currents, intensifying scour and preventing deposition.

North Bay

Seismic profiles in North Bay were only able to image underlying strata near the mouth. In one profile, Unit II was measured at 25.4 m thickness near the entrance sill (Fig. 11). Because of the lack of data, this is likely a gross underestimation of the total thickness of the unit. Similar profiles in East and West Bays show that the maximum thickness of the units fall in the central and head portions of the bay. Little overlying sediment from Unit III and IV indicate that the mouth of North Bay has the same tidal current and morphological characteristics as the mouth of East Bay where there is also little Unit III and IV sediment. An axial line in North Bay shows evidence of Unit IV sediment (Fig. 11). This sediment has some fine strata, but gas deposits not far from the sill prevent further imaging.

Cores

Twenty-two box cores were taken in Simpson Bay to determine sediment accumulation rates in

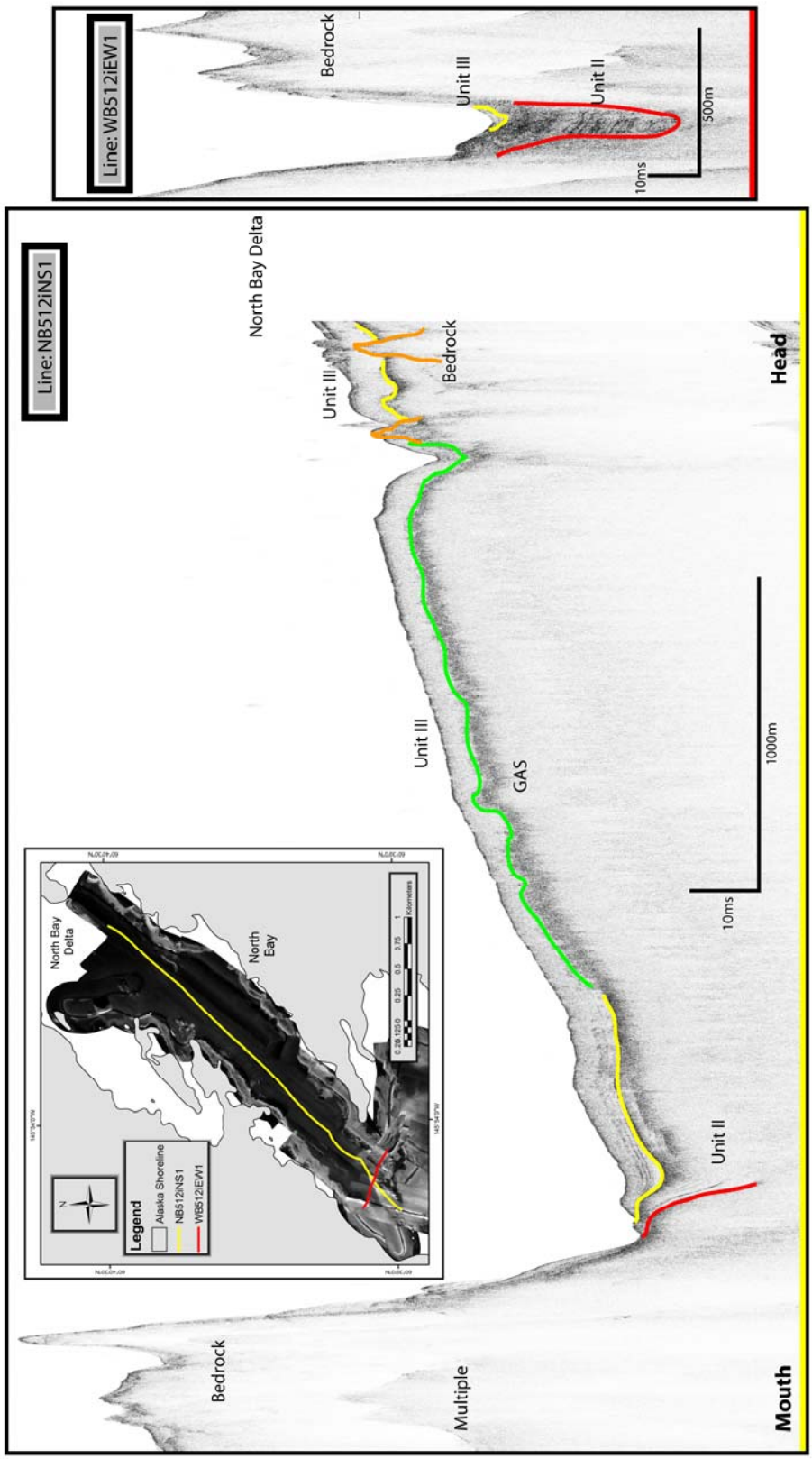

Fig. 11 Seismic profiles from North Bay. NB512iNS1 runs from the mouth of North Bay to the toe of the delta. WB512iEW1 runs across the mouth of North Bay. Tracklines are overlaid on the side scan sonar mosaic. All profiles in North Bay were collected with the Edgetech 512i system

the different sedimentary environments in and will be discussed in more detail in a companion paper to follow. Radioisotope dating of the cores taken in Simpson Bay shows a steep spatial gradient in sedimentation rates. Cores taken in North Bay have high sedimentation rates (0.69 - 1.02 cm yr^{-1}). West Bay cores show lower rates in depositional areas (0.0.30 - 0.52 cm yr^{-1}), and bathymetric highs (composed of relict glacial material) are non-depositional areas (Noll et al. 2008). Cores from East Bay show intermediate sedimentation rates in depositional areas (0.37 - 0.61 cm yr^{-1}).

Two cores were taken at the intersection of seismic lines in the NSB in West Bay. A box core and a piston core were taken specifically to determine an accurate sedimentation rate for the development of a long term geochronology and to determine lithological properties to verify the acoustic data. A sedimentation rate of 0.35 cm yr^{-1} was used to develop the geochronology based on the analysis of the ^{210}Pb data (Fig. 12). The longer piston core crosses a shallow reflector in Unit IV and displays a decrease in porosity and an increase in the mean grain size relative to strata above and below the reflector (Fig. 12). This can be ascribed to cooler, wetter conditions which increased energy in the drainage basin so that hydrodynamic sorting is able to carry larger sediment to the basin.

DISCUSSION

Basin Chronology

A relative chronology of glacial retreat in Simpson Bay is developed by looking at watershed properties, unit thicknesses, water depth, and modern sedimentation rates. The differences in these factors between and within the basins of this system lead to different deglaciation chronologies. Seismic profiles in Simpson Bay are similar to other deglaciated fjords (Knebel 1986; Lysa et al. 2004; Syvitski 1989). A bedrock surface is overlain by a succession of glacial diamicton, proglacial sediment, and glaciomarine sedimentary facies (Knebel 1986). While the seismic profiles in Simpson Bay show comparatively thin total sediment thickness (seafloor to bedrock) when compared to other systems, Holocene deposits are of similar thickness as other deglaciated fjords (Knebel 1986; Lysa et al. 2004).

Watershed and basin morphologies contributed to the timing of deglaciation in Simpson Bay. Watershed:basin surface area ratios and the total sizes of the watersheds are a first order indicator of the

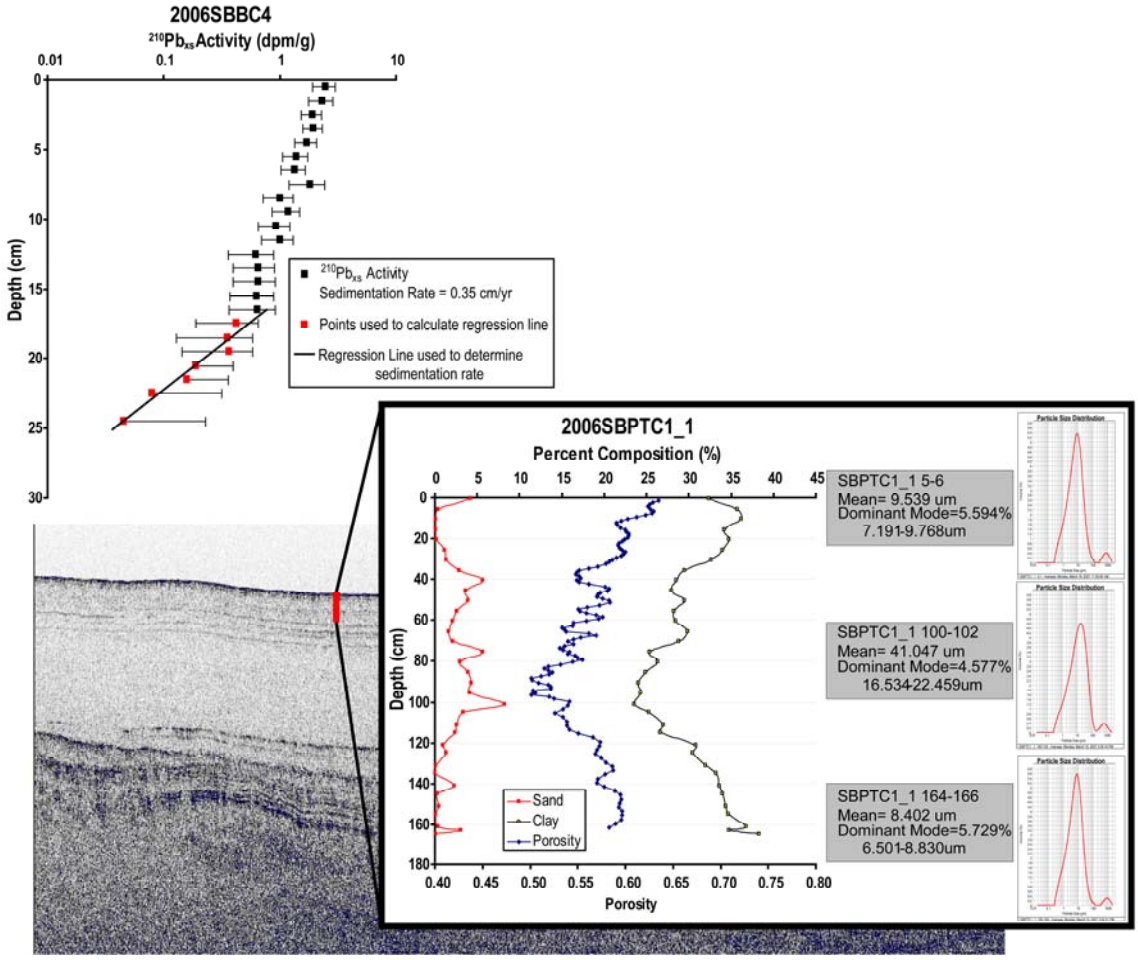

Fig. 12 Cores 2006SBBC4 and 2006SBPTC1_1 used for geochronology and ground-truthing the acoustic data. 2006SBBC4 shows a $^{210}Pb_{xs}$ activity profile. The log-linear decrease in activity below 18cm was identified as a region of steady state sediment accumulation and was used to determine a regression line and accumulation rate of 0.30cm yr^{-1}. 2006SBPTC1_1 shows porosity and grain size data. Clay content and porosity both decrease until about 100cm depth, after which they begin to increase. This minimum in value corresponds to a dark reflector in the seismic data. Particle distribution of selected samples indicates a coarsening in the mean and the position of the dominant mode

length of glacial occupation in each bay (Powell and Molina 1989). The large watershed:basin surface area ratio (20:1) and watershed (112.5 km^2); (Fig. 3) in North Bay indicates that glacial retreat would be delayed with respect to the other watersheds. More ice funneled into a smaller basin would maintain a positive mass balance and stable terminus while others retreated. Also the position of the mouth of North Bay at the head of West Bay would mean that West Bay would need to become completely deglaciated before glacial retreat in North Bay could start. The shallow entrance moraine and the narrow entrance would have both contributed to a longer period of glaciation by significantly reducing the surface area of the face of the glacier (Powell and Molina 1989; Wiles et al. 1995), leaving it less susceptible to changes in oceanographic conditions. East Bay has an intermediate watershed:basin surface area ratio (7:1) and watershed area (51.8 km^2), which combined with a dramatic narrowing at the mouth of the bay serves to promote glaciation and delay glacial retreat. The glacier in East Bay would have been more sensitive to climate changes than the glacier in North Bay because there is not a shallow entrance morainal bank and East Bay exchanges directly with PWS. West Bay has the smallest watershed:basin surface area ratio (1:1) and the smallest watershed (7.5 km^2) indicating that glacial retreat would have begun before retreat in East Bay. Due to the geometry of the entrance of West Bay, the face of the glacier covering West Bay would have a large surface area and would be in direct contact with PWS. This would make it especially susceptible to increased calving associated with changes in climate. Based on basin morphology, glacial retreat began in West Bay before East Bay. Retreat was rapid due to a small watershed and a large glacial surface area interacting with ocean currents. The glacier in East Bay would have maintained its terminus at the mouth longer, but would have been susceptible to increased calving with increasing water temperature. North Bay would have become deglaciated after West Bay due to the entrance geometry and watershed size.

Water depth also suggests different deglaciation histories (Fig. 5). East and North Bays have similar depths and seafloor topography. The seafloor slopes downward from bay head to mouth reaching the deepest point just bayward of the terminal morainal bank before shallowing to the crest of the bank. The deeper maximum depth with respect to West Bay suggests a coupled effect between larger watersheds providing for a longer period of glaciation which in turn excavated more material. This is true for both the

present water depth and the maximum depth to Unit I measured in East Bay and inferred in North Bay.

The thickness and extent of the different sedimentary units in Simpson Bay tell the most about the deglaciation of the system. In West Bay the SSB has a dynamic fill characteristic indicative of sediment exchange between East and West Bay after deglaciation. Unit II is composed of proglacial material deposited during glacial retreat and as the glacier paused at the promontory (Fig. 8). Unit II deposition is thin in the depression on the entrance morainal bank, suggesting deposition during glacial retreat. Unit III is thicker in the SSB than it is in the NSB due to a combination of factors (Fig 8). Deposition would have only occurred in the NSB once the glacier retreated from the central promontory. At this point, proglacial material would be trapped in the NSB and only the finer fraction would bypass the central promontory and deposit in the deeper area between the promontory and the entrance morainal bank. Additional material would come from deposition of sediment from East Bay, advected into West Bay by tidal currents, and deposited in the SSB. Unit III sediment in the depressions on the entrance morainal bank are also a mixture of the two sources, but the unit is thin due to higher tidal velocities on the bank, retarding deposition. Unit IV is thin in the SSB and lacks the number of clearly defined, thin reflectors found in the NSB. This is a combination of higher energy closer to the mouth of the bay and a lack of significant sediment source. There is only a small freshwater source that discharges sediment into the SSB and the SSB is distal to sediment discharge from North Bay. Unit IV in the depressions in the entrance morainal bank does not show the fine scale stratigraphy that is found in the NSB because changes in sediment supply from the short term events that create those layers are diluted by exchange with PWS and input of sediment from East Bay. There is a noticeable change in reflection type to darker tones near the surface that delineates this deposit (Fig. 7). Unit IV in the SSB is thinner that in the NSB because of lower sedimentation rates and the increased effects of exchange with PWS. The small amount of gas found in West Bay (in the SSB in Unit III) indicates that sedimentation rates during Unit III deposition were high enough to bury and preserve the organic matter need for gas generation.

Strata found in the NSB are more influenced by its interaction with North Bay than with East Bay. After the glacier retreated from the promontory, proglacial material was deposited in the depressions left in the exposed bedrock and Unit I. Unit II material continued filling the sub-basin until the glacier

retreated past the bedrock moraine into North Bay. Slump deposits seen in the seismic data are the result of rapid sedimentation and failure at the face of the glacier (Fig. 8). Unit III deposition began once the glacier retreated into North Bay. During this time, Unit II sediment was trapped in North Bay behind the morainal bank and only the suspended fraction was able to escape. The comparatively thin Unit III in the NSB indicates that retreat in North Bay was rapid following its detachment from the terminal morainal bank. The large flux of sediment into the NSB from North Bay was sufficient to overwhelm and dilute the small amount of sediment coming from the drainage basin, prohibiting the formation of high amplitude reflectors. The result of this depositional environment is the homogenous Unit III. It was not until the glacier retreated far up North Bay and became grounded, that Unit IV sediment began depositing. Once the glacier in North Bay became a valley glacier, delta formation began at the head of the bay, sequestering coarse material within the delta and allowing only finer material to reach the estuary. This caused West Bay to transition from a basin influenced by the glacial sediment from North Bay to a basin dominated by watershed runoff and tidal exchange, allowing the preservation of thin reflectors. Fine scale stratigraphy preserved in the NSB is helped by higher modern sedimentation rates (0.48 cm/yr) and the absence of a delta or lake at the head to modulate sediment discharge. This absence reduces the hydrodynamic sorting efficiency of the watershed and allows a broader range of grain sizes to reach the basin, thus preserving a record more indicative of climate variations. The type of strata formation in the NSB is facilitated by a larger drainage basin (compared to the SSB) and the contribution of two small rivers increasing sediment discharge.

Glacial retreat in East Bay began after the retreat of glaciers from West Bay. Seismic reflection profiles in East Bay indicate a period of deglaciation that is conceptually similar, but temporally different to that found in West Bay. This arm of Simpson Bay is significantly deeper than West Bay (Fig. 5) and has more Unit III and about the same amount of Unit IV sediment fill (Fig. 10). This suggests more recent deglaciation when considering the higher sediment input due to the higher watershed:basin surface area ratio and higher modern accumulation rates. The Unit II deposit in East Bay is considerably thicker than in West Bay due to the larger glacier and presumably a longer period of tidewater glaciation with the glacier at the head of the bay. In the northeastern portion of the bay, Unit II is obscured by gas deposits in

Unit III. The slope of Unit I in the imaged portions of the bay suggests that Unit II thickness in the area obscured by gas is greater than the reported values (Fig. 10). Unit III is about the same thickness in the imaged portions of East Bay as in West Bay, but the thickness may also be an underestimation due to the gas deposit obscuring part of the unit. Gas deposits found in Unit III suggest high sedimentation rates, rapid burial, and preservation of organic carbon preventing diagenesis and uptake by benthic organisms during the formation of the unit. The shift from Unit III to Unit IV is more subtle in East Bay than in West Bay. A traceable reflector delineates this boundary, but there is a lack of characteristic thin reflectors and there is not a strong change in reflection amplitude. Although present, fine strata formation may be inhibited by the presence of a small lake near the head of the bay which would serve to modulate sediment input. The lake would trap coarse sediment in the lake and discharge terrigenous material at a more uniform grain size in the face of small climate fluctuations.

North Bay has notably different morphology from the other arms of Simpson Bay, but the limited sub-bottom data suggest that deglaciation was similar to that in East Bay, but temporally different than the rest of the system. An entrance sill at the mouth of the arm restricts exchange and constrains sediment from Simpson Creek to the bay, and like East Bay, this arm is overdeepened with respect to West Bay. In North Bay, sedimentation rates are high (~ 1 cm yr^{-1}) allowing for biogenic gas buildup (Fig. 11). Because most of the sequence in North Bay is obscured by biogenic gas, only a small portion of the seismic profile run at the mouth of the bay shows any subsurface data. One seismic profile shows 25.3 m of Unit II fill, with little overlying strata. This profile was run at the mouth of the bay and the Unit II fill suggests that there is a thick sequence of Unit II material present. Unit II is probably thickest in North Bay and the lack of overlying sediment is due to the thinning of the unit at the mouth (as seen in East Bay), not a lack of deposition. The highest tidal currents would be found in this area, similar to what is found in East Bay. The 4 m of Unit IV material is similar in thickness to that found in the rest of the system, but the measurement made at the mouth is likely an underestimation. Some fine scale strata are found in the unit suggesting that although sedimentation rates were high, lack of exchange and confinement of sediment to the arm allows for the preservation of strata. Unlike gas deposits found in Unit III in the rest of Simpson Bay, gas deposits are found in Unit IV in North Bay. This suggests that modern sedimentation rates in

North Bay are comparable to sedimentation rates when Unit III was deposited in other parts of the system. The only other notable subsurface feature is a large sediment bulge found at the mouth of the bay, north of the morainal bank on the western shore (Fig. 11). This bulge shows onlapping basin fill modified by coreolis and is consistent with an ebb tidal deposit. This deposit is due to high sediment input and the hydrodynamic conditions surrounding the sill. The large intertidal delta at the head of North Bay is unique to Simpson Bay. This delta began forming at the conclusion of tidewater glaciation in North Bay. The delta began capturing the coarse fraction coming out of the glacier and allowed only fine material to enter the bay. The modern delta is composed of sandy silts, while silty clays and clayey silts are found in the basin.

Neoglacial Basin Environments

The neoglacial refers to the period of glacial/interglacial cycles influencing glacial activity beginning at the end of the 'Hypsithermal Warming Interval', which culminated approximately 6000 ybp, to the present (Denton and Porter 1970; Porter and Denton 1967; Sugden and John 1976). Denton and Karlen (1973) used ^{14}C dates throughout the St. Elias Mountains in Alaska and locations in Europe to establish regional and worldwide climate change chronology using glacial activity as a proxy. The St. Elias Mountains are a coastal mountain range in south central Alaska with a large ice cap and expansive alpine, piedmont, and tidewater glaciers. Part of the same orogen that defines the Chugach Mountains, which border and feed glaciers to PWS, the St. Elias Mountains experience similar regional climate changes as are found in the mountains surrounding PWS as it applies to heavy orographic precipitation, temperature and overall climate variability. ^{14}C dates from moraines in the St. Elias Mountains were used to identify three periods of glacial expansion. A synthesis of data presented by Mayewski et al. (2004) identified six periods of Rapid Climate Change (RCC) which correlated well to and validated Denton and Karlen's (1973) chronology with multiple proxies (ice cores, marine sediment cores, etc…). These phases are characterized by polar cooling, tropical aridity, and major atmospheric circulation changes (Mayewski et al. 2004).

The many fjords of PWS have dramatically different subsurface morphologies, watershed:basin surface area ratios, current structures, glacial influence and sediment supply, suggesting that their temporal

glacial histories vary substantially over small spatial scales. Although the fjords within PWS experience climate variations simultaneously, until recently glaciated fjords may have had retreating, advancing, or stable glaciers while many fjords have no glaciers at all. Many fjords, like Simpson Bay, are currently deglaciated, but are still influenced by glaciers in the distal portions of their drainage basin. Because of spatial differences in the modern glacial influence of fjords throughout PWS, it is probable that the differences in stratagraphic successions among the arms of Simpson Bay are due to different glacial responses to the same regional climate fluctuations.

It is well established that fjords act as sediment sinks (Lysa et al. 2004; Syvitski et al. 1987). The morainal banks that delineate the boundaries of Simpson Bay trap sediment and preserve a high resolution record of sedimentary process. Using modern sedimentation rates, a high resolution chronological record is formed for the timing of factors that influence sediment deposition such as climate, glacial activity, and seismic processes. The close association of climate and glacial activity allows climate influences on sediment deposition in Simpson Bay to be determined using seismic profiles. Focusing on Unit IV and the boundary between Units II and III in the seismic record in West Bay, high amplitude continuous internal reflectors suggest that the system has undergone seven phases of glacial expansion/climate fluctuation over the last 2800 yrs. Three of these events are well correlated to Denton and Karlen's (1973) world wide record and provide a contextual framework for our observations. The other four are most likely local to basin scale climate fluctuations causing changes in sediment delivery driven by precipitation. Changes in reflection type in these layers are caused by a decrease in porosity and an increase in the mean grainsize relative to stratal units above and below (Fig. 12). This is verified by core samples taken from the youngest layer (R7). After a chronology was developed, a conceptual model of retreat in Simpson Bay was developed (Fig. 13). This chronology does not negate the possibility that Simpson Bay existed as a fjord before the glacial retreat initiated 2800 ybp. The Hypsithermal Warming Interval (approximately 7000 - 6000 ybp; Sudgen and John 1976) caused worldwide glacial decay and may have caused a previous retreat of glaciers from Simpson Bay. Cooling following the Hypsithermal caused a 'rebirth of glaciers' (Sudgen and John 1976) and may have caused glaciers to reoccupy Simpson Bay. This contingency is only speculation as any evidence left during the Hypsithermal would have been subsequently removed by

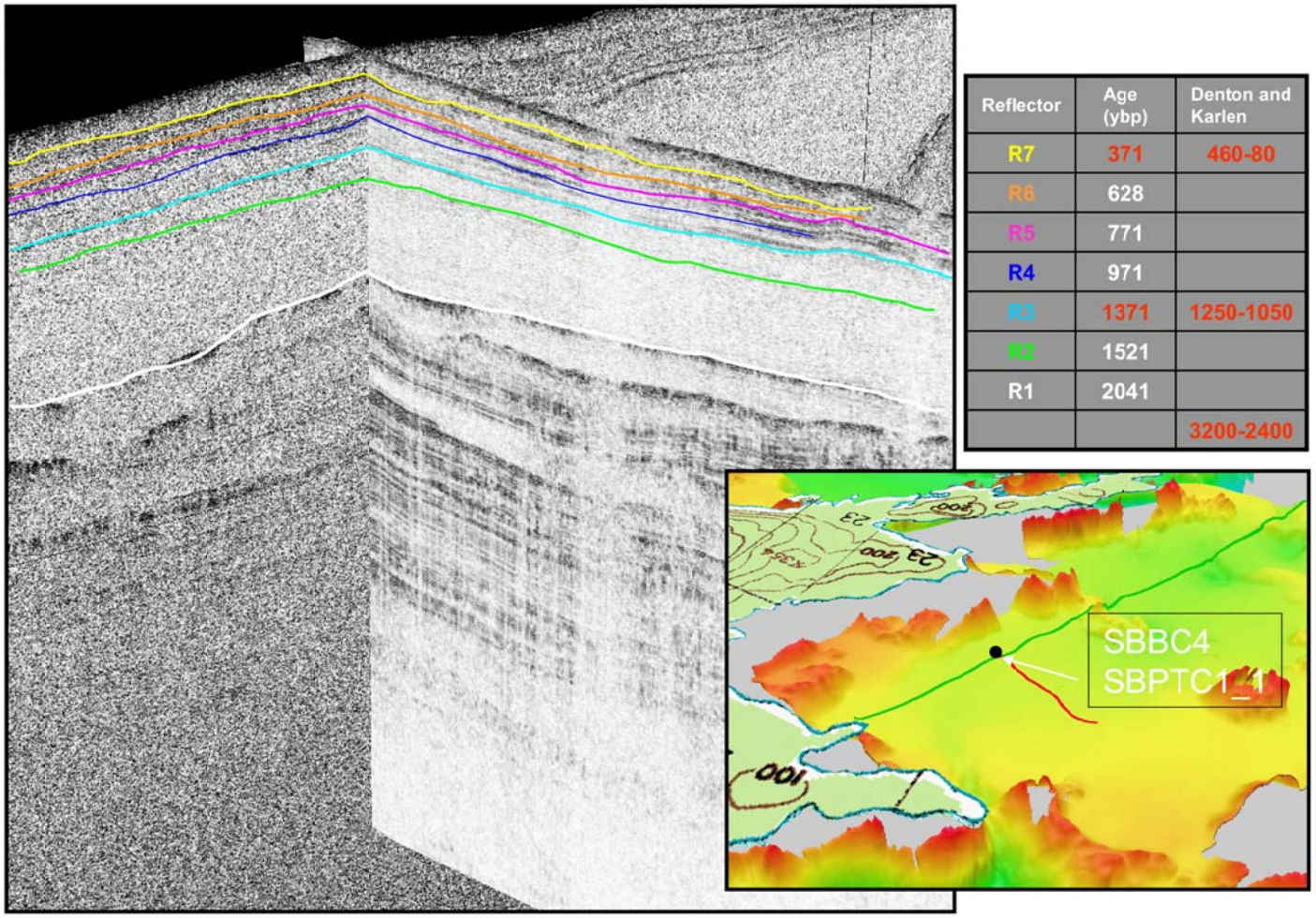

Reflector	Age (ybp)	Denton and Karlen
R7	371	460-80
R6	628	
R5	771	
R4	971	
R3	1371	1250-1050
R2	1521	
R1	2041	
		3200-2400

Fig. 13 Fence diagram of seismic profiles used for the basin chronology. Reflectors were correlated along and cross the axis of the bay and the calculated ages for the reflectors are shown in the table. The red numbers indicate significant periods of glacial expansion by Denton and Karlen (1973). The inset shows the position of cores SBBC4 and SBPTC1_1 to the intersection of the seismic profiles

glacial advance or is beyond our ability to resolve deeper strata.

The dating of the thin reflectors in Unit IV in Simpson Bay was accomplished by the use of short lived radioisotopes (^{210}Pb and ^{137}Cs) to determine modern sedimentation rates and applying those rates to the depths of significant reflectors. The use of short lived radioisotopes in determining sedimentation rates on short (~100 yr) time scales is an important tool that is widely used to investigate sedimentary processes (Jaeger et al. 1998, 1999; Nittrouer et al. 1981; Santschi et al. 2001). It must be noted that using modern sedimentation rates to formulate absolute dates of reflector found in the sedimentary record comes with caveats. Inherent errors due to changes in sedimentation rates over time and instantaneous deposition due to seismic events cause increasing uncertainty in ages with depth. Although these errors exist, first order estimates of ages can be developed which can be correlated to other studies. It is reasonable to apply these modern rates to reflectors in Unit IV as it is composed of sediment resultant processes similar to those found presently. Due to the nature of glacial processes and erosion, sediment input and accumulation rates in fjords decrease with decreasing glacial mass. This would suggest that ages determined deeper in the sedimentary record may be an overestimate of their true age due to the suspected increase in sedimentation rate with depth.

Significant reflectors were identified based on a number of criteria. Intersecting seismic profiles were collected in the NSB of West Bay (Fig. 13). This is a depositional environment which would presumably preserve a record of sediment input. Box and piston cores were taken where the profiles intersect to give accurate sedimentation rates and geotechnical properties. Only reflectors that were correlated between the two profiles and extensively along track were used as they were considered indicative of basin wide changes in sediment deposition. A conceptual model of glacial retreat was then combined with dates to develop a framework for glacial processes and their preserved strata types.

Phase I (Fig. 14) is characterized by the retreat of the glacier from the mouth of Simpson Bay to the entrance to North Bay. The dates 3300 - 2400 ybp are identified as a period of extensive glacial expansion by Denton and Karlen (1973) and presumably the glacier in Simpson Bay was terminated at the mouth of the bay (Fig. 14; Phase 1a). Glacial retreat began after this peak and moved swiftly, depositing Unit I along the way. A pause in retreat created the recessional morainal bank in the middle of the bay

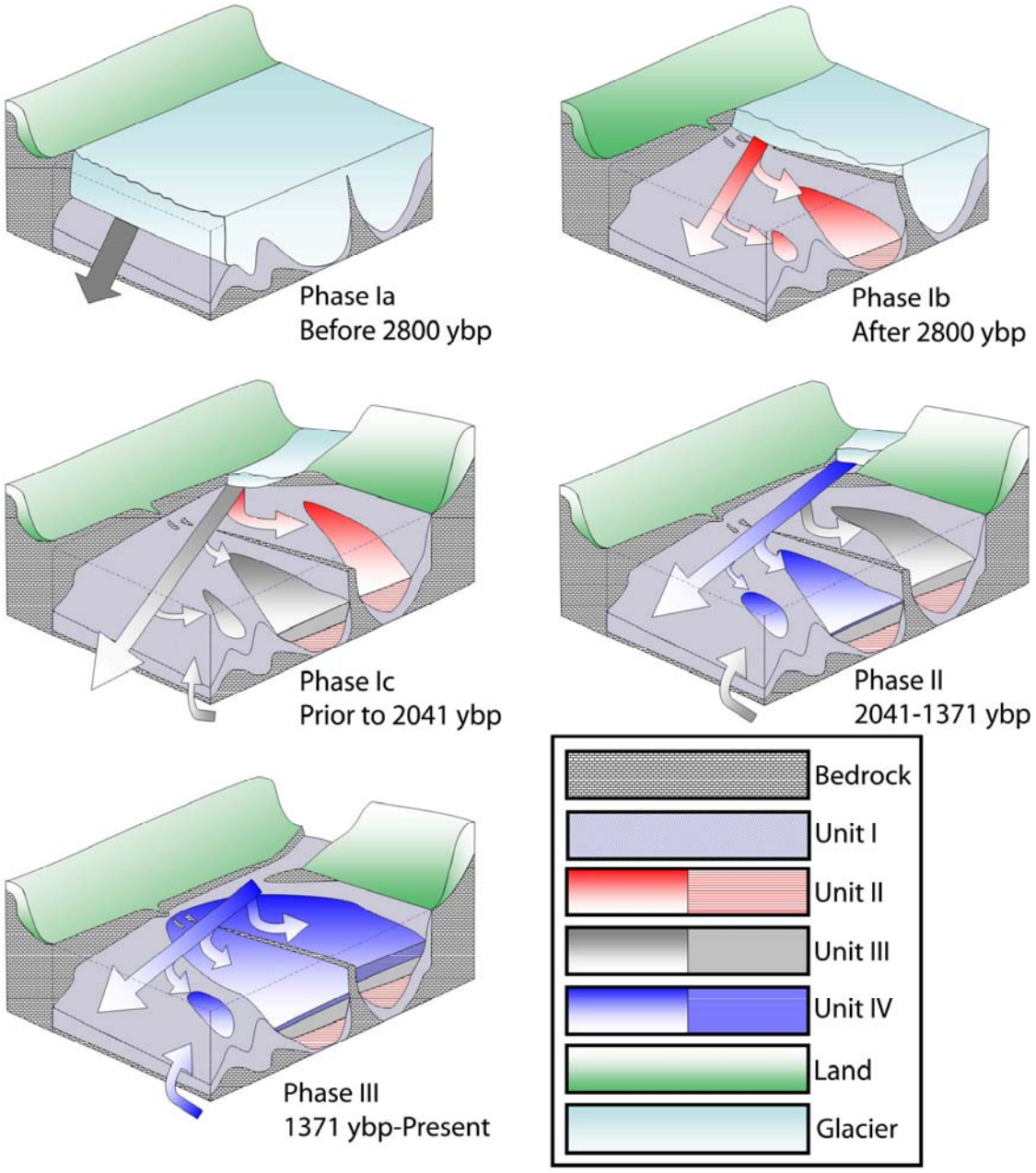

Fig. 14 Conceptual model of glacial retreat in West Bay. The dates assigned to the phases of retreat are taken from the calculated ages of reflectors indicating major shifts in glacial type

(Fig. 14; Phase 1b). Retreat continued until the glacier became grounded at the entrance to North Bay (Fig. 14; Phase 1c). The glacier in North Bay deposited Unit II in NSB until sometime during the peak in glacial retreat (2400 - 1250 ybp; Denton and Karlen 1973) when the glacier retreated past the morainal bank, causing a change in depositional type from Unit II to Unit III and delineating Reflector 1 (R1; Fig. 13), identified as the interface between Units II and III. This marks the retreat of the glacier in North Bay from the morainal bank separating West and North Bay and is dated at 2041 ybp. Coarse sediment from the glacier would have been entrained in North Bay and only the finer, suspended load would escape and deposit in West Bay. Furthermore, Unit III sediment from the glacier in East Bay would be advected into West Bay through tidal exchange and would deposit in the SSB. This peak in retreat most likely marked the retreat of the glacier in East Bay past its terminal morainal bank and back up the fjord. Reflector 2 (R2; Fig. 13) is a faint, but extensive reflector found in Unit III. The age of this reflector (1521 ybp) does not correlate to any world wide climatic event and is attributed to local climate fluctuations. Reflector 3 (R3; Fig. 13) is a significant reflector delineating the boundary between Units III and IV. The age of R3 is 1371 ybp and is correlated to a small period of glacial advance and climate cooling from 1200 - 1000 ybp (Denton and Karlen 1973). This event and the subsequent glacial retreat mark the beginning of modern sedimentation in Simpson Bay. The remaining reflectors are most likely a function of climate fluctuations driving changes in precipitation driven sediment input rather than significant glacial growth and decay and are part of Phase III (Fig. 14). Reflectors 4, 5, and 6 (R4, R5, R6 respectively; Fig. 13) are dated at 971, 771, and 629 ybp. These reflectors were deposited during a period of glacial retreat and are attributed to regional climate changes. Reflector Seven (R7; Fig. 13) is dated at 371 ybp and correlates well to a period of extensive glacial expanse from 460 - 80 ybp (Denton and Karlen 1973).

Age dates are not as well constrained in East Bay, but based on preserved strata, we can still develop a conceptual model of the mechanics of glacial retreat (Fig. 15). Phase I and II in East Bay are similar to Phase I in West Bay. Glaciers occupied the entire bay and a change in climate caused a retreat of the glacier (Fig. 15). This may correlate with the end of a period of extensive glacial expansion by Denton and Karlen (1973) from 3300 - 2400 ybp. Following this period, Phase II began with the retreat of the glacier up the bay to a position as a tidewater glacier resting atop what we identify now as the plateau

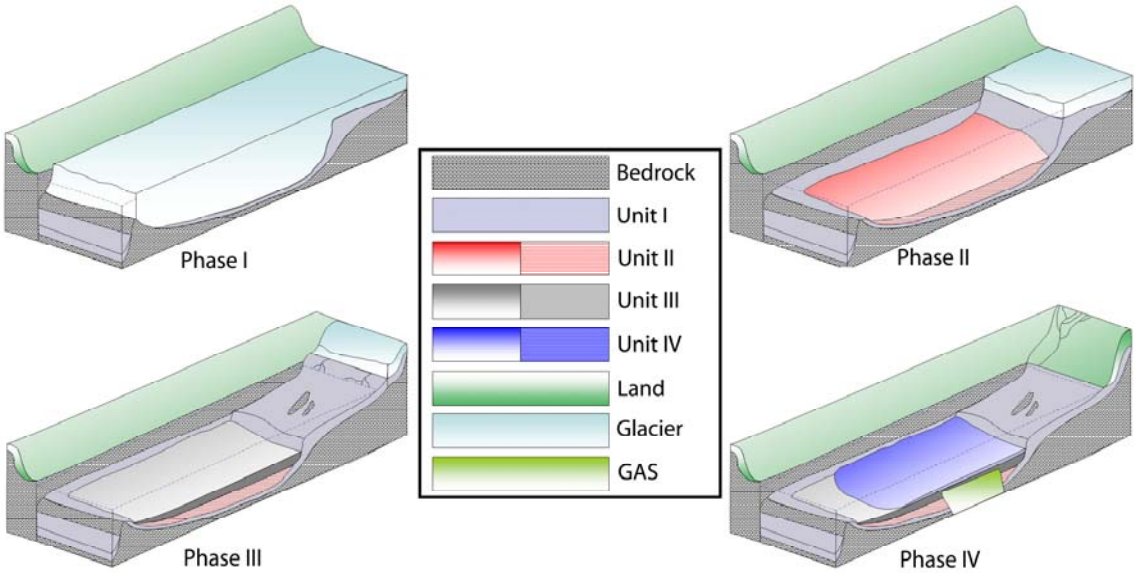

Fig.15 Conceptual model of glacial retreat in East Bay. Calculated dates of reflectors were not possible because gas obscured the maximum depth of the reflectors in the central portion of the bay

at the head of the bay (Fig. 15). This probably coincided, but lagged behind the retreat of the glacier from West Bay and deposited Unit II material. With Phase III, the retreat of the glacier from East Bay initiated capture of coarse material on land and began the formation of Unit III. Modern accumulation rates suggest that this may have happened about 2083 ybp which correlates with glacial retreat from the NSB in West Bay. This would still indicate a lag between the two bays, as glacial retreat from the mouth of West Bay began earlier than the ages reported which are for the NSB in West Bay. Finally, in Phase IV the glacier has retreated from the basin, sediment input is fluvially dominated, and Unit IV sediment is found (Fig. 15). The interface between Unit III and IV is dated at approximately 683 ybp, putting it well after the interface in the NSB in West Bay.

CONCLUSION

1. While on a regional scale glacial retreat is often modeled as simultaneous and directly coupled to

climate change, on a basin scale, changes in basin morphology have a great influence on the chronology of glacial retreat. We have shown that within a small fjord system, individual units show large differences in glacial histories while under the same climatic and oceanographic conditions. These changes are attributed to the differences in watershed and basin morphology and are illustrated in the sedimentary record.

2. The seismic record in Simpson Bay shows punctuated changes in preserved strata indicative of different phases of glacial influence. Because the energy regimes of these different phases differ drastically and the shifts between phases are abrupt, stratal units are easily delineated and can be correlated throughout the system. These units can be correlated to common sedimentary processes, but not chronologically due to the differences in glacial retreat.
3. Seismic profiles can provide a high resolution record of sedimentary processes within a basin. Because fjords are considered reasonably closed systems and major sinks of sediment, they capture a detailed basin chronology with little outside influence. It is because of this that they provide the opportunity to investigate basin responses to climate change. The record must studied with care and certain criteria must be addressed to determine whether the conclusions reached are robust. Most of the changes seen and the questions to be addressed change the nature of sedimentary processes as to confuse any chronological interpretation. Expansion and contraction of glaciers changes sediment input and accumulation rates and lead to inaccuracies when extrapolating modern sedimentation rates through time. Furthermore, strata found in the seismic record accounts for only retreat from the last greatest advance of the glacier. The record of prior, if any, advances and retreats through Simpson Bay would have been destroyed by the last glaciation, precluding preservation of previous events. As such, fjords are only useful for determining recent climate change.
4. Glaciers last occupied a position at the mouth of Simpson Bay approximately 2800 ybp. Glacial retreat began first in West Bay followed by soon by East Bay and began in North Bay after glaciers retreated from West Bay.

CHAPTER III

CONTROLS ON SEDIMENT DISTRIBUTION AND ACCUMULATION IN AN ALASKAN TURBID OUTWASH FJORD: SIMPSON BAY

OVERVIEW

Simpson Bay is a turbid outwash fjord located in south central Alaska. The controls on sediment distribution and accumulation were studied to determine the processes which govern strata formation and preservation in a non-glaciated, macrotidal fjord. Box cores were taken throughout the fjord to calculate accumulation rates and the effects of long term changes in sediment deposition. $^{210}Pb_{xs}$ activity, porosity, grain size and x-radiographs of cores were used to investigate the different sedimentary environments. Analyses of short lived radioisotopes were used to measure accumulation rates at a number of locations throughout the fjord. Three depositional environments were identified in Simpson Bay: physically dominated delta front environments, biologically dominated deepwater environments, and non-depositional relict glacial deposits. Evidence of both physical and biological post-depositional modification was found throughout the system. X-radiographs were used to identify sedimentary structures, validate surface mixed layers, and help identify physically versus biologically mixed environments. $^{210}Pb_{xs}$ derived accumulation rates varied from 0.07 to 1.02 cm yr^{-1} throughout the system. $^{210}Pb_{xs}$ profiles in the diamicton deposits on the morainal banks show a log-linear decrease in activity indicative of steady state accumulation, but because these areas are non-depositional relict glacial deposits, the decrease in activity is modeled as biodiffusivity rather than accumulation. Activity profiles were also used to look at the response and recovery of the seafloor to large earthquakes. Profiles throughout Simpson Bay show evidence of an event signal, correlated with the 1964 Good Friday Earthquake. Biodiffusivity rates from the ^{210}Pb profiles range from 0.75 - 85.31 cm^2 yr^{-1} indicating that the system is well mixed and when combined with grain size profiles and x-radiographs shows that biological mixing does not allow preservation of textural changes in accumulated sediment. When the depths of secondary geochronometers were compared to calculated depths from ^{210}Pb accumulation rates the results showed no evidence of less intense deep mixing below the surface mixed layer. This indicates that although a number

of benthic fauna and burrow types were observed, larger burrows to the base of the mixed layer were responsible for complete mixing on the timescales investigated. Data from and instrumented benthic pod show that seafloor current velocities are insufficient to mobilize coarse material in the relict glacial deposits, but that the resuspension of fine material suggests a coupled bio-physical process where fine sediment it transported to the surface by benthic organisms and transported by tidal currents.

INTRODUCTION

Physical, biological, and chemical processes combine to alter deposited sediment and these alterations can cause misinterpretation when investigating the origin and depositional environments of preserved strata. The factors governing modern sediment deposition and preservation are key components to providing linkages to understand paleo-depositional environments preserved in the rock record. Only when these processes are understood and can be explained, are we able to make an accurate assessment of preserved material.

Fjords, like other estuarine, coastal, and deep sea depositional environments, have multiple processes working in concert that contribute to the deposition, accumulation and post-depositional alterations of sediment. These processes contribute to different degrees depending on the location in the individual fjord and on where the fjord lay in relation to end member systems (Dowdeswell et al. 1994; Jaeger and Nittrouer 1999; Syvitski 1994; Syvitski 1989). Differences in fjord morphology play a large role in the types of alteration. The temperate fjords of coastal Alaska tend to be well mixed, supporting healthy benthic communities where biological processes dominate. Deepwater renewal in these areas provide suitable habitat for a diverse benthic population which rework the seafloor (Powell and Molina 1989; Muench and Heggie 1978; Reed and Schumacher 1987). Deepwater fjords are sometimes seasonally or permanently anoxic/hypoxic, inhibiting the establishment of or destroying benthic populations (Bentley and Nittrouer 1999; Jaeger and Nittrouer 1999; Syvitski and Shaw 1995; Syvitski et al. 1987). In these cases, preserved strata reflect only the physical/energy regime of the system. Chemical alterations play a role in these systems due to their unique chemistry. Furthermore, tidewater fjords have significantly different dynamics when compared to non-glaciated fjords. Glaciers discharge large volumes

of sediment and freshwater directly into the marine environment. Sedimentation rates near the glacier front can be on the order of centimeters per day (Cowan and Powell 1991; Jaeger and Nittrouer 1999; Hoskin and Burrell 1972; Molnia 1983; Powell 1991; Powell and Molnia 1989) which can overwhelm benthic communities, inhibiting development, and preserving primary physical sedimentary fabric. Also, ice rafted debris introduces a wide range of clast sizes, sometimes great distances, through quiescent systems that would otherwise require high energy environments for transport (Syvitski 1989; Syvitski et al. 1987). Sedimentation rates in these systems decrease exponentially with distance from the glacier front (Bogen 1983; Hoskin et al. 1978; Relling and Nordseth 1979; Smith and Walton 1980; Syvitski and Murray 1981; Syvitski and Shaw 1995), and biological processes begin to influence preserved sediment when rates become low enough for the establishment of benthic communities.

Fjords are a type of estuarine system that is generally impacted less by direct anthropogenic disturbances than are other temperate and equatorial estuaries. Some fjords are found in high latitudes where climate is inhospitable (Antarctica, Greenland). Others have rugged topography that make transportation difficult and isolates these systems. As always humans seem to find a way and there are many examples of heavily impacted fjord systems. Some low-latitude, temperate fjords are heavily urbanized and industrialized which can increase sediment load due to land development, increase contaminant input, and alter the biological community through fishing, trawling and trapping (eg. Saguenay Fjord, Quebec; Puget Sound, Washington; Hudson River, New York; etc…). Fjords as a whole bear the signs of anthropogenic impacts on global climate which are altering glacial mass balance, opening up new environments in the face of glacial retreat.

The purpose of this paper is to investigate the relationships between physical and biological processes and preserved strata. Depositional environments in Simpson Bay have already been discussed (Noll et al. 2008), so the focus will rest on post depositional alteration of sediment. These environments range from physically dominated delta fronts to biologically dominated deepwater environments to biologically and physically modified relict glacial deposits. This investigation becomes important in the face of climate change and the disintegration ice bodies. Glaciated systems are becoming sparse and investigations into established, non-glaciated systems become important in understanding the future of

many of these recently deglaciated systems. By choosing a relatively pristine, dynamic system, we can investigate the many possibilities nature presents without having to account for the factors applied by anthropogenic forcing. Simpson Bay has been deglaciated for ~2800 years, so it reflects long term sedimentary properties of a non-glaciated temperate fjord. Geochemical and geotechnical analysis of cores using radioisotopes, sedimentological properties, and qualitative analysis of x-radiographs were used to asses the degree to which sediment is preserved. Cores of different lengths and tracers that work on different time scales will allow assessment of processes that work on decadal to centennial intervals.

BACKGROUND

Geologic Setting

Simpson Bay is a macrotidal turbid outwash fjord located in southcentral Alaska (Fig. 16). The fjord can be morphologically divided into three discrete units each with variations in watershed characteristics, sediment inputs, oceanographic influences, and sedimentary environments. These basins can be further divided into areas of modern deposition and areas of relict glacial deposits (Fig. 17). These relict glacial deposits were deposited as glaciers retreated and where hydrodynamic controls prevent modern deposition and erode fine material, effectively armoring the seafloor (Noll et al. 2008). Both areas show evidence of robust benthic communities which are the dominate mechanism for post depositional alteration of sedimentary strata.

Simpson Bay is Y-shaped and can be divided into three parts: West Bay, North Bay and East Bay with West Bay being the central part of Simpson Bay. This arm has the largest surface area (7.5 km^2), but has a small drainage basin (7.5 km^2), giving it an approximately 1:1 watershed:basin surface area ratio (Fig. 3). This arm is approximately 4 km long and 2 km wide and opens directly into Prince William Sound (PWS). West Bay is morphologically the most dynamic portion of Simpson Bay. On average, it is the shallowest (25 to 55 m; Fig. 5), and the bottom is irregularly shaped (Noll et al. 2008). The side scan sonar and bathymetry data combined with extensive seismic profiles have been used to divide West Bay into Northern and Southern Sub-Basins. These sub-basins show specific stratigraphic differences

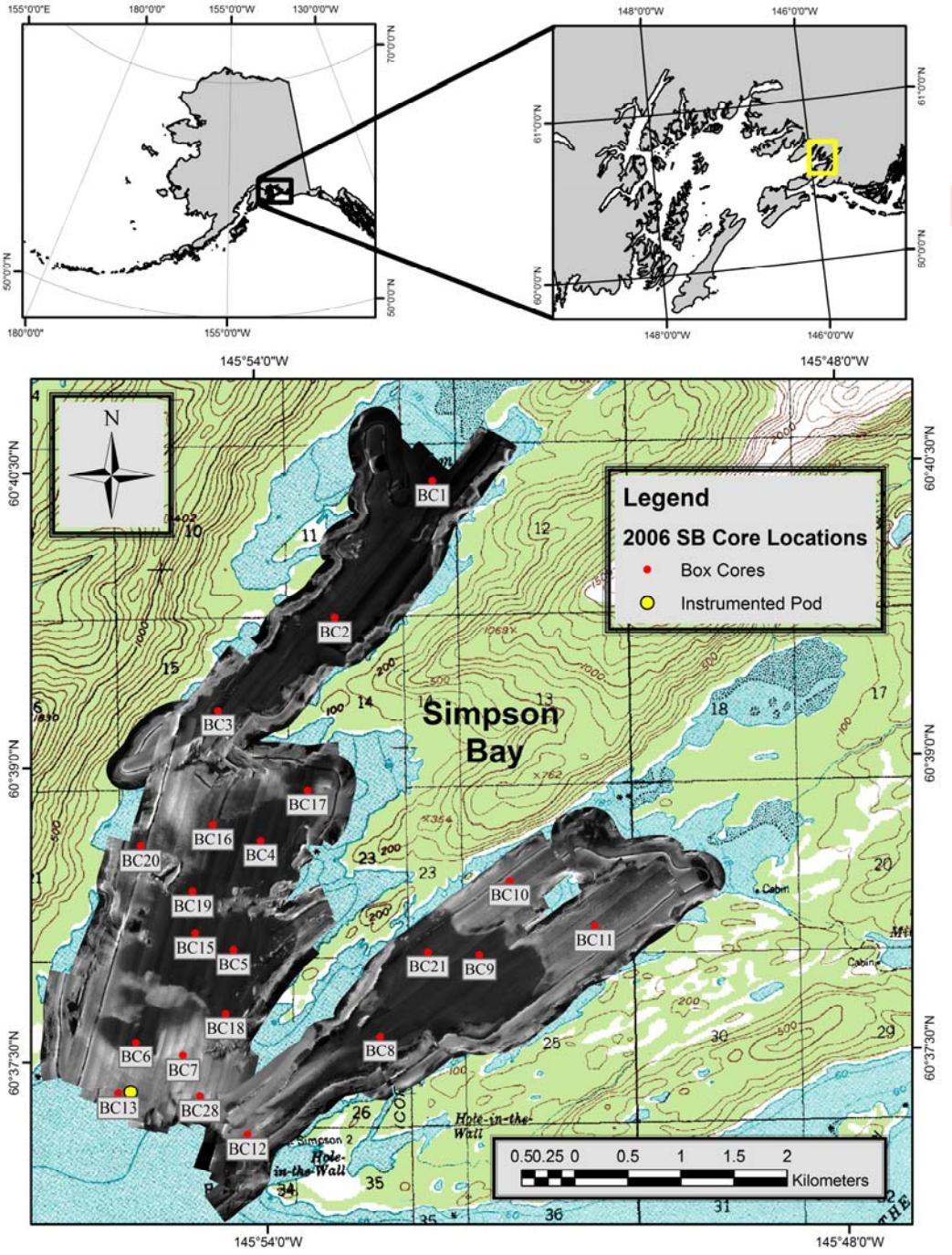

Fig. 16 Box core locations from Simpson Bay. The side scan sonar mosaic shows fine grain estuarine mud in the central portions of the basin and the USGS topo map shows steep shorelines that surround the bay. Simpson Bay is divided into three morphologically distinct units: West Bay, North Bay, and East Bay. Red dots denote the locations of the box cores and the yellow dot denotes the location of the pod deployment

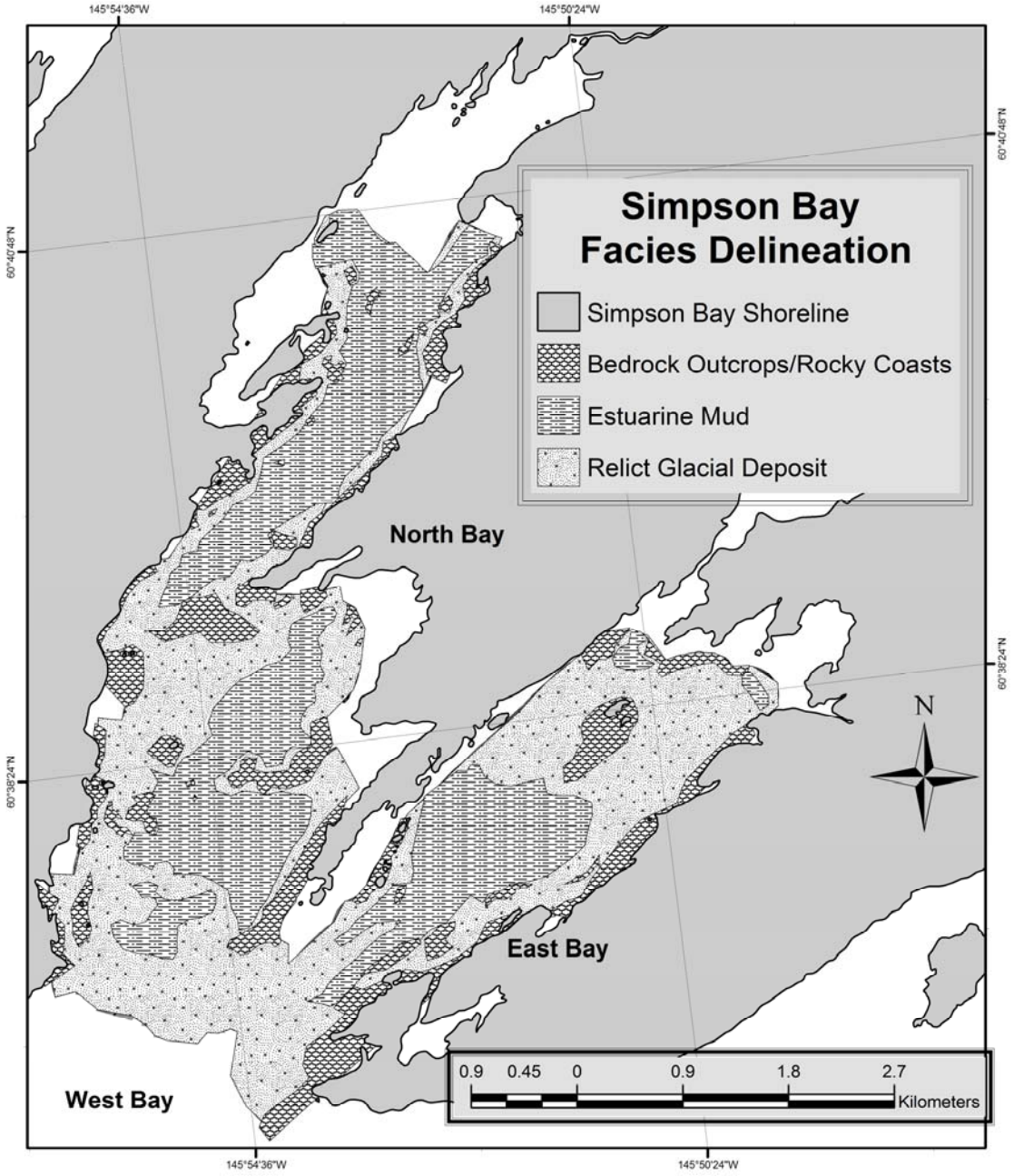

Fig. 17 Facies delineation of modern sediment in Simpson Bay. Fine grain estuarine mud is found ponded in the central portions of the bays, while relict glacial deposits and rocky outcrops are found around the periphery of the bay

indicative of differences in glacial retreat and sediment source. The Northern and Southern Sub-Basins have approximately 70 m of post glacial fill with large spatial and temporal heterogeneities and approximately 5 and 2.5 m of modern sediment, respectively. Side scan sonar and bathymetry data reveal fine grain sediment ponded in bathymetric lows while bathymetric highs are formed by the high backscatter diamicton and bedrock deposits that make up the relict glacial material. This part of Simpson Bay is bounded to the north by the shoreline and the bedrock moraine morainal bank that separates North Bay and West Bay and to the south by a low relief morainal bank and PWS (Noll et al. 2008).

North Bay is the northern arm of Simpson Bay. It has the largest watershed (112 km^2), which encompasses some small alpine glaciers and the smallest surface area (5.5 km^2), giving it a large watershed:basin surface area ratio (20:1; Fig. 3). This is the only part of Simpson Bay that acts as more classically defined fjord (Perillo 1995; Pritchard 1967). It has a narrow entrance with a shallow sill which makes it a semi-restrictive basin, although no seasonal or permanently hypoxic conditions have been noted. North Bay is long (4 km) and narrow (0.7 - 1.3 km) with depths that range from 80 m (Fig. 5) just inside the entrance sill to the intertidal delta. A large sediment supply has helped create a large delta at the head of the bay. This intertidal delta captures most of the coarse particulate load of the river, allowing discharge of only the fine suspended load. Any coarse material that does escape the delta during high discharge periods is quickly deposited at the base of the delta. Side scan sonar data shows that the bottom is composed of estuarine muds with glacial diamicton and bedrock near shorelines and the entrance sill. Biogenic gas in the shallow subsurface does not allow the seismic profiles to image the glacial surface, but other characteristics (comparison with East Bay, watershed morphology, etc…) suggest that there may be >100 m of post glacial fill in the fjord.

East Bay is the eastern arm of Simpson Bay. East Bay has characteristics of both North and West Bay. It is long, narrow and deep (80 m; Fig. 5), but does not have a shallow entrance sill and exchanges directly with PWS. East Bay has almost the same surface area (7 km^2) as West Bay, but its drainage basin is much larger (52 km^2), giving it a 7:1 watershed:basin surface area ratio (Fig. 3). The side scan sonar data show estuarine muds in the deeper areas. The seismic data reveal approximately 100 m of post glacial fill, although this may be a slight underestimate due to the presence of biogenic gas in some areas,

and approximately 4 m of modern sediment. East Bay does not have a delta forming in the bay, but does have a small upland lake in the main freshwater supply that has an actively building delta. At the head of the bay, depths decrease sharply to a high backscatter, shallow plateau composed mainly of coarse grain material with a veneer of estuarine mud on top (Noll et al. 2008).

Rivers draining active orogens produce some of the highest sedimentation rates on earth. The short steep mountainous rivers of the Andes, Oceania, and Alaska have high elevations and small watersheds yielding some of the highest sediment loads on earth (with an increased emphasis on the bedload fraction) and a short residence time in the watershed (Jaeger and Nittrouer 2006; Jaeger and Nittrouer 1999; Jaeger et al 1998; Milliman and Syvitski 1992). Simpson Bay's watershed has peaks as high as 1500 m and has a watershed area of 172 km^2 making it a mountainous river under Milliman and Syvitsky's classification. Orographic precipitation is driven predominantly by the interaction of the Aleutian Low pressure system with the Chugach Mountains. The Chugach Mountains, reach heights in excess of 4000 m less than 60 km from the coast, and St. Elias Mountains just east of the study site make up one of the highest coastal reliefs in the world. These combined with easily erodable fine grain sedimentary bedrock, rapid uplift (several meters per 1000 yrs) and high precipitation suggests that freshwater delivers high sediment loads to Simpson Bay (Fig. 2; AGDC 1998; Jaeger and Nittrouer 1999).

Because freshwater discharge is modulated by changes in precipitation and meltwater discharge, freshwater delivery creates an array of oceanographic conditions that can change on a wide range of timescales (seasonal, annual, interdecadal). Short residence times in the watershed provide a direct feed back between watershed changes and constituent inputs. These inputs can shift the nutrient, salinity, sediment, circulation, and water chemistry balances in the fjord. These changes are directly translated to the benthos and affect the health of the benthic community.

Applications of Short-Lived Radioisotopes

Short-lived radioisotopes are used in a diverse array of lacustrine, estuarine, coastal, shelf and deep water environments (Degeest et al. in press; DeMaster et al. 1985; Jaeger et al. 1998; Kodie et al. 1972; Krishnaswami, et al. 1971; Kuehl et al. 1986; Kuehl et al. 1982; Nittrouer et al. 1979; Sommerfield

and Lee 2003; Sommerfield and Nittrouer 1999; Walsh and Nittrouer 2003). ^{210}Pb has proven a useful tool when looking at sedimentary dynamics on decadal to centennial timescales including surface mixing, accumulation rates, instantaneous deposition, and short term sedimentation rates. These can be used to investigate changes in discharge, benthic community dynamics, mixed layer residence times, and event processes as well as an array of other dynamics.

Biological Mixing

A common use of ^{210}Pb is its application to the quantitative assessment of biological mixing. Biological mixing has been modeled as diffusion under the assumption that the time averaged vertical integration of all processes resembles a one-dimensional diffusive model (Aller and Dodge 1974; Goldberg and Kodie 1962; Guinasso and Schink 1975; Nozaki et al. 1977). This model requires some assumptions be demonstrated. Sediment accumulation must be steady state and the effects of mixing must completely homogenize the Surface Mixed Layer (SML). If these assumptions cannot be met, then the model output will not quantitatively reflect the aspects of biological mixing. In areas where the assumption of steady state deposition and complete mixing of the SML are satisfied, and the activity profiles can be identified as biologically mixed, biodiffusion coefficients or biodiffusivity (D_b, $cm^2\ y^{-1}$) can be calculated in the surface mixed layers using a regression of the down core activity of the isotope and the equation:

$$A(z) = A(o)e^{\left(-z/\sqrt{Db/\lambda}\right)}$$

where D_b = biodiffusion coefficient ($cm^2\ y^{-1}$), z = change in depth of the of the regression (cm), A_z = $^{210}Pb_{xs}$ activity at end of the regression (dpm g^{-1}), A_o = $^{210}Pb_{xs}$ activity at beginning of regression (dpm g^{-1}), and λ = radioisotope decay constant (^{210}Pb, 0.031 yr^{-1}); (Aller and Cochran 1976; Bently and Nittrouer 2003; Wheatcroft et al. 1990).

While this approach is quite robust in most settings, it breaks down when the effects of less intense deep mixing are underestimated (Nittrouer et al. 1984) or if mixing varies considerably with depth (Christensen 1982; Olsen et al. 1981; Schink and Guinasso 1977). To asses the degree to which this

influences the calculations of D_b, independent tracers must be used to verify the results. These include time dependent tracers such as short lived radioisotopes, event layers, and other proxies with a known source function such as contaminates, organic matter, and heavy metals to name a few. ^{137}Cs is a commonly used tracer to verify D_b results and investigate deep mixing in estuarine and coastal environments (Nittrouer et al. 1984). ^{137}Cs is a bomb-produced radioisotope with a first occurrence that coincides with the beginning of atmospheric bomb testing in 1954 (Krishnaswami et al. 1971). When deep mixing is not present, the maximum ^{137}Cs depth should not be deeper than the sediment accumulation rate multiplied by the time elapsed from the beginning of testing plus the SML. If the depth of first occurrence is deeper than this calculated depth, deep mixing is present and the calculations of D_b break down (Nittrouer et al. 1983/1984). Care must be taken in many environments to negate the effects of episodic deposition and either validate the assumption of steady state deposition or account for changes in deposition.

Estimates of biological mixing can be further complicated by the fact that D_b does not take into account the effects of horizontal mixing and cannot be used when vertical advective mixing affects the SML (Smith and Schafer 1984; Wheatcroft et al. 1990). The horizontal component is not accounted for in the one-dimensional model and can cause significant perturbations when considering heterogeneities in bed roughness and faunal abundance (Aller 1982; Jumars et al. 1982; Jumars 1978; Levin et al. 1986; Smith and Schafer 1984). Organisms with branching or U-shaped burrows are found which precipitate horizontal transport of sediment and gradients in grain size distribution due energetic environments and grain size specific faunal foraging preferences promote spatial heterogeneities. These contributions mean that values of D_b may be skewed. The vertical component of advective mixing can be identified by the shape of the ^{210}Pb profile (Nittrouer and Sternberg 1981) and D_b values for those profiles can be discounted. All of these factors taken together conclude that tracer profiles and quantitative measurements of D_b are important and useful tools, but care must be taken satisfy all assumptions and verify values by a combination of approaches.

Physical Mixing

Physically mixed systems in Simpson Bay are confined to the delta front environment. This area is not extensive and is dominated by gravity transport processes. Because of the depth, lack of fetch, and geographical orientation to prevailing wind, Simpson Bay does not receive adequate wave energy to cause physical mixing of bottom sediments. Delta foresets in Simpson Bay are of sufficient slope (up to 30°) and there is adequate sediment supply to generate turbidity currents (Gilbert 1982; Prior et al. 1981; Syvitski and Shaw 1995; Syvitski et al. 1988). These currents are capable of transporting coarse deltaic sediment great distances while eroding sediment along the way. The flows work to maintain slope stability and can be initiated by the oversteepening of the forset or seismic events (Syvitski and Shaw 1995) both of which are significant factors in Simpson Bay. Hyperpycnal flows are also possible. These flows emanate from the river mouth as high density gravity driven flows caused by injection of high turbidity river water along the bottom (Mulder et al. 2003; Mulder and Syvitski 1995). Both of these processes are episodic in nature and form laminated deposits. The frequency and magnitude of the deposits are a result of environmental factors linked to high discharge events, a large tidal range, and seismic events.

METHODS

Box cores were taken over a two day period in the summer of 2006 from the F/V *Miss Kayle* using a 50 cm x 50 cm x 100 cm GOMEX style box corer. Twenty-one stations were occupied for coring based on side scan sonar and seismic data (Noll et al. 2008) to target specific bottom types. A Trimble DGPS was used for positioning throughout the survey. After the box core was brought on board it was sampled with a 15 cm diameter PVC tube and a 2.5 cm x 10 cm plexiglas tray for x-radiographs. Core lengths ranged from 15 - 40 cm depending on substrate. The tubes and trays were sealed and stored upright for the short trip to port. Sediment samples were extruded and sub-sampled on 1 cm intervals and the trays were x- radiographed in port using a digital x- radiograph machine.

Geotechnical Analysis

Sample aliquots were dried to determine porosity which was used to calculate corrected depths and mass accumulation when determining sediment accumulation rates. Dried samples were saved for the ^{210}Pb analysis.

Grain size analysis was carried out using a Malvern 2000 Mastersizer Laser Particle Analyzer. Approximately 10 g of wet sediment was sieved through a 2 mm mesh sieve with de-ionized (DI) water into 200 ml calibrated jars to remove material larger than 2 mm (gravel; Malvern cannot process particles larger than 2 mm). The greater than 2 mm fraction was dried and weighed. 10 ml of a 10% sodium hexametaphosphate solution was added to the jars and they were filled to 200 ml with DI water. Sample jars were homogenized with a magnetic stir plate during analysis. 10 ml was pipetted into aluminum tins and dried to reincorporate the gravel data with the Malvern output. Sample was added to the Malvern using a pipette until optimum obscuration limits were achieved and grain size distribution was determined for the 2 μm to 2 mm fraction. Sand, silt, and clay percentages were determined (clay < 4 μm; silt 4 - 64 μm; sand 64 - 2000 μm) and recombined with the gravel data to determine the gravel, sand, silt, clay distribution for the sample.

Radioisotope Analysis

Activity profiles of short lived (~100 yr) radioisotopes were used to determine sedimentation rates in the different sedimentary environments throughout Simpson Bay. Activities of $^{210}Pb_{xs}$ ($t_{1/2}$ = 22.3 yr) in core samples were measured and plotted to determine sedimentation rates. ^{210}Pb activities were measured indirectly using the ^{210}Po method (Nittrouer et al. 1979; Santschi et al. 2001). Samples were wet sieved with a minimum amount of DI water through a 40 μm sieve and the smaller fraction was used to minimize the influence of changes in surface area on activity. Sample blanks of 100 ml DI water were run with the same method periodically throughout the process to determine if the sieve process had any effect on the activity and no detectable activity was reported. Trials using wet sieved, dry sieved, and bulk dried ground sediment were analyzed and the wet sieved gave the greatest yield. Aliquots (1 g) of dried sample were spiked with a ^{209}Po tracer for yield determination and were prepared by complete digestion with HCl,

HNO_3 and HF (Santchi et al. 2001). ^{210}Po and ^{209}Po were chemically separated and spontaneously deposited onto Ag planchetts. Activity of the Po isotopes was determined by α-spectroscopy using a Canberra surface barrier detector. ^{210}Po is the granddaughter of ^{210}Pb and is assumed to be in secular equilibrium. ^{210}Pb activity was calculated and supported values were subtracted to determine $^{210}Pb_{xs}$ activity. Supported values were determined by assuming that the activity at the bottom of the core where $^{210}Pb_{total}$ becomes constant is the supported value.

Sediment accumulation rates were determined by calculating a regression line in an area of the core consistent with steady state deposition and using the equation:

$$A(z) = A(0)e^{(-\lambda z / S)}$$

where S = sediment accumulation rate, z = change in depth of the of the regression (cm), $A_z = {}^{210}Pb_{xs}$ activity at end of the regression (dpm g^{-1}), $A_o = {}^{210}Pb_{xs}$ activity at beginning of regression (dpm g^{-1}), and λ = radioisotope decay constant (^{210}Pb, 0.031 yr^{-1}); (Bentley and Nittrouer 2003; Nittrouer et al. 1984).

Residence time for sediment in the Surface Mixed Layer (SML) was determined to look at the timescales over which the benthic community is able to mix the SML and the time through which sediment remains biologically mobile.

A time dependent mixing parameter G was calculated according to Guinasso and Schink (1975) for cores where D_b was calculated. This parameter is an indicator of strata preservation where small values of G (<0.1) indicate weak mixing and large values (>10) suggest that the profile is homogenized, effectively eliminating textural heterogeneities (Nittrouer 1981):

$$G = \frac{D_b / L_b}{A}$$

^{137}Cs ($t_{1/2}$ = 30yr; 662 keV peak) activity was determined using a low-background, high efficiency, high-purity Germanium (HPGe) planar γ-detector coupled to a multi channel analyzer. Samples were wet packed and counted for approximately 24 hrs to determine the first occurrence of ^{137}Cs in the core. ^{137}Cs was produced by bomb fallout as a result of atmospheric nuclear bomb testing in the

1950's and early 1960's (Krishnaswami et al. 1971). The depth of first appearance will coincide with the beginning of atmospheric bomb testing in 1954.

Instrumented Pod

From June 16th through July 1st 2008, an instrumented pod was deployed at the mouth of West Bay over relict glacial material (Fig 18). The deployment was designed to look at the resuspension of fine material deposited on the seafloor through vertical transport of material in the sediment column by benthic fauna. The pod included a Laser In-Situ Scattering and Transmissometry (LISST) particle size analyze (2 – 500 μm), a 2 MHz Nortek Aquadopp upward looking ADCP, and a Seabird CTD with OBS and dissolved oxygen (DO) sensors. All the devices have internal power supplies and recording. The devices were timed synchronized to UTC time using the same computer and were set to sample every ten minutes. Current velocity and direction data were extracted from the first bin of the ADCP data. The device was attached 0.8 m above the base of the pod. The blanking distance was 0.2 m and the cell size 0.5 m making the mid point of the first cell 0.7 m above the ADCP and 1.5 m above the seafloor. The CTD and LISST were positioned below the ADCP approximately 0.5 m above the seafloor.

RESULTS

Biologically Dominated Systems

Biologically dominated systems are found throughout the deeper parts of Simpson Bay. These areas are composed of predominantly fine grain sediment. Cores of this type show a Surface Mixed Layer (SML) of constant activity followed by a log-linear decrease in activity to supported levels where activity becomes constant again. Not all cores show constant activity in the SML, but the porosity profiles, evidence of burrowing, and the lack of any preserved strata indicate that the sediment is actively biologically mixed.

Fig 18 Picture of the instrumented pod. The pod was tethered to a surface line with float for retrieval

North Bay

Three cores were taken in North Bay, two of which were taken in biologically dominated areas and the other in the physically dominated delta front (Fig. 19). SBBC2 was taken in the middle of North Bay and has the highest sedimentation rates found in Simpson Bay (1.12 cm yr^{-1}; Table 1). The core shows intense burrowing in the upper 5 cm and longer burrows to 10.5 cm (D_b = 4.66; Fig. 20). ^{137}Cs was found to the bottom of all the cores in North Bay supporting the high ^{210}Pb accumulation rates. Silt content is variable, but relatively constant to 16 cm where it decreases through the interval from

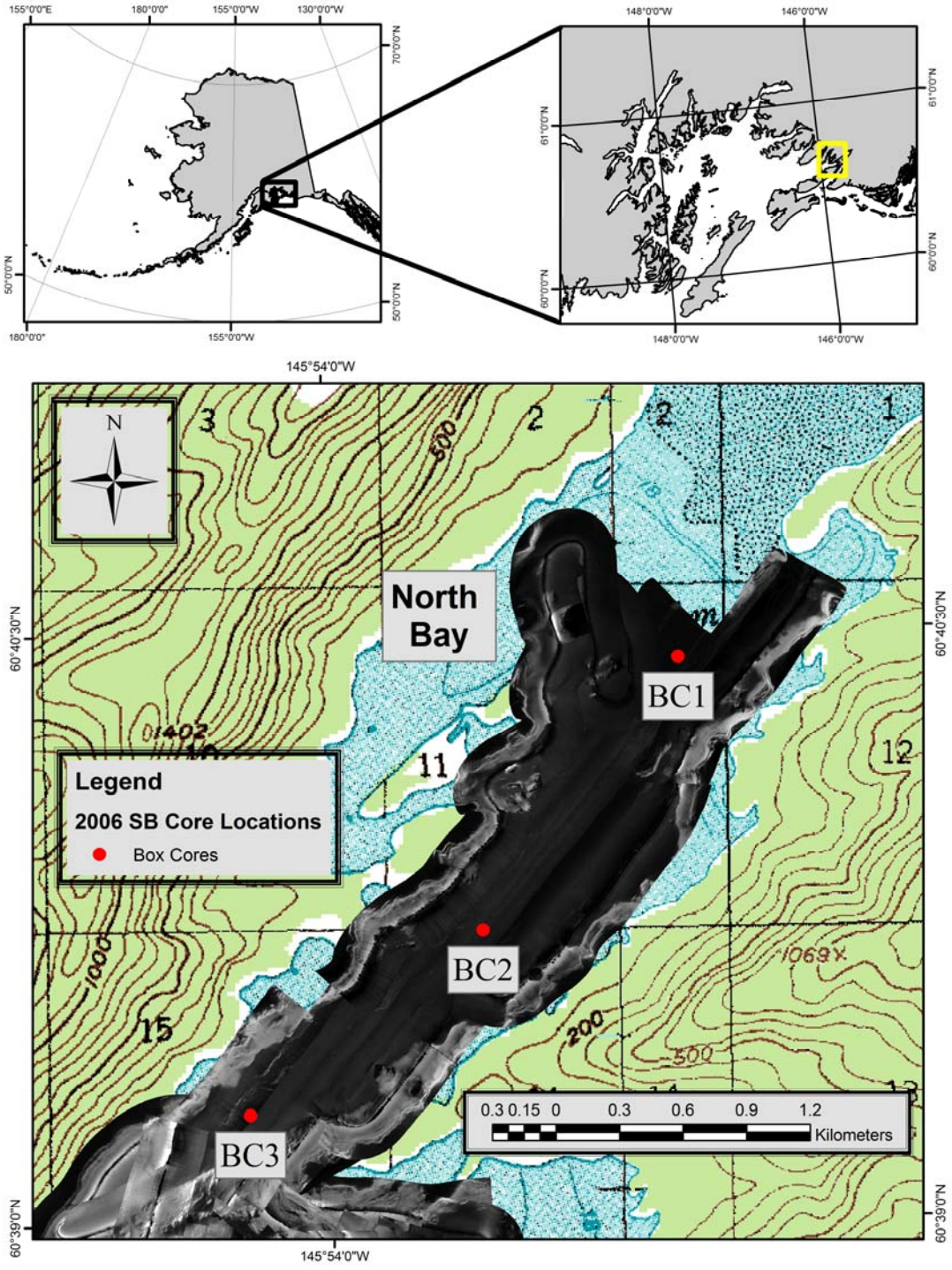

Fig. 19 Box core locations in North Bay are overlaid on side scan sonar and USGS topo maps

Table 1 List of $^{210}Pb_{xs}$ derived attributes for box cores taken from Simpson Bay

[a]RDL = Relict Glacial Deposits

[b]SML = Surface Mixed Layer

[c]Cores taken in relict glacial deposits are non-depositional precluding the calculation of accumulation rates

[d]RDL = Thickness of the Rapidly Deposited Layer; I = The depth of the inflection. Depths are not available for the RGD

[e]Biodiffisivity rates were calculated from the regression of data points in the SML. Cores with two D_b values showed evidence of deep mixing by two or more faunal groups. Cores with Advective mixing have reversed SML profiles.

[f]G = Time dependant mixing parameter. Cannot be calculated without an accumulation rate.

[g]EOC = ^{137}Cs was found to the End of the Core

Core	Bay	Mixing[a]	SML[b] (cm)	Accumulation Rate (cm y^{-1})[c]	1964 Response[d]	Accumulation Rate (cm y^{-1})	Biodiffusivity (cm^2 y^{-1})[e]	G[f]	Residence Time (y)	Maximum ^{137}Cs Penetration (cm)[g]	%OC	Mean GRNZ (µm)
SBBC1	North Bay	Physical	10.5	0.69	-	1.00	23.61	2.41	20.87	EOC	0.91	36.64
SBBC2	North Bay	Biological	10.5	1.02	-	-	4.66	0.43	12.47	EOC	1.76	16.84
SBBC3	North Bay	Biological	15.5	0.80	-	-	85.31	4.78	27.68	EOC	1.29	11.07
SBBC4	West Bay	Biological	3.5	0.39	RDL=5	0.30	1.18	0.72	10.90	18.5	1.13	14.27
SBBC5	West Bay	Biological	7.5	0.30	I=14.5	0.07	0.75	0.23	37.88	17.5	0.96	15.45
SBBC6	West Bay	Biological	3.5	0.34	I=15.5	0.15	360.96	233.72	13.44	14.5	0.87	26.07
SBBC7	West Bay	RGD	5.5	-	-	-	0.05	-	-	6.5	1.06	-
SBBC13	West Bay	RGD	6.5	-	-	-	0.02	-	-	5.5	1.11	-
SBBC15	West Bay	Biological	5.5	0.37	I=15.5	0.10	Advective	6.43	19.01	17.5	0.90	17.96
SBBC16	West Bay	Transitional	11.0	0.33	I=11.5	0.13	Advective	3.12	8.93		1.30	-
SBBC17	West Bay	Biological	6.5	0.52	RDL=3	0.31	1.98	0.60	12.08	22.5	0.92	18.27
SBBC18	West Bay	Biological	6.5	0.34	I=13.5	0.11	1.38	0.49	23.73	16.5	1.00	22.32
SBBC19	West Bay	Biological	3.5	0.43	RDL=4	0.26	Advective	5.34	8.75	21.5	-	17.73
SBBC20	West Bay	Transitional	11.5	0.08	-		0.51	0.51	143.42	11.5	1.35	-
SBBC8	East Bay	Biological	4.5	0.61	RDL=6	0.16	3.89	1.10	9.35	25.5	1.05	29.53
SBBC9	East Bay	Biological	4.5	0.50	RDL=5	0.17	Advective	10.15	12.66	20.5	1.10	23.33
SBBC10	East Bay	RGD	14.5	-	-	-	2.03 and 0.23	-	-	EOC	1.44	-
SBBC11	East Bay	RGD		-	-	-	0.15 and 0.005	-	-	11.5	1.81	-
SBBC12	East Bay	RGD	7.5	-	-	-	0.05	-	-	8.5	1.05	-
SBBC21	East Bay	Biological	6.5	0.37	RDL=5	0.23	4.72	0.98	34.94	25.5	-	18.43
SBBC28	East Bay	RGD	13.5	-	-	-	0.03	-	-	6.5	0.95	-

16 – 23 cm. Silt content increases slightly to 30 cm before dropping rapidly again through the end of the core at 37 cm. SBBC3 was taken in the deep area behind Seaworld Reef. The activity profile was similar to SBBC2 with a high accumulation rate of 0.8 cm yr^{-1}. Intense burrowing was found in the upper 5 cm and longer burrows were found to 14.5 cm indicated by the $^{210}Pb_{xs}$ profile and x-radiographs (D_b = 85.31; Fig. 21). The x- radiograph shows a filled burrow with a bivalve at the bottom to a depth of 14 cm. Silt values are variable from the surface to 27 cm where they decrease rapidly to 33 cm. At 33 cm silt values hold relatively constant through the end of the core.

West Bay

Northern Sub-Basin (NSB)

Six cores were taken in the different depositional areas of West Bay and can be separated into two groups based on their position in the sub-basins of West Bay (Fig. 16). Cores SBBC17, SBBC4, and SBBC19 are in the NSB of West Bay (Fig. 22). These cores have a SML (3.5 - 4.5 cm), followed by a region of log-linear decrease in activity (Table 1). A 4 - 5 cm thick Rapidly Deposited Layer (RDL) is followed by log-linear decrease in activity to supported values (Jaeger 1998; Smith and Walton 1980). Some of the cores did not reach supported levels so an appropriate supported value from other cores was used. Sedimentation rates below the RDL are lower than rates above it and ^{137}Cs is found at varying depths, but is normally below the RDL.

SBBC17 is located at the extreme head of West Bay near the northern shoreline and closest to the small creeks that provide the only significant freshwater source to West Bay (Fig. 22). The $^{210}Pb_{xs}$ profile for core SBBC17 shows the typical profile described above (Fig. 23). The $^{210}Pb_{xs}$ activity shows a slight decrease in the region defined as the SML, indicating diffusive mixing (D_b = 1.98 $cm^2\ yr^{-1}$). Burrows in the x-radiographs verify that mixing is present otherwise the x-radiographs were largely homogenous. Accumulation rates (0.52 cm yr^{-1} above the RDL) are moderate for the system and suggest an 11.56 yr residence time for sediment in the SML. Below the RDL sedimentation rates are lower, 0.31 cm yr^{-1}. Silt content varies from ~60-70%. Silt decreases from the bottom of the core to about 22 cm and increases further with depth. This change happens at the same interval that the porosity profile changes from

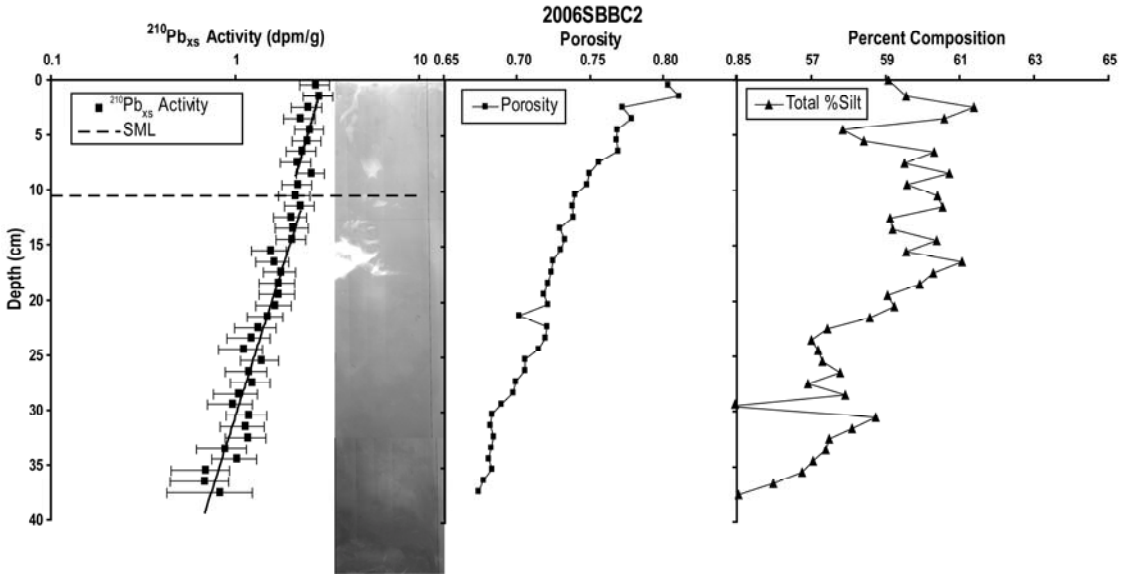

Fig 20 $^{210}Pb_{xs}$ activity, x-radiograph, porosity, and total silt content profiles for core SBBC2

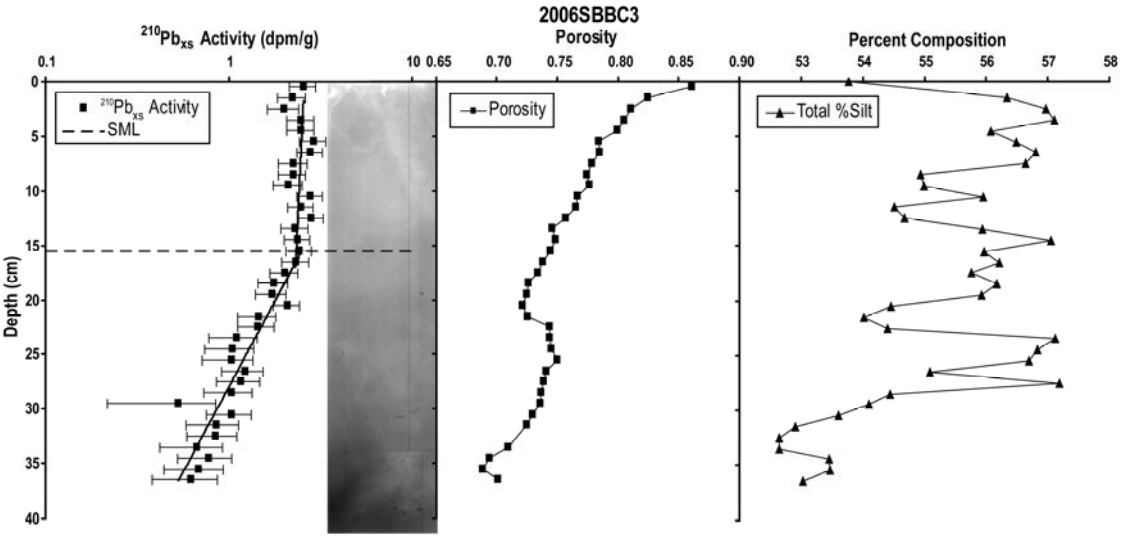

Fig 21 $^{210}Pb_{xs}$ activity, x-radiograph, porosity, and total silt content profiles for core SBBC3

constant to increasing porosity. Above 22 cm the silt content increases steadily to the top of the RDL, where it begins to increase irregularly. Sand is negligible throughout the core indicating that changes in grain size are due to changes in the silt and clay content.

SBBC4 is located in the center of the NSB (Fig. 22). SBBC4 shows the same typical profile, but accumulation rates (0.39 cm yr^{-1} above the RDL and 0.30 cm yr^{-1} below) and biodiffusivity (D_b = 1.18 cm^2 yr^{-1}) were lower than in SBBC17 (Fig. 24). X-radiographs showed a diverse assemblage of burrow types. These range from deep, thick lined and unlined burrows to shallow, narrow burrows. One burrow branches at right angles at approximately 3 cm and radiates laterally indicating that horizontal mixing may play an important in surface mixing. The porosity profile shows an exponentially increasing gradient to higher values, but never reaches a constant value. Silt content generally increases up core and becomes more variable above the RDL.

SBBC19 is the last core in this group. It shows the typical activity profile (Fig. 25), and is located at the southern end of the SSB near the rocky outcrop that separates the basin (Fig. 22). The SML (3.5 cm) in this profile has a reverse activity profile (activity increases with depth) indicating that mixing may resemble advective more than diffusive processes (Nittrouer 1981). X-radiographs show a greater density of biogenic structures than cores SBBC17 or SBBC4 and show a bivalve in live position within an open burrow. Accumulation rates are 0.43 and 0.26 cm yr^{-1} above and below the mixed layer and porosity contents decrease down to ~19 cm where they become constant. Silt content increases from the bottom of the core to the top of the RDL where it continues to increase, but irregularly.

Southern Sub-Basin (SSB)

The SSB consists of cores SBBC15, SBBC5, and SBBC18 (Fig. 26). These cores have lower accumulation rates (0.07 - 0.36 cm yr^{-1}) and thicker SML (5.5 - 7.5 cm) than are found in the NSB. These cores do not have a RDL, but instead have an inflection point mid-core. Above the inflection is an interval of high accumulation and below the inflection is an interval of low accumulation. At the inflection, there is an interval of anomalously low activity. The first occurrence of ^{137}Cs is found at varying depths, but always below the inflection.

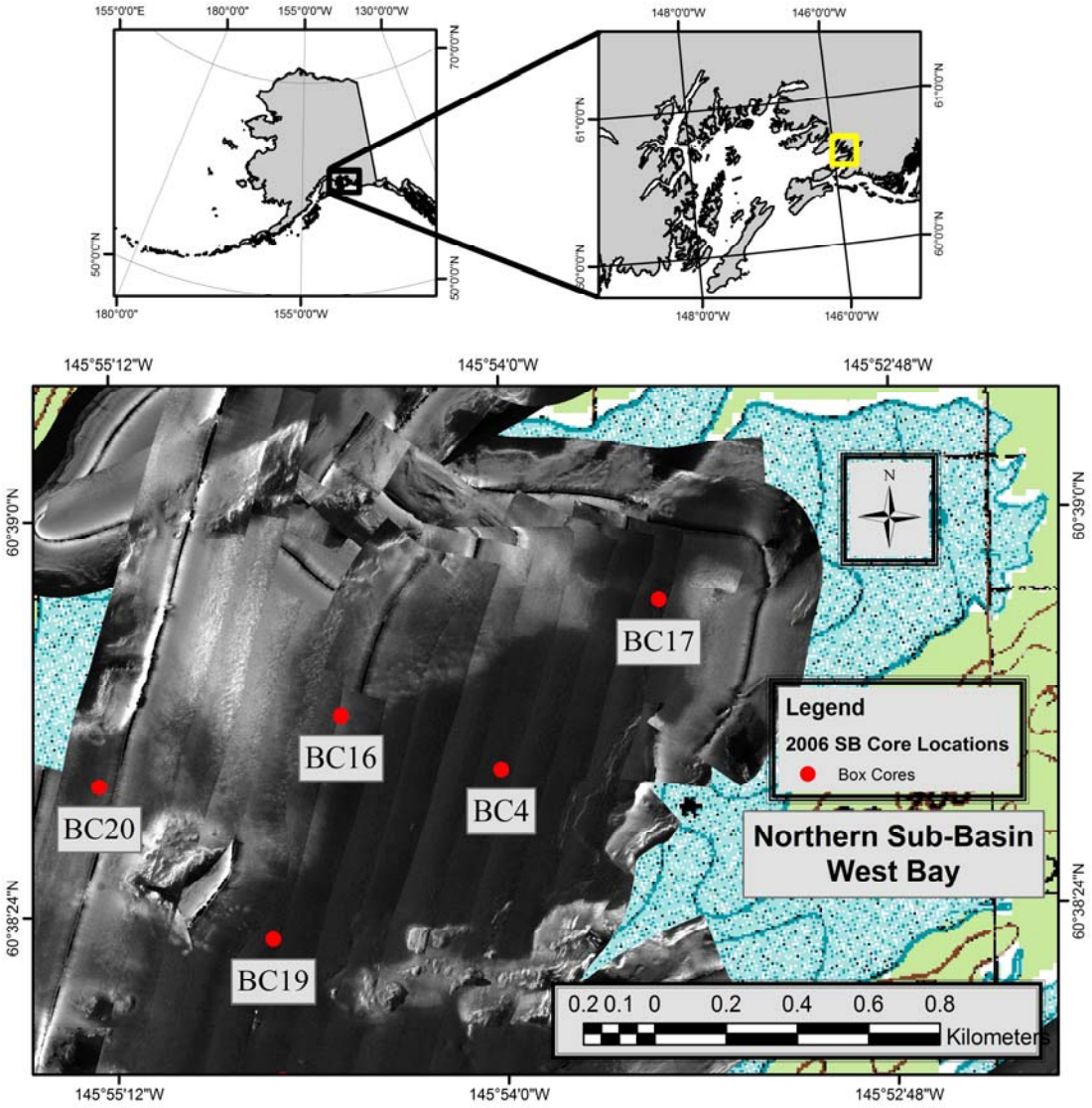

Fig 22 Core locations for the NSB in West Bay are overlaid on the side scan sonar and USGS topo maps. Cores BC17, BC4, and BC19 are found in fine grain estuarine mud, while BC16 and BC20 and BC16 are found in transitional areas

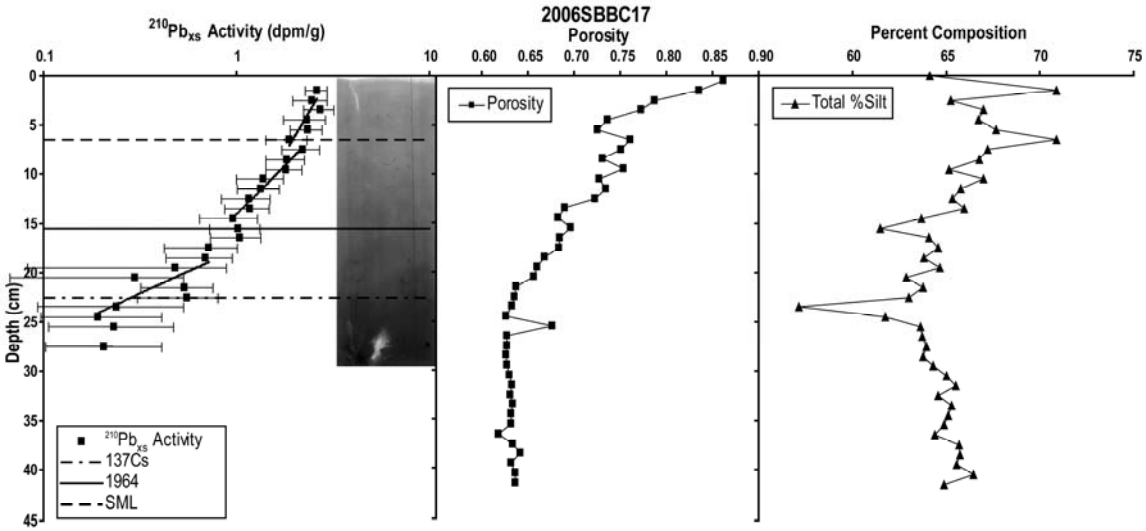

Fig. 23 $^{210}Pb_{xs}$ activity, x-radiographs, porosity, and total silt content profiles for core SBBC17

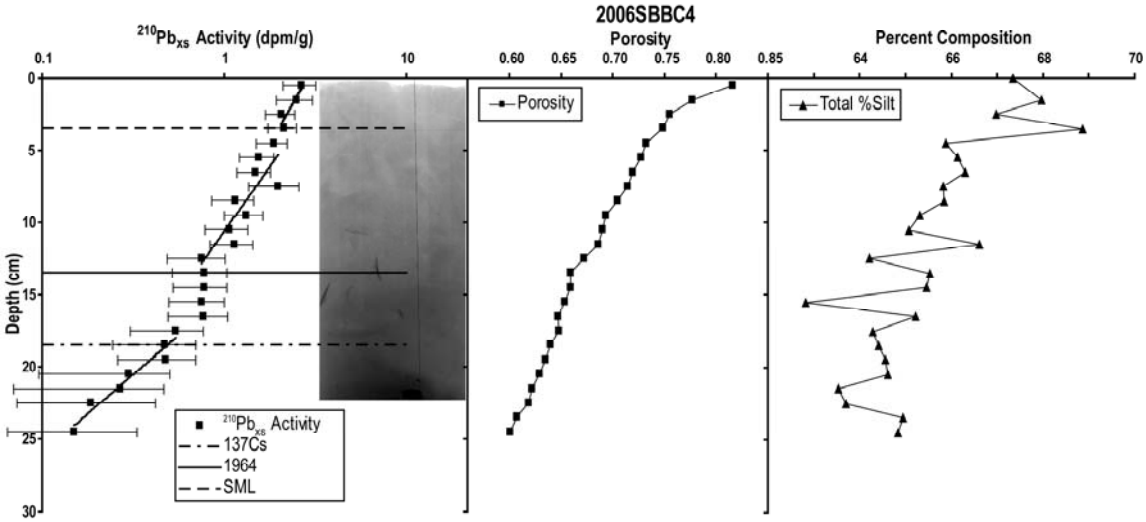

Fig. 24 $^{210}Pb_{xs}$ activity, x-radiographs, porosity, and total silt content profiles for core SBBC4

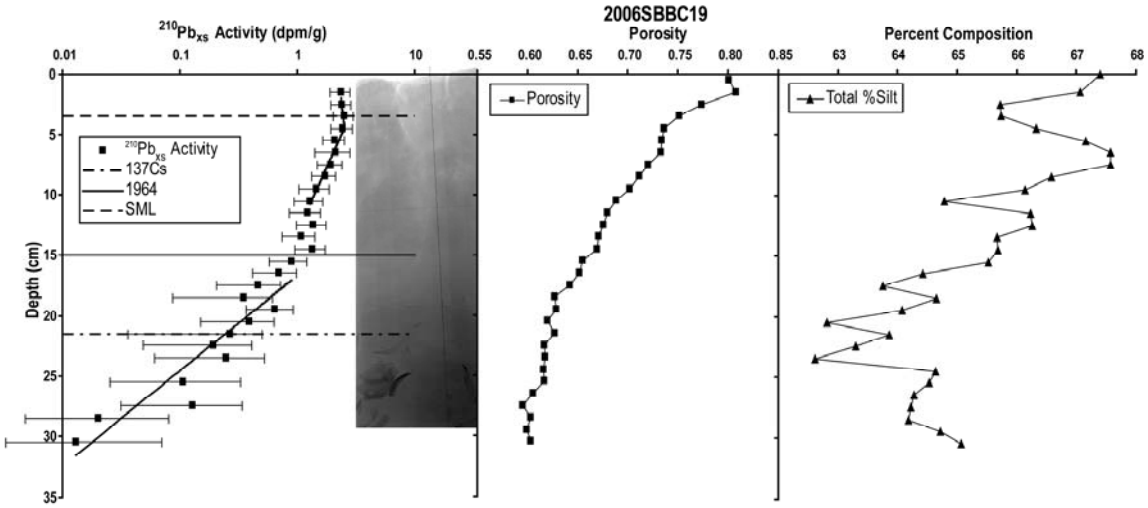

Fig 25 $^{210}Pb_{xs}$ activity, x-radiographs, porosity, and total silt content profiles for core SBBC19

SBBC15 is the most northern core in the SSB and is located closest to the rocky outcrop that divides the basin (Fig. 26). Surface mixing in core SBBC15 is more appropriately modeled as advective mixing based on the reversed activity profile and x-radiograph (Fig. 27). A u-shaped burrow, typical of Fat Innkeeper worms (*Urechis campo*; Fisher and MacGinite 1928), and a small bivalve are found in the x-radiograph and the $^{210}Pb_{xs}$ profile of the SML (5.5 cm) is reversed (Nittrouer 1981). Below the SML the core shows a profile typical of the SSB. There is an inflection at 15cm and accumulation rates of 0.37 cm yr^{-1} above it and 0.10 cm yr^{-1} below it. The silt content decreases from the bottom of the core to about 19 cm above where it begins to increase. This trend is correlated to the interval in the porosity profile where the porosity values become uniform.

Core SBBC5, in the center of the SSB (Fig. 26), has a relatively deep SML (7.5 cm) and accumulation rates are 0.3 and 0.07 cm yr^{-1} above and below the inflection. Mixing is less intense than in the NSB (D_b = 0.75 cm^2 yr^{-1}; Fig. 28) and lower accumulation rates result in longer residence times in the SML (37.9 yr). A hiatal surface associated with a change in silt and porosity is found at approximately

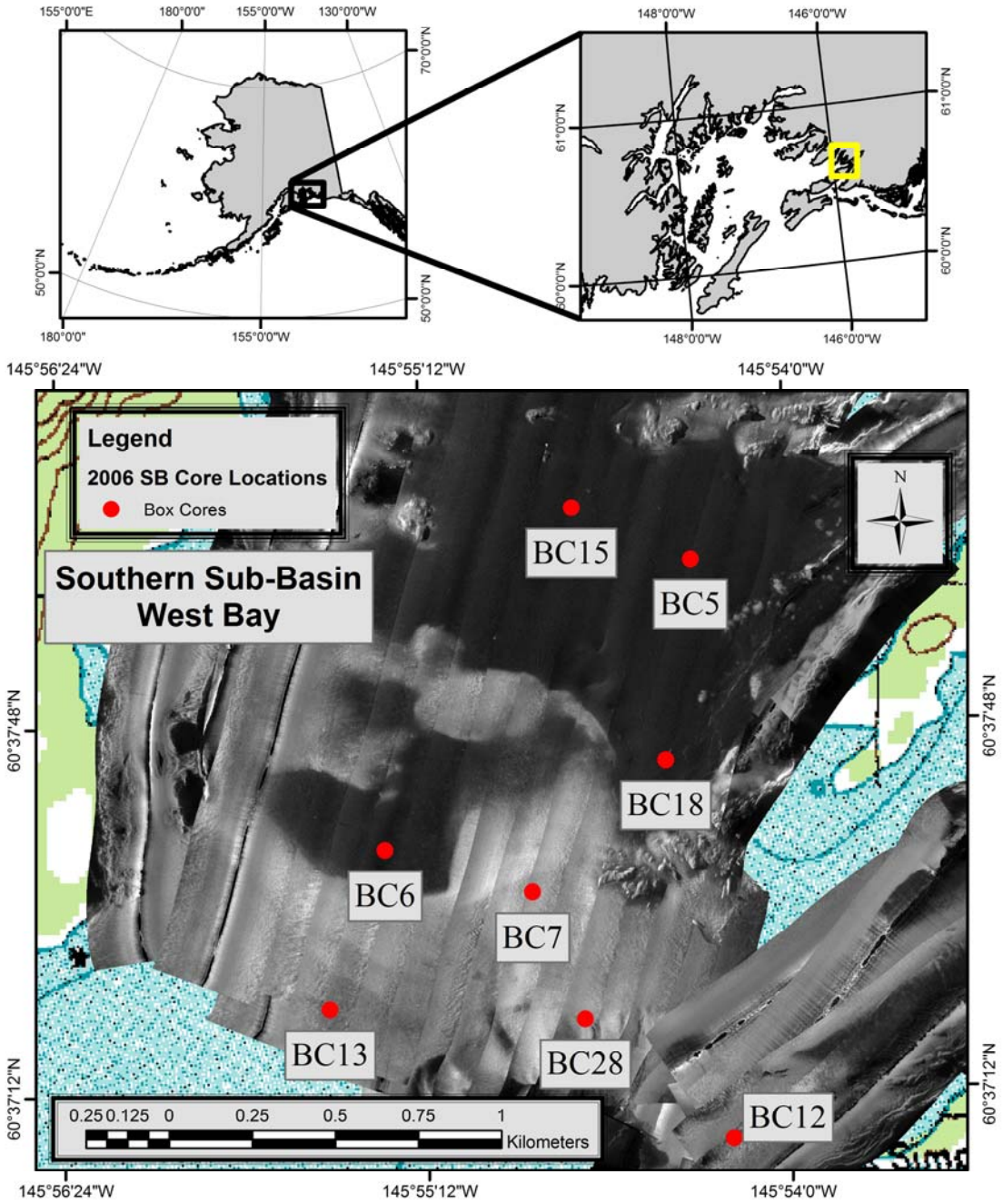

Fig. 26 Core locations for the SSB in West Bay overlaid on the side scan sonar and USGS topo maps. BC18, BC5, BC6, and BC15 are found in the fine grain estuarine mud while cores BC7, BC13, BC28, and BC12 are found in relict glacial deposits

18.5 cm. Porosity profiles show a high porosity surface layer, and there were few burrows observed in the x-radiographs.

SBBC18 is located near a small embayment on the eastern shore of West Bay (Fig. 26) in an area that contains patchy distribution of biogenic gas in the subsurface and evidence of intense burrowing. The x-radiograph shows numerous small burrows in the upper 3.5 cm and larger burrows to 6.5 cm. The $^{210}Pb_{xs}$ profile indicates that surface mixing (D_b = 1.38 $cm^2\ yr^{-1}$) and a high accumulation rate (0.34 cm yr^{-1}; Fig. 29) results in a longer residence time in the SML (23.72 yr). The inflection point in core SBBC18 is at 10.5 cm and accumulation rates below it are 0.11 cm yr^{-1}.

Core SBBC6 is a unique core, located in a fine grain sediment pond in the middle of the relict glacial deposit at the mouth of West Bay (Fig. 22). X-radiographs show abundant narrow burrows in the upper 2 cm and few larger, deeper burrows to 4 cm (Fig. 30), as well as some large pieces of broken shell deeper in the core. The $^{210}Pb_{xs}$ profile is shows a similar response to the cores in the SSB. A shallow, well mixed SML (D_b=360.96 $cm^2\ yr^{-1}$) and high accumulation (0.34 cm yr^{-1}) above the inflection (15.5 cm) result in a short residence time in the SML of 11.0 yrs. The extremely high Db value is most likely due to mixing significantly more rapid than the decay of the isotope used. ^{137}Cs is found above the inflection (14.5 cm) in this case. Accumulation rates below the inflection are 0.15 cm yr^{-1}. SBBC6 has higher sand content than is found in most of the other depositional areas (5-10%) with a maximum at ~20 cm. This higher sand content and proximity to the relict glacial deposits may promote the higher accumulation rates and more intense biological mixing which contributes to the higher Db.

East Bay

Cores SBBC8, SBBC9, and SBBC21 are from the depositional area of East Bay (Fig. 31). These cores show the same characteristics as the cores from the NSB in West Bay. SML thicknesses range from 2.5 - 6.5 cm and accumulation rates range from 0.37 - 0.61 cm yr^{-1} above the RDL and from 0.16 - 0.2 cm yr^{-1} below the RDL (Table 1).

Core SBBC8 is located at the mouth of East Bay (Fig. 31) and has the highest sedimentation rates in East Bay (0.65 cm yr^{-1}). Although the SML is thin (2.5 cm), abundant burrows in the x-radiographs and

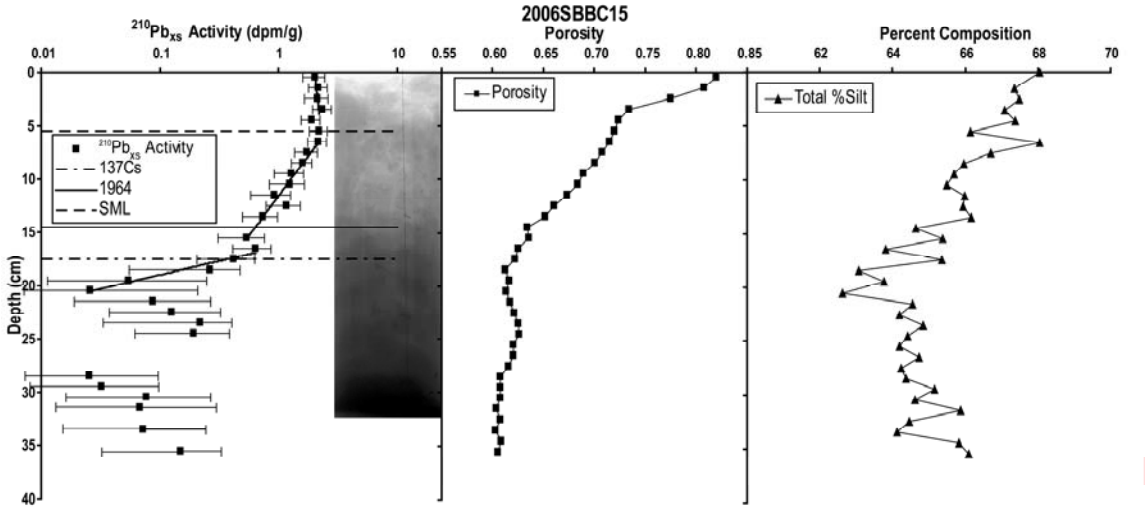

Fig 27 $^{210}Pb_{xs}$ activity, x-radiographs, porosity, and total silt content profiles for core SBBC15

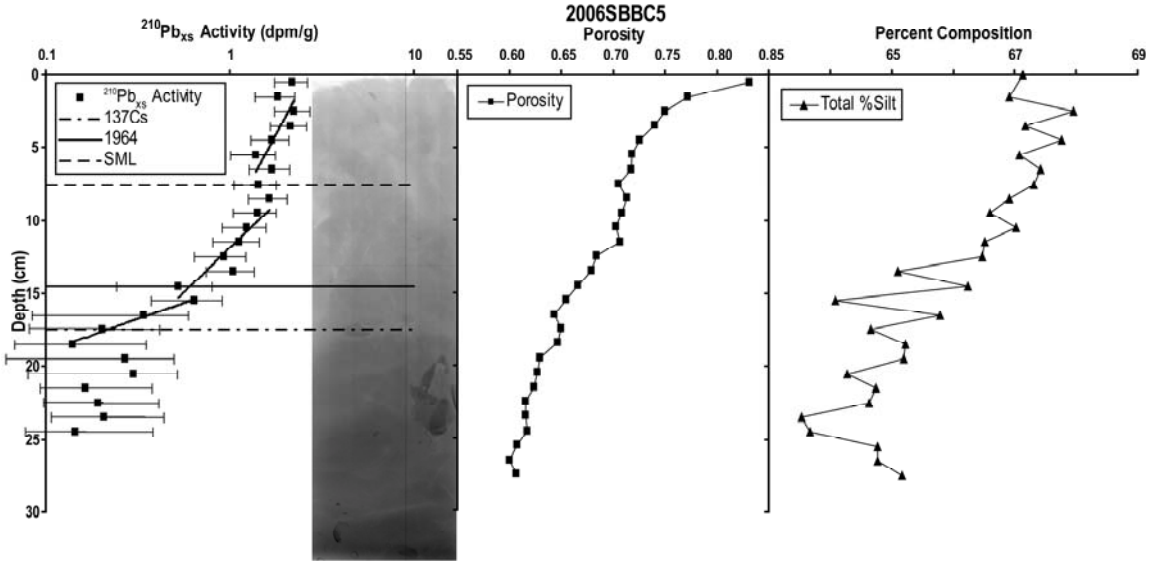

Fig 28 $^{210}Pb_{xs}$ activity, x-radiographs, porosity, and total silt content profiles for core SBBC5

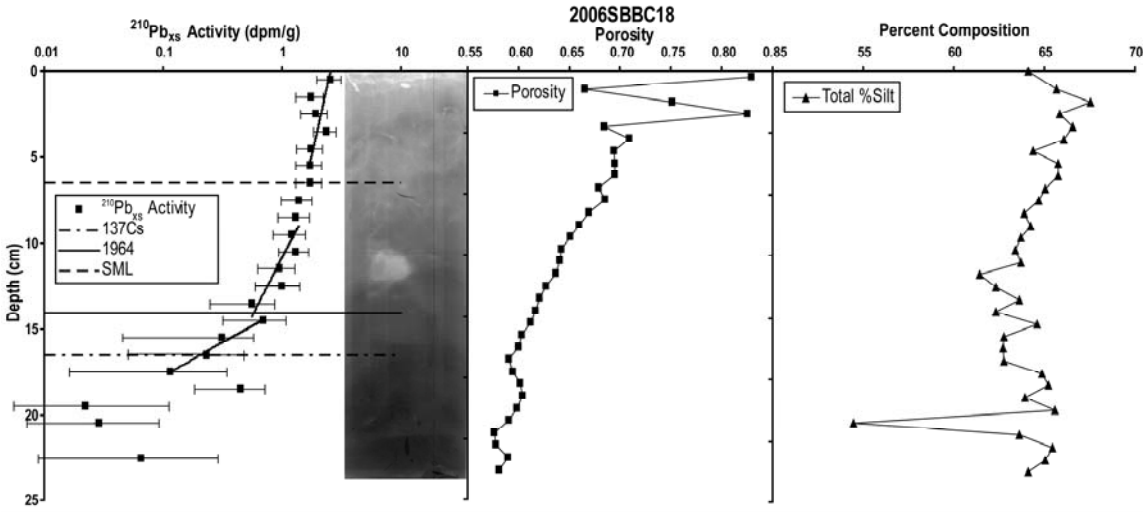

Fig 29 $^{210}Pb_{xs}$ activity, x-radiographs, porosity, and total silt content profiles for core SBBC18

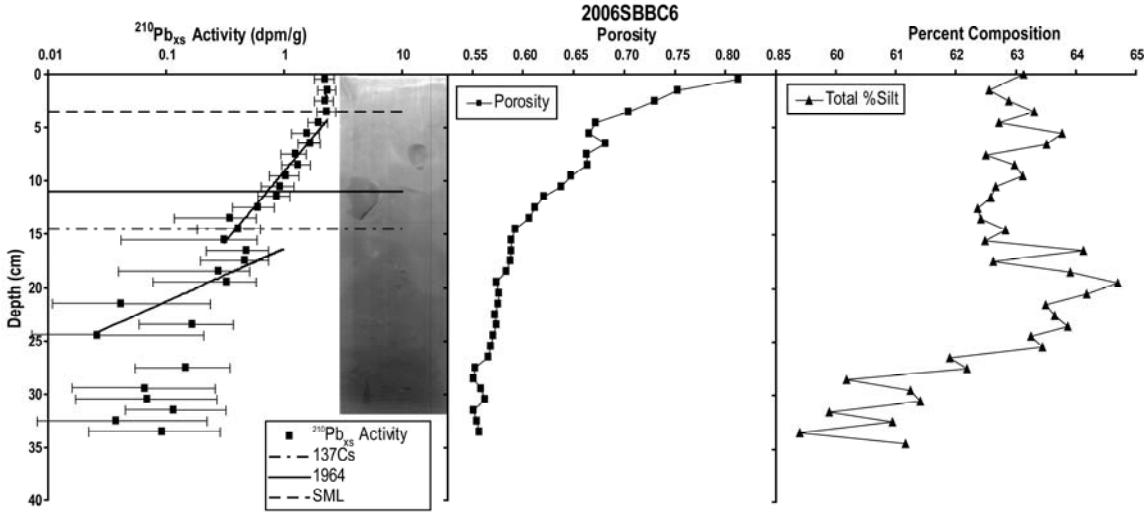

Fig 30 $^{210}Pb_{xs}$ activity, x-radiographs, porosity, and total silt content profiles for core SBBC6

the $^{210}Pb_{xs}$ profile (D_b = 3.89 cm^2yr^{-1}) indicate that this core is well mixed (Fig. 32). Porosity decreases from the surface to 4.5 cm and is uniform below the SML. The silt profile shows a generally uniform value from the base of the core to approximately 22 cm (top of the RDL) above which it follows a coarsening upward trend to 10 cm. Sand content is noticeably higher in this core (4 - 8%), but no significant trend is observed. The first occurrence of ^{137}Cs is found in the RDL in this core.

SBBC21 is located along the north western shoreline of East Bay (Fig. 31) and surface mixing is complicated by the presence of abundant shallow burrows and occasional lined burrows (Fig. 33). The SML, from the $^{210}Pb_{xs}$ profile, is 6.5 cm thick and that portion of the profile has irregular behavior. A diffusivity coefficient of 4.72 $cm^2\ yr^{-1}$ was calculated, but deep, non-uniform mixing is apparent by the longer burrows although comparison of accumulation rates with the RDL suggests this is not the case. Grain size profiles show a coarsening upward trend of the silt and clay fractions, starting at the base of the RDL, but have a low sand content with no significant changes.

SBBC9 is located at the base of the plateau at the head of East Bay (Fig. 31). The $^{210}Pb_{xs}$ profile in SBBC9 is similar to the other two cores in East Bay except that the SML is reversed suggesting advective mixing (Fig. 34). The profile indicates that the SML is well mixed and is corroborated by x-radiographs that show abundant, narrow burrows and bivalves. Although not actively feeding in this case, these bivalves may contribute to the advective nature of the profile. The porosity profile for SBBC9 is irregular with anomalously low values. Silt and clay profiles show a generally coarsening upward trend and sand content is low.

Physically Dominated Systems

Core SBBC1 was taken in front of the delta at the head of the Northern Arm (Fig. 19 and 35). The core contains three fining upward sequences. The core does not penetrate to the bottom of the basal sequence and the upper sequence extends to the top of the core. Each is truncated by erosional surfaces and the subsequent sequence is deposited atop the erosional surface. The surface sequence is deeply bioturbated (10.5 cm; D_b = 23.61 $cm^2\ yr^{-1}$; Table 1). The SML has long burrows and a small bivalve in live position. The $^{210}Pb_{xs}$ profile is irregular, due to non-steady state deposition and discharge at the delta

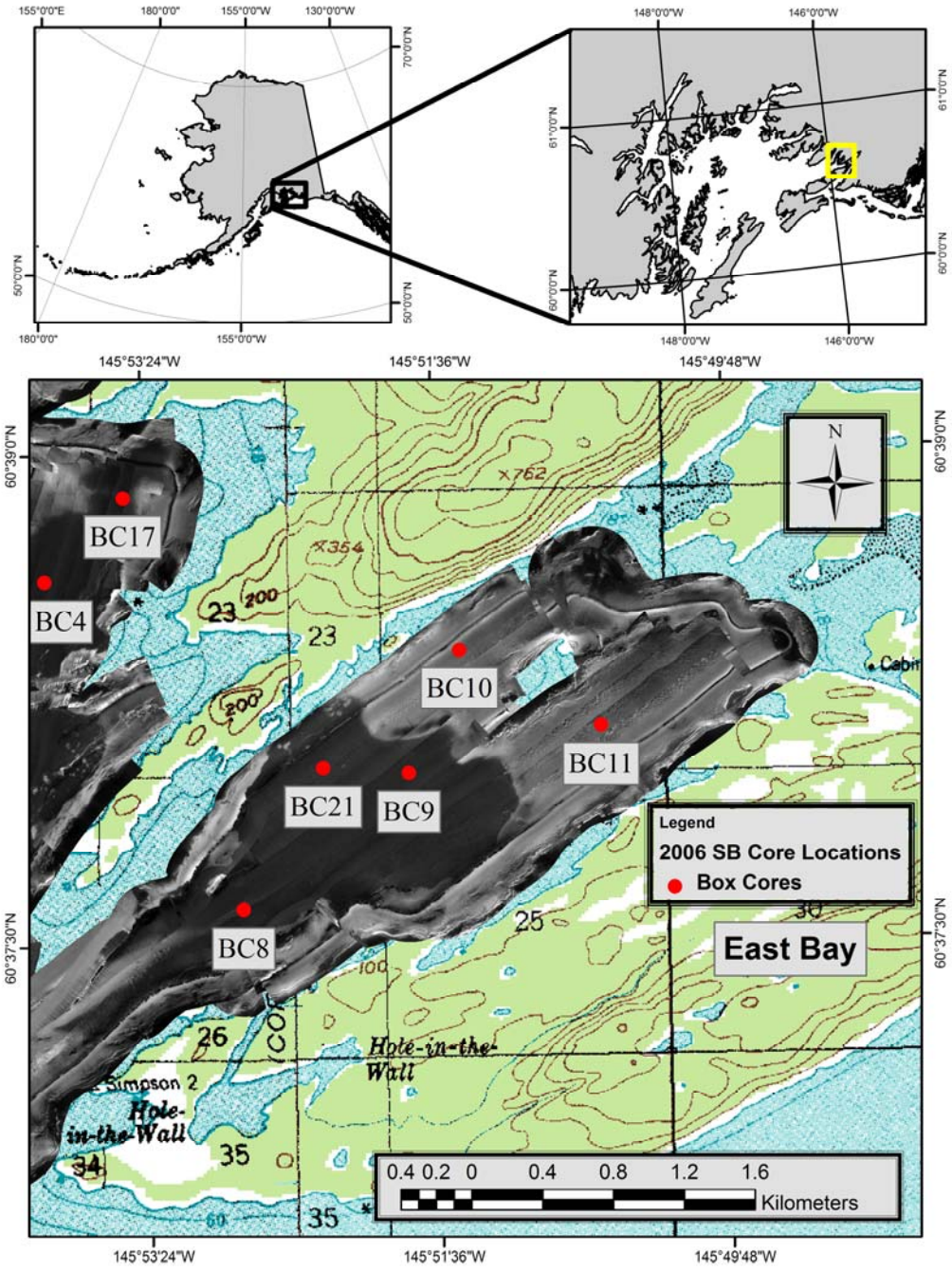

Fig 31 Core locations for East Bay overlaid on the side scan sonar and USGS topo maps. BC21, BC9, and BC8 are found in the fine grain estuarine mud while cores BC10 and BC11 are found in relict glacial deposits

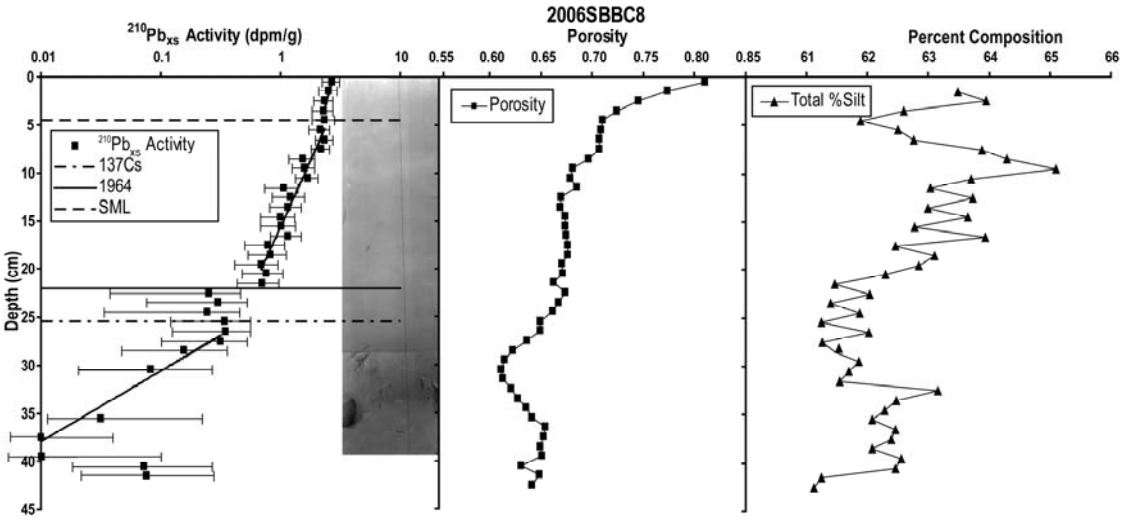

Fig 32 $^{210}Pb_{xs}$ activity, x-radiograph, porosity, and total silt content profiles for core SBBC8

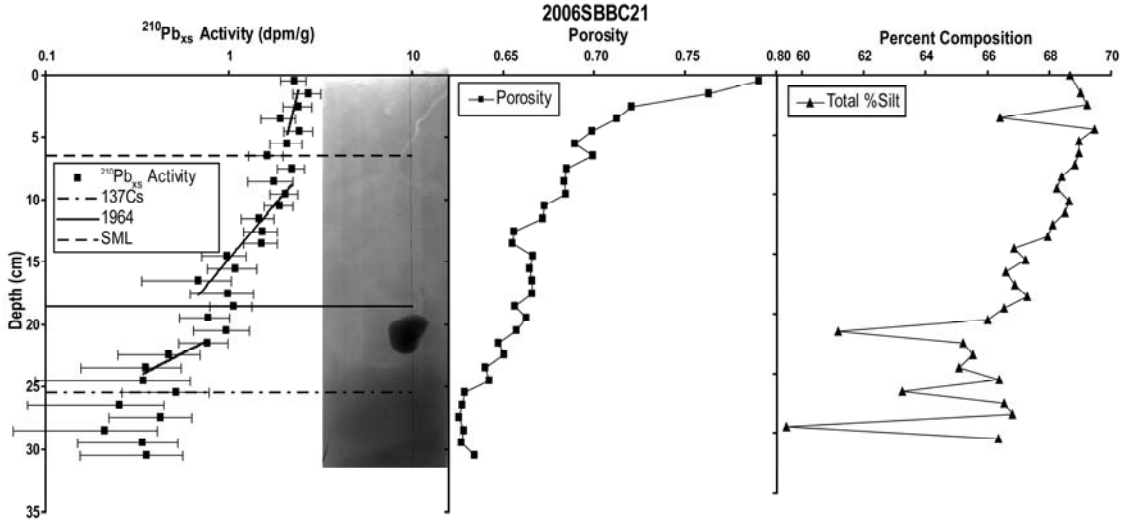

Fig 33 $^{210}Pb_{xs}$ activity, x-radiograph, porosity, and total silt content profiles for core SBBC21

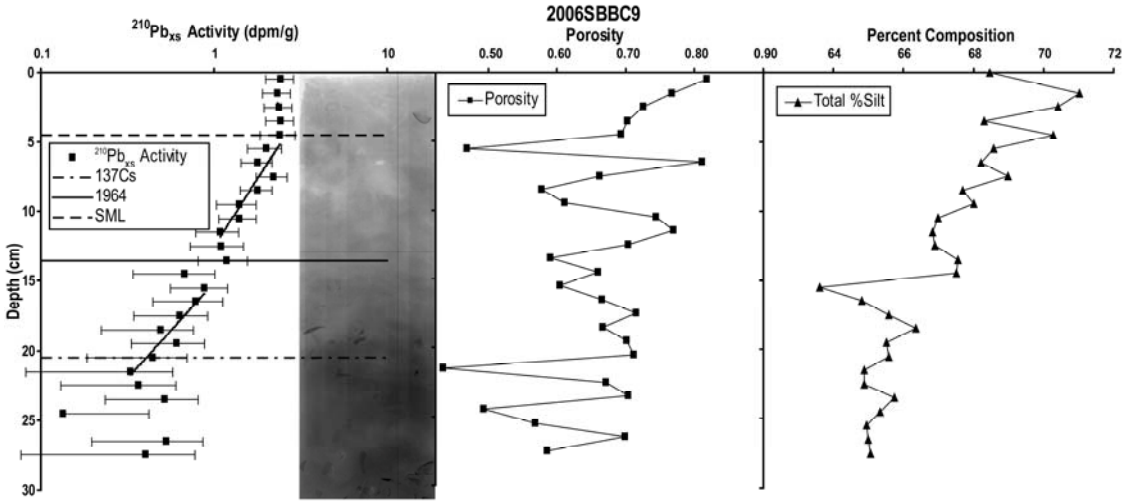

Fig 34 $^{210}Pb_{xs}$ activity, x-radiograph, porosity, and total silt content profiles for core SBBC9

front. This environment is susceptible to mass wasting and gravity driven transport of sediment off the delta seen as erosional surfaces in the x-radiographs and RDLs in the $^{210}Pb_{xs}$ activities are irregular. Some regions of the profile show log-linear decrease in activity and accumulation rates in these areas range from 0.69 - 1.0 cm yr^{-1}. The porosity profile is variable, indicative of episodic deposition of graded beds. A higher overall sand percentage results in a larger mean grain size. Silt content is similar to that of the rest of the system (~60%), but sand content increases (~15%) at the expense of the clay fraction (~20%). The preservation of small features near the base of the beds indicates that the RDLs and subsequent 'normal' deposition was adequately thick to prevent biological mixing to the base of the beds. The lack of evidence of biological activity in the lower sequences suggests that physical processes act more frequent to and/or to a greater extent than biological activities, thus making physical processes the dominate control on the nature of preserved strata.

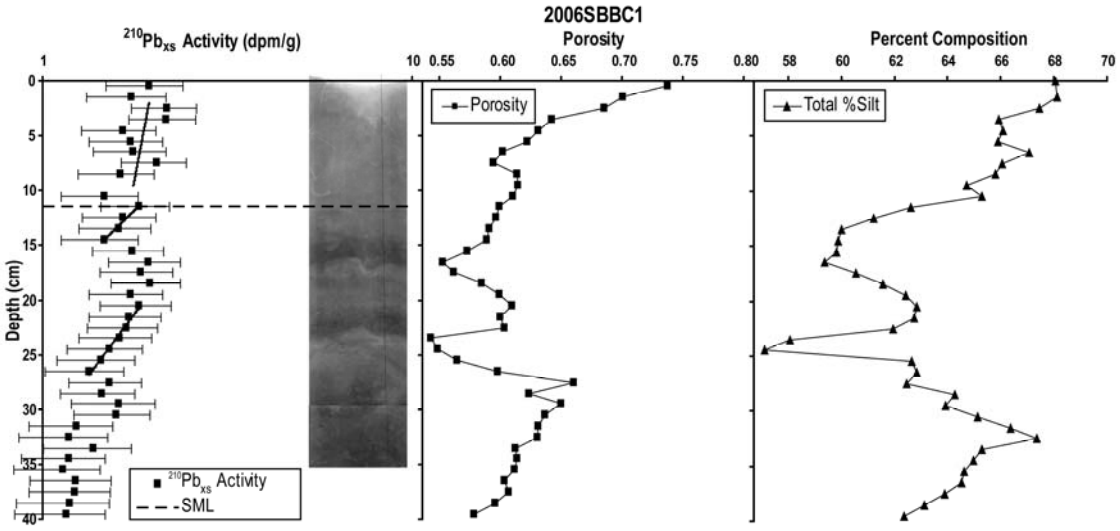

Fig. 35 $^{210}Pb_{xs}$ activity, x-radiograph, porosity, and total silt content profiles for core SBBC1 (See Fig. 19 for location)

Relict Glacial Deposits

The relict glacial deposits are the poorly sorted diamicton and proglacial deposits that make up the non-depositional morainal banks at the head and mouth of East and West Bay (Fig. 16). The morainal bank separating North and West Bay is predominantly composed of bedrock surrounded by diamicton, and was not sampled. These environments cannot be characterized as exclusively biologically or physically modified systems because they have characteristics of both. Benthic organisms mix the upper portions of the sediment profiles by moving fine material to the surface as they penetrate the seabed. This fine material is then transported by the swift bottom currents that keep these areas non-depositional. These modifications effectively winnow and armor surface sediments in these deposits as evidenced in the grain size profiles and x-radiographs as a mud supported gravel grading to a gravel supported mud. Because there is no accumulation, the log-linear decrease in $^{210}Pb_{xs}$ activity seen in the profiles is modeled as biological mixing. This is corroborated by the presence of ^{137}Cs at or near the base of the $^{210}Pb_{xs}$ profile.

Some profiles show an intensely burrowed SML with constant activity followed by a decrease in activity with depth. This suggests benthic communities with variations in mixing intensity. This profile type is associated with cores SBBC10 and SBBC11 (Figs. 36 and 37) located at the head of East Bay (D_b = 10.12 and 2.50 $cm^2\ yr^{-1}$ respectively; Fig. 31). These cores have higher organic carbon percentage (1.17% and 1.48%) than the other relict cores and deep mixing (SML = 14.5 and 11.5 cm respectively; Table 1), suggesting that organic carbon levels and mixing timescales are coupled. Cores SBBC10 and SBBC11 have abundant large articulated carbonate shells, mixed with the gravel, not found in the other relict cores. Cores at the mouth of East and West Bay (Figs. 26 and 38) have much shallower mixing depths (4.5 - 7.5 cm), less intense mixing (D_b = 0.25 - 0.98 $cm^2\ yr^{-1}$), and lower organic carbon contents (0.8 - 0.88%).

Transition Systems

In some areas core profiles have characteristics of the depositional and relict systems. These cores are in areas that are transitioning from relict to depositional due to basin filling. Cores were able to penetrate the soft modern sediment into the relict material below. Side scan sonar data show these to be areas of intermediate backscatter, indicative of higher sand content and some reflection from material just below the surface (Noll et al. 2008; Fig. 16). Core SBBC16 was taken south of Seaworld reef and shows a shallow SML (3.5 cm; Table 1) with a reversed slope (Figs. 22 and 39). Below this is a layer with high accumulation rates (0.33 cm yr^{-1}), similar to other cores in the NSB. An inflection is seen in the profile at 11.5 cm which corresponds to the calculated 1964 depth, with lower accumulation rates below (0.13 cm yr^{-1}). This inflection is similar to the earthquake signal found in the SSB. X-radiographs show a slight increase of coarse material below the inflection. The base of $^{210}Pb_{xs}$ activity (13.5 cm) is at a hiatal surface seen in the x-radiographs with coarse material below and the first occurrence of ^{137}Cs is 5 cm farther below. Silt content is relatively high from 9.5 to 22.5 cm due to a decrease in sand content. Above this interval silt content steadily increases to a maximum near the surface because of a reduction in clay content. Above 9.5 cm, sand content stays relatively constant at about 12%. Core SBBC20 is in an area of intermediate side scan sonar backscatter near the western shore line of West Bay (Fig. 22). Swift

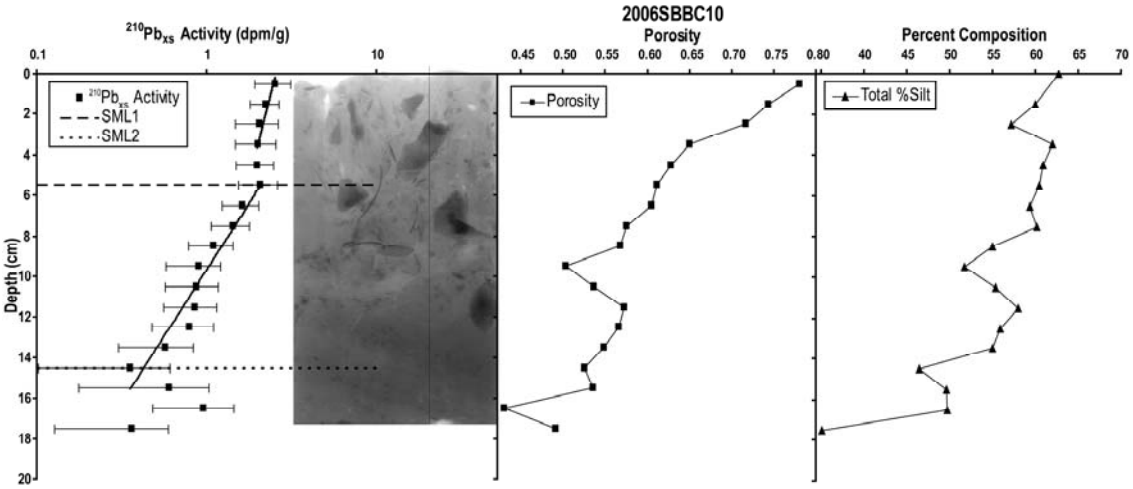

Fig. 36 $^{210}Pb_{xs}$ activity, x-radiograph, porosity, and total silt content profiles for core SBBC10

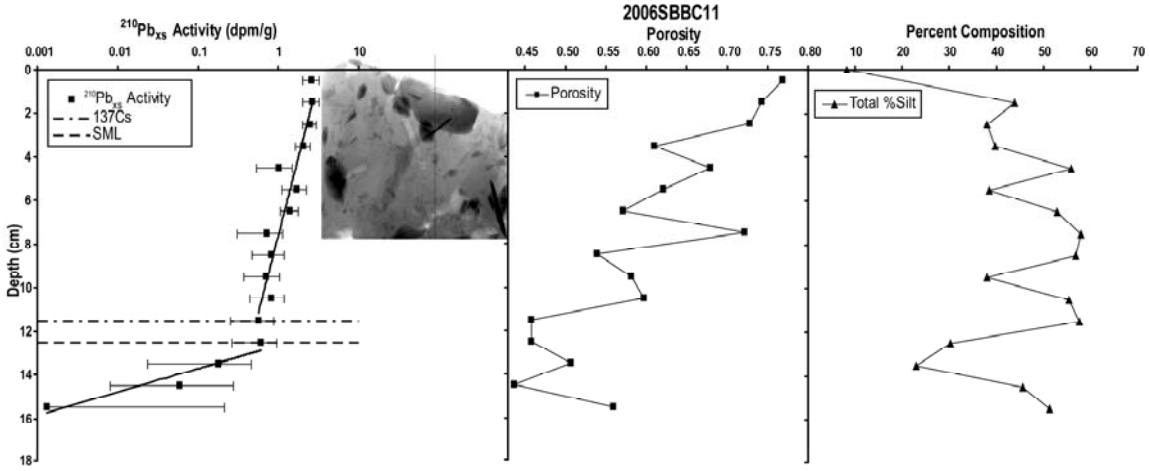

Fig. 37 $^{210}Pb_{xs}$ activity, x-radiograph, porosity, and total silt content profiles for core SBBC11

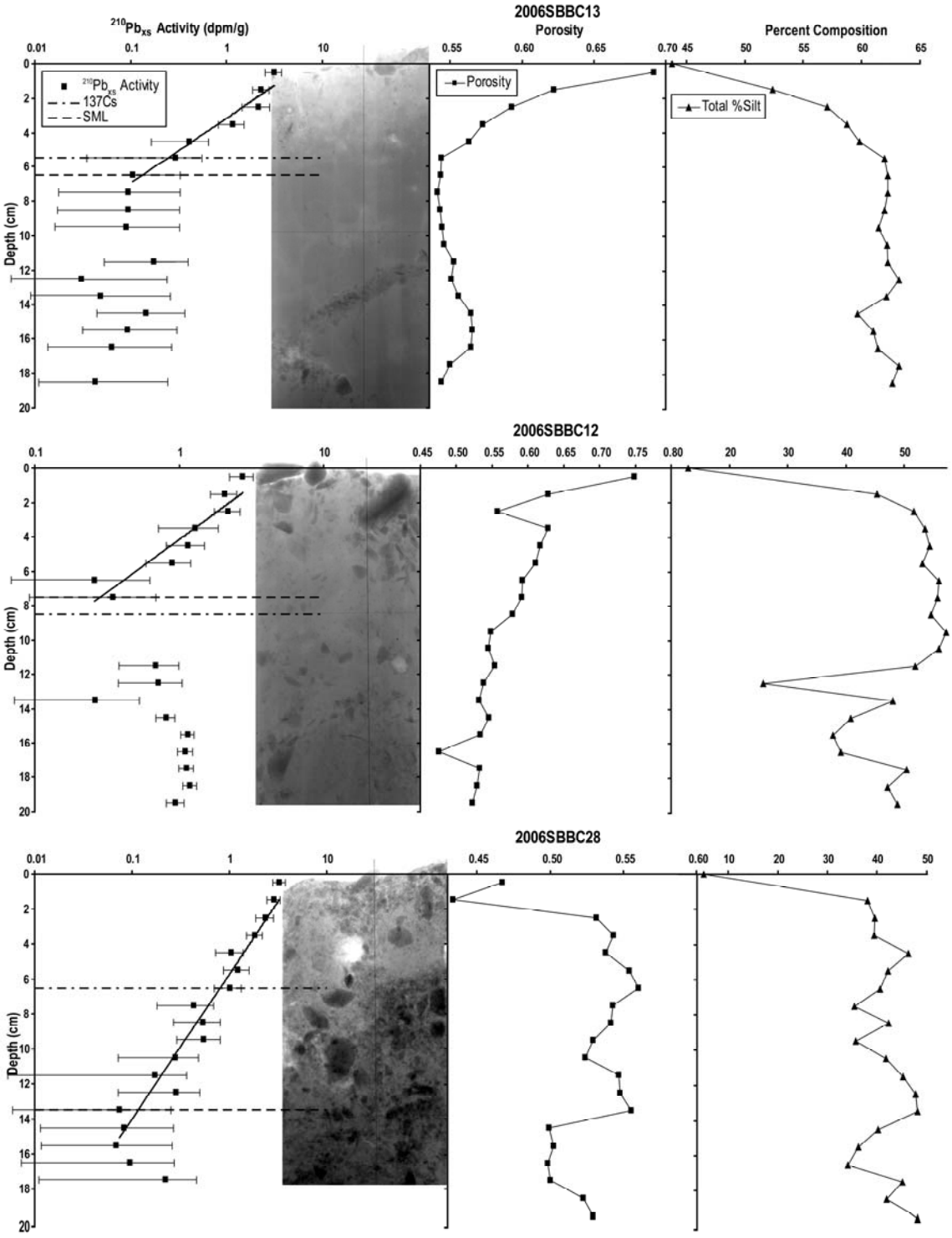

Fig. 38 $^{210}Pb_{xs}$ activity, x-radiograph, porosity, and total silt content profiles for cores SBBC13, SBBC12, SBBC28, and SBBC7 taken in the relict glacial deposit at the head of West Bay (See Fig. 26 for locations)

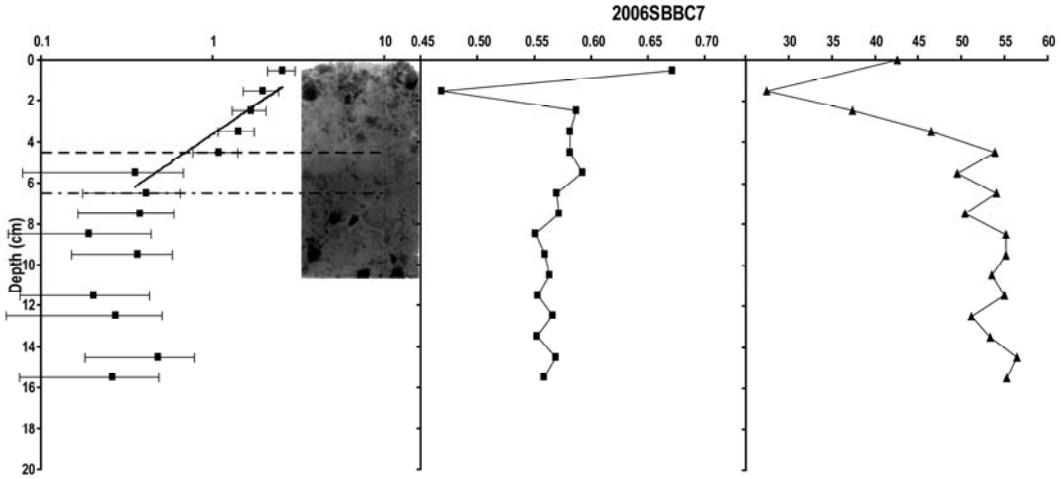

Fig. 38 Continued

currents are reported over the relict glacial deposits on the western side of the mouth of West Bay (Shelton Gay, personal comm.), but SBBC20 may be in an area of localized deposition, partially protected from the most intense tidal currents. Silt content is marginally higher (suggesting the possibility of lower current velocities) than SBBC16 and the x-radiographs do not show as many large particles (Fig. 40). Log-linear decrease in activity to an inflection at 11.5 cm is most likely due to deep mixing and the decrease below is due to less intense mixing at depth ($D_b = 0.51$ cm^2 yr^{-1}). This inflection may also mark the depth of mixing in the relict glacial material, before modern deposition started. A sharp decrease in silt at 20.5 cm is correlated with an increase in coarse material in the x-radiograph and the gravel content. Sand content decreases throughout the profile indicating a decreasing contribution of sand transported by the tidal currents although the content is higher than in SBBC16.

Oceanographic Data

An instrumented pod was deployed over the relict glacial material at the mouth of West Bay (Fig 16). The pod was deployed for 15 days and was able to record two events (as defined by the ADCP

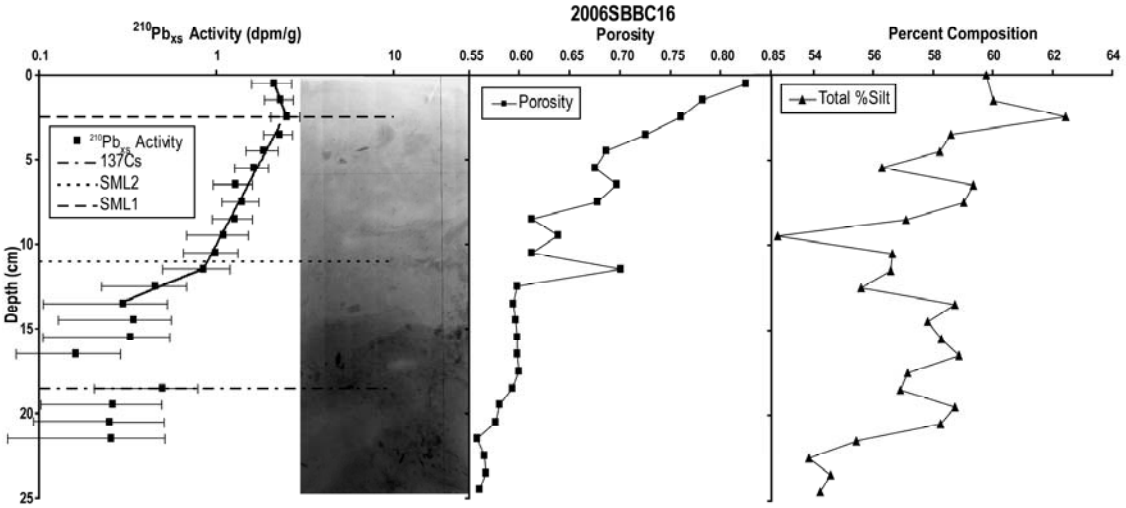

Fig 39 $^{210}Pb_{xs}$ activity, x-radiograph, porosity, and total silt content profiles for core SBBC16

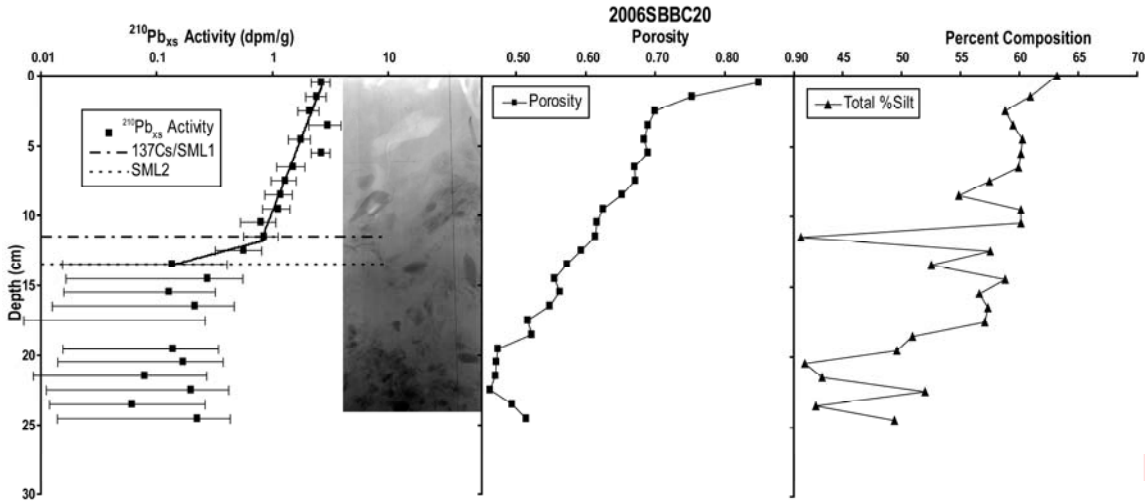

Fig 40 $^{210}Pb_{xs}$ activity, x-radiograph, porosity, and total silt content profiles for core SBBC20

direction data). The pods collected data under "normal conditions" for 8 days before the first of the events. The data shows that under normal conditions temperature, salinity, suspended sediment concentration, dissolved oxygen, and current direction are correlated to tidal motion (Fig. 41). Salinity ranges from 27.5 - 28.0, temperature ranges from 4.8 - 5.2 °C, and dissolved oxygen ranges from 10.6 - 10.7 mg l^{-1}. The current speed from the ADCP is variable (0 - 0.3 m s^{-1}) and poorly correlated to not only the tidal direction, but also the height (Fig. 42). The LISST data shows correlations between tidal height and suspended sediment concentration in specific fractions at the seafloor over the relict glacial deposits (Fig. 43). Because it measures sediment concentration in size bins rather than bulk concentration, sediment concentrations of discrete grain sizes were measured. The data showed a bimodal distribution with modes in the 23.4 and 280 µm fractions (Fig. 44) and that even though maximum velocities under normal conditions were less than 0.30 m s^{-1}, the highest concentrations were found in the 280 µm fraction (1 - 5 µl l^{-1}). Sediment in this fraction had relatively constant values and was not well correlated to tidal motion (Fig. 43). The 23.4 µm fraction was well correlated with tidal height as were most fractions less than 87.9 µm. The correlation shows higher suspended concentration in the outgoing tide and lower concentration in the incoming tide (Fig. 43).

The two events captured by the pod showed warmer, fresher water with lower dissolved oxygen and higher suspended sediment exiting the bay (Fig. 45). The first event began at 175.667 Julian Days (JD) and lasted approximately 30 hrs until 176.944 JD and the second began 178.694 JD and lasted approximately 40 hrs until 180.590 JD (based on the ADCP current direction data). Progressive vector diagrams show that the residual current direction during normal conditions has a tidal signal and is north-eastward across the mouth of the bay (Fig. 46) suggesting a net inflow at the seafloor. At the beginning of each event the current direction breaks phase from the tides and shifts to ~140° ±16° and remains constant through the event. This direction suggests a net outflow of water at the seafloor. After each event the current direction went back into phase with the tides (Fig. 42). The response to each event from the CTD data was significantly different although in both cases the response was offset slightly in time (Fig. 45). In the first event temperature rose slightly while salinity and dissolved oxygen decreased slightly. The effects of the first event are not dramatic, but are noticeable in that the values for each of these parameters

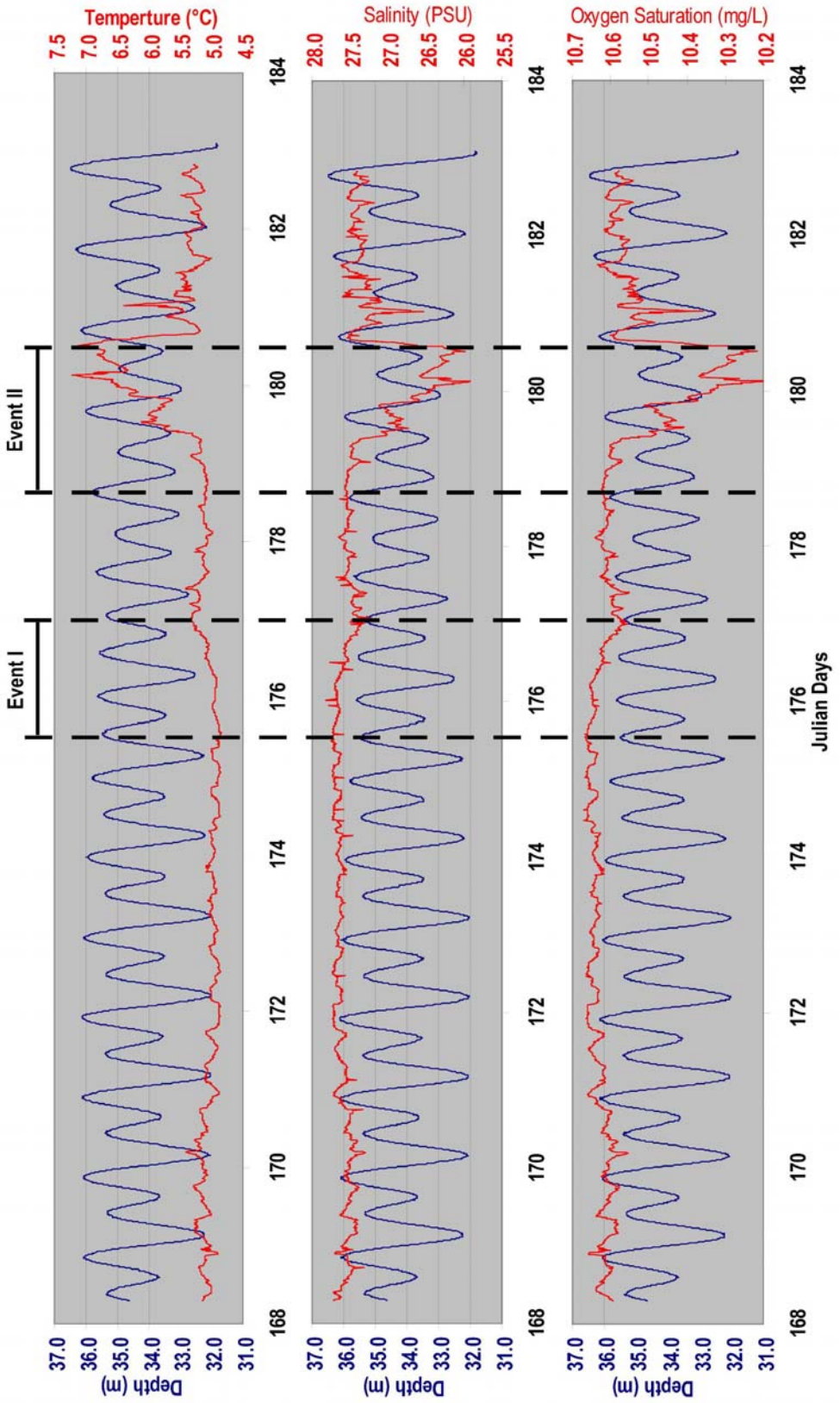

Fig. 41 Time series of CTD data and tide data from the instrumented pod for the period from 06-16 to 7-1-2008 (UTC). Blue lines show tide height while red lines denote values for the different CTD measurements. The deployment recorded two events as defined by the direction data. The events are characterized by generally warmer temperature, lower salinity, and lower oxygen saturation

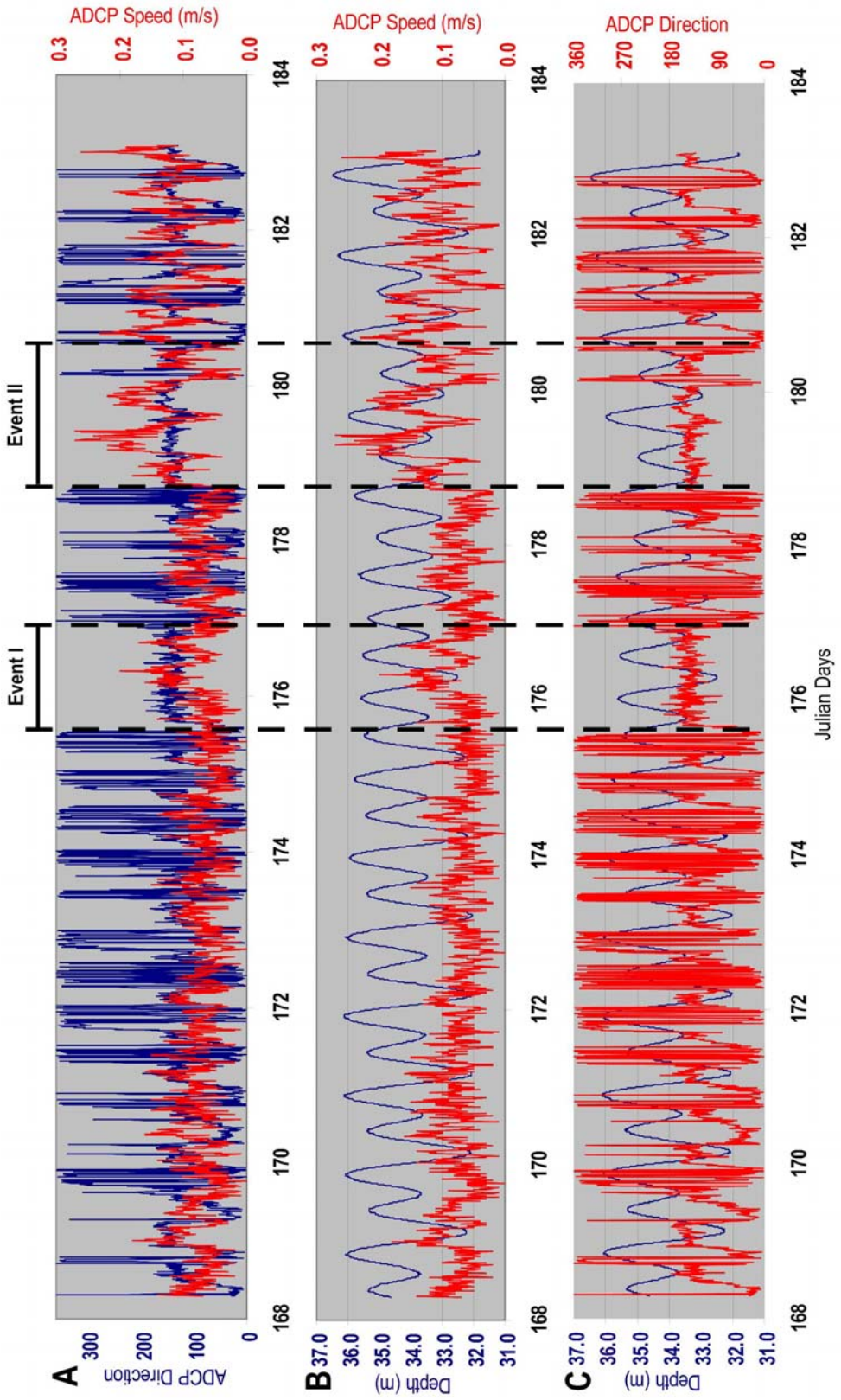

Fig. 42 Time series of ADCP direction, speed, and tide data from the instrumented pod for the period from 06-16 to 7-1-2008 (UTC). The deployment recorded two events as defined by the direction data. The event is characterized by generally higher current velocities and caused the current direction to go out of phase with the dominate tidal forcing causing an outflow for the period of the event . Panel A shows the current direction (blue) and velocity (red). Panels B and C show depth (blue) versus velocity and direction (red) data

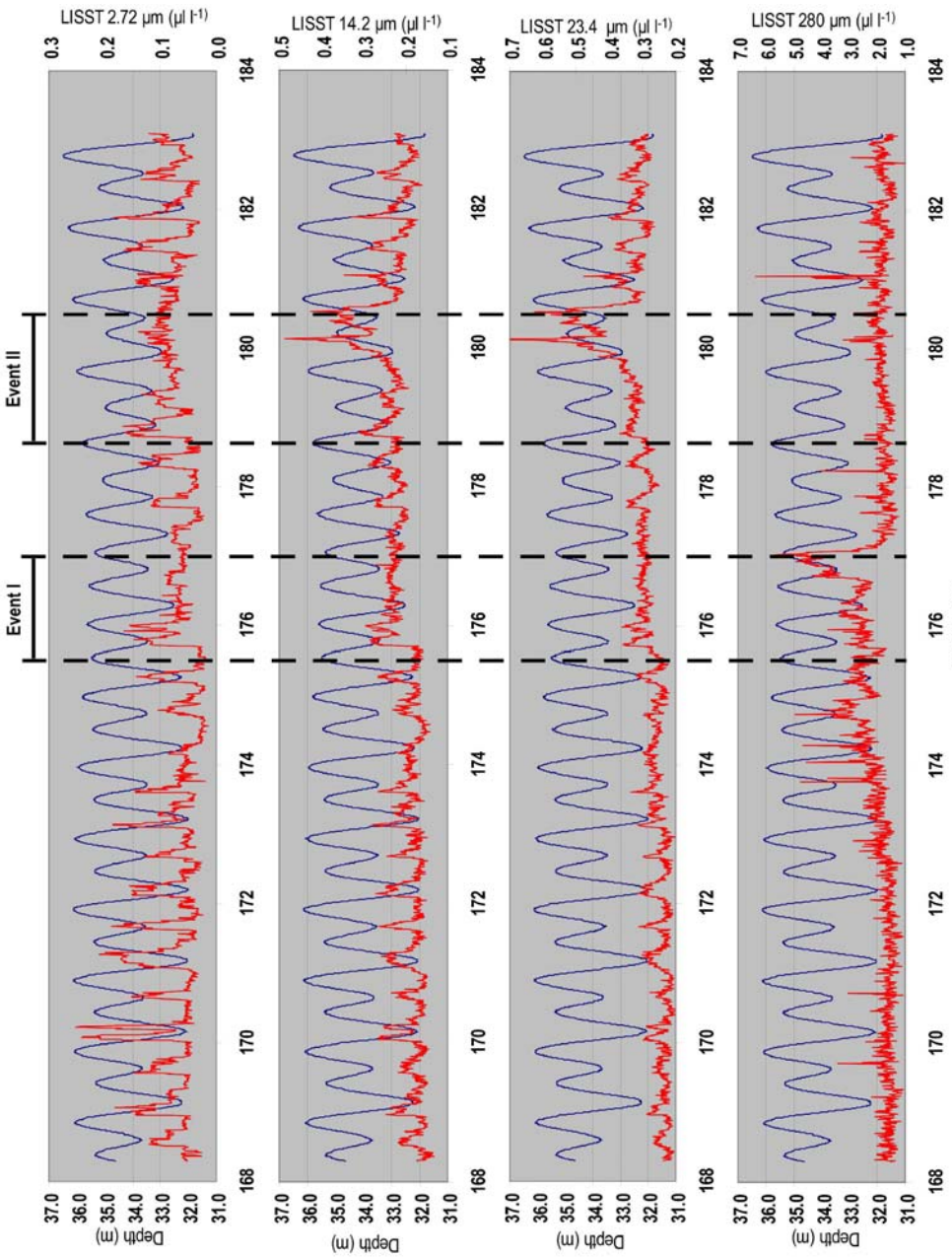

Fig. 43 Time series of LISST particle size and tide data from the instrumented pod for the period from 06-16 to 7-1-2008 (UTC). The deployment recorded two events as defined by the direction data. The 14.3 µm and 23.4 µm concentrations increase, but with a time lag from the beginning of the event. The 2.72 µm, and 280 µm fractions do not show a significant response. Tide data is shown in blue while the LISST data is shown in red

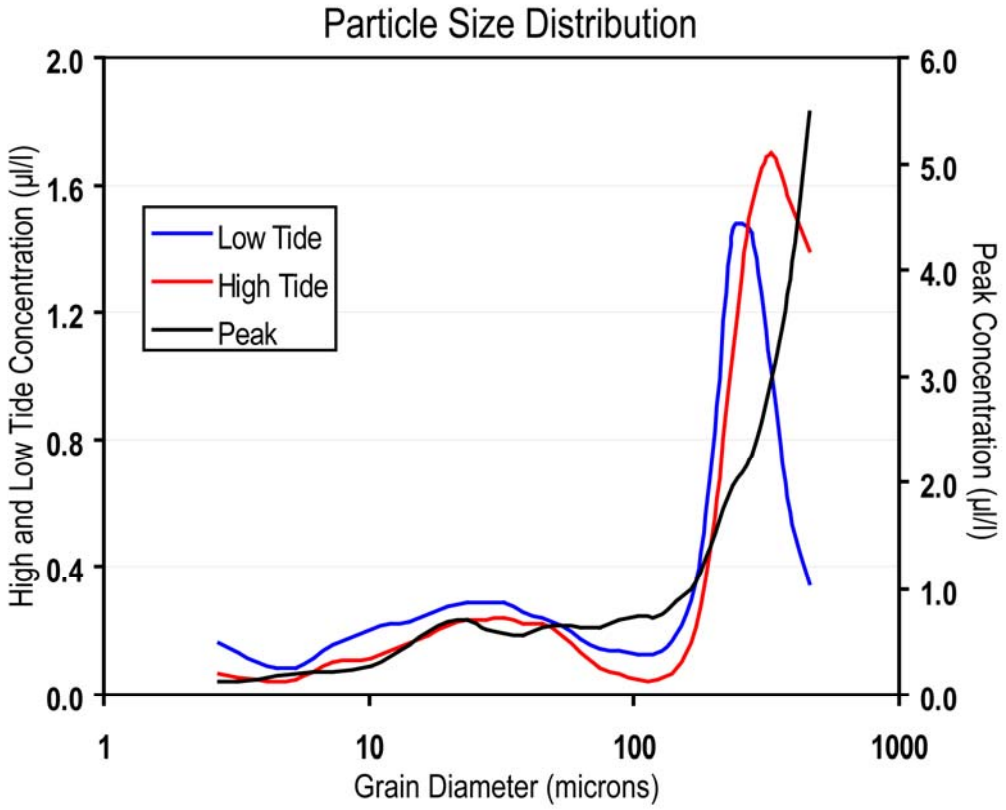

Fig. 44 Particle size distribution graphs for representative high and low tide and for the grain size corresponding with the end of the second event. Mean grain size shifts to higher values following low tide. The peak shows an increase in the larger grain size fraction and a small increase at approximately 40 µm

go out of phase with the tides and result in broad peaks. The values peak at the end of the event, but do not return to pre-event values. The second event shows the same trends and the values go out of phase with the tides, but the peaks are more significant. The values peak at the end of the event and the values do not return to levels recorded at the beginning of the deployment. Both events show a slight increase in current velocity, but the velocity data display high frequency scatter and was not well correlated to any of the other measurements (direction, tide, LISST, CTD; Fig. 42). Both events have low velocity spikes in

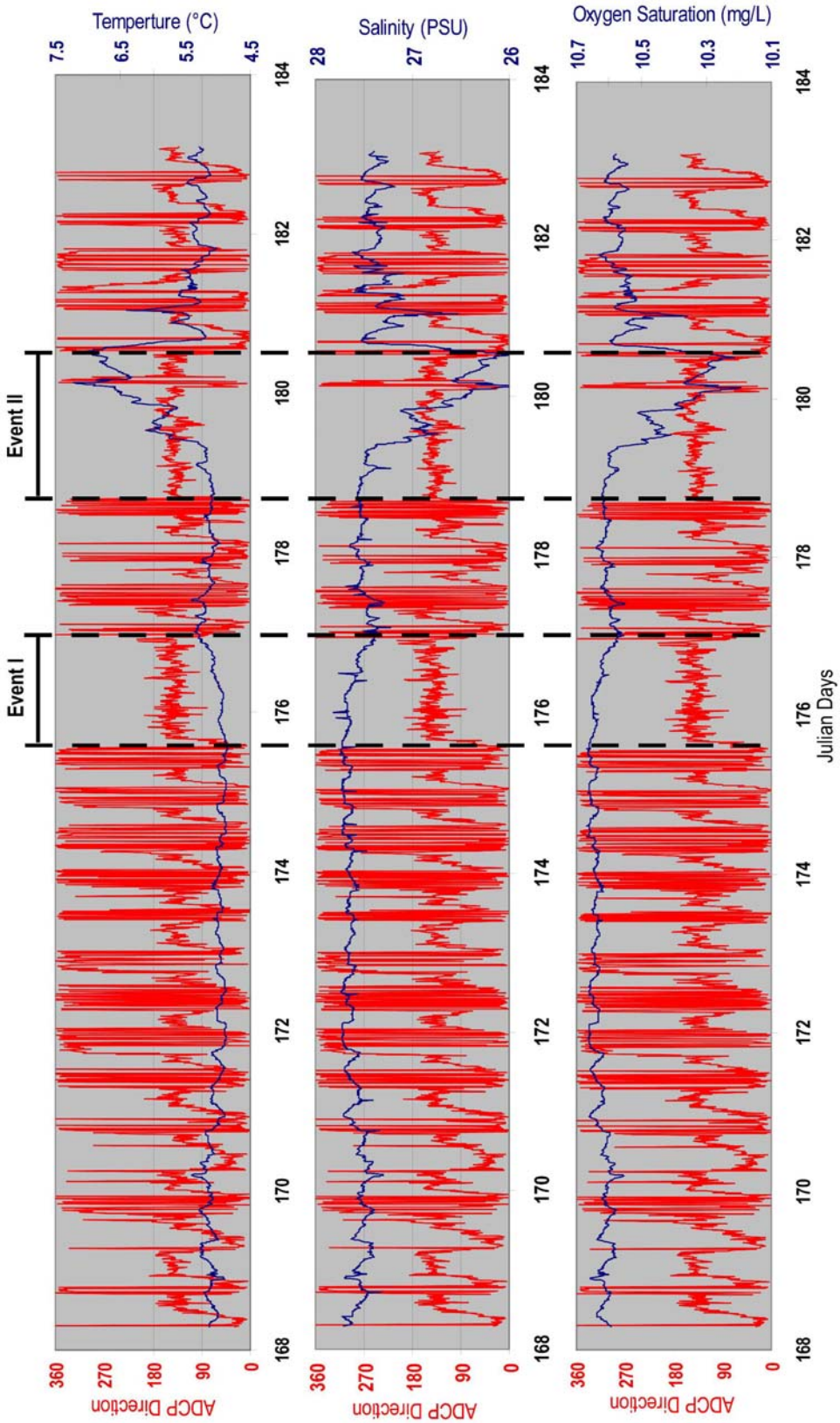

Fig. 45 Time series of CTD (blue) and directional (red) data from the instrumented pod for the period from 06-16 to 7-1-2008 (UTC). The two events show responses in each measurement

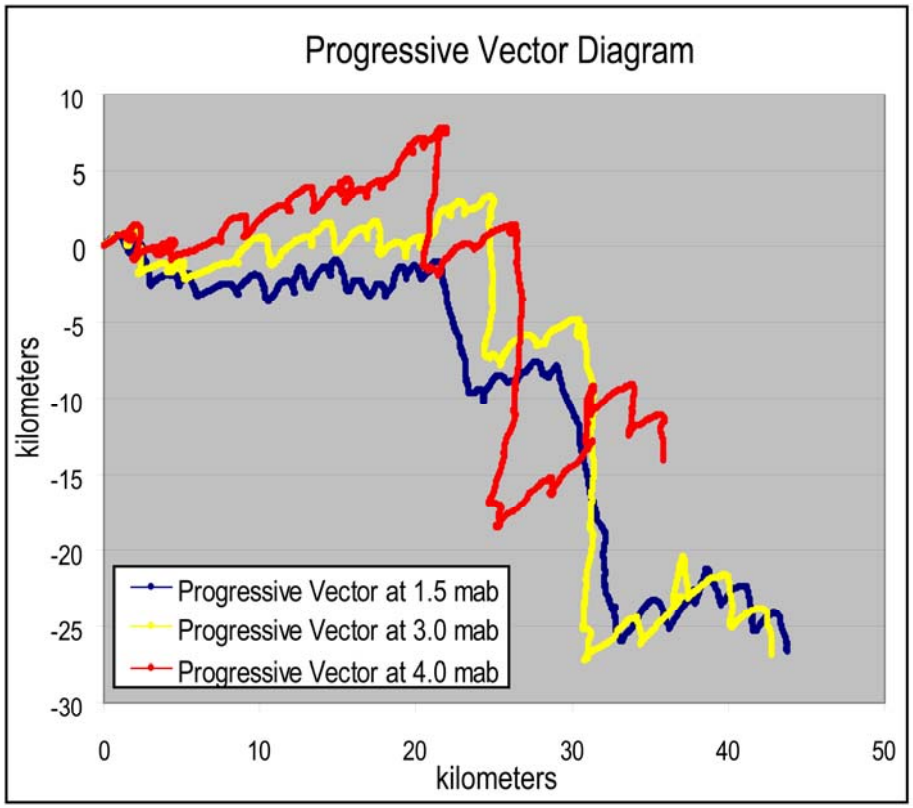

Fig. 46 Progressive vector diagram from the ADCP data for different heights above the bottom. The diagram shows an east-north-east direction under normal conditions with a shift due south during the events. Heights are given in Meters Above Bottom (mab)

the middle of the event (Fig. 42). The LISST data does not show a strong response to the first event except that it goes out of phase with the tides and remains constant at ~0.3 µl l^{-1} (normal conditions range from 0.2 - 0.3 µl l^{-1}) in the 23.4 µm fraction (Fig. 43). During the second event the 23.4 µm fraction goes out of phase with the tides at the beginning of the event and rises to a peak (0.7 µl l^{-1}) at the end of the event (Fig. 43). Plots of current direction versus concentration show that during the second event, higher concentrations were associated with the outflow but the highest concentrations were found during the brief switch in direction (Fig. 47). The LISST data shows higher concentrations associated with the event

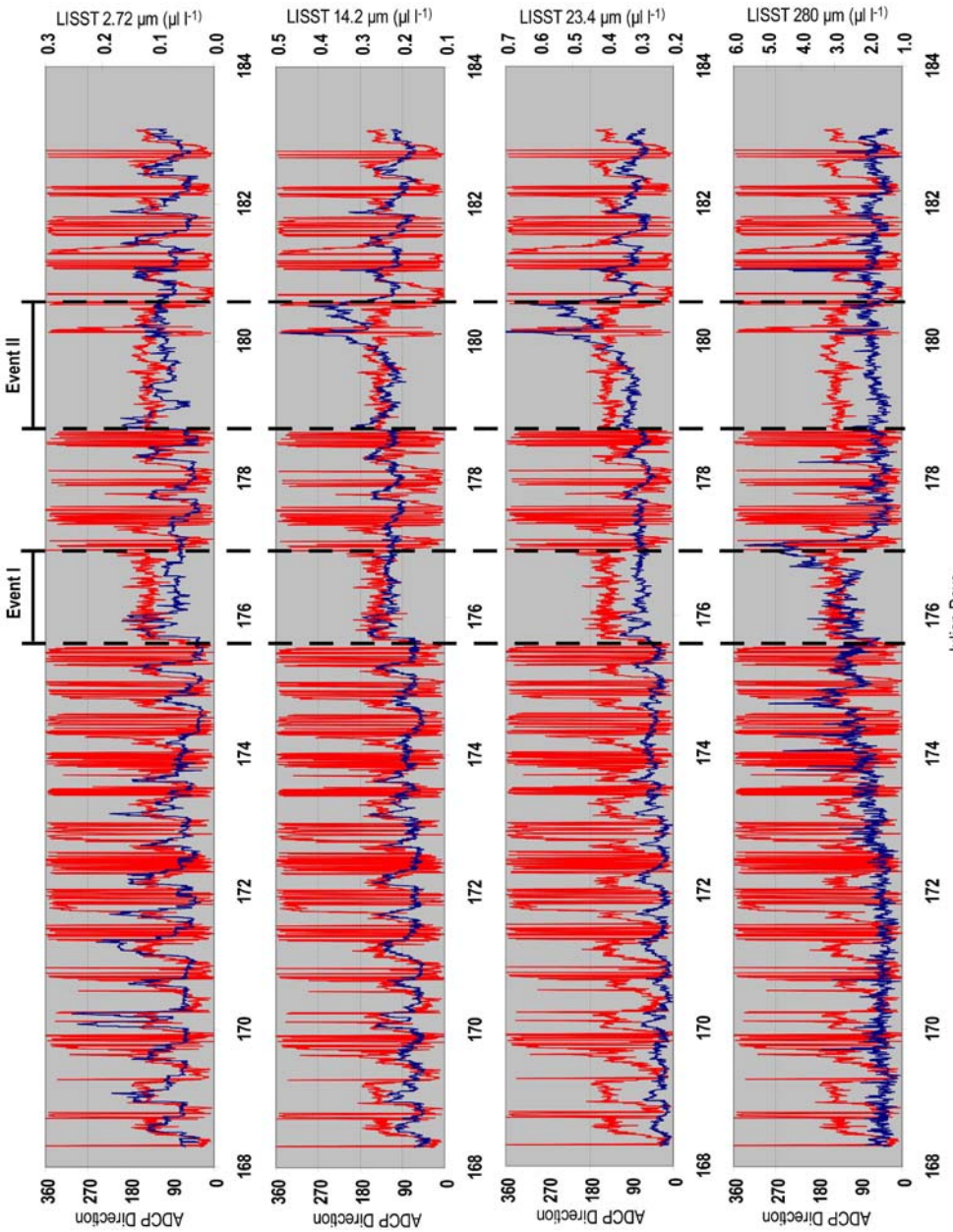

Fig. 47 Time series of LISST (blue) and directional (red) data from the instrumented pod for the period from 06-16 to 7-1-2008 (UTC). The 14.3 µm and 23.4 µm fractions show the strongest response to the event, while the 2.72 µm fraction does not seem to show a significant response to the event. The 280 µm fraction shows a response to the first event with increasing concentration then a rapid fall to low concentration

across a range of velocities, but the highest concentrations were at lower velocities. The event has two peaks superimposed on the second event. The first shows the maximum concentrations in the 23.4 μm fraction. This peak coincides with a short counterclockwise rotation in current direction (Fig. 47). The second peak coincides with counterclockwise rotation of current direction at the end of the event. The LISST peaks are well correlated to peaks in the CTD data. Post event sediment concentrations in the 23.4 μm fraction are again tidally influenced, but at higher concentrations than before (0.3-0.4 $\mu l\ l^{-1}$). Data from the 280 μm fraction shows no correlation to any of the other data. Values are relatively constant (no tidal variability) at ~1.5 $\mu l\ l^{-1}$ until ~173 JD when they begin to increase. At 177.035 JD the values peak at 5.7 $\mu l\ l^{-1}$ then drop back to ~1.5 $\mu l\ l^{-1}$ for the rest of the deployment (Fig. 47).

Two other grain size fractions were investigated with the LISST data. The 14.2 μm fraction corresponds with the mean grain size of material in the depositional area north of the sill in West Bay. This fraction behaves in the same manner as the 23.4 μm fraction, but at lower concentrations. The 2.72 μm fraction is the smallest fraction available with the instrument. This fraction behaves differently in that the concentration varies with the tides, but during the events concentrations remain at a constant value. After the events the concentrations return to levels seen at the beginning of the deployment and correlate well with the tidal data (Fig 47).

DISCUSSION

Surface Mixing

Three factors conspire to prevent the preservation of seafloor heterogeneities in the depositional environments throughout Simpson Bay; they are: 1) the efficiencies of the delta and lake systems at modulating sediment input so that episodic discharges do not impart a strong textural signal; 2) lack of physical mixing due to the water depth and geographical orientation to prevailing winds and waves; and 3) a robust benthic community able to homogenize the sediment column within the residence time of material in the SML. The only physical process working to modify the bottom (excluding deltaic processes in SBBC1) are the erosion of fine material transported to the surface by deposit feeders in the coarse grain relict glacial deposits. This is a coupled process because vertical sediment transport is mediated by

benthic infauna and subsurface heterogeneities are created by size selective particle transport. While interdecadal climate shifts do vary rainfall and runoff rates, residence times in the surface mixed layer (8-30 yrs) allow ample time for vertical integration of those climate signals. These lines of reasoning lead to the idea that surface mixing in the depositional areas of Simpson Bay can be modeled as biologically modified (as opposed to physical or combined biological/physical modification) and as diffusive in most cases. G values throughout the depositional portions of the system range from 0.23 to 6.43 (with most values below 1; Table 1) indicating that preservation of signals is not likely. One value of 233.72 was calculated due to high biodiffusivities as a result of an almost vertical profile in the SML. This value is probably not reasonable and another tracer with a shorter half-life would be more appropriate. A few cases show subsurface peaks in $^{210}Pb_{xs}$ activity resulting from species specific mixing dynamics and appear to conform to an advective mixing model (Fig. 25 and 27).

Core SBBC19, taken in a muddy, depositional area of Simpson Bay near a rocky outcrop, shows evidence of advective mixing, indicated by an increase in $^{210}Pb_{xs}$ activity with depth and a maximum activity at the base of the SML (Fig. 25); (Nittrouer 1981). In this case, the x-radiograph showed a small (~2 cm) bivalve in live feeding position. Due to water depth, size and substrate this bivalve is most likely a Nuttall's Cockle (*Clinocardium nuttallii;* Flora and Fairbanks 1976; Kozloff 1996, 1987; Smith and Carlton 1975) or Fat Gaper Clam (*Tresus capax*; Gould 1850; Kozloff 1987; Smith and Carlton 1975). Burrowing and feeding activities by these benthic organisms causes advection of high activity material directly to the base of the SML instead of downward diffusive transport (Rice 1986; Wheatcroft 1990). Core SBBC15 shows a similar SML profile. A U-shaped burrow (*Urichis campo*) may be responsible for this type of profile, but the activity profile becomes constant near the base of the SML indicating that these burrows are the exception and that deeper, diffusive mixing by other organisms may play a larger role in the overall dynamics of the SML.

The other cores in the depositional areas of Simpson Bay have varying degrees of diffusive mixing. These cores are dominated by two polychaete assemblages based on burrow types and depths. Specific species could not be identified based on the x-radiographs, but further work is being conducted to investigate the benthic community structure in Simpson Bay. The $^{210}Pb_{xs}$ profiles and x-radiographs were

used to distinguish between the two and investigate the contributions of each to the greater dynamics of the SML. Activity profiles from cores SBBC17 (Fig. 23) and SBBC5 (Fig. 28) show a log linear decrease in activity with depth. These cores show few of the short narrow burrows found in other cores. The majority of burrows are the longer lined burrows suggesting that the sediment column is mixed by a smaller number of larger individuals. Cores SBBC18 (Fig. 29) and SBBC8 (Fig. 32) have an activity profile in the SML with two slopes. At the surface, the activity decreases steeply to a depth below which activity becomes uniform. X-radiographs show that the depth where the slope changes is at the bottom of a layer of abundant short narrow burrows. Through and below this layer are longer lined and unlined burrows suggesting deep, intense mixing, but by fewer, larger individuals. Core SBBC4 (Fig. 24) has the same type of profile and has deep lined burrows, but is the only example of burrows that branch laterally at depth (other cores show surface burrows that coalesce at depth, but none that branch). This suggests that there is a lateral component to sediment mixing, below the surface, in some areas.

While there is evidence of two polychaete assemblages in Simpson Bay, less intense, deeper mixing does not seem to be an issue when quantifying biodiffusivity and calculating sedimentation rates. $^{210}Pb_{xs}$ profiles show that ^{137}Cs is a difficult proxy for validating deep mixing in this case. Rapidly deposited layers and changes in sedimentation rates in specific regions of the profile can be resolved, but introduce uncertainty when determining a calculated first occurrence of ^{137}Cs. The seafloor response to the 1964 earthquake provides a better reference. The same rapidly deposited layers and changes in rate that cause difficulties when calculating ^{137}Cs depths can be useful when pinpointing the depth of the 1964 Earthquake deposit. Because sediment accumulation after the earthquake conforms to the assumption of steady state deposition, the change in depth from the base of the SML to the earthquake signal provides a well defined chronological marker. Furthermore, this marker does not have the same issues with post depositional mobility that ^{137}Cs can display. In most cores where the 1964 earthquake signal was established, the calculated depth of 1964, using the modern sedimentation rates fell at or below the observed signal. This not only discounts deep mixing, but also indicates that the longer, lined burrows found in most cores play the dominate role in surface mixing with regards to time scales on the order of

the half-life of ^{210}Pb and that because physical mixing can be discounted, biological mixing by larger polychaetes is the dominate mechanism mixing surface sediment in Simpson Bay.

Surface mixing in the relict glacial deposits has created an armored surface by selectively transporting finer material to the surface which has been subsequently winnowed by bottom currents. This can be seen in the $^{210}Pb_{xs}$ profile of SBBC13 (Fig. 38) by a linear decrease in activity to ~6 cm. This coincides with the maximum depth of ^{137}Cs. The grain size profile shows a maximum grain size at the surface followed by a fining downward trend. This is also seen in the x-radiographs as well as a number of burrows in the coarse surface sediments. The proximity of other cores to these features influences the mean grain sizes found in the cores. Cores SBBC4 (Fig. 22 and 24) and SBBC5 (Fig. 26 and 28) are found in the center of their respective depositional environments in the NSB and the SSB. Core SBBC4 has a mean grain size of 14.2 um while cores adjacent to it have higher mean grain sizes (SBBC17 18.2 μm and SBBC19 17.7 μm). Core SBBC5 has a mean grain size of 14.4 μm while core SBBC15 has a mean grain size of 17.9 μm and core SBBC18 has a mean grain size of 22.3 μm. SBBC6, collected within the depression on the morainal bank at the mouth of West Bay (Fig. 26), contains high sand content for its depositional setting due to its close proximity to relict glacial deposits. Accumulation rates are high considering the fact that it is so far from any riverine inputs. Because this site receives material from the relict glacial deposits regardless of current direction, the high accumulation rates indicate that winnowing of sediments from the relict glacial deposits may provide a significant source of fine sediment for deposits far removed from sediment sources. The changes in the mean grain sizes of these cores indicate that there is some component of coarser sediment transport off these features. This is especially evident in East Bay (Fig. 31) where core SBBC8 at the mouth of the bay has a mean grain size of 29.52 μm and core SBBC9 at the head of the bay and at the base of the plateau has a mean grain size of 23.3 μm. Core SBBC21 located in the middle of the bay has a mean of 18.4 μm. The variability in the grain size distribution and the porosity from samples in SBBC9 suggests that periodically there is significant transport of sand size material (up to 5%) off the plateau. The changes in the sand content correlates with changes in porosity, suggesting that they are linked.

Transitional areas show a particular change in activity profile indicative of the change from mixing of relict material to mixing of modern material. Core SBBC16 is found in the gyre set up at the head of West Bay. This increase in available sediment may account for the observation that there is a component of accumulation not found in SBBC20. The first occurrence of ^{137}Cs below the hiatal surface in coarse material suggests that this was once a relict glacial area and that the benthic community transposed the ^{137}Cs signal downward. Once sediment accumulation began, rates were low until the earthquake (similar to other cores in the area) and the benthic community mixed relict coarse and modern fine sediment. After the earthquake, accumulation rates were high, and the higher sand and presence of bivalves is due to the proximity to the other relict glacial deposits. SBBC20 is found along the western shoreline. This core has a deep SML with little to no accumulation. The benthic community here is able to mix a thick portion of the sediment column down to the depth of the relict deposit. This may be because of high nutrients from the localized source (OC = 1.14% vs. 0.94%). While these cores are a combination of mixing regimes, they do not display one on top of the other. There is a period of transition where the benthic community may reincorporate the modern fine material back into the glacial material. This reincorporation may define the shape of the profile in the area of accumulation below the inflection point.

North Bay Depositional Continuum

North Bay is the only portion of Simpson Bay that conforms to the more classical definition of a fjord (Pritchard 1967; Syvitski and Shaw 1995). The depositional continuum in North Bay begins on the delta where coarse material (gravel, sand, woody fragments) from the watershed are deposited. Proximal to the delta (SBBC1; Fig. 23) coarse material that escapes the delta is rapidly deposited. Sand values as high as 25% are found in SBBC1 near the delta front though mean grain size is silt sized (36.6 μm). Physical processes are the dominant factor affecting sediment preservation. Evidence of turbidity flows is found in x-radiographs and grain size profiles. The hiatal surfaces and fining upward sequences are evidence of the erosion/deposition dynamics of prograding, high discharge delta fronts (Gilbert 1982; Kostaschuk and McCann 1983; Prior et al. 1981; Syvitski and Hein 1991; Syvitski et al. 1988). The

preservation of the physical structures is a function of the frequency and magnitude of the events juxtaposed against the ability of the benthic communities to recover and mix the sediment column. Because discharge at the delta front is heavily influenced by seasonal and annual variability, a geochronology of these events cannot be developed with the available radioisotopes. Also, the erosion of strata by subsequent events prevents the measurement of the total thickness of the previous event and the thickness of post event deposition. That said, the presence of undisturbed strata at the base of each sequence indicates that the magnitude of event deposit was thicker than the benthic communities ability to bioturbate (ie. the benthic community could not mix through the depth of the event into the base of the previous event; Nittrouer and Sternberg 1981; Wheatcroft 1990; Wheatcroft and Drake 2003) and/or that the events are so frequent that the benthic communities do not have the time necessary to mix the previous event before the next event. The frequency argument is supported by the observation that in other cores in North Bay, the SML is thicker (14.5 cm) and biological mixing is more intense (D_b = 4.66 - 85.31 $cm^2\ yr^{-1}$). This indicates that the biological community has the potential for deep mixing, but that it may be disrupted and becomes depauparate before it can reach that potential. Also, because inputs of sediment are so variable, the regions of log-linear decay may be artifacts and cannot be relied upon for accumulation rates. The magnitude argument is supported by the facts that burrows do not reach to the base of the modern turbidite deposit and that there do seem to be periods of steady state deposition in the ^{210}Pb profile. This indicates that between events there are periods of high accumulation rates and that the communities are well established, but do not penetrate the base of the physically stratified layer. The latter seems to be the better argument considering that changes in the benthic community can occur over the short spatial scales seen in North Bay and that because the depositional environments are so different, those changes may be due to grain size variations, differences in accumulation rates, frequency of disturbances, and high frequency discharge related hydrographic variability (temperature, salinity, nutrient inputs, etc…). It is further supported by the observation that the SML is thicker than SMLs found in the rest of Simpson Bay suggesting that the benthic community is healthy and that a more robust, shallower mixing benthic community is present at the head of North Bay. These questions will take a detailed investigation of the benthic community structure beyond the scope of this study to resolve.

Core SBBC2 (Fig. 20) indicates the presence of a mid-bay depocenter in North Bay. Accumulation rates are significantly higher here than in any other part of Simpson Bay. Higher accumulation rates are correlated to higher % organic carbon content (with respect to the rest of Simpson Bay; 1.76%) in surface sediment, which may contribute to the total volume of sediment deposited. The grain size distribution, when considering the series of cores down the axis of North Bay, displays the classic fining distally characteristic well established in other fjords (Syvitski, 1989; Syvitski and Shaw, 1995; Syvitski et al., 1987). Core SBBC1 has a non-steady state sedimentary environment with a higher energy regime and higher mean grain size (36.64 μm; SD = 4.7) than the other North Bay cores. SBBC3 has lower sedimentation rates than SBBC2 (mean grain size 16.83 μm) and slightly finer mean grain size (11.07 μm; SD = 6.8). This is a function of the hydrodynamic properties of the basin which create a velocity regime in this area that allows silt size particles to fall out of suspension. The mode is quite stable (6.4 μm; SD = 0.29), but large shifts in the mean (16.8 μm; SD = 7.8) indicate that there is periodic transport of coarser riverine sediment to this point in the surface plume during extreme discharge events.

Core SBBC3 is located at the base of the sill separating North and West Bays near an erosional/non-depositional feature. This feature is due to hydraulic jump erosion or possibly down slope cascading of water from West Bay. Channels around the base of Seaworld Reef suggest that there may be tidally driven bottom currents around this feature. Because of the lower sedimentation rates and fine mean grain size the currents which maintain this feature are probably not erosional, but are non-depositional. Erosional features would transport coarse material and increase the mean grain size in the surrounding sediments. A non-depositional feature would allow for limited deposition of the very fine silt and clay fraction only during slack water (hence the low accumulation rates) and keep the area around the base of Seaworld Reef, free of deposition during high flow. While the mean grain size in core SBBC3 does vary somewhat, the mode is quite constant (5.7 μm; SD = 0.12). Further analysis shows that when there is sand (material > 63 μm) it is in the fine to very fine fractions (90 – 63 μm). This indicates that there may be short periods of down slope bottom currents sufficient to carry fine sand.

Throughout North Bay, high accumulation (0.80 – 1.02 cm yr^{-1}) and high organic carbon content (0.29 – 1.76%) are responsible for the extensive presence of biogenic gas buildup in the shallow

subsurface (Noll et al. 2008). By constraining these parameters, we can conjecture that gas found in other parts of Simpson Bay was mediated by similar depositional conditions, specifically higher accumulation rates and organic carbon content. This allows us to make better speculation about accumulation rates in periods below our core control. Gas deposits are found in specific locations in specific strata in the rest of Simpson Bay indicating that at the time of deposition, accumulation rates were at or exceeded 1.0 cm yr^{-1} and that organic carbon content was greater than ~1.3%. These conditions are only found in North Bay (with one exception) and provide a good model for paleodepositional environments in Simpson Bay.

Oceanographic Controls on Sediment Distribution

Oceanographic conditions in Simpson Bay are controlled by basin morphology, atmospheric forcing, and tidal motion. The most interesting of these may be tidal dynamics interacting with bathymetric features. Preliminary work by Shelton Gay with Prince William Sound Science Center, using a towed ADCP, suggests that surface currents due to flood tides form a northeastward jet flowing across the sill on the western side of the mouth of West Bay. This is supported by data from the instrumented pod at the mouth of West Bay in ~35 m water depth by the ADCP directional data from 1.7 m above the seafloor. This flow in turn generates a southward flow along the eastern shoreline, causing an anticyclonic gyre at the mouth of the bay. The pod shows that as at the beginning of the flood tide, the direction changes rapidly to a northeastward direction (~60°) which it maintains through slack tide. After the peak flood, the bottom flow begins a gradual turn clockwise towards a southwestward flow (~210°) leading into the slack ebb tide. The ebb tide initially generates an outflow of water from North Bay along the western shoreline, but eventually turns east, creating an anticyclonic gyre around Seaworld Reef. The initial outflow of the ebb tide along the western shore line works to discharge sediment out of Simpson Bay. These tidal interactions are seen in the ADCP data collected by Gay in both the surface currents (bin centered at 2 m) to at least 10 m depth, although the magnitudes diminish with depth. There is no evidence of accumulation of fine material which is prevented by the stronger tidal currents. The gyre around the reef and at the entrance work to hydrodynamically separate the two West Bay Sub-basins and sequester material from North Bay and from the streams at the head of West Bay in the NSB, leading to

higher accumulation rates (0.4 - 0.55 cm y^{-1}) as opposed to those in the SSB (0.3 - 0.36 cm y^{-1}). Material in the SSB is deposited by the southward flow along the eastern shoreline during the flood tide by water advected from East Bay and Orca Bay. Gay's data shows that this water is possibly advected from the mouth of West Bay into North Bay, which would contribute to accumulation in the NSB.

The sediment concentration data collected by the LISST in the 23.4 μm fraction shows a strong tidal signal under normal circumstances. Specifically, higher concentrations are found on the outflow of more turbid estuarine water as opposed to the inflow of less turbid PWS water, suggesting that there is a net export of sediment from Simpson Bay. Mean grain size in the depositional areas north of the sill are finer (10 - 20 μm) and unimodal with the dominate mode at approximately 10 μm. Therefore, the increase in concentration may be a result of local resuspension as opposed to transport of material from the upper parts of the bay because there is no mechanism to deposit fine material while transporting coarser material seaward in this system. Material in the 2.34 μm fraction may be influenced by transport from the head of West Bay. This fraction remains constant during the event while the other fraction increases suggesting that it may be from a non-local source.

Material in the 280 μm fraction behaves differently than all the other fractions. A differentiation between sediment and material must be made when discussing this fraction because the changes in concentration do not change in respect to the hydrodynamic regime. There is no tidal or velocity signal and the size is too coarse for transport at the range of measured velocities (0.1 - 0.3 m s^{-1}). This material can be explained by the presence of plankton or other organic particles in the water column. The presence of these organisms would not be dependent on tide, but rather nutrient and photic conditions. Concentrations of this fraction steadily increase until the end of the first event when they decrease sharply to levels at the beginning of the deployment. Environmental conditions after the event may not have been conducive to plankton production, causing a decrease in abundance. Plots, of concentration in the 280 μm fraction versus current direction and velocity, show higher concentrations at lower velocities, suggesting that periods of low flow are needed for these particles to settle rather than high flow needed for local resuspension and transport. A range of concentrations at each of the tidal modes was found suggesting that there is not a correlation between concentration and current direction.

CONCLUSION

1. Preservation of sedimentary strata in Simpson Bay is dominated by biological processes which serve to destroy sedimentary fabric and integrate high frequency signals. The benthic community is robust enough to sufficiently mix the sediment column, eliminating the possibility of preserving textural heterogeneities. A sampling scheme with high spatial coverage showed that spatial heterogeneities are preserved in Simpson Bay. Basin morphologies throughout Simpson Bay influence sediment transport and deposition which in turn control sediment texture and accumulation rates. Changes in benthic community structure, both species and size of benthic fauna, alter the SML and residence times such that large spatial heterogeneities are found in biologically dominated depositional environments.
2. The benthic community actively modifies relict glacial deposits, winnowing and armoring them, making them less susceptible to erosion over time. These processes are a coupled bio-physical activity linking vertical biological transport of sediment to the surface and horizontal transport of material by physical processes.
3. The pod data suggest that tidal velocities over the relict glacial deposits at the mouth of West Bay are not sufficient to transport coarse material. The resuspension of fine material observed in the LISST data suggests that biological processes work to transport fine material to the surface which is then transported off the bank. This coupled bio/physical interaction armors the seafloor creating a surface layer of mud supported gravel which grades to gravel supported muds with depth in the core.

CHAPTER IV

SEAFLOOR RESPONSE AND RECOVERY TO LARGE SEISMIC EVENTS IN A TURBID OUTWASH FJORD: THE GREAT ALASKAN EARTHQUAKE MARCH 27, 1964 IN SIMPSON BAY, PRINCE WILLIAM SOUND, ALASKA

OVERVIEW

Profiles of multiple parameters from sediment cores taken in Simpson Bay were used to determine seafloor response and recovery to the Great Alaskan Earthquake, March 27, 1964. The epicenter of this M_s 9.2 earthquake was located in northwestern Prince William Sound and is the second largest earthquake in recorded history. The earthquake caused maximum vertical uplifts of 11m near Montague Island while locally Simpson Bay was uplifted ~1.5 m. $^{210}Pb_{xs}$ profiles of cores taken throughout the bay show characteristic event profiles. Cores from the eastern arm and those from the head of the central basin show a distinctive Rapidly Deposited Layer (RDL) of material with uniform activity ranging from 3 - 6 cm thick. Cores taken in the southern part of the central basin do not have this layer, but do have a sharp inflection in the slope of the activity profile. Sedimentation rates after the event increase by at least a factor of two. Post-event accumulation rates indicate that the calculated depth of 1964 lies at or slightly below the top of the RDL validating the accumulation rates and identifying the event that caused the RDL. None of the cores show a significant textural change associated with the RDL, making it difficult to determine the mode of deposition. Furthermore, there is no post-event change in sedimentary fabric, indicating that even though there may be significant changes in the watershed (land slides, shifting of river courses, etc…), the grain size distribution in the receiving basin continue to be modulated by the deltas and lakes that sort material prior to entering Simpson Bay. Analysis of lignin biomarkers was used to determine the type of material in the event layer and the nature of post-event sediment and indicate that the response in East and West Bay to the earthquake differs. The core in West Bay shows a peak in lignin concentration in the event while the core in East Bay does not. This is due to the higher trapping efficiency in the northern part of West Bay, while the lack of peak in East Bay is most likely a function of increased dilution of the terrestrial signal with distance from the source and the

increased importance of locally resuspended basin material. Basin recovery in each system is similar. $^{210}Pb_{xs}$ activities are slightly more variable possibly because discharge is more coupled to changes in precipitation and because of increased shoreline erosion. Lignin signatures indicate that while total lignin values decrease to pre-event levels, the material is composed of more degraded material and some samples show enhanced deposition of resuspended material with non-terrestrial lignin signatures.

INTRODUCTION

Large earthquakes are common in Alaska (five M_s 7.0 or greater earthquakes have been recorded since 1979); (Jaeger et. al 1998; Johnson et. al 1996; Nishenko and Jacob 1990) and include the second largest earthquake ever recorded, the Great Alaskan Earthquake March 27, 1964 (M_s 9.2). These earthquakes have shown the potential to cause catastrophic aerial, intertidal, and subtidal failures. The shorelines of the area moved by this event are dominated by glaciated and non-glaciated fjords. This makes it especially susceptible to failure due to a number of factors: high sedimentation rates have left the glacially carved steep, rocky subtidal shorelines covered by veneers of poorly consolidated fine grain sediment; glaciers have deposited thick sequences of poorly sorted glacial diamicton with steep slopes above and below sea level; and non-glaciated fjords have built extensive deltas where glaciers previously exited, composed of saturated silty sand and gravel (Coulter 1965; Lemke 1967). The 1964 earthquake caused extensive regional deformation (Fig. 6); (Plafker 1990; Plafker 1965), but caused relatively little monetary loss or loss of life due to the sparsely populated area. Previous work by the USGS immediately after the quake outlined the source, extent, and cause of the quake (The Alaska Earthquake Series USGS Professional Paper 542 A-G), but technology did not exist to conduct detailed investigations in the subtidal environment, although a few surveys using single beam echosounders showed extensive deepening near delta fronts in Seward (Lemke 1967; Plafker and Mayo 1965). More recent efforts using seismic, core, and multibeam bathymetry data have delineated the subtidal effects of slope failure in a few sites that received the bulk of the damage, specifically Valdez and Seward, Alaska (Lee 2006). At these sites, large-scale, catastrophic shoreline failure due to the collapse of unconsolidated deltaic sediment upon which the cities were built was documented, but what of the post-event seafloor response and recovery?

Furthermore what was the seafloor response in areas affected by the earthquake, but did not experience massive failure? This study gives an example of an Alaskan fjord near the epicenter of the earthquake (~110 km southeast of the epicenter) that did not undergo catastrophic subtidal seafloor changes, but did show specific geochemical responses to the earthquake and has experienced basin specific changes during the time following the earthquake.

BACKGROUND

Geologic Setting

Simpson Bay is a small macrotidal (> 5 m) fjord located in Prince William Sound (PWS) on the south central coast of Alaska (Fig. 48). Because of its morphology and hydrographic conditions, it is classified as a partially mixed, shallow fjord (Gay and Vaughn 2001). Simpson Bay is Y-shaped with distinct morphological features partitioning the system into three discrete basins. The western and eastern arms exchange directly with PWS and a northern arm feeds into the head of the western arm. In Simpson Bay, freshwater originates as precipitation (355-460 cm yr^{-1}; Fig. 2); (AGDC 1998) in the large watershed of Simpson Bay (Fig. 3) and from the melt water of high alpine glaciers in the northern and eastern arms (Fig. 3); (Gay and Vaughn 2001; AGDC 1998). Fresh water input delivers sediment to the heads of each bay through bayhead deltas and along the shoreline through small creeks. The presence of glaciers and the comparatively large watershed:basin surface area ratio (8:1) suggest a high sediment load may be introduced to Simpson Bay. The drainage basin morphology of Simpson Bay creates large differences in the watershed:basin surface area ratio of each arm. The western arm, with the largest surface area, has by far the smallest drainage basin. In contrast, the small northern arm has a drainage basin 15 times larger than the western arm. These data have great implications about the source, distribution and fate of sediment in Simpson Bay (Noll et al. 2008).

Side scan sonar and bathymetry surveys of Simpson Bay (Noll et al. 2008) have classified bottom types and described basin morphology. West Bay is the western arm of Simpson Bay (Fig. 48). This arm has the largest surface area (7.5 km^2), but has a small drainage basin (7.5 km^2) giving it an approximately 1:1 watershed:basin surface area ratio (Fig. 3). This arm is approximately 4 km long and 2 km wide and

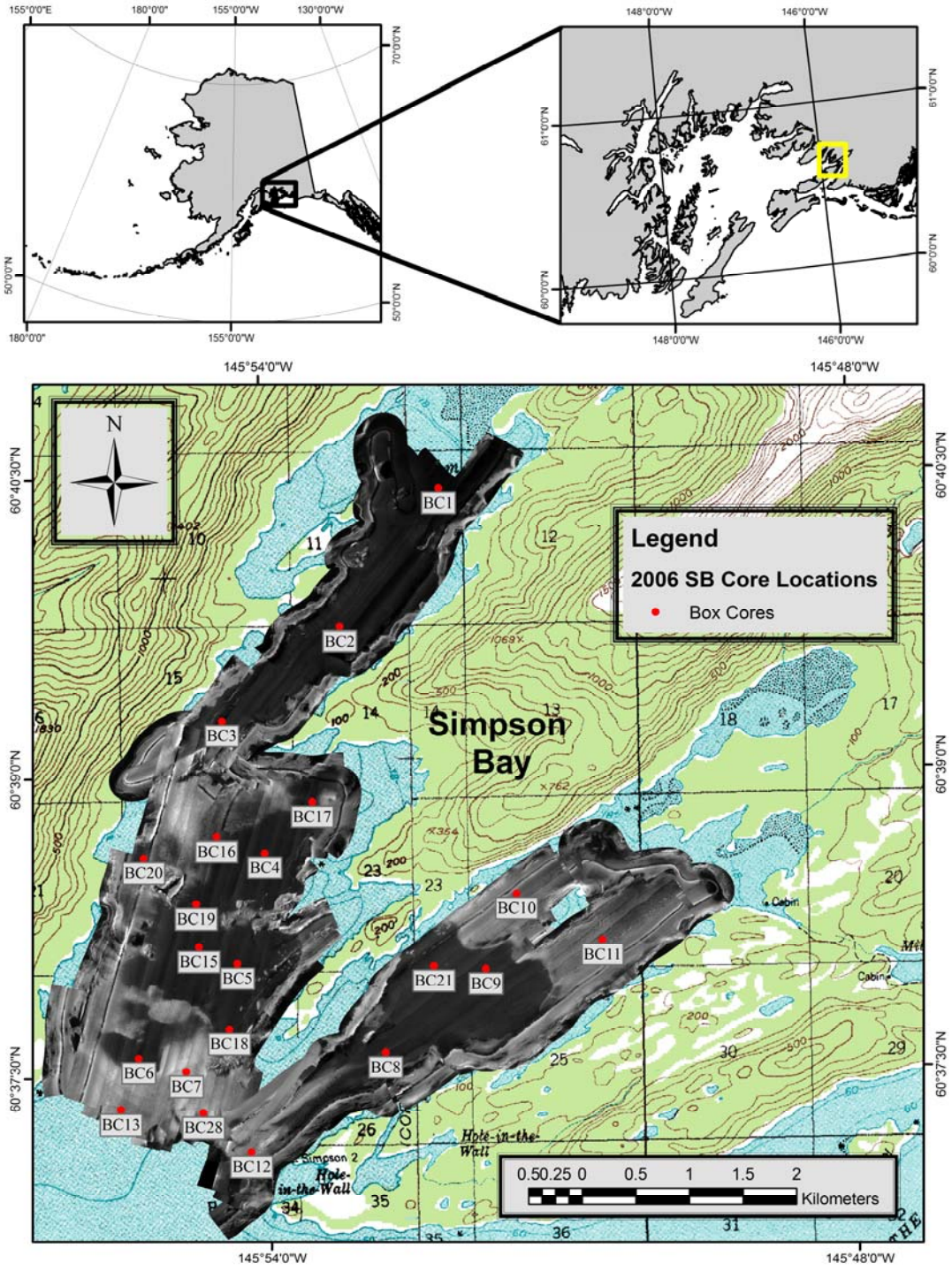

Fig. 48 Study site showing box core locations and side scan sonar mosaic overlaid on a USGS topo map

opens directly into PWS. West Bay is morphologically the most dynamic portion of Simpson Bay. On average, it is the shallowest (25 to 55 m); (Fig. 5), and the bottom is irregularly shaped. Fine grain sediment is found ponded in bathymetric lows while high backscatter bedrock and diamicton deposits form bathymetric highs (Fig. 48). This portion of Simpson Bay is bounded to the north by the shoreline and the bedrock morainal bank that separates North Bay and West Bay and to the south by a low relief morainal bank and PWS. Side scan sonar and bathymetry data combined with extensive seismic profiles were used to divide West Bay into northern and southern sub-basins. These sub-basins are separated by a rocky promontory that extends from land on the eastern shoreline across the majority of the bay in the subtidal and emerges on the western shoreline in a series of small islands and intertidal outcrops. Seismic data show that although a portion of the promontory is covered by modern sediment the feature extends across the bay in the shallow subsurface. East Bay is a northeast/southwest oriented basin which is long (4 km) and narrow, thinning from 2 km at the head to 1 km at the mouth with depths ranging from 10 - 80 m (Figs. 5 and 48). East Bay has almost the same surface area (7 km^2) as West Bay, but its drainage basin is much larger (52 km^2), giving it a 7:1 watershed:basin surface area ratio (Fig. 3). The mouth of East Bay is at the southern end of Simpson Bay, and unlike North Bay, water masses exchange directly with PWS. There is no sill at the mouth that restricts circulation, but there is a low relief (~15 m), high backscatter morainal bank that separates East Bay from the rest of Simpson Bay (Fig. 5). The deep area of East Bay is composed of low backscatter fine grain estuarine mud that transitions to rocky shoreline along the periphery (Fig. 48). At the head of the bay, depths decrease sharply to a high backscatter, shallow plateau composed mainly of coarse grain material with a veneer of estuarine mud. North Bay is the long (4 km) and narrow (0.7 - 1.3 km) northern arm of Simpson Bay (Fig. 48). Depths range from 5 - 80 m (Fig. 5), and this arm has steep sides (5° to 25°) composed of diamicton and bedrock that transition to shoreline. In some areas, bathymetry data show sheer rock faces that descend from above the water to the bottom of the fjord. North Bay is the smallest arm of Simpson Bay (5.5 km^2), but has the largest drainage basin (112 km^2) resulting in a 20:1 watershed:basin surface area ratio (Fig. 3). Bedrock is exposed at the morainal bank complex at the mouth of North Bay making this the only portion of Simpson Bay that has a true restrictive sill (Figs. 5 and 48). Aerial photography shows riverine input is somewhat restricted to North

Bay by this sill. The rest of the bay is composed of estuarine mud and rocky shorelines except for the delta at the head of the bay.

Sediment input into Simpson Bay is driven by unique morphological features and hydrography. Orogeny in the south central coast of Alaska has created one of the highest coastal reliefs in the world. Simpson Bay is part of the Orca Group, a component of the Prince William lithotectonic terrane. The Orca Group is composed of a deep-sea fan complex of flyschoid greywacke and minor pelite interbedded with subordinate oceanic volcanic rocks and minor pelagic sediment (Farmer et al. 1993). Fine grain sedimentary rock and conglomerates are found throughout Simpson Bay (Lethcoe 1990). PWS has shoreline mountains that reach 1000 m in elevation and is bordered to the north by the Chugach Mountains that reach heights in excess of 4000 m, less than 60 km from the coast (Gay and Vaughn 2001). The Aleutian Low is a low pressure atmospheric system that dominates the weather patterns of Alaska's southern coast. The interaction of the Aleutian Low with this coastline produces meters of precipitation each year that supply snow to the high altitude ice fields that feed massive glaciers and rain/snow to low altitude temperate rainforests. These factors, coupled with a rapidly uplifting (several meters per 1000 yrs), easily erodable coastal mountain range, create a drainage system with some of the highest sedimentation rates in the world (Hallet et al.1996; Jaeger et al. 1998; Powell and Molinia 1989). A high freshwater flow during the late summer maximum brings sediment into the Simpson Bay at the fjord head and along the shoreline. Rivers at the head of the two upper arms tap large drainage basins and bring sediment laden glacial water to the fjord. Coarse sediment is trapped in prograding fjord head deltas found at the heads of both arms of Simpson Bay. The northern arm drains a larger area and more glaciers than the eastern arm and consequently a larger delta has built at the head of the northern arm (Gay and Vaughn 2001; Noll et al. 2008).

The Great Alaskan Earthquake March 27, 1964

On March 27, 1964, a magnitude 9.2 earthquake (Johnson 1996) shook an 800 km long section of south central coastal Alaska in the vicinity of PWS (Fig. 6). A land area of approximately 170,000 to 200,000 km^2 from Kodiak Island extending through the Kenai Peninsula and Prince William Sound to

Yakataga including Cook Inlet and the coastal portions of the Chugach Mountains was rotated along an axis roughly parallel to the Aleutian Trench. This ranked the event as causing the largest area of crustal deformation associated with a single earthquake at the time (Plafker 1965). Maximum uplift of 11 m was observed on Montague Island and areas to the northwest of the axis, extending from Kodiak Island to Port Valdez, were depressed as much as 2 m.

The earthquake occurred along the convergent margin where the Pacific plate is subducted at a rate of 6 cm yr^{-1} below the North American plate. The complexity of terrane accretion along this margin causes the Pacific plate to subduct at different angles. Near the Prince William Sound asperity the plate interface is shallow and broad dipping at 3° - 4°. Farther south, near the Kodiak asperity, subduction is steeper, dipping at 8° - 10° (Johnson et al. 1996). The Yakutat terrane is the most recent addition to the coastal terrane complex, and it is the plane between the North American Plate and the Yakutat terrane, (which is loosely coupled to the underlying Pacific Plate) know as the Alaskan megathrust, on which the earthquake occurred (Doser et. al 1999; Johnson et al. 1996).

Areas that saw the most human damage were in towns built on poorly consolidated alluvial/glacial deposits. The deposits on which the cities such as Seward and Valdez were built on experienced liquefaction during the event and the resultant failure caused portions of the town to fall into the fjord (Coulter 1965; Lemke 1967). These failures generated localized tsunamis, with wave runup exceeding 50 m in some cases, causing some of the greatest damage (Plafker and Mayo 1965). Observations along shorelines throughout the area noted highly localized, erratic damage with no preferential direction. This indicates that damage due to seismic sea waves was due to localized sources such as: submarine slides, tectonic tilting, seiching, local submarine faulting, and subaerial landslides (Plafker and Mayo 1965). Large scale seismic sea waves were generated due to crustal deformation in the Gulf of Alaska. These waves caused damage to areas of coastal Alaska, Hawaii, and the US Pacific coast and were measured as far away as Antarctica (Johnson et al. 1996). Seismic sea waves in PWS were relatively mild. The highest seen were approximately 5 m above normal tide (the earthquake occurred at lower low water) in northern and western PWS, but with a normal tide range on the order of 5 m, the effects were only seen when the waves reached above the highest high tide. In eastern PWS where areas

were uplifted and sea waves were the smallest, little effect was observed (Plafker and Mayo 1965).

Rapid Deposited Layers (RDL)

Many cores in the depositional areas of Simpson Bay show radiochemical evidence of layers of sediment deposited in a short timeframe relative to the half-life of the isotope used for analysis. Using ^{210}Pb geochronology we were able to identify these layers and determine their age, which agrees well with the occurrence of the 1964 earthquake. The term RDL will be used extensively throughout this text because, while we can determine that the layers are due to earthquake triggered episodes of rapid sedimentation, the layer shows few indicators as to the processes that deposited the layer. ^{210}Pb is not able to give any genetic indicators as to the type of flow (turbidite, hyperpycnal, etc…), and there is not a significant textural signal. This generic term encompasses all forms of rapid sedimentation and is preferred so as not to make assumptions or create confusion as to the type of processes that distribute sediment due to these events.

Terrestrial Biomarkers

Terrestrial biomarkers are used in a number of diverse environments to determine the contribution, distribution, and fate of terrestrial organic material in estuarine, coastal, and marine sediments (Bianchi et al. 1997; Goni et al. 2000; Houel et al. 2006; Loh et al. 2008; Louchouarn et al. 1999; Nuwer and Keil 2005). Lignin is a useful tracer because it is a recalcitrant biomacropolymer which ranks second only to cellulose in abundance (de Leeuw and Largeau 1993; Louchouarn et. al. 1999). Lignin Oxidation Products (LOP) are composed of a suite of eight lignin-derived phenolic biomarkers found exclusively in terrestrial vascular plants. Concentrations of these eight biomarkers were determine by copper oxidation of bulk sediment and are used to determine the source (angiosperm/gymnosperm), dilution, degradation, and preservation of the material as well as establish diagenetic processes (Louchouarn et al., 1999; Louchouarn et al., 1997). These tools were used to help determine the source of the material preserved in the RDL and how the basin and watershed have recovered following the earthquake.

METHODS

Box cores were taken over a two day period in the summer of 2006 from the F/V Miss Kayle using a 50cm x 50cm x 100cm GOMEX style box corer. Twenty-one stations were occupied for coring based on side scan sonar and seismic data to target specific bottom types. A Trimble DGPS was used for positioning throughout the survey. After the box core was brought on board it was sampled with a 15 cm diameter PVC tube and a 2.5 cm x 10 cm plexiglas tray for x-radiographs. Core lengths ranged from 15 - 40 cm depending on substrate. The tubes and trays were sealed and stored upright for the short trip to port. All box cores were acquired, sub-sampled, and x-radiographs were taken within 72 hrs. Sediment samples were extruded and sub-sampled on 1 cm intervals and the trays were x-radiographed in port using a digital x-radiograph machine.

Geotechnical Analysis

Sample aliquots were dried to determine porosity which was used to calculate corrected depths and mass accumulation when determining sediment accumulation rates. Dried sample was saved for the ^{210}Pb analysis.

Grain size analysis was carried out using a Malvern 2000 Mastersizer Laser Particle Analyzer. Approximately 10 g of wet sediment was sieved through a 2 mm mesh sieve with de-ionized (DI) water into 200 ml calibrated jars to remove material larger than 2 mm (gravel; Malvern cannot process particles larger than 2 mm). The greater than 2 mm fraction was dried and weighed. 10 ml of a 10% sodium hexametaphosphate solution was added to the jars and they were filled to 200 ml with DI water. Sample jars were homogenized with a magnetic stir plate during analysis. 10 ml was pipetted into aluminum tins and dried to reincorporate the gravel data with the Malvern output. Sample was added to the Malvern using a pipette until optimum obscuration limits were achieved and grain size distribution was determined for the 2 μm to 2 mm fraction. Sand, silt, and clay content was determined (clay < 4 μm; silt 2 - 64 μm; sand 64 - 2000 μm) and recombined with the gravel data to determine the gravel, sand, silt, clay distribution for the sample.

Radioisotope Analysis

Activity profiles of short lived (~100 yr) radioisotopes were used to determine sedimentation rates in the different sedimentary environments throughout Simpson Bay. Activities of $^{210}Pb_{xs}$ ($t_{1/2}$ = 22.3 y) in core samples were measured and plotted to determine sedimentation rates. ^{210}Pb activities were measured indirectly using the ^{210}Po method (Nittrouer et al. 1979; Santschi et al. 2001). Samples were wet sieved with a minimum amount of DI water through a 40 μm sieve and the smaller fraction was used to minimize the influence of changes in surface area on activity. Samples blanks of 100 ml DI water were run with the same method periodically throughout the process to determine if the water had any effect on the activity and no detectable activity was reported. Trials using wet sieved, dry sieved, and bulk dried ground sediment were analyzed and the wet sieved gave the greatest yield. Aliquots (1 g) of dried sample were spiked with a ^{209}Po tracer was added to the sample for yield determination and were prepared by complete digestion with HCl, HNO_3 and HF. ^{210}Po and ^{209}Po were chemically separated and spontaneously deposited onto Ag planchetts (Santchi et al. 2001). Activity of the Po isotopes was determined by α-spectroscopy using a Canberra surface barrier detector. ^{210}Po is the granddaughter of ^{210}Pb and is assumed to be in secular equilibrium. ^{210}Pb activity was calculated and supported values were subtracted to determine $^{210}Pb_{xs}$ activity. Supported values were determined by assuming that the activity at the bottom of the core where $^{210}Pb_{total}$ becomes constant is the supported value.

Sediment accumulation rates were determined by calculating a regression line in an area of the core consistent with steady state deposition and using the equation:

$$A(z) = A(o)e^{\left(-\lambda z / S\right)}$$

where S = sediment accumulation rate, z = change in depth of the of the regression (cm), A_d = $^{210}Pb_{xs}$ activity at end of the regression (dpm g^{-1}), A_o = $^{210}Pb_{xs}$ activity at beginning of regression (dpm g^{-1}), and λ = radioisotope decay constant (^{210}Pb = 0.031 y^{-1}) (Bentley and Nittrouer 2003; Nittrouer et al. 1984).

^{137}Cs ($t_{1/2}$ = 30 y; 662 keV peak) activity was determined using a low-background, high efficiency, high-purity Germanium (HPGe) planar γ-detector coupled to a multi channel analyzer. Samples were wet packed and counted for approximately 24 hrs to determine the first occurrence of ^{137}Cs

in the core. ^{137}Cs was produced by bomb fallout as a result of atmospheric nuclear bomb testing in the 1950's and early 1960's (Krishnaswami et al. 1971). The depth of first appearance will coincide with the beginning of atmospheric bomb testing in 1954.

Geochemical Analysis

Sediment samples from Simpson Bay were analyzed for a number of different chemical components. Elemental and biomarker analysis were all used to determine the marine vs. terrestrial source of both surficial and down-core samples.

Elemental

Total carbon (%OC) and nitrogen (%N) values were determined using a Perkin Elmer 2400 CHNS/O Carbon Hydrogen Nitrogen analyzer. 4 - 5 mg dried ground sediment was packed in silver capsules, fumigated with concentrated HCl for 24 hr to remove inorganic carbon, and dried at 40°C for > 24 hrs before analysis. NIST standards (NIST SRM 1941b – Organics in Marine Sediment) and duplicate samples were run in each batch to assure instrument precision and accuracy.

Biomarker

Biomarker analysis was performed using the CuO method of Hedges and Ertel (1982) and Goni and Hedges (1992) with modifications by Louchouarn et al. (1997). In order to assure at least 4 mg carbon was available for analysis, > 300 mg dried pulverized sample was digested in the absence of O_2 with CuO and $Fe(NH_4)_2(SO_4)_2*6H_2O$ under alkaline conditions in stainless steel bombs. The bombs were heated to 150°C for 90 min. to complete the oxidation, and then an ethyl vanillin standard was added to the sample at room temperature for yield determination. Samples were acidified using HCl and a liquid-liquid extraction was preformed three times using ethyl acetate. After drying, samples were dissolved in pyridine and derivatized with BSTFA/TMCS to form trimethylsilyl derivatives. Analyses were run on a Hewlett-Packard 5890 GC fitted with a fused capillary column attached to a flame ionization detector (FID). Batches of 12 samples were run with one duplicate and one standard (NIST SRM 1941b – Organics in Marine Sediment). The quantification of the 8 lignin oxidation products (LOP) was determined from their FID response.

RESULTS

$^{210}Pb_{xs}$ Earthquake Response

Cores from West Bay show two different earthquake responses based on their location in the northern or southern sub-basin. Core profiles in the northern sub-basin (SBBC4, SBBC17, and SBBC19); (Fig. 22) have a 3.5 - 4.5 cm thick surface mixed layer (SML), followed by a region of linear decrease in activity to a RDL approximately 4 - 5 cm thick. Below the RDL there is a log-linear decrease in activity to supported levels (Jaeger 1998; Smith and Walton 1980); (Fig. 49). Accumulation rates above the RDL range from 0.39 - 0.52 cm yr^{-1} and 0.26 - 0.31 cm yr^{-1} below. In each case the maximum ^{137}Cs penetration was found below the base of the RDL, verifying that the layer was deposited after the 1954 first occurrence of ^{137}Cs. Using the post-event accumulation rates, the calculated 1964 depth is at or near the top of the RDL (Table 1).

Cores in the southern sub-basin (SBBC5, SBBC15, and SBBC18; Fig. 26) show a completely different signal the earthquake. These cores do not have a RDL, but instead have an inflection in the activity profile (Fig. 50), as seen in SBBC5, which contains a typical profile for this record. Above and below this inflection point, activity decreases in a log-linear fashion. In each case, the first occurrence of ^{137}Cs is below the inflection and in each case the calculated depth of the 1964 layer falls at the inflection. The SML in the southern sub-basin ranges from 5.5 - 7.5 cm and the inflection lies from 13.5 - 15.5 cm below the surface from core to core. Accumulation rates above the inflection range from 0.3 - 0.37 cm yr^{-1} and range from 0.07 - 0.11 cm yr^{-1} below it (Table 1). Core SBBC6, in the sediment pond on the morainal bank at the head of West Bay, has a profile similar to the profile from the core from the southern sub-basin. Accumulation rates above the inflection (15.5 cm) are relatively high (0.34 cm yr^{-1}) and are lower below the inflection (0.15 cm yr^{-1}). Large articulated bivalve shells in the x-radiograph are not a result of mass transport. Instead they are discarded by the large population of sea otters that live in the area. Core SBBC16 was collected in the transitional area at the head of West Bay. This core penetrates the relict glacial deposit below the modern fine sediment. The earthquake signal within the $^{210}Pb_{xs}$ profile from this core is similar to that found in the southern sub-basin, with an inflection at 11.5 cm.

The radioisotope signal in the East Bay cores is similar to that of the cores from the northern sub-basin (Fig. 31). RDL thicknesses in cores SBBC8, SBBC9, and SBBC21 range from 5 - 6 cm and are bound above and below by intervals of log-linear activity decay (Fig. 51). Surface mixed layers range

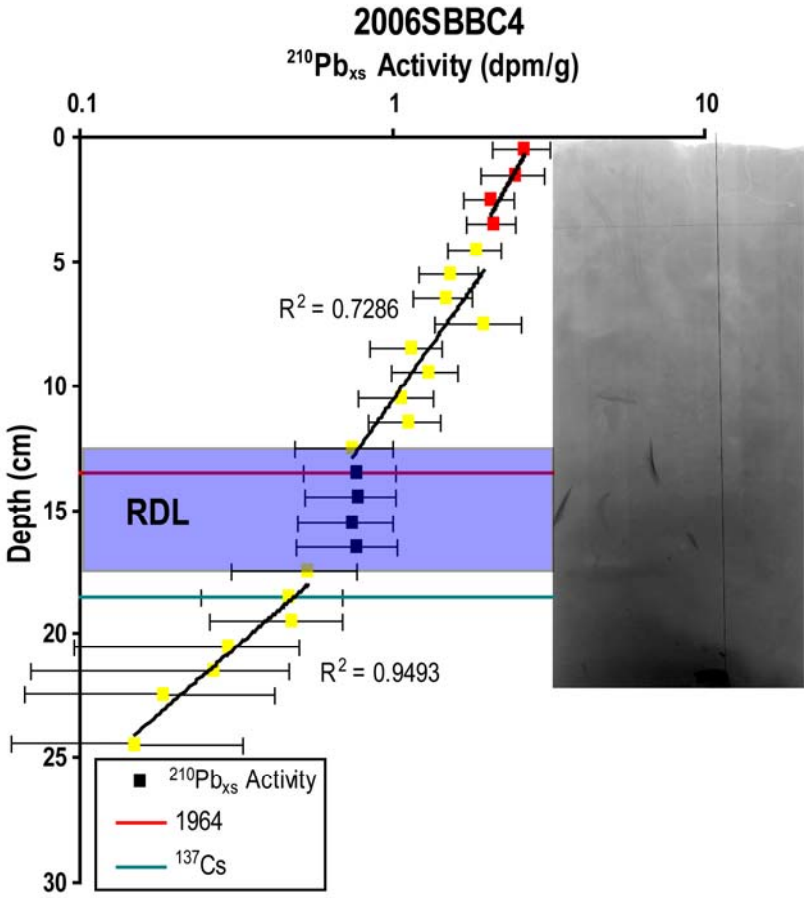

Fig. 49 Core SBBC4, taken in the NSB in West Bay, showing the x-radiograph, the region defined as the RDL (in blue), the maximum penetration of ^{137}Cs (green line) below the RDL, and the calculated depth of 1964 (red line) near the top of the RDL. The yellow points are the ^{210}Pb activity data used to determine accumulation rates above and below the RDL, and the red points are the ^{210}Pb activity data defining the SML

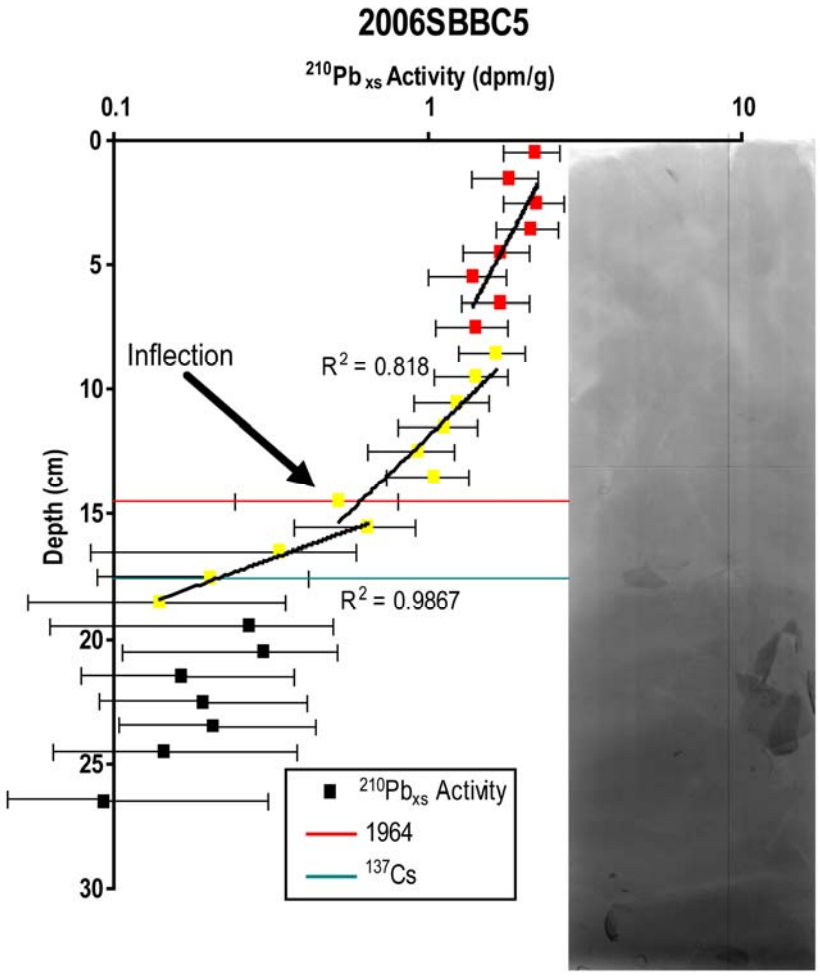

Fig. 50 Core SBBC5, taken in the SSB in West Bay, showing the x-radiograph, the inflection point, maximum penetration of ^{137}Cs (green line) below the inflection, and the calculated depth of 1964 (red line) at the inflection. The yellow points are the ^{210}Pb activity data used to determine accumulation rates above and below the inflection, and the red points are the ^{210}Pb activity data defining the SML

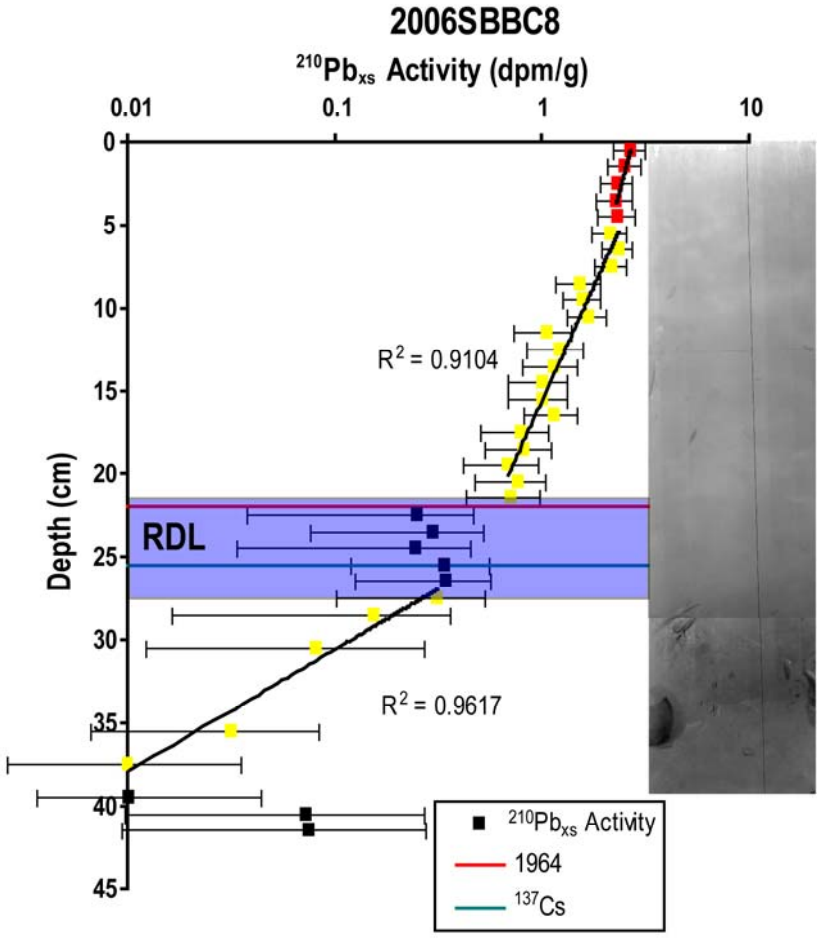

Fig. 51 Core SBBC8, taken in East Bay, showing the x-radiograph, the region defined as the RDL (in blue), the maximum penetration of ^{137}Cs (green line) in the RDL, and the calculated depth of 1964 (red line) near the top of the RDL. The yellow points are the ^{210}Pb activity data used to determine accumulation rates above and below the RDL, and the red points are the ^{210}Pb activity data defining the SML. The line in the x-radiograph at 30 cm is where two portions of the x-radiographs were merged

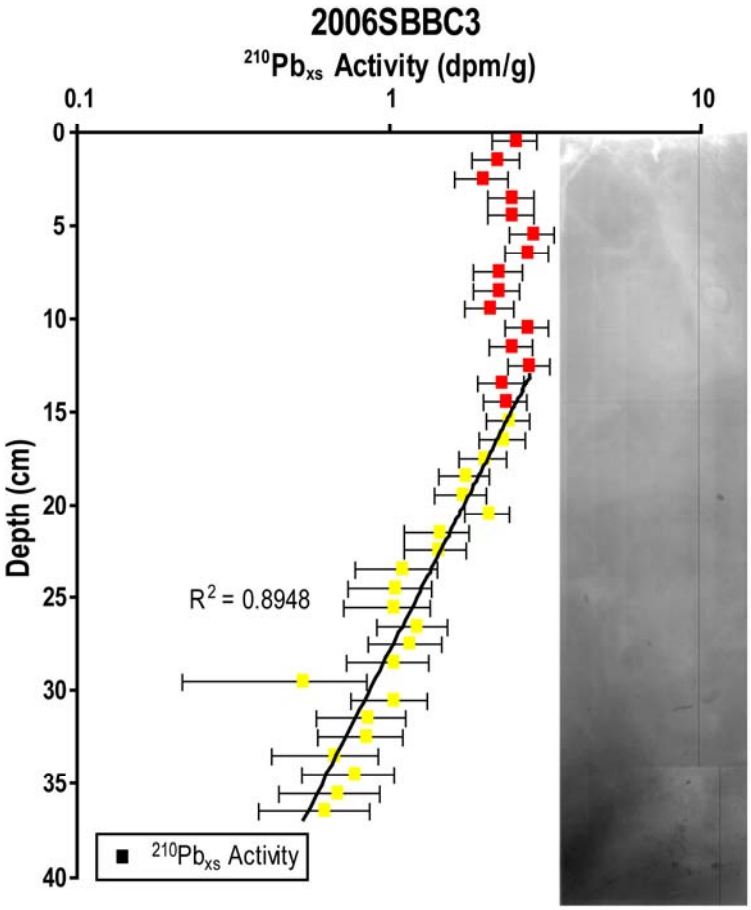

Fig. 52 Core SBBC3 taken at the mouth of North Bay behind Seaworld Reef showing the x-radiograph and the ^{210}Pb activity data. The yellow points are the ^{210}Pb activity data used to determine accumulation rates and the red points are the ^{210}Pb activity data defining the SML. Note that the maximum ^{137}Cs penetration was not reached or the calculated 1964 depth. High accumulation rates confirm that the core was not long enough to reach these layers

from 4.5 - 6.5 cm and accumulation rates above and below the RDL are 0.37 - 0.61 cm yr^{-1} and 0.16 - 0.23 cm yr^{-1} respectively. SBBC8 is the only core where the first occurrence of ^{137}Cs falls within the RDL, but otherwise the first occurrence of ^{137}Cs falls below the RDL and the calculated 1964 depth falls at or near the surface of the RDL (Table 1).

$^{210}Pb_{xs}$ for some of the cores in Simpson Bay did not contain a record of the earthquake response for a number of reasons. Accumulation rates in North Bay are so high (0.8 – 1.02 cm yr^{-1}) that cores SBBC2 and SBBC3 (Figs. 19 and 52) were not long enough to penetrate the earthquake layer and SBBC1 is located in the delta front environment where $^{210}Pb_{xs}$ geochronology was not reliable (Fig. 53). ^{137}Cs was found to the base of all cores in North Bay. Cores taken in the relict glacial deposits did not show a record of the response because they were collected from non-depositional areas (Fig. 54). Transitional core SBBC20 lacks sufficient sedimentation rates to contain a record of an earthquake response. The $^{210}Pb_{xs}$ profile contains a record of deep biological mixing to the surface of the relict glacial material.

Geotechnical Signal

One of the interesting aspects of the results from the cores taken in Simpson Bay is that there is not a conclusive, ubiquitous textural signal in the RDL defined with the $^{210}Pb_{xs}$. A few of the cores contain higher grainsize variability in the post event part of the profile, but there is no "Golden Spike" in the grain size or porosity data. SBBC1 contains dramatic changes in porosity and grain size that can also be seen in the x-radiographs (Fig. 55). Although these sequences are event driven, it is impossible to determine a reliable geochronology because of the erosional component of the deposits. Because we cannot determine the frequency of events with any great certainty, it is possible that one of the events is the 1964 deposit, but because it is in a highly dynamic delta front environment, the sequences observed are likely due to more frequently occuring events. Unlike other cores in Simpson Bay, increases in silt are coupled to decreases in sand and indicate a relative fining in the profile. Other cores contain a coupling between the silt and clay fractions indicating that an increase in silt reflects a relative coarsening. Cores SBBC4 and SBBC8 are cores that show changes in grain size distribution associated with the RDL, though it should be noted that the changes only range from 5 – 10% over the entire length of the core. In core SBBC4, silt increases, clay decreases, and sand content increased by ~2% after the event (Fig. 56). Below the RDL content for all the fractions were relatively constant. These changes are all minute, on the order of 5% for the silt and clay and only 1% for the sand, but measurable. Slightly darker tones (coarser material) are seen in x-radiographs in the interval identified as the RDL as well as a few shell fragments. In core SBBC8, silt and clay content is relatively constant below and through the RDL, but above it, silt

content increases and clay content decreases to the base of the SLM (Fig. 57). In the SML, silt content decreases and clay content increases. Sand content is relatively constant throughout the profile and 2 - 6% higher than the other cores due to its close proximity to nearby relict glacial deposits. The core shows a

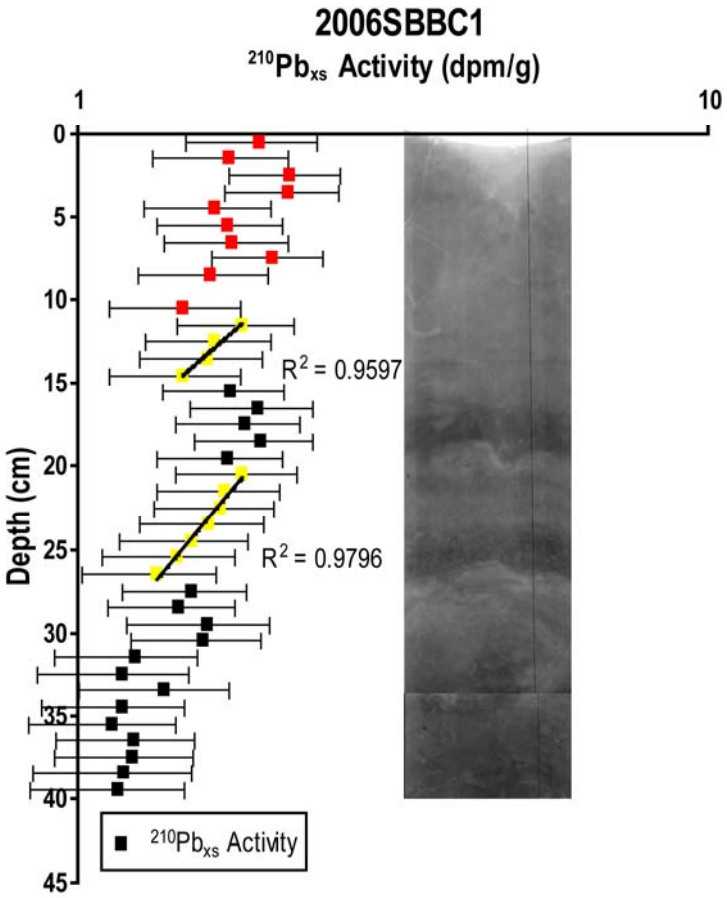

Fig. 53 Core SBBC1 taken at the delta front at the head of North Bay showing the x-radiograph and the ^{210}Pb activity profile. Red points indicate the ^{210}Pb activity data used to define the SML, while yellow points are regions of log-linear ^{210}Pb activity decay used to calculate accumulations. Do to the dynamic nature of the depositional environment, these rates are probably not accurate and the episodic nature of deposition did not allow a confident geochronology to be defined

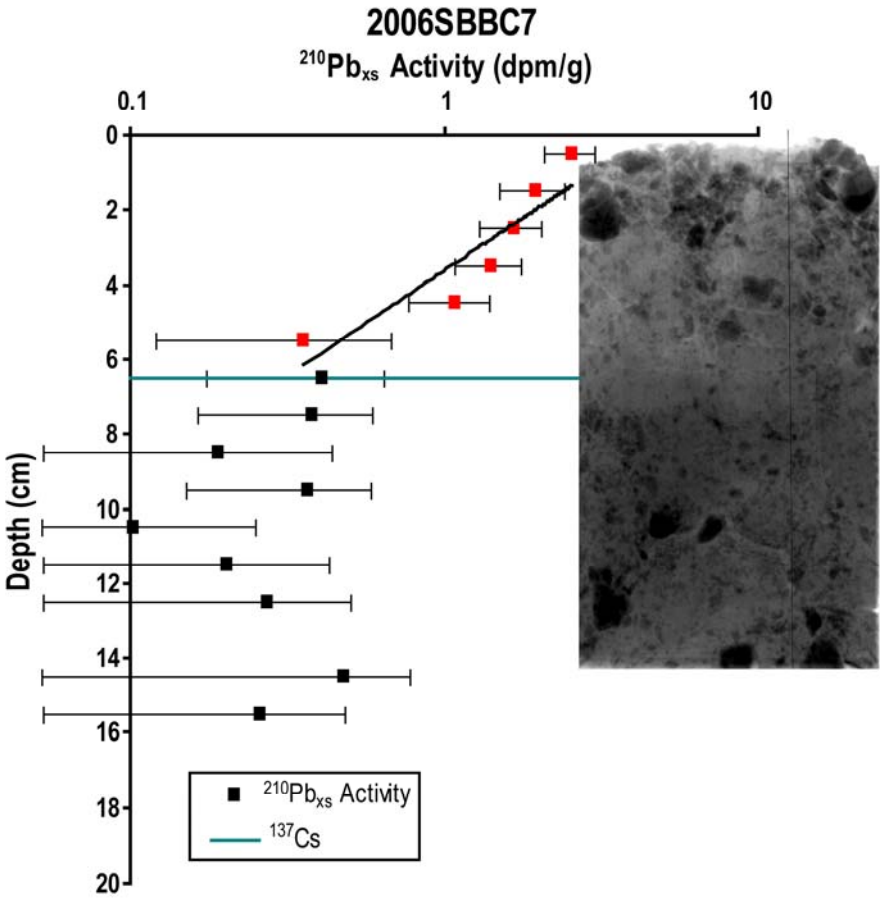

Fig. 54 Core SBBC7 taken in the relict glacial deposits at the mouth of West Bay showing the x-radiograph and the ^{210}Pb activity profile. Red points define the region of bioturbation and were used to calculate a biodiffusion coefficient

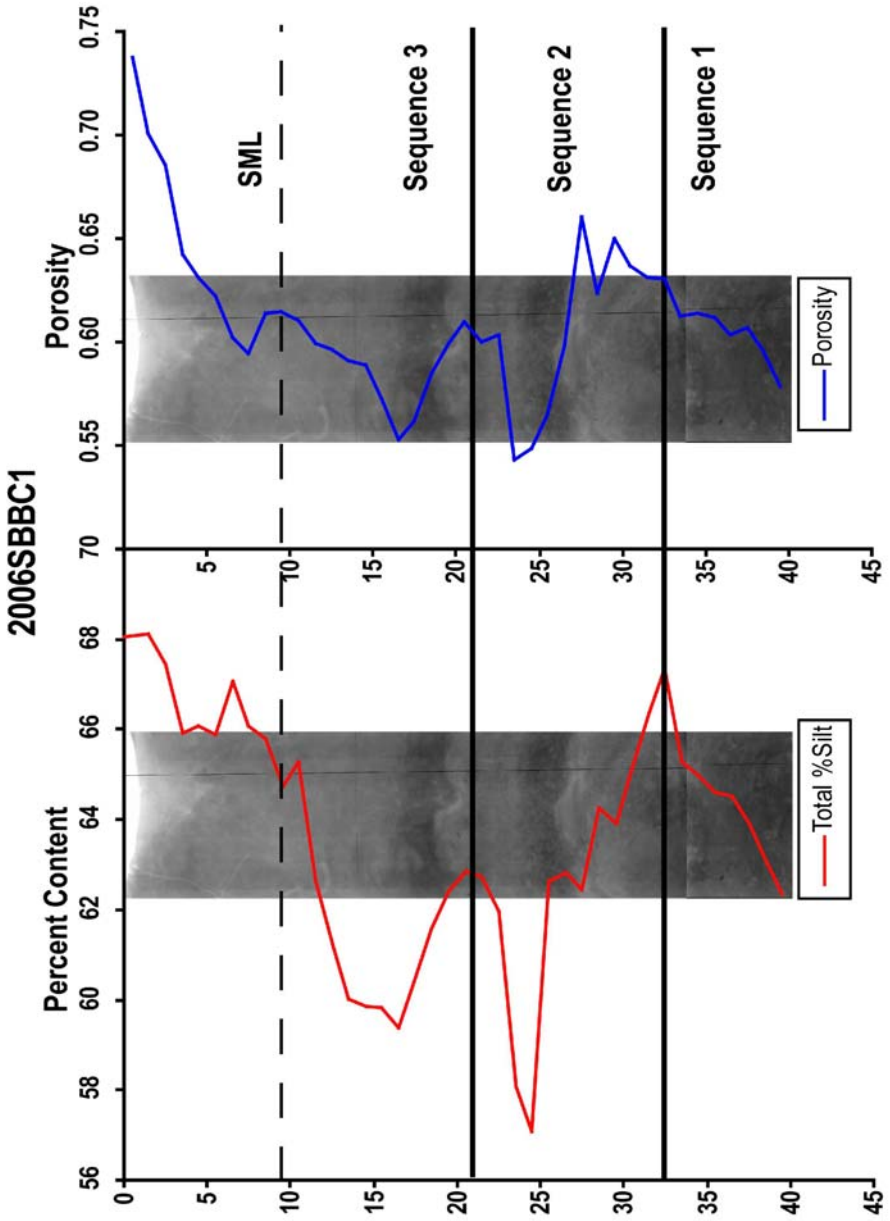

Fig. 55 Silt content (red line) and porosity (blue line) profiles from SBBC1. These parameters were used with the x-radiographs to define three sequences indicative of hyperpycnal flows. Each flow displays a coarsening fining upward sequence interrupted by an erosional layer. Sequence 3 is the most recent sequence which includes a bioturbated SML

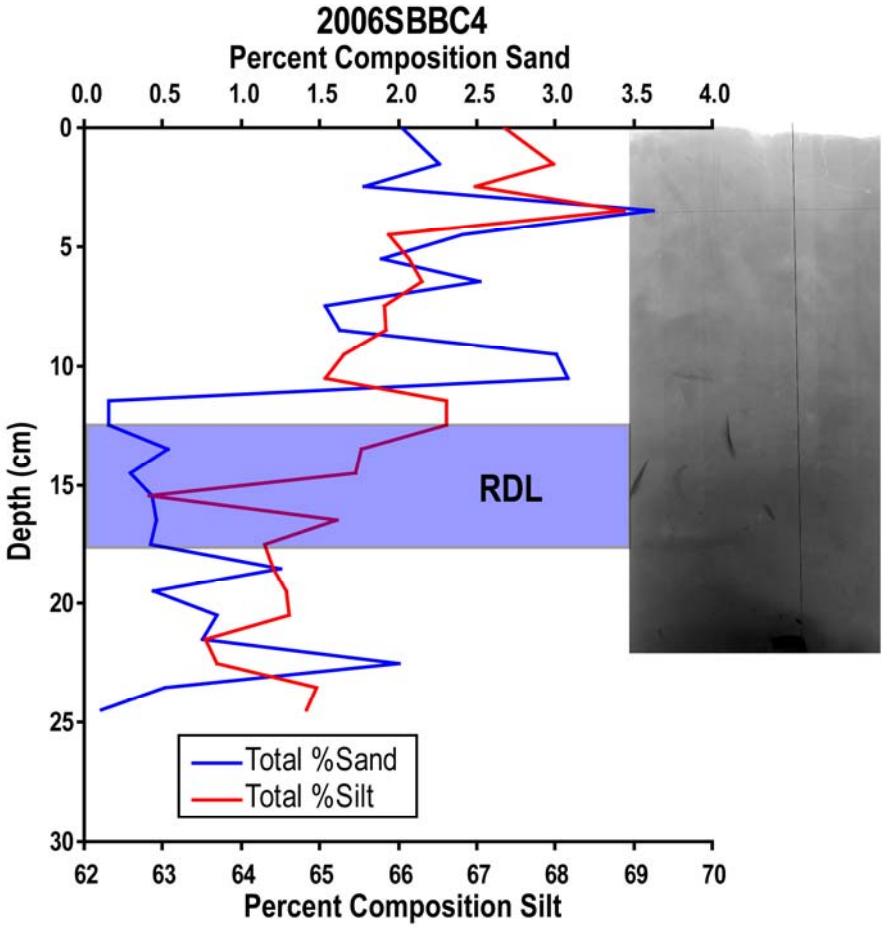

Fig. 56 Silt (red line) and sand (blue line) content profiles from core SBBC4 combined with the x-radiograph show a slight post-event response to the 1964 earthquake

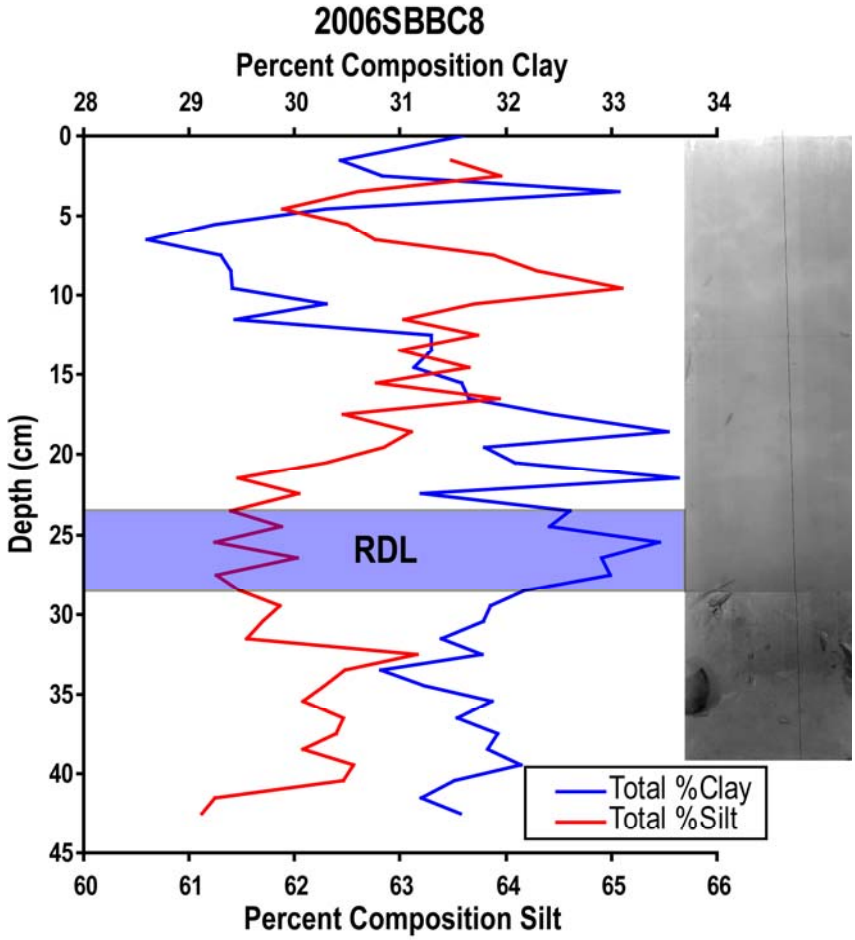

Fig. 57 Silt (red line) and clay (blue line) content profiles from core SBBC8 combined with the x-radiograph show a slight post-event response to the 1964 earthquake

peak in silt content and a decrease in porosity at ~33 cm, which is illustrated in the x-radiographs as a layer of coarse material.

Geochemical Signal

Mass-normalized (Σ_8 mg per gram) and carbon-normalized (λ_8 mg per 100mg C_{org}) concentrations of lignin as well as ratios of the eight LOP were used to investigate the source of the sediment preserved in the RDL. Syringyl (S) over Vanillyl (V) and Cinnamyl (C) over Vanillyl ratios were used to determine plant groups (gymnosperm vs. angiosperm) and tissue type (woody vs. leafy; Louchouarn et al., 1999; Goni and Hedges, 1992; Goni et al., 1993). Other markers were used to determine diagenetic state and alteration (degredation) of the material. Ratios of acid over aldehyde moieties for both V and S phenols ($(Ad/Al)_v$ and $(Ad/Al)_s$) indicate the freshness of the material. 3,5-dihydroxybenzoic acid over V (3,5Bd/V) is used as an indicator of soil degradation (Houel et al. 2006; Louchouarn et al. 1999). One caveat to using LOP is that the 3,5Bd and p-hydroxyl phenols (P) are not exclusive to terrestrial plants and may be elevated when brown macroalgae and kelps are prevalent. Ratios of p-hydroxyacetophenone to P (PON/P) are used as an indicator of whether there is a non-terrigenous component to the P over the sum of S and V (P/(V+S) degradation pathway (Houel et al. 2006; Louchouarn et al. 1999). Down-core profiles of these geochemical properties were generated for cores SBBC1, SBBC3, SBBC4, and SBBC8. Theses cores are representative of the depositional environments from each of the bays. Core SBBC3, taken at the mouth of North Bay showed no significant variation over the length of the core. This core did not penetrate the earthquake layer so observations made about the recovery of the system assume that the system is returning to pre-event conditions. The only significant change observed was in the SML where a bivalve had burrowed into the upper 6 cm of the profile (Fig. 52).

Core SBBC1 was taken in the physically dominated delta front environment at the head of North Bay (Fig. 19). The core shows repeated cycles of rapid deposition and erosion indicative of hyperpycnal flows (Fig. 55); (Mulder et al. 2003). Three sequences characterized by erosional surfaces followed by coarsening then fining upward sequences indicative of hyperpycnal deposits. Deposition resulting from

these events show a coarse lag atop the erosional surface composed of riverine/deltaic sediment. The deposit fines to the top of the deposit after which steady state, mixed marine/terrigenous deposition begins. Because these sequences have an erosional component, the tops of each previous sequence (containing the steady state deposition) are not preserved. Thus the uppermost sequence is the only example of steady state deposition. Elemental analysis was not well correlated to the grain size profiles, most of the LOP did not show significant variation over the length of the core, and none showed a RDL signature. Some of the LOP show a perturbation between 13.5 and 15.5 cm possibly indicating the top of the most recent event. PON/P values are low and constant (~0.17) from the surface to 13.5 cm before jumping to higher values (~0.19) and remaining relatively constant to the base of the core. This shift in PON/P is inversely correlated to a shift in P/(V+S) values (Fig. 58).

Core SBBC4 was taken in the northern sub-basin in West Bay and was the only core to show a significant geochemical signal of the earthquake. This site is the main depocenter of the northern sub-basin and is the depocenter for material trapped in the gyre set up in the northern sub-basin. The $^{210}Pb_{xs}$ profile contains a well defined, relatively thick RDL which was used as a reference for the changes in the geochemical properties (Fig. 49). The total lignin values measured in Simpson Bay (0.52 – 2.78 mg per mg OC) generally agree with a range of global values (0.06 – 6.8 mg per mg OC; Loh et al. 2008), but the net change in values does not change significantly down core when viewed in the context of anthropogenic changes to natural systems (Houel et al. 2006; Louchouarn et al. 1999; Louchouarn et al. 1997). When looked at in the context of variations to non-anthropogenic changes in basin properties, the changes seen do show identifiable trends within the analytical precision of the techniques used for the analysis. C/N ratios show a peak (8.75) at the base of the RDL (15.5 cm) and a trough (7.47) at the top of the RDL (13.5 cm); (Fig. 59). Above the RDL, C/N values increase sharply to values slightly higher than before the event. The peak and trough within the RDL are driven more by the %N values than the %OC. %N values are variable below and through the RDL, but are constant above the RDL. %OC values are relatively constant though the profile, but shows a gentle increase from the RDL through the surface interval. Σ_8 and λ_8 have highly variable profiles that diverge toward the surface (Fig. 59), but both signatures peak in the RDL. λ_8 decreases steadily after the event, while Σ_8 does not show a post event earthquake signal and

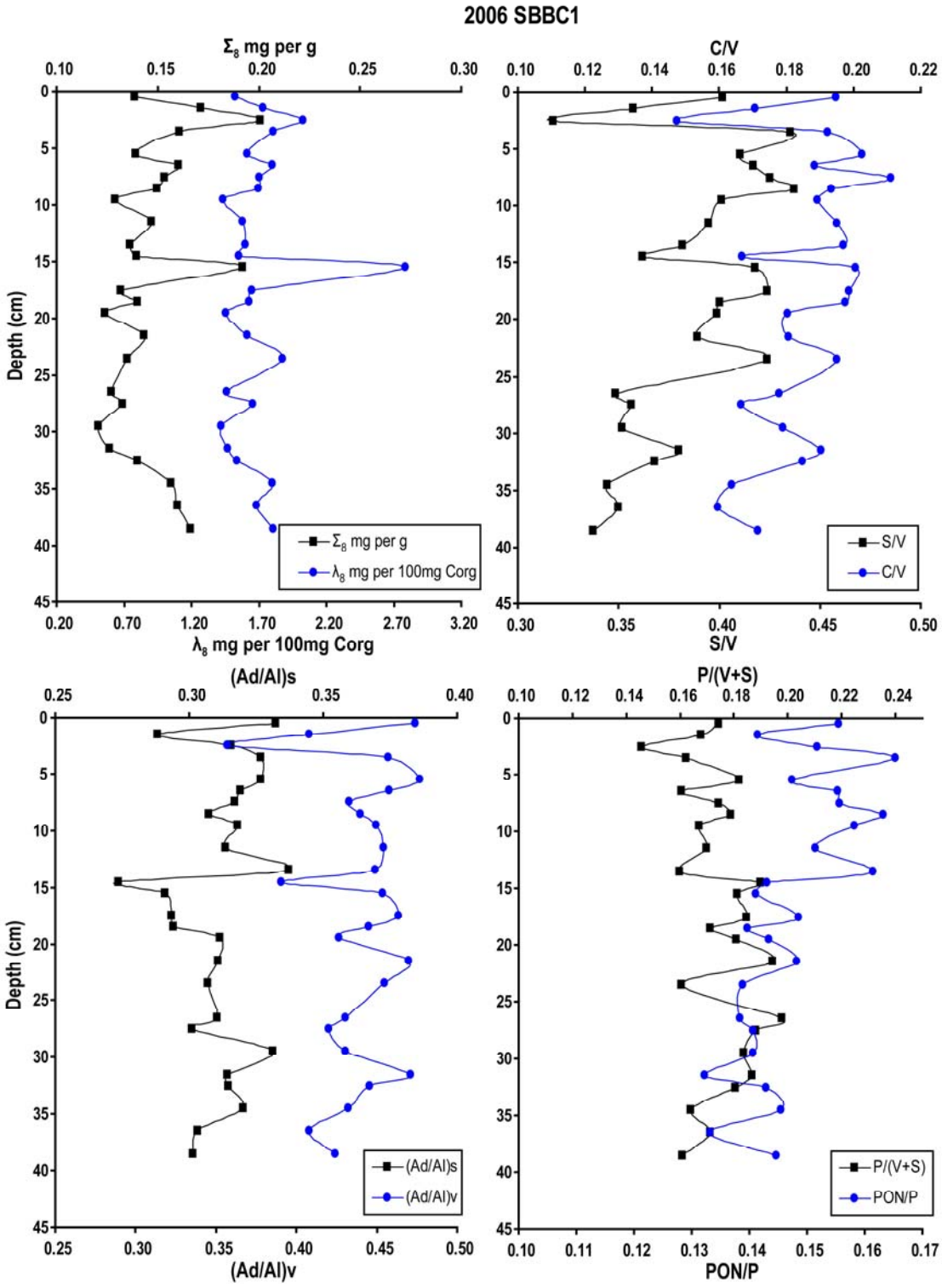

Fig. 58 LOP profiles for core SBBC1

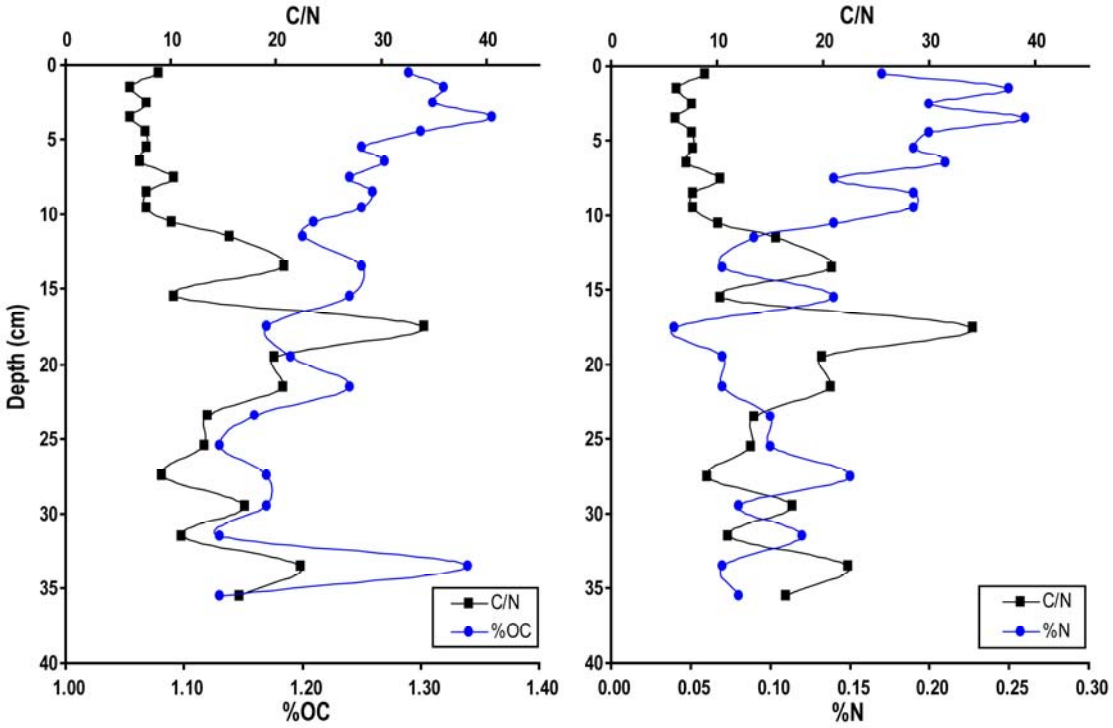

Fig. 58 Continued

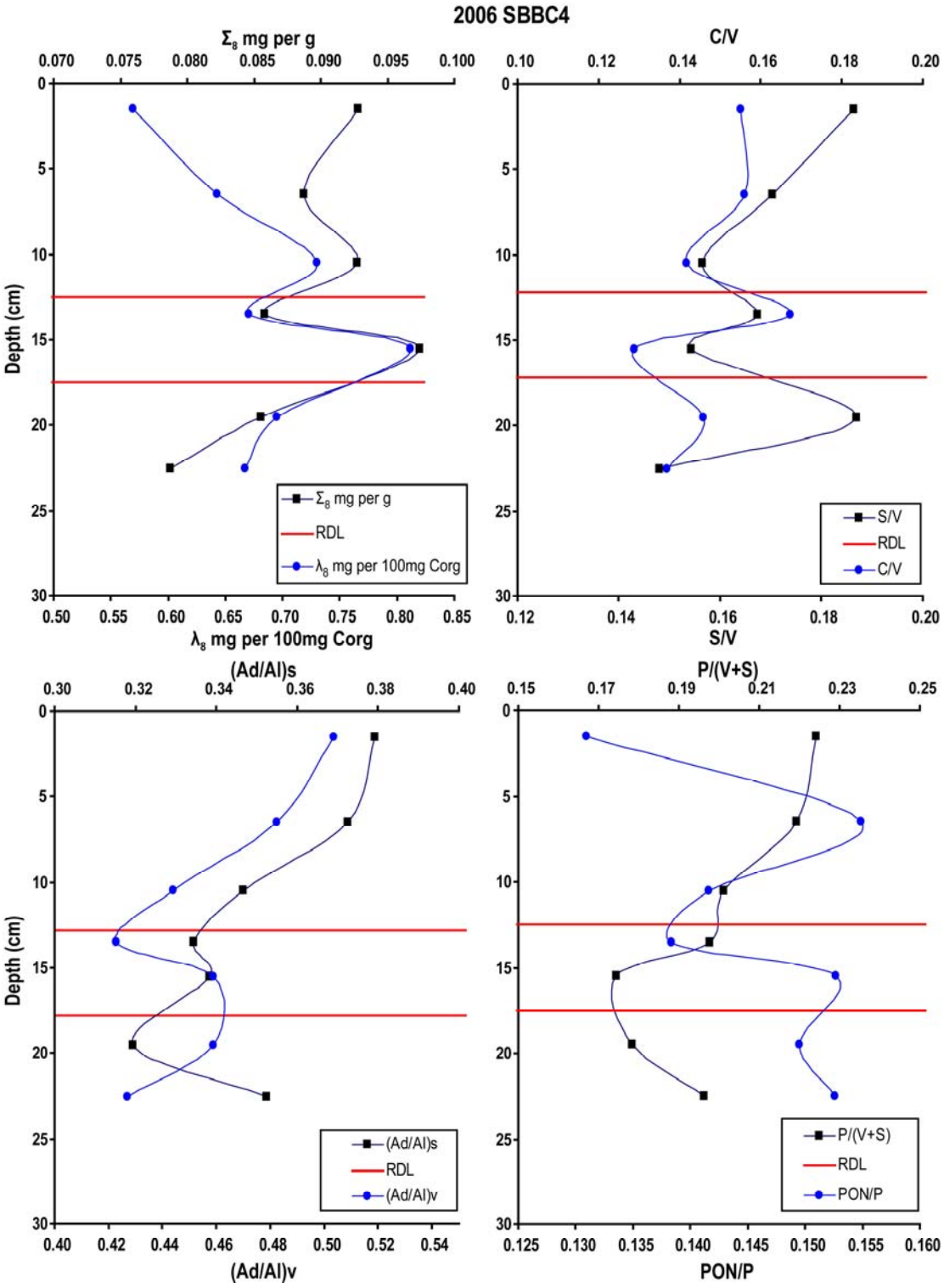

Fig. 59 LOP profiles for core SBBC4

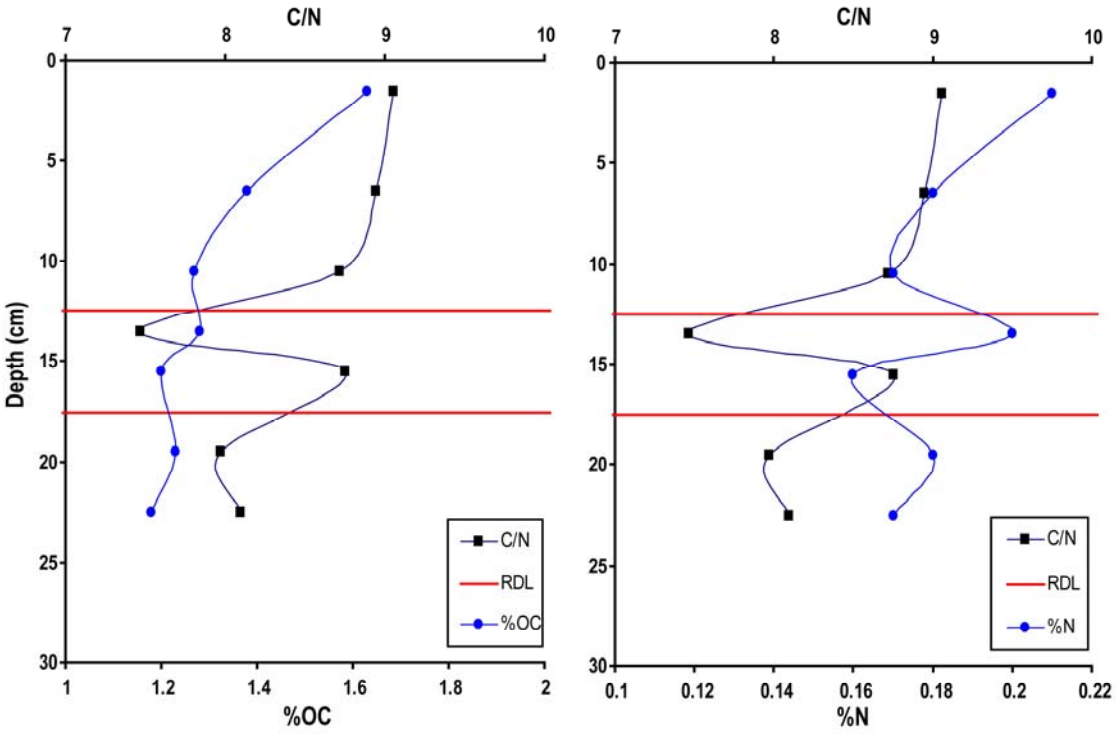

Fig. 59 Continued

remains relatively constant above the RDL. C/V and S/V ratios show large shifts below and through the event (Fig. 59), but the peak in Σ_8 and λ_8 are characterized by low values in these ratios. The LOP parameters that characterize the degree to which the material is degraded all display a trough correlated with the peak in Σ_8 and λ_8 and a general shift to more degraded values pre- and post-event. Both (Ad/Al)v and (Ad/Al)s are generally high (all greater than 0.3) indicating degraded terrestrial inputs even under normal conditions, and show an increase in post RDL values (as high as (Ad/Al)v = 0.5 and (Ad/Al)s = 0.38); (Fig. 59). PON/P values remain low and relatively constant through the profile indicating that marine signatures (kelps and brown macroalgae) do not contribute significantly to either the 3,5Bd/V or P/(V+S) ratios (Figs. 59 and 60). This is further supported by lower ratios than are found on the delta at the head of North Bay. The delta has an abundance of kelp which would likely skew the values. 3,5Bd/V

and P/(V+S) ratios increase steadily after the event. Comparisons of geochemical values to geotechnical properties do not show significant correlations because there is a lack of a strong textural signal in the core.

Core SBBC8 was taken in the depositional environment near the mouth of East Bay. This location has more of a marine contribution than SBBC4, but because it is landward of the point where the mouth of East Bay constricts, it is not an open marine environment. %OC, %N, and C/N values do not show an explicit record of event response in the RDL. C/N values maintain a steady increase from the base of the RDL to the surface, mirrored by the N values, but show a small net change. %OC values are more variable, and display a steep increase from the base of the RDL to 13.5 cm below which they become uniform to the surface (Fig. 61). These uniform values may be related to dynamics in the SML, but extend to twice the depth. The $^{210}Pb_{xs}$ profile does not show evidence of deep mixing, indicating that the system may be reaching equilibrium at higher values than before the event. Σ_8 and λ_8 values are uniform through the event, and decrease well below the event (15.5 cm) before increasing again (Fig. 61). λ_8 values in this case show a strong correlation to the clay fraction indicating that lignin is most likely found in DOM which is subsequently bound to the high surface area clay material (Fig. 62). S/V and C/V do not show a significant signal of the event, indicating that the terrigenous source material did not change (Fig. 60). As with SBBC4, all the constituents that measure degradation increase. Acid:aldehyde ratios, 3,5 Bd/V, and P/(V+S) all steadily increase throughout the core. PON/P values are generally low, but do show a sharp increase in the same interval that λ_8 increases (Figs. 60 and 61).

DISCUSSION

Earthquake Signal

Seafloor response to the 1964 earthquake throughout Simpson Bay varies in response to sediment supply and oceanographic conditions. The two responses in West Bay are most likely due to the current structure created by the interaction of tidal motion and basin morphology. Areas in Simpson Bay that are efficient sediment traps display a RDL that can be identified by a layer of uniform $^{210}Pb_{xs}$ activity. The first occurrence of ^{137}Cs is below this layer in most cores, indicating that the RDL was deposited after the

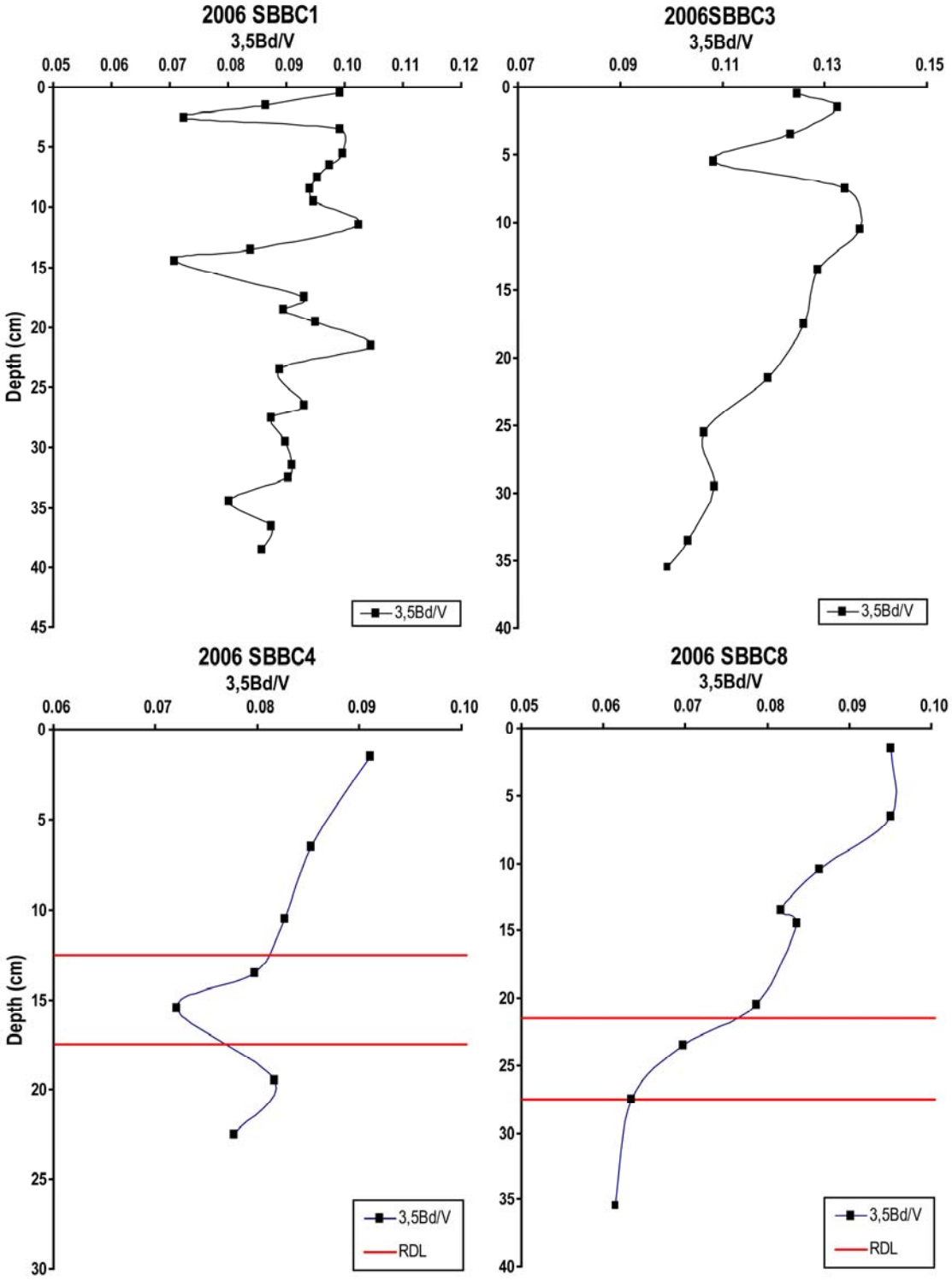

Fig. 60 3,5BdV profiles for the four cores chosen for LOP analysis

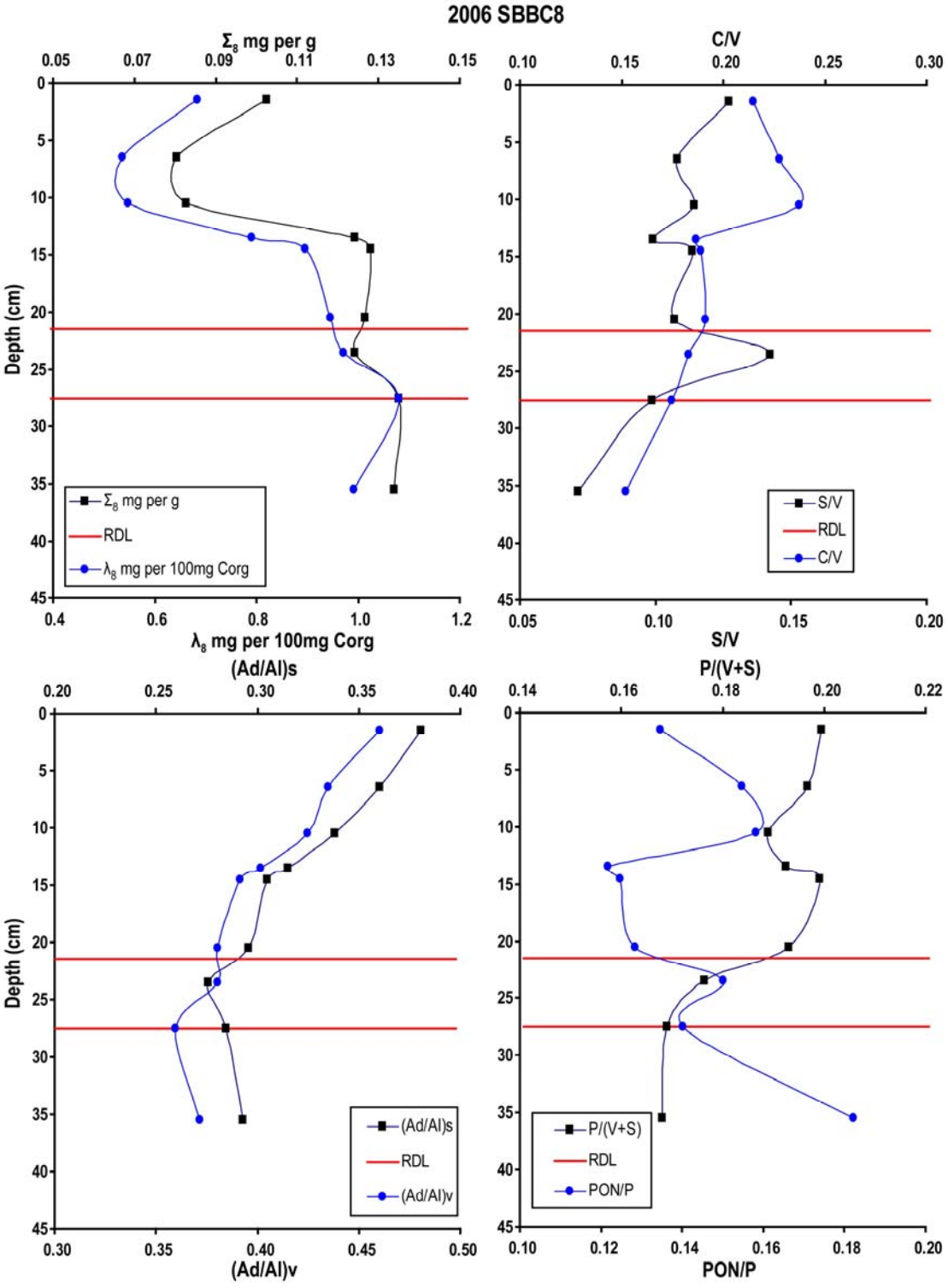

Fig. 61 LOP profiles for core SBBC8

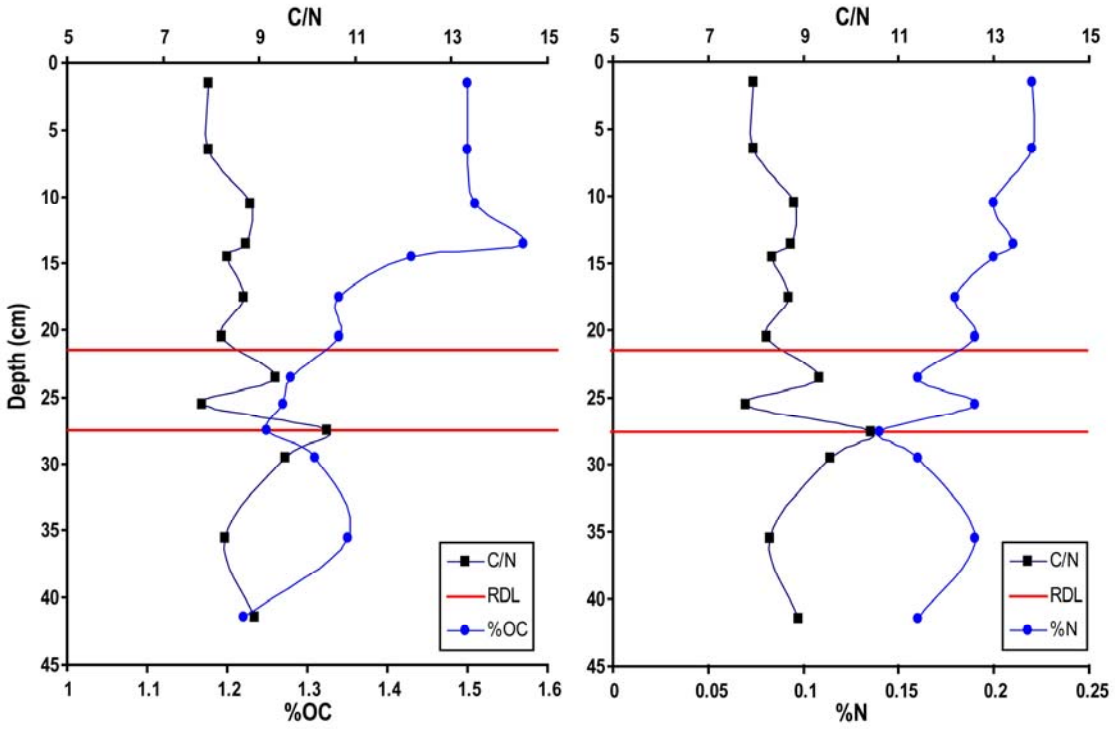

Fig. 61 Continued

1954 first occurrence of ^{137}Cs (Fig. 49). This helps validate the layer as the signal of the 1964 earthquake. Furthermore, by calculating the depth of 1964 using accumulation rates determined from $^{210}Pb_{xs}$ activity above the RDL, we find that the top of the RDL is at or above the calculated depth (Table 1). The observation that the depth falls below the top of the RDL validates the assumption that there is not less frequent, deep mixing below the identified SML and that the $^{210}Pb_{xs}$ derived accumulation rates are valid. Areas that are not efficient traps display an inflection above the first occurrence of ^{137}Cs, near the calculated 1964 depth using $^{210}Pb_{xs}$ accumulation rates from the interval above the inflection (Fig. 50).

Based on preliminary hydrographic data collected by Shelton Gay, tidal currents set up an anti-cyclonic gyre in the northern sub-basin (personal comm. 2008). This gyre traps sediment transported out of North Bay and from the river at the head of West Bay, contributing to the higher accumulation rates.

Cores SBBC17, SBBC4, and SBBC19 (Fig. 22) show well defined RDL ranging from 3 - 5 cm thick. A lack of definitive textural signal of the earthquake makes it difficult to determine the type of RDL and source of the RDL material. A lag deposit or fining upward sequence would provide some genetic information, but the lack of a significant signal requires the use of other parameters. This is where the stable isotopes and biomarkers become useful. Because biomarkers are found exclusively in terrestrial plant material, the presence, absence or relative abundance of the material gives evidence of the source of the material and can indicate transport mechanisms (de Leeuw et al. 1993; Louchouarn et al. 1999). Biomarker profiles from core SBBC4 in the northern sub-basin show that organic matter in the RDL has a more terrestrial signal than pre-event material. This indicates that the source of the RDL material has a significant terrestrial signal, most likely from discharge of deltaic material and transport of fresh material from the drainage basin. Pre- and post-event λ_8 values are low, indicating that the organic carbon signature in the northern sub-basin quickly returns to equilibrium. The low λ_8 contribution in the SML is correlated with high %OC. This correlation combined with the uniform Σ_8 values indicate that λ_8 is diluted in the SML with marine %OC and that preferential uptake of marine %OC over lignin by benthic fauna decreases this dilution with depth in the core. The lack of a strong textural signal indicates that mass wasting or gravity flows are not a probable transport mechanism, and that the slight changes in the textural signal after the event are in response to changes in the watershed.

Cores in the southern sub-basin (Figs. 26 and 50) show a signal of the earthquake, but it is not the RDL seen in the cores in East Bay and the northern sub-basin. Instead of having and RDL, these cores have an inflection in the $^{210}Pb_{xs}$ profile that corresponds to the 1964 depth. Accumulation rates above the event are higher than those below it. The lack of RDL is due to oceanographic processes that prevent the rapid deposition of significant amounts of sediment. Lower sedimentation rates reflect the effectiveness of the gyre in the northern sub-basin at keeping sediment in the head of the bay. The lack of significant freshwater input and shoreline available for erosion precludes the rapid discharge and resuspension of material. The two-fold increase in accumulation rate following the event indicates that there is a basin wide response to the event, but all responses are not created equal.

$^{210}Pb_{xs}$ profiles from East Bay are similar to those found in the northern sub-basin of West Bay indicating that it is also an efficient sediment trap. There is no gyre to trap sediment, but the narrow mouth may restrict flow enough to enhance deposition and reduce export (Fig. 48). Cores SBBC8, SBBC9, and SBBC21 (Fig. 31) all show well defined RDL's ranging from 5 - 6 cm thick and accumulation rates above the RDL range from 0.37 - 0.61 cm yr^{-1} (Table 1). Higher sand content in SBBC8 indicates that while it is an efficient trap of material discharged from the head of the bay, there is a higher content of coarser material transported from the relict glacial deposits at the mouth of the bay.

Although the sequences found in core SBBC1 at the head of North Bay cannot be ascribed specifically to the 1964 earthquake, they are none the less RDL (Fig. 55). These sequences display the classic coarsening fining trend observed in hyperpycnal flow deposits (Mulder and Syvitski 1995; Mulder, et al. 2003; St-Onge et al. 2004). In this core, none of the LOP show a RDL signature (Figs. 58), but some show an event signal at the top of the most modern hyperpycnal deposit (~14.5 cm). (Ad/Al)s and PON/P values increase while P/(V+S) and 3,5Bd/V values decrease. This combined with a sharp decrease in the S/V ratio indicates that there is a rapid, though small, change in the LOP signature at the interface between steady state deposition and hyperpycnal deposits. This shift represents a shift towards degraded woody material which is sequestered in the delta under normal circumstances, but eroded from the delta and discharged from the river during hyperpycnal flows. The inverse relationship between high PON/P versus lower P/(V+S) and 3,5Bd/V values indicates that kelps and macroalgae may contribute to the total lignin concentration (Figs. 58 and 60). This is the case due to significant amounts of kelps on the intertidal portion of the delta. Because the core is close to the delta, it is in the part of the flow that has a strong erosive component. Thus, the interface between the modern and hyperpycnal deposit is not preserved in the deeper sequences.

Cores SBBC4 and SBBC8 show different geochemical signals of the earthquake. Core SBBC4 shows a peak in both Σ_8 and λ_8 in the earthquake layer (~15.5 cm); (Figs. 59 and 62), as defined by the $^{210}Pb_{xs}$. This peak is correlated with low 3,5Bd/V and %N values (Figs. 59 and 60). These indicate a discharge of concentrated, fresh lignin. λ_8 values before and after the event are relatively similar, suggesting that the nature of sediment discharged into the system rapidly returns to pre-event values. This

interval also has a peak in the gravel fraction. The gravel component is less than 4% of the total grain size distribution and is composed of shell (marine) and plant material greater than 2 mm as opposed to lithic fragments. The reaction of each geochemical signature in the RDL suggests that the earthquake deposit has a terrestrial component which is diluted to a small degree by resuspended basin material.

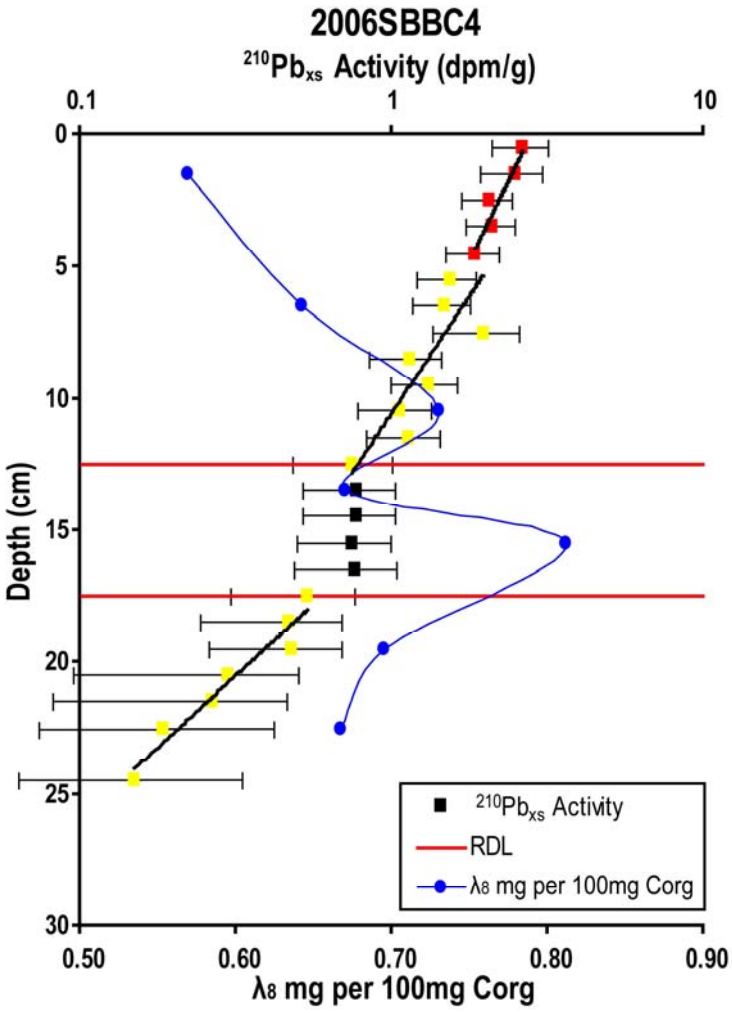

Fig. 62 $^{210}Pb_{xs}$ and λ_8 profiles for SBBC4 showing the earthquake response in both parameters. λ_8 values peak in the RDL indicating a pulse of terrigenous sediment

Σ_8 and λ_8 concentrations in SBBC8 provide signals in response to the earthquake because of their correlation to changes in the clay fraction (R^2 = 0.93 and 0.85 respectively; Fig. 63). They do not, however, have signatures in the RDL, as is found in SBBC4. Clay content below the RDL is uniform and increases slightly through the RDL. Clay content remains uniform, but at the higher content to 13.5 cm (7 cm above the top of the RDL), below which it gradually decreases to the base of the SML (Fig. 64). The lack of a pulse of terrigenous material suggests two possible response scenarios. The first scenario is that

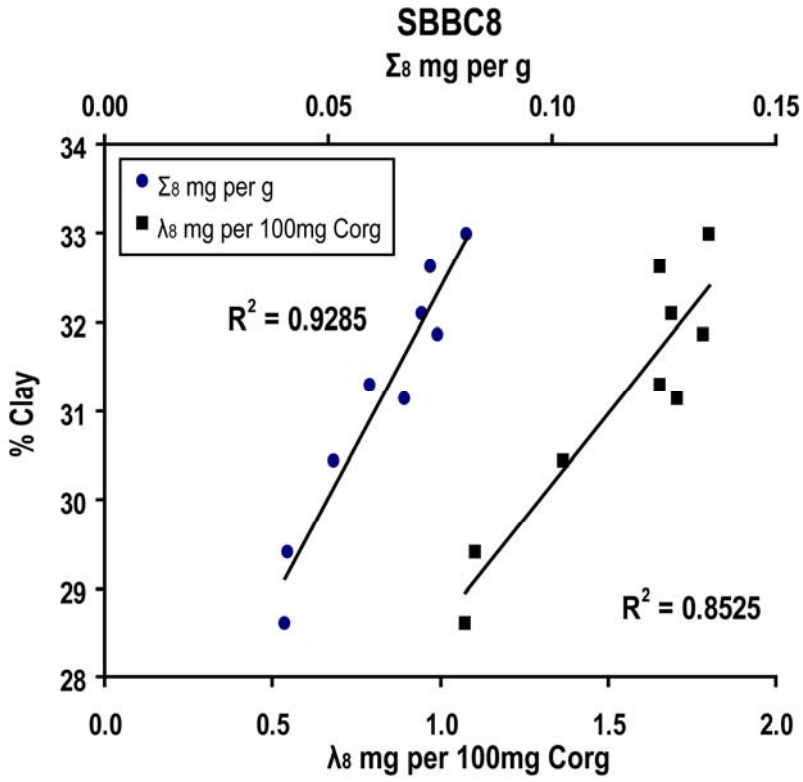

Fig. 63 λ_8 and Σ_8 versus clay content for core SBBC8. The regression shows good correlation between clay content and LOP parameters

East Bay has a more extensive deltaic system than West Bay and is better able to buffer terrestrial inputs. Regardless of the magnitude of the earthquake, the lake would sequester material and the strata preserved in the lake would record the effects of the earthquake. This may in fact be true. Satellite images show a small lake with a delta in the East Bay watershed, while there is no delta in West Bay. The second scenario is that there is a pulse of terrigenous material, but that SBBC8 is located sufficiently far from the source that the LOP are diluted to the point that there is no signal. Grain size data in the RDL show a

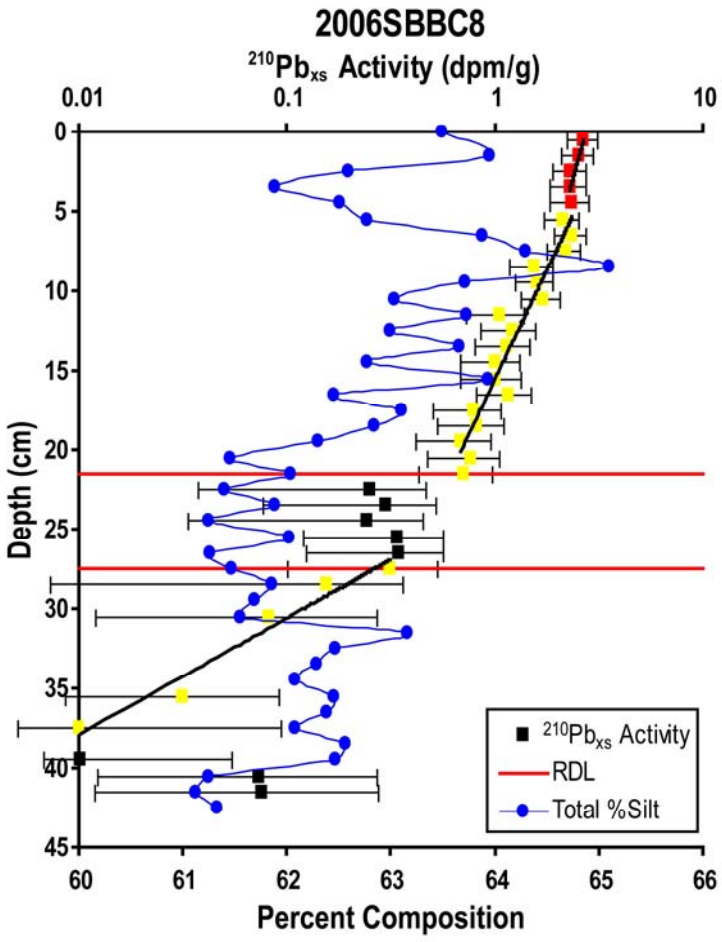

Fig. 64 $^{210}Pb_{xs}$ activity and silt content (blue line) profiles for core SBBC8 showing a slight earthquake response and recovery to the earthquake

small (< 1.5%) component of gravel size shell and organic debris, but the lignin signature varies little, indicating that the organic material may be basin derived sediment. Cores taken closer to the head of the bay have λ_8 concentrations in the surface interval two times higher than found in core SBBC8 and concentrations in the core taken on the plateau at the head of the bay are two times higher than SBBC9 (Fig. 31). Because of the closer proximity to the terrestrial source, profiles of SBBC9 may display a signal in the earthquake layer, but SBBC8 does not. In this scenario, the material in the RDL in SBBC8 is composed predominantly of resuspended basin material. Grain size profiles show a shift to finer material at the base of the RDL, which remains uniform through and above the RDL before gradually returning to pre-event values. A shift to finer material would be expected because a higher percentage of fine material would be resuspended and would be transported farther. Because each scenario would result in similar profiles, the probable solution is that there is a component of each scenario.

Basin Recovery

All of the cores in Simpson Bay, where an earthquake signal was identified, show an increase in sedimentation rates following the earthquake. This increase is the result of erosion of previously deposited subtidal shoreline material (basin material) and deltaic deposits. The area was uplifted ~1.5 m so it is reasonable to presume that a significant portion of sediment that was sequestered below the wave base became available for erosion and transport. Also, due to loss of accommodation, sediment would bypass deltas and erode river channels until a new equilibrium is reached. In some cases, regression lines generated from the decay of $^{210}Pb_{xs}$ activity have slightly lower confidence above the RDL, suggesting that there may be post-event variability in sediment discharge. Again, there is little overwhelming geotechnical evidence to support any basin wide recovery to the event.

Core SBBC4 shows not only the earthquake generated RDL, but also the recovery of the watershed to the disturbances. λ_8 profiles show that after the spike in the RDL, values rapidly return to lower, pre-event levels (Figs. 59 and 60). Elevated %OC values and uniform Σ_8 values in the SML indicate that low λ_8 values are forced by diagenetic processes. λ_8 is diluted by marine organic matter that is consumed quickly in the SML, causing relatively lower carbon normalized concentrations (Fig. 59).

Higher %OC and %N indicate that the organic material in the SML has a higher marine component than material below the SML. The divergence of the Σ_8 and λ_8 signatures above the RDL indicates that during the earthquake recovery, variations in the signatures of the LOP in the profile are driven by diagenetic processes as opposed to the dilution of terrestrial material in the system. Slightly higher total lignin concentrations and higher sedimentation rates after the event can be attributed to a greater component of marine sourced LOP, specifically, the continued erosion of uplifted basin and deltaic sediment with a kelp and brown macroalgae signature. Below the RDL, changes in Σ_8 and λ_8 values are coupled, suggesting that while in equilibrium, variations in the profile are due to watershed changes and dilution of lignin (Fig. 59). Before the event, shoreline sediment was not eroded and the low lignin concentrations are representative of watershed discharge. This leads to the conclusion that the nature of carbon in a natural system is driven by dilution of the terrestrial signal while changes in a perturbed system are influenced by diagenetic processes and the inclusion of marine derived LOP. West Bay has not totally recovered from the event, evidenced by increased %OC and Σ_8 and higher accumulation rates due to erosion caused by uplift. The erosion of basin material is supported by increases in 3,5Bd/V, P/(V+S), and the acid:aldehyde ratios (Figs. 59 and 60).

Changes in the geochemical profiles in East Bay reflect the recovery to the earthquake, but are correlated to changes in grain size distribution (Figs. 61 and 63). Σ_8 and λ_8 are bound to the clay fraction, and responds as the clay content increases after the earthquake. 3,5Bd/V, P/(V+S), and the acid:aldehyde ratios all continuously increase from the base of the core to the surface (Figs. 60 and 61) and are not as well correlated to the grain size. This may reflect underpinning environment changes that have changed the signature of lignin in the system. This is also reflected in the correlated variations of Σ_8 and λ_8 indicating that dilution is more important than diagenisis.

The recovery of North Bay to the earthquake is less well defined due to the lack of information during and before the event. In general lignin values decrease, indicating a possible shift to pre earthquake conditions mirrored by an increase in the degredation signature in the 3,5Bd/V, P/(V+S), and the acid:aldehyde ratios, though these changes are all small and the evidence is circumstantial (Figs. 60 and 65). The slight inverse correlation of PON/P to 3,5Bd/V indicates that changes in degredation may be due

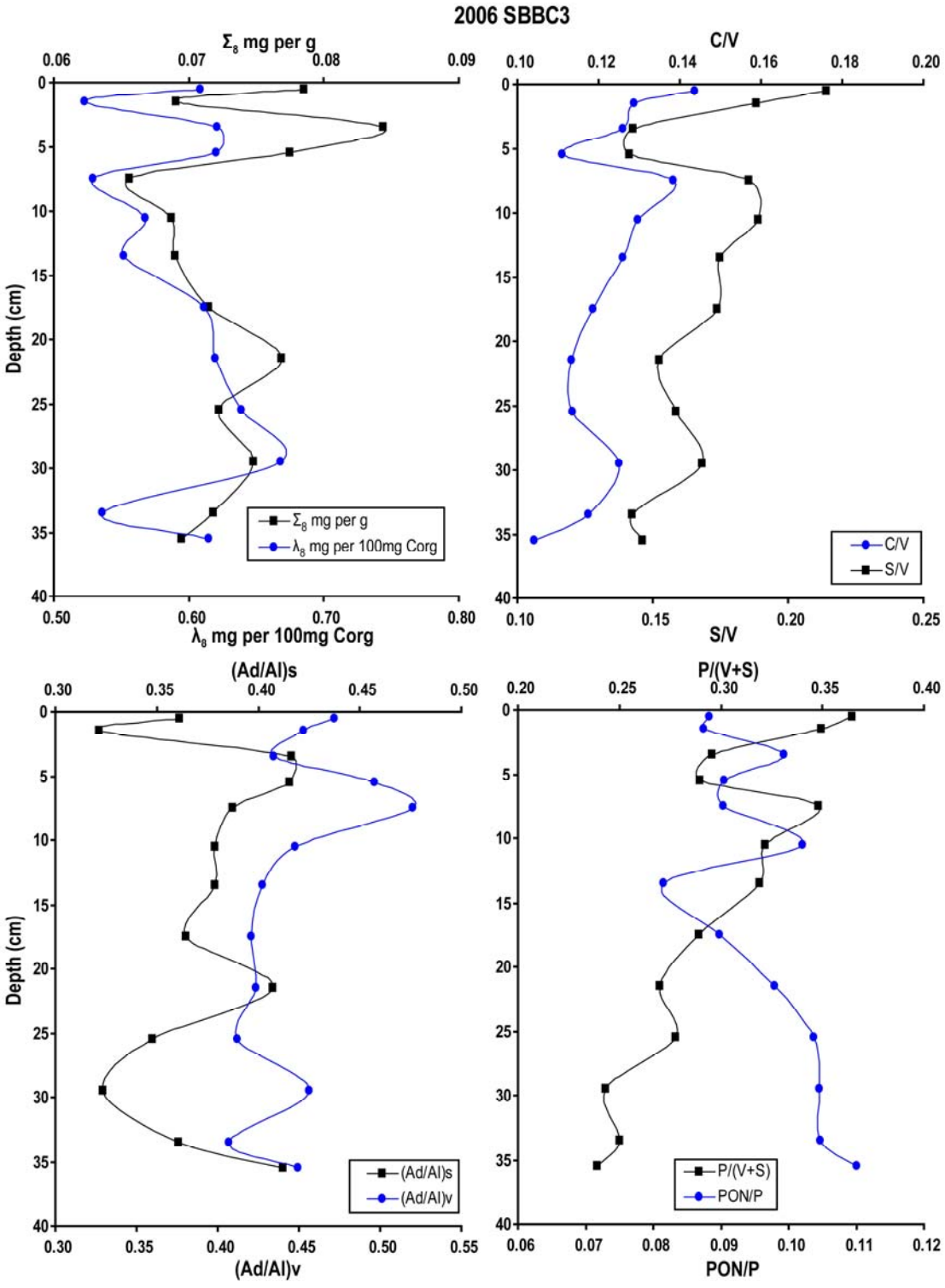

Fig. 65 LOP profiles for core SBBC3

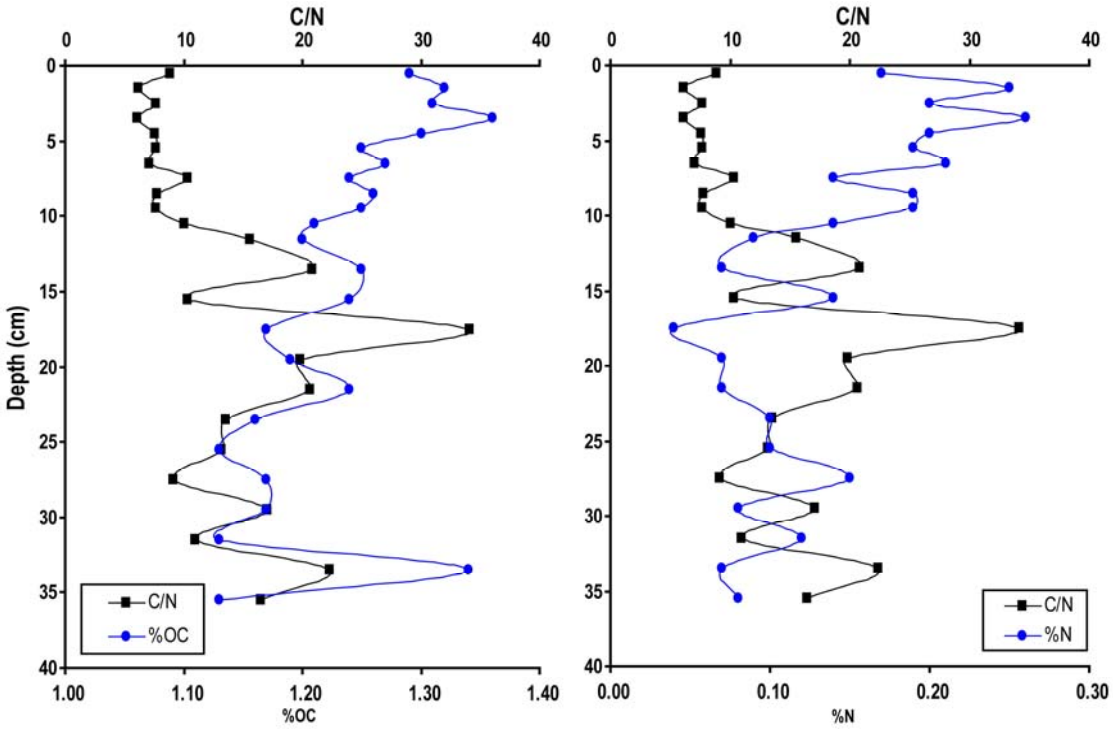

Fig. 65 Continued

to a decreasing component of eroded uplifted basin sediment, while decreasing clay content may indicate a possible return to a previous equilibrium. Variability in the SML is a result of a bivalve burrow seen in the x-radiograph (Fig. 52).

CONCLUSION

1. The geotechnical indicators (grain size, porosity, etc…) used to identify rapidly deposited layer in many systems throughout the world were not useful in conclusively determining the extent of event deposits in Simpson Bay. Though it was in close proximity to the second largest earthquake in recorded history, there were not significant textural changes that confidently identified the event in the short sediment cores taken throughout the basin. Because of this, radioisotope and geochemical tools proved invaluable in identifying the seafloor response and

recovery to this large event. Throughout the system we find that each watershed:basin system responds differently to the event and recovers at different rates.

2. The event signal relied on a number of factors: oceanographic conditions, watershed properties, and proximity to sediment sources. Environments close to the delta front receive episodic inputs of sediment at both seasonal (changes in runoff) and event (hyperpycnal and turbidity flows) frequencies. Because the seasonal changes in discharge do not allow for reliable geochronologies and events erode material, it is not possible to ascribe individual sequences to specific events. Environments sufficiently far from the delta front to be unaffected by these changes, but close enough to receive sediment from terrestrial sources see a direct radioisotope and geochemical signal of the earthquake. Radioisotope profiles show a deposit of sediment with uniform activity bound above and below by log-linearly decaying activity. The core near the terrestrial input showed a peak in biomarkers associated with fresh terrestrial material. After the rapidly deposited layer, lignin concentrations returned to lower levels with higher degredation ratios indicative of a mature basin. Environments that are removed from a terrestrial source show a rapidly deposited layer in the radioisotope signature, but do not show the same peak in terrestrial material that is seen closer to the terrestrial source. This may be due to a combination of factors, including dilution of the lignin signal and the basin specific trapping of sediment.
3. Oceanographic processes work to intensify or prevent the preservation of the event signal. Protected areas such as East Bay display event deposits, while open areas such as the southern sub-basin in West Bay show inflections in the radioisotope profiles, but no deposit. The interaction of oceanographic process on basin morphology can create mini-basins with drastically different event signatures. The northern sub-basin, separated from the southern sub-basin by a rock promontory, shows radioisotope profiles more similar to those found in East Bay than the southern sub-basin. This is due to a gyre set up at the head of the bay that traps sediment. The southern sub-basin is more influenced by marine conditions in PWS and did not preserve a rapidly deposited layer.

4. While the response to the event is different throughout the system, the recovery is similar. Most radioisotope profiles have higher variability (lower confidence in the regression) and higher sedimentation rates after the earthquake. This could be due to flushing of material from the watershed and shoreline erosion. Lignin values suggest that there may be a significant component of marine material with a lignin signature in the post earthquake sediment. This may come from eroded shorelines and deltaic deposits with lignin rich brown macroalgae and kelps. Some cores do show a small change in grain size as a result of the event, but the changes are not significant.

REFERENCES

Aarseth I (1997) Western Norwegian fjord sediments: age, volume, stratigraphy, and the role as temporary depository during glacial cycles. Mar Geol 143:39-53

ADNR (1964) Earthquake 1964 1:2,000,000. Alaska Department of Natural Resources, EVOS: Alaska Dept. of Natural Resources/Lands Record Information Service

ADNR (1998) Alaska glaciers 1:1,000,000. Alaska Department of Natural Resources, Land Records Information Service

AGDC (1998) Alaska precipitation 1:2,000,000. USGS, Water Resources for Alaska GIS Datasets, Alaska Geospatial Data Clearinghouse

Aller RC (1982) The effects of macrobenthos on chemical properties of marine sediment and overlying water. In: McCall PL, Tevesz MJS (eds) Animal-sediment relations. Plenum Press NY, pp 53-102

Aller RC, Dodge RE (1974) Animal-sediment relations in a tropical logoon, Discovery Bay, Jamaica. J Mar Res 32:209-232

Andrews JT, Syvitski JPM (1994) Sediment fluxes along high latitude glaciated continental margins: Northeast Canada and Eastern Greenland. In: Hay W (ed.) Global sedimentary geofluxes. National Academy of Sciences Press, Washington, pp 99-115

Barrie JV, Conway KW (1999) Late Quaternary and postglacial stratigraphy of the Northern Pacific margin of Canada. Quat Res 51:113–123

Bentley SJ, Nittrouer CA (1999) Physical and Biological Influences of the formation of Sedimentary Fabric in an oxygen-restricted depositional environment: Eckernforde Bay, Southwestern Baltic Sea. Palaios 14:585-600

Bentley SJ, Nittrouer CA (2003) Emplacement, modification, and preservation of event strata on a flood-dominated continental shelf: Eel shelf, Northern California. Cont Shelf Res 23:1465-1493

Bianchi TS, Lambert CD, Santschi PH, Gou L (1997) Sources and transport of Land-derived particulate and dissolved organic matter in the Gulf of Mexico (Texas shelf/slope): the use of lignin-phenols and loliolides as biomarkers. Org Geochem vol 27(1/2):65-78

Bogen J (1983) Morphology and sedimentology of deltas in fjord and fjord-valley lakes. Sedimentary Geol 36:245-267

Cai J, Powell RD, Cowan EA, Carlson PR (1997) Lithofacies and seismic-reflection interpretation of temperate glacimarine sedimentation in Tarr Inlet, Glacier Bay, Alaska. Mar Geol 143:5-37

Carlson PR (1989) Seismic reflection characteristics of glacial and glacimarine sediment in the Gulf of Alaska and adjacent fjords. Mar Geol 85:391–416

Christensen ER (1982) A model for radionuclides in sediments influenced by mixing and compaction. J Geophys Res 87(C1):566-572

Coulter HW, Migliaccio RR (1965) Effects of the Earthquake of March 27, 1964, at Valdez, Alaska. The Alaska Earthquake, March 27, 1964: Effects on Communities. U. S. Geological Survey Prof Paper 542-C p 44

Cowan EA, Powell RD (1991) Ice-proximal sediment accumulation rates in a temperate glacial fjord, southeaster Alaska. In: Anderson JB, Ashley GM (eds) Glacial marine sedimentation: Paleoclimatic significance. Geol Soc Amer Special Paper 261 pp 61-73

Davidson G (1904) The glaciers of Alaska: that are shown on Russian charts or mentioned in older narratives. Extracted from the Transactions and Proceedings of The Geological Society of the Pacific; vol III, Series II, June 1904. Cunningham, Curtis & Welch, San Francisco, CA

DeGeest AL, Mullenbach BL, Puig P, Nittrouer CA, Drexler TM, Durrieu de Madron X, Orange DL (2008) Sediment accumulation in the western Gulf of Lions, Fance: the role of Cap de Creus Canyon in linking shelf and slope sediment dispersal systems. Continental Shelf Research Continental Shelf Research (in press) doi:10.1016/j.csr.2008.02.008

de Leeuw JW, Largeau C (1993) A review of macromolecular organic compounds that comprise living organisms and their role in lerogen, coal, and petroleum formation. In: Engel MH, Macko SA (eds) Organic geochemistry: principles and applications. Plenum Press NY pp 23-72

DeMaster DJ, McKee BA, Nittrouer CA, Qian J, Cheng G (1985) Rates of sediment accumulation and particle reworking based on radiochemical measurements from continental shelf deposits in the East China Sea. Cont Shelf Res 4(1-2):143-158

Denton GH, Porter SC (1970) Neoglatiation. Sci Amer 222:101-110

Denton GH, Karlen W (1973) Holocene climatic variation – their pattern and possible cause. Quat Res 3:155-205

Doser DI, Veilleux AM, Velasquez M (1999) Seismicity of the Prince William Sound region for over thirty years following the 1964 Great Alaskan Earthquake. Pure App Geophysics 154:593-632

Dowdeswell JA, Whittington RJ, Jennings AE, Andrews JT, Mackensen A, Marienfeld P (2000) An origin for laminated glacimarine sediments through sea-ice build-up and suppressed iceberg rafting. Sedimentology 47:557–576

Earth Explorer: Data Set Selection (1992) USGS, http://edcsns17.cr.usgs.gov/EarthExplorer/.

Farmer GL, Ayuso R, Plafker G (1993) A coast mountains provenance for the Valdez and Orca groups, southern Alaska, based on Nd, Sr, and Pb isotopic evidence. Earth Planet Sci Lett 116:9–21

Gay SM III, Vaughn SL (2001) Seasonal hydrography and tidal currents of bays and fjords in Prince William Sound, Alaska. Fish Oceanogr 10 Suppl 1:159–193

Gilbert R (1982) Contemporary sedimentary environments on Baffin Island, N.W.T. Canada: Glaciomarine processes in fjords of eastern Cumberland Peninsula. Arctic Alpine Res 14:1-12

Goldberg ED, Kodie M (1962) Geochronological studies of deep-sea sediments by the thorium-ionioum method. Geochim Cosmochim Acta 26:417-450

Goni MA, Hedges JI (1992) Lignin dimmers: Structures, distribution, and potential geochemical applications. Geochim Cosmochim Acta 56:4025-4043

Goni MA, Nelson B, Blanchette RA, Hedges JI (1993) Fungal degradation of wood lignins: Geochemical perspectives from CuO-derived phenolic dimmers and monomers. Geochim Cosmochim Acta 57:3985-4002

Goni MA, Yunker MB, Macdonald RW, Eglinton TI (2000) Distribution and sources of organic biomarkers in arctic sediments from the Mackenzie River and Beaufort Shelf. Mar Chem 71:23-51

Guinasso Jr NL, Schink DR (1975) Quantitative estimates of biological mixing rates in abyssal sediments. J Geophys Res 80:3032-3043

Hallet B, Hunter L, Bogen J (1996) Rates of erosion and sediment evacuation by glaciers: a review of field data and their implications. Global Planet Change 12:213–235

Hayes SP, Schumacher J D (1977) Gulf of Alaska study of mesoscale oceanographic processes. NOAA/OCSEAP RU 138, Ann Rep 14:251-328

Hedges JI, Ertel JR (1982) Characterization of lignin by gas capillary chromatography of cupric oxide oxidation products. Analyt Chem 54:174-178

Hoskin CM, Burell DC (1972) Sediment transport and accumulation in a fjord basin, Glacier Bay, Alaska. J Geol 80:539-551

Hoskin CM, Burell DC, Freitag GR (1978) Suspended sediment dynamics in Blue Fjord, Western Prince William Sound Alaska Estuarine Coastal Mar Sci 7:1-16

Houel S, Louchouarn P, Lucotte M, Canuel R, Ghaleb B (2006) Translocation of soil organic matter following reservoir impoundment in boreal systems: Implications for in situ productivity. Lim Oceanogr 51(3):1497-1513

Hunter LE, Powell RD, Lawson DE (1996) Flux of debris by ice at three Alaskan tidewater glaciers. J Glaciology 12(140):123-135

Jaeger JM, Nittrouer CA (1999) Sediment deposition in an Alaskan fjord: Controls on the formation and preservation of sedimentary structures in Icy Bay. J Sedimentary Res 69(5):1011-1026

Jaeger JM, Nittrouer CA (2006) A quantitative examination of modern sedimentary lithofacies formation on the glacially influenced Gulf of Alaska continental shelf. Cont Shelf Res 26(17-18):2178-2204

Jaeger JM, Nittrouer CA, Scott ND, Milliman JD (1998) Sediment accumulation along a glacially impacted mountainous coastline: North-East Gulf of Alaska. Basin Res 10:155–173

Jaeger J, Hallet B, Pavlis T, Sauber J, Lawson D, Millman J, Powell R, Anderson SP, Anderson R (2001) Orogenic and glacial research in pristine Southern Alaska. Eos Trans Am Geophys Union 82(19):213–216

Jin M, Wang J (2004) Interannual variability and sensitivity study of the ocean circulation and thermohaline structure in Prince William Sound, Alaska. Cont Shelf Res 24:393-411

Johnson JM, Satake K, Holdahl SR, Sauber J (1996). The 1964 Prince William Sound earthquake: joint inversion of tsunami and geodetic data. J of Geophys Res 101(B1):523-532

Jumars PA, 1978. Spatial autocorrelation with RUM (Remote Underwater Manipulator): vertical and horizontal structure of a bathyal benthic community. Deep-Sea Research 25 589-604

Jumars PA, Self RFL, and Nowell ARM, 1982. Mechanics of particle selection by tentaculate deposit-feeders. Journal of Experimental Marine Biological Ecology 64 47-70

Knebel HJ (1986) Holocene depositional history of a large glaciated estuary, Penobscot Bay, Maine. Mar Geol 73:215–236

Kodie M, Soutar A, Goldberg ED (1972) Marine geochronology with 210Pb. Earth Planet Sci Lett 14:422-446

Kostaschuk RA, McCann SB (1983) Observations on delta-forming processes in a fjordhead delta, British Columbia. In: Syvitski JPM, Skei J (eds), Sedimentology of fjords. Sedimenaty Geol 36 pp 269-288

Krishnaswami Lal SD, Martin JM, Meybeck M (1971) Geochronology of lake sediments. Earth Planet Sci Lett 11:407-414

Kuehl SA, Nittrouer CA, DeMaster DJ, 1982. Modern sediment accumulation and strata formation on the Amazon continental shelf. Mar Geol 49:279-300

Kuehl SA, DeMaster DJ, Nittrouer CA (1986) Nature of sediment accumulation on the Amazon continental shelf. ContShelf Res 6(1-2):209-225

Landsat.org (2005) http://bsri.msu.edu/cgi-bin/access7g.pl

Lee H, Ryan H, Kayen RE, Haeussler PJ, Dartnell P, Hampton MA (2007) Varieties of submarine failure morphologies of seismically-induced landslides in Alaskan fjords. Norwegian J Geol vol 86:221-230

Lemke RW (1967) Effects of the Earthquake of March 27, 1964, at Seward, Alaska. The Alaska Earthquake, March 27, 1964: effects on communities. U. S. Geological Survey Prof Paper 542-E p 51

Lethcoe J (1990) An observer's guide to the geology of Prince William Sound, Alaska. Prince William Sound Books Valdez, Alaska

Levin LA, DeMaster DJ, McCann LD, Thomas CL (1986) Effects of giant protozoans (class:Xenophyophorea) on deep-seamount benthos. Mar Ecological Program Series 29:99-104

Loh PS, Reeves SM, Harvey SM, Overnell J, Miller AEJ (2008) The fate of terrestrial organic matter in two Scottish sea lochs. Estuarine Coastal Shelf Sci 76:566-579

Louchouarn P, Lucotte M, Canuel R, Gagne J-P, Richard L-P (1997) Sources and early diagenesis of lignin and bulk organic matter in the sediments of the Lower St. Lawrence Estuary and the Saguenay Fjord. Mar Chem 58:3-26

Louchouarn P, Loucotte M, Farella N (1999) Historical and geographical variations of sources and transport of terrigenous organic matter within a large-scale coastal environment. Org Geochem 30:675-699

Lysa A, Sejrup H P, Aarseth I (2004) The late glacial-Holocene seismic stratigraphy and sedimentary environment in Ranafjorden, northern Norway. Mar Geol 211:45-78

Manley WF, Kaufman DS (2002) Alaska PaleoGlacier Atlas: Institute of Arctic and Alpine Research (INSTAAR) University of Colorado http://instaar.colorado.edu/QGISL/ak_paleoglacier_atlas, v1

Milliman JD, Syvitski JPM (1992) Geomorphic/tectonic control of sediment discharge to the ocean: the importance of small mountainous rivers. J Geol 100:525–544

Molnia BF, (1983) Subarctic glacial-marine sedimentation: a model. In: Molnia BF (ed) Glacial-marine sedimentation. Plenum Press NY pp 95-114

Muench RD, Heggie DT (1978) Deepwater exchange in Alaskan subarctic fjords. In: Kjerfic B (ed) Estuarine Transport Processes. Univ South Carolina Press, Columbia, South Carolina pp 239-267

Mulder T, Syvitski JPM (1995) Turbidity currents generated at river mouths during exceptional discharges to the world ocean. J Geol 103:285-299

Mulder T, Syvitski JPM, Migeon S, Faugeres J-C, Savoye B (2003) Marine hyperpycnal flows: initiation, behavior and related deposits. Mar Pet Geol 20:861-882

Nishenko SP, Jacob KH (1990) Seismic potential of the Queen Charlotte Alaskan Aleutian seismic zone. J Geophys Res 95:2511-2532

Nittrouer CA, Sternberg RW (1981) The formation of sedimentary strata in an allochthonous shelf environment: the Washington continental shelf. Mar Geol 42:201-232

Nittrouer CA, Sternberg RW, Carpenter R, Bennett JT (1979) The use of Pb-210 geochronology as a sedimentological tool: application to the Washington continental shelf. Mar Geol 31:297–316

Nittrouer CA, Demaster DJ, McKee BA, Cutshall NH, Larsen IL (1983/1984) The effect of sediment mixing on Pb-210 accumulation rates for the Washington continental shelf. Mar Geol 54:201-221

Nittrouer CA, DeMaster DJ, McKee BA (1984) Fine-scale stratigraphy in proximal and distal deposits of sediment dispersal systems in the East China Sea. Mar Geol 61:13-24

Noll CJ, Dellapenna TM, Gilkinson A, Davis RW (2008) A high resolution geophysical investigation of sediment distribution controlled by catchment size and tides in a multi-basin turbid outwash fjord: Simpson Bay, Prince William Sound, Alaska. Geo-Mar Lett (in press) DOI 10.1007/s00367-008-0120-8

Nozaki Y, Cochran JK, Turekian KK, Kellerr G (1977) Radiocarbon and ^{210}Pb distribution in submersible taken deep-sea cores from project FAMOUS. Earth Planet Sci Lett 34:167-173

Nuwer JM, Keil RG (2005) Sedimetnary Organic Matter Geochemistry of Clayoquot Sound, Vancouver Island, British Columbia. LimnOceanogr 50(4):1119-1128

Olsen CR, Simpson HJ, Peng TH, Bopp RF, Trier RM (1981) Sediment mixing and accumulation rates effects on radionuclide depth profiles in Hudson estuary sediments. J Geophys Res 86(C11):11020-11028

Perillo GME (1995) Definitions and geomorphologic definitions of estuaries. In: Perillo GME (ed) Geomorphology and sedimentology of estuaries. Development in Sedimentology vol 53 Elsevier Science BV, Amsterdam pp 17-47

Plafker G (1965) Tectonic deformation associated with the 1964 Alaska Earthquake. Science, vol 148(3678):1675-1687

Pflaker G (1990) Regional tectonic displacement of shorelines in south-central Alaska during and between great earthquakes. Northwest Sci 64:250-25

Plafker G, Mayo LR (1965) Tectonic deformation, subaqueous slides and destructive waves associated with the Alaskan March 27, 1964 earthquake; an Interim geologic evaluation. US Geological Survey OFR p 21

Porter SC, Denton GH (1967) Chronology of Neoglatiation in the North American Cordillera. Amer J Sci 265:177-210Powell RD, Molnia BF (1989) Glacimarine sedimentary processes, facies and morphology of the South-Southeast Alaska shelf and fjords. Mar Geol 85:359–390

Powell RD (1991) Grounding-line systems as second-order controls on fluctuations of tidewater termini of temperate glaciers. In: Anderson JB, Ashley GM (eds) Glacial Marine Sedimentation: Paleoclimatic Significance. Geol Society Amer Special Paper 261 pp 75-93

Prior DB, Wiseman Jr. WJ and Gilbert R, 1981. Submarine slope processes on a fan delta, Howe Sound, British Columbia. Geo-Marine Letters, 1: 85-90.

Pritchard DW (1967) What is an estuary: physical viewpoint. In: Lauff GH (ed) Amer Assoc for the Advancement Sci Pub No 83:3-5 Baltimore MD: Horn-Schafner

Reed RK, Schumacher JD (1987) Physical oceanography. In: Hood DW, Zimmerman ST (eds) The Gulf of Alaska. NOAA, US Dept Commerce pp 57-91

Relling O, Nordseth K (1979) Sedimentation of a river suspension into a fjord basin. Gaupne fjord in Western Norway. Norsk Geogr Tidsskr 33:187-203

Santschi PH, Guo L, Asbill S, Allison M, Kepple AB, Wen L (2001) Accumulation rates and sources of sediments and organic carbon on the Palos Verdes shelf based on radioisotopic tracers (^{137}Cs, ^{239,240}Pu, ^{210}Pb, ^{234}Th, ^{238}U, ^{14}C). Mar Chem 73:125–152

Schink DR, Guinasso NL (1977) Effects of bioturbation on sediment-seawater interaction. Mar Geol 23:133-154

Smith JN, Walton A (1980) Sediment accumulation rates and geochronologies measured in the Saguenay Fjord using the 210Pb dating method. Geochim Cosmochim Acta vol 44(2):225-240

Smith JN, Schaffer CT (1984) Bioturbation processes in continental slope and rise sediments delineated by Pb-210, microfossil and textural indicators. J Mar Res 42:1117-1145

Sommerfield CK, Nittrouer CA (1999) Modern accumulation rates and a sediment budget for the Eel shelf: a flood dominated depositional environment. Mar Geol 154:227-241

Sommerfield CK, Lee HJ, (2003) Magnitude and variability of Holocene sediment accumulation in Santa Monica Bay, California. Mar Environ Res 56:151-176

St-Onge G, Mulder T, Piper DJW, Hillaire-Marcel C, Stoner JS (2004) Earthquake and flood-induced turbidites in the Saguenay Fjord (Quebec): a Holocene paleoseismicity record. Quat Sci Rev 23:283-294

Sugden DE, John BS (eds) (1976) Glaciers and Landscape. Routledge, Chapman and Hall, Inc New York 120-125

Syvitski, JPM (1989) On the deposition of sediment within glacier-influenced fjords: Oceanographic controls. Mar Geol 85:301-329

Syvitski JPM (1994) Glacial sedimentation processes. Terra Antarctica 1:351-253

Syvitski JPM, Murray JW (1981) Particle interaction in Fjord suspended sediment. Mar Geol 39:215-242

Syvitski JPM, Hein FJ (1991) Sedimentology of an Arctic basin: Itirbilung Fiord, Baffin Island, Canada. Geol Survey Canada Prof Paper 91-11 p 67

Syvitski JPM, Shaw J (1995) Sedimentology and geomorphology of fjords. In: Perillo GME (ed) Geomorphology and sedimentology of estuaries. Development in Sedimentology vol 53 Elsevier Science BV, Amsterdam p 113-178

Syvitski JPM, Burrell DC, Skei JM (eds) (1987) Fjords: processes and products. Springer, Berlin Heidelberg New York

Syvitski JPM, Smith JN, Boudreau B, Calabrese EA (1988) Basin sedimentation and the growth of prograding deltas. J Geophys Res 93:6895-6908

Syvitski JPM, Stoker MS, Cooper AK (1997) Seismic facies of glacial deposits from marine and lacustrine environments. Mar Geol 143:1–4

USDA (1998) Watershed 1:31,380. United States Department of Agriculture Forest Service, Chugach National Forest

USDA (2002) Freshwater streams 1:31,380. United States Department of Agriculture Forest Service, Chugach National Forest

Vorren TO, Lebesbye E, Andreassen K, Larsen KB (1989) Glacigenic sediments on a passive continental margin as exemplified by the Barents Sea. Mar Geol 85:251-272.

Walsh JP, Nittrouer CA (2003) Contrasting styles of off-shelf accumulation in New Guinea. Mar Geol 196:105-125

Wiles GC, Calkin PE, Post A (1995) Glacier fluctuations in the Kenai Fjords, Alaska, U.S.A.: An evaluation of controls on iceberg-calving glaciers. Arctic Alpine Res vol 27(3):234-245

Wheatcroft RA (1990) Preservation potential of sedimentary event layers. Geology 18:843-845

Wheatcroft RA, Jumars PA, Smith CR, Nowell ARM (1990) A mechanistic view of the particulate biodiffusion coefficient: step lengths, rest periods and transport directions. J Mar Res 48:177-207

Wheatcroft RA, Drake DE (2003) Post-depositional alteration and preservation of sedimentary event layers on continental margins, I. The role of episodic sedimentation. Mar Geol 199:123-137

APPENDIX A

SBBC1	Interval	Depth	Weight (g)	Gross Po-209	Gross Po-210	Total Activity	Excess Activity	Error
	0-1	0.5	1.0234	745	376	3.083	1.940	0.455
	1-2	1.5	1.0088	887.5	413.5	2.887	1.738	0.421
	2-3	2.5	1.0101	1443	772	3.311	2.175	0.439
	3-4	3.5	1.0117	1244	663	3.293	2.156	0.446
	4-5	4.5	1.0069	1534	685	2.800	1.649	0.373
	5-6	5.5	1.0197	1282.5	595.5	2.875	1.726	0.390
	6-7	6.5	1.0086	1366	635	2.910	1.762	0.391
	7-8	7.5	1.0269	1649.5	853	3.180	2.040	0.409
	8-9	8.5	1.02	1256	561	2.779	1.627	0.377
	9-10	9.5	1.0144	286.5	98.5	2.151	0.980	0.417
	10-11	10.5	1.0038	1679	697	2.624	1.468	0.347
	11-12	11.5	1.0045	1794.5	843	2.968	1.821	0.381
	12-13	12.5	1.0095	1425	632	2.802	1.651	0.370
	13-14	13.5	1.0287	1730.5	770.5	2.760	1.608	0.356
	14-15	14.5	1.0233	1567	660	2.625	1.468	0.346
	14-15a	15.5	1.0019	1504.5	684	2.894	1.745	0.378
	15-16	16.5	1.0158	928	455	3.079	1.936	0.424
	16-17	17.5	1.0161	1060.5	504.5	2.986	1.841	0.406
	17-18	18.5	1.0091	1170	572	3.090	1.948	0.412
	18-19	19.5	1.0027	1154.5	522	2.876	1.727	0.390
	19-20	20.5	1.0021	1152	535	2.971	1.825	0.397
	20-21	21.5	1.0119	1293.5	584.5	2.863	1.713	0.378
	21-22	22.5	1.0059	1622	722	2.837	1.687	0.365
	22-23	23.5	1.0132	1517.5	664	2.768	1.616	0.360
	23-24	24.5	1.0027	1384	575	2.669	1.514	0.352
	24-25	25.5	1.0069	1373.5	556.5	2.592	1.435	0.344
	25-26	26.5	1.0079	1844	721	2.499	1.339	0.321
	26-27	27.5	1.0073	2019.5	843	2.670	1.515	0.335
	27-28	28.5	1.0063	1787	724	2.607	1.450	0.331
	28-29	29.5	1.0049	589.5	252.5	2.760	1.607	0.412
	29-30	30.5	1.0069	1147	488	2.736	1.583	0.365
	30-31	31.5	1.0016	1585.5	588	2.397	1.234	0.314
	31-32	32.5	1.0104	1167	425	2.346	1.180	0.319
	32-33	33.5	1.0074	738.5	289.5	2.532	1.373	0.366
	33-34	34.5	1.0223	1752	645	2.343	1.178	0.301
	34-35	35.5	1.0214	1723.5	622	2.299	1.133	0.297
	35-36	36.5	1.0066	1699	626	2.394	1.230	0.305
	36-37	37.5	1.0173	1771.5	657.5	2.386	1.222	0.302
	37-38	38.5	1.0097	1098	408	2.347	1.183	0.334
	38-39	39.5	1.0074	1458.5	535	2.323	1.157	0.318

SBBC2	Interval	Depth	Weight (g)	Gross Po-209	Gross Po-210	Total Activity	Excess Activity	Error
	0-1	0.5	1.0139	954	582	3.877	2.760	0.501
	1-2	1.5	1.0099	934.5	583.5	3.984	2.870	0.514
	2-3	2.5	1.0252	1029	592	3.616	2.490	0.467
	3-4	3.5	1.0111	1214.5	650	3.410	2.279	0.436
	4-5	4.5	1.0117	1297	746	3.681	2.558	0.456
	5-6	5.5	1.0248	1454.5	828.5	3.599	2.473	0.441
	6-7	6.5	1.0179	1596	865	3.448	2.317	0.421
	7-8	7.5	1.0083	1682.5	867	3.309	2.175	0.405
	8-9	8.5	1.0157	1533	890	3.720	2.598	0.447
	9-10	9.5	1.0271	1512.5	795.5	3.333	2.199	0.407
	10-11	10.5	1.0152	1207	616	3.272	2.136	0.414
	11-12	11.5	1.0081	1578.5	831	3.399	2.267	0.413
	12-13	12.5	1.0259	1059	526	3.167	2.028	0.406
	13-14	13.5	1.0062	1057.5	522.5	3.212	2.074	0.413
	14-15	14.5	1.0057	1785	874	3.185	2.046	0.383
	15-16	15.5	1.0206	1786.5	759	2.723	1.570	0.335
	16-17	16.5	1.007	1854	790	2.782	1.631	0.338
	17-18	17.5	1.0032	1525.5	681.5	2.927	1.781	0.361
	18-19	18.5	1.014	985	442	2.880	1.732	0.385
	19-20	19.5	1.0199	1179.5	531	2.873	1.725	0.374
	20-21	20.5	1.0079	1187	514	2.810	1.660	0.364
	21-22	21.5	1.0124	1788.5	734.5	2.653	1.499	0.329
	22-23	22.5	1.0257	1035	405	2.495	1.336	0.338
	23-24	23.5	1.0186	990.5	369	2.392	1.229	0.329
	24-25	24.5	1.0269	1426	508	2.281	1.114	0.297
	25-26	25.5	1.0258	1232.5	491.5	2.556	1.398	0.332
	26-27	26.5	1.0293	1347	496	2.352	1.188	0.307
	27-28	27.5	1.0095	1617.5	598	2.408	1.245	0.306
	28-29	28.5	1.0099	1746	591	2.215	1.046	0.281
	29-30	29.5	1.0142	2005.5	660.5	2.146	0.975	0.268
	30-31	30.5	1.0171	1896	687	2.354	1.190	0.291
	31-32	31.5	1.0124	1182.5	418	2.307	1.141	0.306
	32-33	32.5	1.008	1667	592	2.340	1.175	0.292
	33-34	33.5	1.0083	1632.5	510.5	2.059	0.886	0.265
	34-35	34.5	1.0166	1619	544	2.195	1.026	0.279
	35-36	35.5	1.0292	1765.5	512	1.871	0.692	0.242
	36-37	36.5	1.0084	1864	522	1.863	0.683	0.237
	37-38	37.5	1.004	194.5	58.5	2.009	0.835	0.407

SBBC3	Interval	Depth	Weight (g)	Gross Po-209	Gross Po-210	Total Activity	Excess Activity	Error
	0-1	0.5	1.0058	1613	889	3.676	2.553	0.417
	1-2	1.5	1.0096	1679.5	851	3.366	2.234	0.386
	2-3	2.5	1.01	956	449	3.151	2.012	0.388
	3-4	3.5	1.0089	1267.5	681.5	3.611	2.487	0.416
	4-5	4.5	1.0108	1222	659	3.615	2.491	0.418
	5-6	5.5	1.0111	811.5	487	4.022	2.910	0.483
	6-7	6.5	1.0065	1138	658	3.912	2.797	0.447
	7-8	7.5	1.01	1027.5	516.5	3.389	2.258	0.403
	8-9	8.5	1.0245	1672	850	3.379	2.248	0.376
	9-10	9.5	1.0155	1110.5	540	3.261	2.126	0.386
	10-11	10.5	1.0054	1065	612	3.912	2.797	0.447
	11-12	11.5	1.0035	1752.5	927.5	3.610	2.485	0.393
	12-13	12.5	0.9403	1370	743	3.948	2.834	0.441
	13-14	13.5	1.0073	1327.5	673	3.445	2.315	0.391
	14-15	14.5	1.0205	1693	881	3.508	2.380	0.381
	15-16	15.5	1.0231	1656.5	877.5	3.562	2.436	0.386
	16-17	16.5	1.0172	1378	707	3.470	2.341	0.387
	17-18	17.5	1.0171	1705.5	799	3.168	2.030	0.350
	18-19	18.5	1.0079	1447	615	2.915	1.769	0.332
	19-20	19.5	1.0061	1546.5	646.5	2.873	1.725	0.325
	20-21	20.5	1.012	1636	766	3.231	2.095	0.348
	21-22	21.5	1.0168	1406.5	577.5	2.616	1.462	0.341
	22-23	22.5	1.0136	1860	757	2.601	1.447	0.327
	23-24	23.5	1.0069	957.5	338	2.271	1.106	0.324
	24-25	24.5	1.0153	913	316	2.219	1.053	0.318
	25-26	25.5	1.0172	885.5	304.5	2.201	1.034	0.317
	26-27	26.5	1.0135	1416	526	2.386	1.225	0.314
	27-28	27.5	1.0045	1294.5	465	2.328	1.165	0.312
	28-29	28.5	1.0124	1089	371	2.202	1.035	0.304
	29-30	29.5	1.0145	381.5	101.5	1.716	0.533	0.315
	30-31	30.5	1.0142	1508	516	2.208	1.041	0.290
	31-32	31.5	1.0083	1529.5	478	2.028	0.855	0.271
	32-33	32.5	1.0198	1856	582	2.022	0.849	0.260
	33-34	33.5	1.0019	1536.5	432.5	1.848	0.669	0.250
	34-35	34.5	1.0169	1777	538	1.958	0.783	0.255
	35-36	35.5	1.0062	1859.5	531	1.866	0.688	0.245
	36-37	36.5	1.0088	1547	426	1.804	0.624	0.243

SBBC4	Interval	Depth	Weight (g)	Gross Po-209	Gross Po-210	Total Activity	Excess Activity	Error
	0-1	0.5	1.0081	387.5	222.5	3.765	2.752	0.545
	1-2	1.5	1.0087	290	160	3.615	2.597	0.563
	2-3	2.5	1.0194	1675.5	827	3.200	2.169	0.379
	3-4	3.5	1.0133	1697	841	3.249	2.219	0.380
	4-5	4.5	1.0187	1547.5	712.5	3.002	1.964	0.360
	5-6	5.5	1.0122	1446	594	2.696	1.648	0.333
	6-7	6.5	1.0082	1957.5	784	2.639	1.589	0.315
	7-8	7.5	1.0179	142	68	3.110	2.076	0.608
	8-9	8.5	1.0047	1455.5	511.5	2.312	1.252	0.298
	9-10	9.5	1.0093	1401	529	2.473	1.418	0.315
	10-11	10.5	1.0199	1605.5	553	2.232	1.169	0.285
	11-12	11.5	1.0116	1283	449	2.298	1.237	0.299
	12-13	12.5	1.0168	1217.5	358.5	1.924	0.851	0.262
	13-14	13.5	1.0132	1587	472	1.950	0.878	0.255
	14-15	14.5	1.0068	1632.5	483	1.952	0.880	0.254
	15-16	15.5	1.011	1498	437	1.926	0.854	0.252
	16-17	16.5	1.0164	904.5	267.5	1.943	0.870	0.276
	17-18	17.5	1.0062	1504	390	1.721	0.641	0.232
	18-19	18.5	1.0189	1485.5	375	1.654	0.572	0.225
	19-20	19.5	1.0077	1762	440	1.663	0.581	0.218
	20-21	20.5	1.0067	1603.5	358.5	1.490	0.403	0.204
	21-22	21.5	1.0043	1763	385	1.459	0.371	0.198
	22-23	22.5	1.0216	585.5	123	1.380	0.289	0.234
	23-24	23.5	1.0082	1683	382	1.518	0.432	0.204
	24-25	24.5	1.0131	1872.5	378.5	1.346	0.254	0.183

SBBC5	Interval	Depth	Weight (g)	Gross Po-209	Gross Po-210	Total Activity	Excess Activity	Error
	0-1	0.5	1.0086	1378	745	3.321	2.403	0.449
	1-2	1.5	1.0022	850.5	406.5	2.954	2.024	0.438
	2-3	2.5	1.0056	778	424	3.357	2.441	0.492
	3-4	3.5	1.004	796.5	421	3.261	2.342	0.479
	4-5	4.5	1.0159	1140	529	2.844	1.909	0.402
	5-6	5.5	1.0049	875.5	359.5	2.544	1.599	0.384
	6-7	6.5	1.0177	872	405	2.841	1.907	0.418
	7-8	7.5	1.0097	1174.5	491	2.578	1.634	0.370
	8-9	8.5	1.0092	1183	533	2.794	1.857	0.391
	9-10	9.5	1.0026	1054.5	434.5	2.572	1.627	0.373
	10-11	10.5	1.0063	1486	573	2.398	1.447	0.335
	11-12	11.5	1.0106	1583.5	585	2.287	1.333	0.320
	12-13	12.5	1.0082	1738	579	2.099	1.138	0.287
	13-14	13.5	1.007	1485.5	520.5	2.210	1.253	0.306
	14-15	14.5	1.0091	779	211	1.705	0.730	0.280
	15-16	15.5	1.0092	1282.5	371	1.821	0.850	0.269
	16-17	16.5	1.0092	795	192	1.528	0.547	0.255
	17-18	17.5	1.0073	1427.5	314.5	1.396	0.411	0.215
	18-19	18.5	1.0044	1276	268	1.335	0.347	0.212
	19-20	19.5	1.0131	1152.5	267	1.460	0.476	0.230
	20-21	20.5	1.0135	1530	358	1.489	0.506	0.219
	21-22	21.5	1.0069	1241.5	263.5	1.359	0.372	0.212
	22-23	22.5	1.0191	1109	243	1.387	0.400	0.219
	23-24	23.5	1.0156	875.5	193	1.400	0.414	0.231
	24-25	24.5	1.0188	622	131	1.340	0.352	0.239
	25-26	25.5	1.0087	919.5	167.5	1.171	0.177	0.200
	26-27	26.5	1.0028	955	191	1.293	0.303	0.214
	27-28	27.5	1.0057	844.5	143	1.091	0.095	0.195

SBBC6	Interval	Depth	Weight (g)	Gross Po-209	Gross Po-210	Total Activity	Excess Activity	Error
	0-1	0.5	1.0043	1077	556	3.349	2.235	0.428
	1-2	1.5	1.001	1476.5	781.5	3.444	2.335	0.420
	2-3	2.5	1.0188	1416	736	3.323	2.209	0.409
	3-4	3.5	1.0174	1381.5	737	3.416	2.305	0.420
	4-5	4.5	1.0016	1625	760	3.073	1.949	0.371
	5-6	5.5	1.0188	462.5	193.5	2.702	1.566	0.411
	6-7	6.5	1.0186	1468	637	2.803	1.670	0.348
	7-8	7.5	1.0084	1601.5	587	2.392	1.244	0.303
	8-9	8.5	1.0121	647	243	2.454	1.309	0.355
	9-10	9.5	1.0037	1414.5	470.5	2.192	1.037	0.286
	10-11	10.5	1.005	1107	351	2.086	0.928	0.286
	11-12	11.5	1.0176	1564.5	487	2.023	0.863	0.264
	12-13	12.5	1.0139	1636	441	1.767	0.598	0.234
	13-14	13.5	1.0063	976.5	225.5	1.525	0.347	0.230
	14-15	14.5	1.009	1374	330	1.582	0.406	0.222
	15-16	15.5	1.0164	420.5	96	1.493	0.314	0.272
	16-17	16.5	1.0109	877	227	1.651	0.478	0.260
	17-18	17.5	1.0031	703.5	179.5	1.641	0.467	0.271
	18-19	18.5	1.0048	894	203	1.458	0.277	0.237
	19-20	19.5	1.0037	776.5	182	1.506	0.328	0.250
	20-21	20.5	1.0081	837	156	1.198	0.009	0.208
	21-22	21.5	1.004	1267.5	241.5	1.230	0.042	0.195
	22-23	22.5	1.016	1408	246	1.115	-0.078	0.178
	23-24	23.5	1.0137	1547.5	327	1.351	0.167	0.201
	24-25	24.5	1.004	1618	303	1.215	0.026	0.184
	25-26	25.5	1.0065	1534.5	272.5	1.149	-0.042	0.178
	26-27	26.5	1.0052	1585	287	1.174	-0.017	0.180
	27-28	27.5	1.0026	1541.5	316	1.332	0.147	0.198
	28-29	28.5	1.0152	91	16	1.134	-0.058	0.395
	29-30	29.5	1.0165	1215.5	236.5	1.253	0.066	0.196
	30-31	30.5	1.0174	1075	210	1.257	0.070	0.201
	31-32	31.5	1.0052	1106.5	221	1.301	0.115	0.205
	32-33	32.5	1.0099	1546	291	1.227	0.038	0.183
	33-34	33.5	1.0062	1285.5	251.5	1.280	0.093	0.195

SBBC7	Interval	Depth	Weight (g)	Gross Po-209	Gross Po-210	Total Activity	Excess Activity	Error
	0-1	0.5	1.0163	826	464	3.644	2.555	0.463
	1-2	1.5	1.0062	415.5	195.5	3.083	1.968	0.461
	2-3	2.5	1.012	901	387	2.798	1.671	0.371
	3-4	3.5	1.016	1028.5	405	2.555	1.417	0.338
	4-5	4.5	1.0081	790	269	2.238	1.085	0.317
	5-6	5.5	1.0073	245.5	57.5	1.541	0.356	0.323
	6-7	6.5	1.0035	1016	245	1.592	0.410	0.235
	7-8	7.5	1.0057	1593.5	378	1.563	0.379	0.215
	8-9	8.5	1.0031	473	98	1.382	0.191	0.248
	9-10	9.5	1.0184	1315.5	310.5	1.551	0.367	0.216
	10-11	10.5	1.0023	940	176	1.250	0.053	0.198
	11-12	11.5	1.0197	774.5	167	1.394	0.203	0.227
	12-13	12.5	1.0123	788	176	1.462	0.274	0.232
	13-14	13.5	1.0123	178.5	34.5	1.265	0.068	0.317
	14-15	14.5	1.0164	373	95	1.661	0.482	0.301
	15-16	15.5	1.0024	871.5	191	1.449	0.260	0.226

SBBC8	Interval	Depth	Weight (g)	Gross Po-209	Gross Po-210	Total Activity	Excess Activity	Error
	0-1	0.5	1.0027	1168.5	670.5	3.786	2.681	0.455
	1-2	1.5	1.0043	1030	570	3.645	2.535	0.449
	2-3	2.5	1.0055	1418.5	741	3.437	2.319	0.410
	3-4	3.5	1.0181	538	278	3.408	2.290	0.459
	4-5	4.5	1.0179	409.5	214.5	3.456	2.339	0.489
	5-6	5.5	1.003	890	434	3.265	2.141	0.409
	6-7	6.5	1.0045	1496.5	775	3.462	2.346	0.399
	7-8	7.5	1.0183	1231	614	3.306	2.184	0.389
	8-9	8.5	1.0128	613.5	247.5	2.688	1.543	0.371
	9-10	9.5	1.0043	1384	562	2.729	1.585	0.329
	10-11	10.5	1.009	997.5	422	2.830	1.690	0.355
	11-12	11.5	1.0167	971	347	2.223	1.062	0.330
	12-13	12.5	1.0026	732.5	275.5	2.372	1.217	0.365
	13-14	13.5	1.0143	988	365	2.303	1.146	0.338
	14-15	14.5	1.012	1084.5	376	2.167	1.004	0.318
	15-16	15.5	1.0114	891	308	2.172	1.010	0.326
	16-17	16.5	1.0005	1064.5	387.5	2.313	1.155	0.333
	17-18	17.5	1.0162	1198	376	1.963	0.792	0.287
	18-19	18.5	1.0053	1272.5	401	1.992	0.823	0.288
	19-20	19.5	1.0035	1330	389	1.862	0.687	0.269
	20-21	20.5	1.007	1063.5	324.5	1.936	0.764	0.288
	21-22	21.5	1.018	1329	398	1.879	0.705	0.271
	22-23	22.5	1.045	1589.5	375	1.442	0.251	0.214
	23-24	23.5	1.052	1286	314	1.490	0.301	0.225
	24-25	24.5	1.0128	1675.5	379.5	1.436	0.245	0.211
	25-26	25.5	1.0035	1716	410	1.529	0.341	0.221
	26-27	26.5	1.0155	1736.5	421	1.533	0.346	0.220
	27-28	27.5	1.0163	1854	439	1.503	0.315	0.213
	28-29	28.5	1.0099	1497.5	316.5	1.350	0.156	0.204
	29-30	29.5	1.0143	750	146	1.238	0.040	0.219
	30-31	30.5	1.005	1842.5	367	1.279	0.082	0.190
	31-32	31.5	1.0042	452	93	1.329	0.134	0.257
	32-33	32.5	1.0162	442.5	98.5	1.421	0.229	0.270
	33-34	33.5	1.0058	1466	277	1.176	-0.025	0.194
	34-35	34.5	1.0145	1100.5	210	1.178	-0.023	0.205
	35-36	35.5	1.0164	1842	366	1.230	0.031	0.191
	36-37	36.5	1.0178	1796.5	350.5	1.206	0.007	0.189
	37-38	37.5	1.0138	780	152	1.210	0.010	0.222
	38-39	38.5	1.0163	1521.5	281	1.144	-0.059	0.187
	39-40	39.5	1.0171	1501	292	1.210	0.010	0.194
	40-41	40.5	1.0136	1687.5	343.5	1.270	0.073	0.197
	41-42	41.5	1.0065	1550	314	1.273	0.076	0.201
	42-43	42.5	1.0079	1811.5	425	1.472	0.283	0.218

SBBC9	Interval	Depth	Weight (g)	Gross Po-209	Gross Po-210	Total Activity	Excess Activity	Error
	0-1	0.5	1.0038	1755	981	3.540	2.431	0.439
	1-2	1.5	1.0172	1947.5	1074.5	3.448	2.335	0.423
	2-3	2.5	1.0136	1524	848	3.490	2.379	0.440
	3-4	3.5	1.009	1581.5	891	3.549	2.441	0.445
	4-5	4.5	1.0166	389	217	3.506	2.395	0.544
	5-6	5.5	1.0164	676.5	337.5	3.136	2.011	0.450
	6-7	6.5	1.005	1944	895	2.927	1.794	0.367
	7-8	7.5	1.0117	966.5	508	3.319	2.202	0.445
	8-9	8.5	1.0044	1534	701	2.921	1.788	0.374
	9-10	9.5	1.003	952.5	378.5	2.544	1.396	0.359
	10-11	10.5	1.0174	1476	597	2.553	1.405	0.336
	11-12	11.5	1.0087	1472.5	519	2.244	1.084	0.304
	12-13	12.5	1.0079	706	262	2.260	1.102	0.372
	13-14	13.5	1.0148	786.5	303.5	2.334	1.179	0.373
	14-15	14.5	1.0119	554	169	1.850	0.676	0.337
	15-16	15.5	1.0089	1080.5	363	2.044	0.878	0.320
	16-17	16.5	1.0063	593	189	1.954	0.784	0.343
	17-18	17.5	1.0112	1054.5	312.5	1.808	0.632	0.290
	18-19	18.5	1.013	1154	317	1.673	0.492	0.269
	19-20	19.5	1.0035	1440.5	418	1.784	0.607	0.273
	20-21	20.5	1.0072	1234	326	1.626	0.443	0.258
	21-22	21.5	1.0077	1178.5	290.5	1.517	0.329	0.247
	22-23	22.5	1.0131	1686	428	1.554	0.368	0.237
	23-24	23.5	1.0035	831.5	229	1.702	0.522	0.287
	24-25	24.5	1.0071	391	84	1.329	0.134	0.284
	25-26	25.5	1.0128	1038.5	207.5	1.229	0.031	0.215
	26-27	26.5	1.0182	412	115	1.708	0.528	0.332
	27-28	27.5	1.0101	221.5	57	1.588	0.403	0.375

SBBC10	Interval	Depth	Weight (g)	Gross Po-209	Gross Po-210	Total Activity	Excess Activity	Error
	0-1	0.5	1.0032	349	203	3.631	2.528	0.593
	1-2	1.5	1.0113	1445.5	783.5	3.357	2.242	0.441
	2-3	2.5	1.006	253	129	3.174	2.053	0.577
	3-4	3.5	1.0073	325.5	164	3.133	2.009	0.539
	4-5	4.5	1.0054	447	221	3.111	1.987	0.493
	5-6	5.5	1.0163	323.5	166.5	3.204	2.083	0.538
	6-7	6.5	1.0057	1226	552	2.762	1.625	0.394
	7-8	7.5	1.0036	1550.5	649	2.573	1.428	0.361
	8-9	8.5	1.017	1439	534	2.263	1.105	0.325
	9-10	9.5	1.017	1039.5	351.5	2.062	0.896	0.318
	10-11	10.5	1.0109	1347	448	2.040	0.874	0.303
	11-12	11.5	1.0065	1547.5	507	2.018	0.851	0.294
	12-13	12.5	1.007	871	276	1.961	0.792	0.313
	13-14	13.5	1.0185	1378.5	393.5	1.747	0.569	0.265
	14-15	14.5	1.0037	1018	253	1.543	0.357	0.255
	15-16	15.5	1.0086	187.5	54	1.780	0.603	0.425
	16-17	16.5	1.0159	174	60	2.126	0.963	0.483
	17-18	17.5	1.0184	1611.5	405.5	1.548	0.362	0.234

SBBC11	Interval	Depth	Weight (g)	Gross Po-209	Gross Po-210	Total Activity	Excess Activity	Error
	0-1	0.5	1.0143	294	177	3.718	2.619	0.624
	1-2	1.5	1.0035	345.5	207	3.740	2.642	0.608
	2-3	2.5	1.0033	1500	856	3.581	2.476	0.459
	3-4	3.5	1.0049	1294.5	654.5	3.167	2.046	0.422
	4-5	4.5	1.0097	183	64	2.180	1.020	0.481
	5-6	5.5	1.0055	184	83	2.824	1.689	0.572
	6-7	6.5	1.0117	1134	464	2.559	1.413	0.359
	7-8	7.5	1.0162	215.5	65.5	1.892	0.720	0.413
	8-9	8.5	1.0156	673	230	1.995	0.828	0.362
	9-10	9.5	1.0055	881.5	280	1.873	0.700	0.329
	10-11	10.5	1.0159	565	191	1.983	0.815	0.370
	11-12	11.5	1.0197	816.5	243.5	1.742	0.565	0.312
	12-13	12.5	1.0062	548	165	1.783	0.607	0.345
	13-14	13.5	1.0042	643.5	149	1.374	0.181	0.277
	14-15	14.5	1.0102	1434	301	1.257	0.059	0.216
	15-16	15.5	1.0038	1261.5	251.5	1.201	0.001	0.214

SBBC12	Interval	Depth	Weight (g)	Gross Po-209	Gross Po-210	Total Activity	Excess Activity	Error
	0-1	0.5	1.0044	1464	920	3.784	2.743	0.518
	1-2	1.5	1.0187	1660.5	880	3.147	2.079	0.436
	2-3	2.5	1.0061	1596	860	3.256	2.193	0.447
	3-4	3.5	1.0097	152.5	60.5	2.388	1.290	0.571
	4-5	4.5	1.0034	1347	502	2.258	1.154	0.340
	5-6	5.5	1.0087	1508.5	503	2.009	0.895	0.304
	6-7	6.5	1.0115	207	48	1.401	0.261	0.365
	7-8	7.5	1.0134	290.5	71.5	1.484	0.348	0.342
	8-9	8.5	1.0105	359	58	0.977	-0.180	0.246
	9-10	9.5	1.0178	1401.5	259	1.109	-0.042	0.195
	10-11	10.5	1.0065	1005	191	1.159	0.010	0.213
	11-12	11.5	1.0111	816.5	243.5	1.811	0.688	0.306
	12-13	12.5	1.0061	548	165	1.838	0.716	0.336
	13-14	13.5	1.014	643.5	149	1.402	0.263	0.267
	14-15	14.5	1.0179	720	123	1.937	0.811	0.122
	15-16	15.5	1.0057	1182.5	235.5	2.263	1.147	0.125
	16-17	16.5	1.0067	980	192	2.224	1.106	0.128
	17-18	17.5	1.0075	1037.5	205	2.241	1.124	0.127
	18-19	18.5	1.0029	1045	210	2.301	1.186	0.128
	19-20	19.5	1.0138	615.5	112.5	2.070	0.948	0.133
	20-21	20.5	1.0057	1382	250	2.066	0.944	0.114
	21-22	21.5	1.0043	791.5	148	2.138	1.018	0.129
	22-23	22.5	1.0159	694	131	2.155	1.036	0.131
	23-24	23.5	1.0203	951.5	187.5	2.240	1.124	0.126
	24-25	24.5	1.0092	8	1	1.437	0.296	0.781
	25-26	25.5	1.0022	1272.5	264	2.401	1.289	0.126
	26-27	26.5	1.0086	1644	304	2.148	1.029	0.110
	27-28	27.5	1.0094	289.5	45.5	1.824	0.695	0.146
	28-29	28.5	1.0132	391	56	1.656	0.522	0.127

SBBC13	Interval	Depth	Weight (g)	Gross Po-209	Gross Po-210	Total Activity	Excess Activity	Error
	0-1	0.5	1.0036	640.5	436	4.103	3.130	0.620
	1-2	1.5	1.0112	1673	924	3.321	2.314	0.452
	2-3	2.5	1.0086	157.5	82.5	3.158	2.144	0.682
	3-4	3.5	1.0137	1098	407	2.223	1.171	0.345
	4-5	4.5	1.014	1378.5	343	1.492	0.408	0.245
	5-6	5.5	1.0128	935	222	1.383	0.296	0.261
	6-7	6.5	1.0157	1298.5	268.5	1.201	0.106	0.221
	7-8	7.5	1.0099	888	181	1.191	0.095	0.237
	8-9	8.5	1.0119	1018.5	208	1.191	0.095	0.230
	9-10	9.5	1.005	945	190	1.186	0.090	0.231
	10-11	10.5	1.0155	1198.5	228.5	1.113	0.014	0.211
	11-12	11.5	1.0116	1493	323	1.268	0.176	0.223
	12-13	12.5	1.0144	1366.5	264	1.129	0.031	0.208
	13-14	13.5	1.0141	1358	265	1.147	0.049	0.209
	14-15	14.5	1.0134	1323.5	278.5	1.238	0.144	0.222
	15-16	15.5	1.0173	1562	317	1.189	0.093	0.209
	16-17	16.5	1.0272	1554	311	1.161	0.064	0.205
	17-18	17.5	1.0192	1637	280	1.015	-0.088	0.180
	18-19	18.5	1.0126	1432.5	273.5	1.141	0.043	0.201
	19-20	19.5	1.003	264	46	1.051	-0.051	0.288
	20-21	20.5	1.0201	785.5	147	1.110	0.010	0.221
	21-22	21.5	1.0136	1375	262	1.143	0.045	0.201
	22-23	22.5	1.0135	1300.5	231.5	1.068	-0.033	0.193
	23-24	23.5	1.0171	1556	308	1.183	0.087	0.202
	24-25	24.5	1.0228	671.5	129	1.142	0.044	0.232
	25-26	25.5	1.0073	603	116	1.167	0.070	0.241
	26-27	26.5	1.0146	1644.5	306.5	1.123	0.024	0.191
	27-28	27.5	1.0075	985	192	1.142	0.044	0.225

SBBC15	Interval	Depth	Weight (g)	Gross Po-209	Gross Po-210	Total Activity	Excess Activity	Error
	0-1	0.5	1.0143	672	321	3.137	2.025	0.418
	1-2	1.5	1.0101	1464.5	726.5	3.271	2.165	0.385
	2-3	2.5	1.0117	388	191	3.241	2.134	0.477
	3-4	3.5	1.0204	981.5	519	3.451	2.354	0.424
	4-5	4.5	1.0112	1615	734	3.009	1.891	0.352
	5-6	5.5	1.0134	1444.5	721.5	3.299	2.195	0.385
	6-7	6.5	1.0116	1152	566	3.251	2.144	0.392
	7-8	7.5	1.0095	909.5	393	2.865	1.741	0.368
	8-9	8.5	1.0161	1700	700	2.726	1.596	0.320
	9-10	9.5	1.0054	577.5	208.5	2.416	1.271	0.348
	10-11	10.5	1.0092	287	103	2.392	1.247	0.405
	11-12	11.5	1.0114	403.5	126	2.077	0.917	0.337
	12-13	12.5	1.0128	327	113	2.307	1.157	0.378
	13-14	13.5	1.0107	1631.5	464.5	1.905	0.737	0.240
	14-15	14.5	1.0051	146	28	1.290	0.094	0.335
	15-16	15.5	1.0056	1513.5	385	1.710	0.534	0.224
	16-17	16.5	1.0029	1618	430	1.810	0.638	0.228
	17-18	17.5	1.0113	1481.5	354.5	1.600	0.418	0.214
	18-19	18.5	1.0184	1139	249	1.451	0.263	0.208
	19-20	19.5	1.0082	1012.5	189	1.252	0.054	0.192
	20-21	20.5	1.0186	1155	212	1.225	0.026	0.182
	21-22	21.5	1.0067	1417.5	269.5	1.283	0.087	0.182
	22-23	22.5	1.015	1015	200	1.319	0.125	0.197
	23-24	23.5	1.0152	1915	403	1.409	0.218	0.185
	24-25	24.5	1.0181	1310	270	1.383	0.191	0.192
	25-26	25.5	1.0117	1575.5	261.5	1.121	-0.083	0.161
	26-27	26.5	1.0041	1861	328	1.199	-0.001	0.164
	27-28	27.5	1.0159	1721.5	299	1.168	-0.034	0.163
	28-29	28.5	1.0082	1574	283	1.224	0.025	0.170
	29-30	29.5	1.0065	1803.5	325.5	1.231	0.032	0.167
	30-31	30.5	1.015	998	188	1.274	0.077	0.190
	31-32	31.5	1.0074	425.5	79	1.265	0.068	0.231
	32-33	32.5	1.0061	719	115	1.097	-0.108	0.183
	33-34	33.5	1.0044	1707.5	315.5	1.269	0.072	0.171
	34-35	34.5	1.0086	126	18	0.977	-0.233	0.295
	35-36	35.5	1.0153	1547.5	306	1.344	0.150	0.180

SBBC16	Interval	Depth	Weight (g)	Gross Po-209	Gross Po-210	Total Activity	Excess Activity	Error
	0-1	0.5	1.0116	311.5	161	3.236	2.127	0.545
	1-2	1.5	1.0027	1630	871	3.392	2.291	0.425
	2-3	2.5	1.0191	1124.5	645.5	3.585	2.493	0.465
	3-4	3.5	1.0173	1681	908	3.380	2.278	0.421
	4-5	4.5	1.0076	1772.5	833	2.969	1.848	0.376
	5-6	5.5	1.0067	1652	716	2.754	1.624	0.354
	6-7	6.5	1.0205	1444.5	558.5	2.424	1.279	0.324
	7-8	7.5	1.0118	1699	683	2.542	1.402	0.330
	8-9	8.5	1.0051	1401.5	533	2.420	1.276	0.326
	9-10	9.5	1.0075	285	100	2.250	1.098	0.415
	10-11	10.5	1.0061	621.5	207.5	2.144	0.987	0.336
	11-12	11.5	1.0136	419	132	2.008	0.845	0.348
	12-13	12.5	1.0196	1766.5	455	1.632	0.452	0.227
	13-14	13.5	1.0022	1004	230	1.484	0.297	0.232
	14-15	14.5	1.0139	1787.5	426.5	1.528	0.343	0.214
	15-16	15.5	1.01	1386	326	1.512	0.326	0.221
	16-17	16.5	1.0056	717.5	152	1.354	0.161	0.236
	17-18	17.5	1.0181	53	10	1.210	0.010	0.518
	18-19	18.5	1.0033	491.5	126.5	1.674	0.496	0.291
	19-20	19.5	1.013	845	190	1.449	0.260	0.233
	20-21	20.5	1.0027	511.5	113	1.438	0.249	0.260
	21-22	21.5	1.0104	530	118	1.446	0.257	0.256
	22-23	22.5	1.0107	907.5	158.5	1.134	-0.069	0.192
	23-24	23.5	1.0199	1151	196	1.095	-0.109	0.178
	24-25	24.5	1.0124	1046.5	211	1.306	0.111	0.206

SBBC17	Interval	Depth	Weight (g)	Gross Po-209	Gross Po-210	Total Activity	Excess Activity	Error
	0-1	0.5	1.0061	1804	766	2.680	1.530	0.349
	1-2	1.5	1.0181	1074.5	657	3.814	2.703	0.497
	2-3	2.5	1.0051	1007	580	3.657	2.541	0.482
	3-4	3.5	1.0061	526.5	324.5	3.910	2.802	0.563
	4-5	4.5	1.0115	1444	806	3.522	2.401	0.445
	5-6	5.5	1.0146	1285.5	724	3.543	2.422	0.453
	6-7	6.5	1.0067	402	194	3.075	1.939	0.489
	7-8	7.5	1.0122	1763.5	946.5	3.401	2.276	0.418
	8-9	8.5	1.001	1613	763	3.031	1.893	0.385
	9-10	9.5	1.0033	1889.5	888	3.005	1.866	0.375
	10-11	10.5	1.0082	1815	730	2.572	1.418	0.328
	11-12	11.5	1.0066	1548.5	614.5	2.542	1.387	0.332
	12-13	12.5	1.007	1864	688	2.363	1.202	0.305
	13-14	13.5	1.0195	1279.5	480	2.372	1.212	0.322
	14-15	14.5	1.0031	1283	430	2.165	0.998	0.298
	15-16	15.5	1.0182	1343.5	469.5	2.224	1.059	0.301
	16-17	16.5	1.0186	1578	555	2.237	1.072	0.296
	17-18	17.5	1.0196	1660.5	501	1.917	0.742	0.260
	18-19	18.5	1.0143	207	61	1.892	0.715	0.401
	19-20	19.5	1.0073	1741.5	453.5	1.684	0.500	0.232
	20-21	20.5	1.017	1538	360	1.499	0.309	0.216
	21-22	21.5	1.0036	1378.5	369	1.737	0.555	0.247
	22-23	22.5	1.0074	694	194	1.754	0.573	0.295
	23-24	23.5	1.013	1654.5	381.5	1.438	0.247	0.218
	24-25	24.5	1.0028	811	179	1.391	0.198	0.242
	25-26	25.5	1.0088	1628.5	372	1.431	0.239	0.218
	26-27	26.5	1.01	933	174	1.179	-0.022	0.206
	27-28	27.5	1.0049	1037.5	229.5	1.405	0.212	0.229
	28-29	28.5	1.0079	1302	245	1.192	-0.009	0.195
	29-30	29.5	1.0046	1675.5	274	1.039	-0.166	0.169
	30-31	30.5	1.0067	1932	325	1.077	-0.127	0.167
	31-32	31.5	1.0145	1706.5	322.5	1.201	0.001	0.183
	32-33	32.5	1.0027	1711	317	1.191	-0.009	0.183
	33-34	33.5	1.0174	1828.5	353	1.223	0.024	0.184
	34-35	34.5	1.0192	1425	275	1.227	0.028	0.190
	35-36	35.5	1.0116	416.5	92.5	1.423	0.230	0.275
	36-37	36.5	1.012	442	77	1.116	-0.087	0.231
	37-38	37.5	1.0037	1427.5	283	1.280	0.083	0.197
	38-39	38.5	1.0133	833	139	1.073	-0.132	0.191
	39-40	39.5	1.0114	1239.5	257.5	1.338	0.143	0.206
	40-41	40.5	1.0055	1119	203	1.175	-0.026	0.192
	41-42	41.5	1.0106	2544.5	314	0.795	-0.419	0.127

SBBC18	Interval	Depth	Weight (g)	Gross Po-209	Gross Po-210	Total Activity	Excess Activity	Error
	0-1	0.5	1.0106	784.5	502	3.737	2.543	0.580
	1-2	1.5	1.0189	1108	566	2.989	1.763	0.451
	2-3	2.5	1.0178	861.5	463.5	3.151	1.932	0.489
	3-4	3.5	1.0036	1186	710	3.556	2.355	0.517
	4-5	4.5	1.009	1802.5	909.5	2.981	1.755	0.424
	5-6	5.5	1.0164	1777	892	2.959	1.731	0.417
	6-7	6.5	1.0014	1452.5	716.5	2.951	1.723	0.428
	7-8	7.5	1.008	1331	588	2.626	1.384	0.393
	8-9	8.5	1.0084	1410.5	607	2.557	1.312	0.382
	9-10	9.5	1.012	1491	614	2.450	1.201	0.362
	10-11	10.5	1.0105	1579.5	676.5	2.552	1.307	0.372
	11-12	11.5	1.0068	1628	603	2.215	0.955	0.331
	12-13	12.5	1.0037	498.5	188	2.262	1.005	0.412
	13-14	13.5	1.0089	896	274	1.834	0.558	0.311
	14-15	14.5	1.0174	405.5	134.5	1.973	0.702	0.386
	15-16	15.5	1.0116	1205	322	1.599	0.312	0.266
	16-17	16.5	1.0071	1761.5	447	1.525	0.235	0.242
	17-18	17.5	1.0067	1671	390	1.410	0.115	0.228
	18-19	18.5	1.0093	1601	460.5	1.733	0.452	0.268
	19-20	19.5	1.0095	285	62.5	1.321	0.022	0.321
	20-21	20.5	1.013	1618.5	358	1.328	0.029	0.218
	21-22	21.5	1.012	1452	299	1.231	-0.072	0.212
	22-23	22.5	1.0042	1602.5	362.5	1.363	0.066	0.225
	23-24	23.5	1.0094	958	190	1.189	-0.116	0.223
	24-25	24.5	1.0167	1077.5	198	1.094	-0.215	0.205
	25-26	25.5	1.0161	1196	213	1.066	-0.244	0.196
	26-27	26.5	1.0189	1479.5	304.5	1.229	-0.075	0.209
	27-28	27.5	1.0103	1682	323	1.156	-0.150	0.196
	28-29	28.5	1.0093	1175.5	216	1.107	-0.201	0.202
	29-30	29.5	1.004	1770	380	1.307	0.007	0.211
	30-31	30.5	1.0045	1281.5	237.5	1.128	-0.180	0.200
	31-32	31.5	1.0121	1471	278	1.141	-0.166	0.197
	32-33	32.5	1.0088	1654.5	334	1.223	-0.080	0.203

SBBC19	Interval	Depth	Weight (g)	Gross Po-209	Gross Po-210	Total Activity	Excess Activity	Error
	0-1	0.5						
	1-2	1.5	1.0126	1794	1021	3.453	2.352	0.454
	2-3	2.5	1.0132	1512.5	874.5	3.506	2.407	0.469
	3-4	3.5	1.0172	1554	926	3.599	2.505	0.477
	4-5	4.5	1.0079	829.5	480	3.527	2.430	0.512
	5-6	5.5	1.0029	1430	743	3.199	2.087	0.434
	6-7	6.5	1.0101	137.5	72.5	3.223	2.112	0.700
	7-8	7.5	1.0045	687	342	3.060	1.942	0.467
	8-9	8.5	1.0124	1534.5	717	2.850	1.722	0.391
	9-10	9.5	1.0045	740	318	2.589	1.451	0.419
	10-11	10.5	1.0197	1498.5	614.5	2.434	1.289	0.356
	11-12	11.5	1.0209	1079	431	2.368	1.220	0.366
	12-13	12.5	1.0163	967.5	408	2.511	1.370	0.390
	13-14	13.5	1.0061	1357	502	2.237	1.083	0.336
	14-15	14.5	1.0071	969.5	398.5	2.483	1.340	0.384
	15-16	15.5	1.0095	1381	471	2.055	0.893	0.313
	16-17	16.5	1.0149	1637.5	511	1.870	0.700	0.283
	17-18	17.5	1.0146	1563	426	1.642	0.462	0.255
	18-19	18.5	1.0044	940.5	237.5	1.537	0.352	0.266
	19-20	19.5	1.0088	1456	437	1.819	0.646	0.280
	20-21	20.5	1.0071	1817.5	471.5	1.575	0.391	0.242
	21-22	21.5	1.006	1478	353	1.459	0.270	0.234
	22-23	22.5	1.0181	1620.5	371.5	1.384	0.192	0.221
	23-24	23.5	1.0191	612	146	1.438	0.249	0.273
	24-25	24.5	1.0021	998.5	166	1.009	-0.199	0.196
	25-26	25.5	1.0136	1114	238	1.302	0.106	0.224
	26-27	26.5	1.0189	1544.5	273.5	1.073	-0.132	0.183
	27-28	27.5	1.018	1679	366	1.322	0.128	0.211
	28-29	28.5	1.0047	1290.5	256	1.219	0.020	0.208
	29-30	29.5	1.0079	1815	335	1.142	-0.060	0.184
	30-31	30.5	1.0029	1382.5	269.5	1.212	0.013	0.202

SBBC20	Interval	Depth	Weight (g)	Gross Po-209	Gross Po-210	Total Activity	Excess Activity	Error
	0-1	0.5	1.0041	1163	691	3.654	2.668	0.498
	1-2	1.5	1.0064	1058.5	590	3.420	2.424	0.477
	2-3	2.5	1.0144	1261	639	3.100	2.090	0.425
	3-4	3.5	1.0019	88.5	56.5	3.955	2.982	0.913
	4-5	4.5	1.0162	1442	656	2.778	1.753	0.382
	5-6	5.5	1.0185	1248.5	744	3.631	2.644	0.485
	6-7	6.5	1.0057	567	232	2.538	1.502	0.411
	7-8	7.5	1.0186	1674.5	639.5	2.339	1.294	0.323
	8-9	8.5	1.0064	1562	562	2.230	1.180	0.314
	9-10	9.5	1.0158	1799.5	637	2.174	1.122	0.301
	10-11	10.5	1.0097	1643	493	1.863	0.797	0.268
	11-12	11.5	1.0061	1623.5	496.5	1.906	0.842	0.274
	12-13	12.5	1.0047	1539	405	1.642	0.566	0.246
	13-14	13.5	1.0179	360.5	72	1.230	0.136	0.272
	14-15	14.5	1.0123	354	76	1.363	0.275	0.282
	15-16	15.5	1.0017	1456.6	277.5	1.223	0.128	0.191
	16-17	16.5	1.005	500	102	1.305	0.214	0.250
	17-18	17.5	1.0078	300.5	52	1.104	0.004	0.259
	18-19	18.5	1.0035	1671	280	1.079	-0.022	0.169
	19-20	19.5	1.0019	1212.5	237.5	1.232	0.138	0.205
	20-21	20.5	1.0024	1196	240	1.261	0.169	0.209
	21-22	21.5	1.0176	1412.5	268	1.175	0.078	0.192
	22-23	22.5	1.0051	933	191	1.290	0.198	0.221
	23-24	23.5	1.0015	1039.5	190.5	1.159	0.062	0.201
	24-25	24.5	1.014	1351	284	1.313	0.223	0.209

SBBC21	Interval	Depth	Weight (g)	Gross Po-209	Gross Po-210	Total Activity	Excess Activity	Error
	0-1	0.5	1.0066	1476	724	3.379	2.278	0.368
	1-2	1.5	1.0165	715.5	412.5	3.797	2.717	0.476
	2-3	2.5	1.0083	941	495	3.493	2.399	0.428
	3-4	3.5	1.0118	630.5	288	3.022	1.907	0.407
	4-5	4.5	1.0168	750	400	3.529	2.437	0.442
	5-6	5.5	1.0185	735.5	355.5	3.193	2.085	0.410
	6-7	6.5	1.0036	985	405	2.757	1.629	0.349
	7-8	7.5	1.0027	1652.5	816	3.314	2.211	0.377
	8-9	8.5	1.0189	201	86	2.883	1.761	0.488
	9-10	9.5	1.0201	1362.5	635.5	3.139	2.029	0.356
	10-11	10.5	1.0177	1532	684	3.012	1.896	0.339
	11-12	11.5	1.0054	1472.5	561	2.601	1.466	0.303
	12-13	12.5	1.0031	1109	429	2.661	1.528	0.319
	13-14	13.5	1.0027	1275.5	491.5	2.652	1.519	0.312
	14-15	14.5	1.0161	1232	387	2.133	0.976	0.264
	15-16	15.5	1.0183	498.5	165	2.243	1.091	0.324
	16-17	16.5	1.0076	219	59	1.854	0.684	0.351
	17-18	17.5	1.0208	235.5	74.5	2.149	0.993	0.376
	18-19	18.5	1.0061	1252	402	2.213	1.060	0.269
	19-20	19.5	1.0192	1391.5	397	1.941	0.776	0.239
	20-21	20.5	1.01	400	123	2.122	0.965	0.323
	21-22	21.5	1.0124	1721.5	482.5	1.929	0.763	0.229
	22-23	22.5	1.0036	950	226	1.652	0.473	0.225
	23-24	23.5	1.0053	1670.5	374	1.537	0.352	0.197
	24-25	24.5	1.0055	336	74	1.527	0.342	0.271
	25-26	25.5	1.0056	537.5	131.5	1.696	0.519	0.258
	26-27	26.5	1.0142	1387	291	1.442	0.253	0.190
	27-28	27.5	1.0193	1495.5	351	1.605	0.424	0.203
	28-29	28.5	1.0116	1004	203	1.400	0.209	0.196
	29-30	29.5	1.0128	1722.5	379.5	1.524	0.339	0.190
	30-31	30.5	1.0054	1248	276	1.541	0.357	0.202

SBBC28	Interval	Depth	Weight (g)	Gross Po-209	Gross Po-210	Total Activity	Excess Activity	Error
	0-1	0.5	1.0135	1752	1146	4.247	3.261	0.481
	1-2	1.5	1.0033	1879.5	1114	3.888	2.888	0.444
	2-3	2.5	1.0107	440	226	3.361	2.343	0.486
	3-4	3.5	1.0075	1603.5	703.5	2.880	1.844	0.349
	4-5	4.5	1.0185	565	185	2.116	1.052	0.329
	5-6	5.5	1.0044	485.5	169	2.281	1.224	0.360
	6-5	6.5	1.0183	720	230	2.075	1.010	0.306
	6-7	7.5	1.0022	601.5	138.5	1.520	0.435	0.255
	7-8	8.5	1.0025	584	143	1.616	0.534	0.268
	8-9	9.5	1.0064	669.5	166	1.630	0.549	0.262
	9-10	10.5	1.0047	1146	237	1.368	0.278	0.206
	10-11	11.5	1.0186	1233.5	239.5	1.267	0.173	0.192
	11-12	12.5	1.0078	964	201	1.375	0.285	0.214
	12-13	13.5	1.0075	1520.5	270	1.172	0.074	0.175
	13-14	14.5	1.0164	1081	194	1.180	0.083	0.186
	14-15	15.5	1.009	979.5	172.5	1.166	0.068	0.188
	15-16	16.5	1.005	1467	263	1.192	0.095	0.177
	16-17	17.5	1.0127	472.5	94	1.312	0.220	0.241
	17-18	18.5	1.009	1035	161	1.040	-0.062	0.169
	19-20	20.5	1.0141	1047	165	1.049	-0.053	0.170
	20-21	21.5	1.0126	1290.5	200	1.033	-0.070	0.161
	21-22	22.5	1.008	1205	193	1.078	-0.023	0.167
	22-23	23.5	1.0046	1145.5	189.5	1.117	0.018	0.173
	23-24	24.5	1.0194	548	93	1.085	-0.016	0.212
	24-25	25.5	1.0185	1076.5	182	1.082	-0.019	0.182
	25-26	26.5	1.0185	338	56	1.065	-0.036	0.238
	26-27	27.5	1.0049	1273.5	213.5	1.093	-0.008	0.176
	27-28	28.5	1.0012	779	136	1.142	0.044	0.201
	28-29	29.5	1.0161	672.5	101	0.968	-0.137	0.186
	29-30	30.5	1.0079	277	51	1.202	0.106	0.271
	30-31	31.5	1.0162	1395.5	268.5	1.246	0.152	0.188
	31-32	32.5	1.0105	1272	238	1.219	0.123	0.189
	32-33	33.5	1.016	1325.5	244	1.193	0.096	0.184
	33-34	34.5	1.0177	1268	212	1.087	-0.014	0.173

APPENDIX B

SBBC1	Interval	Depth	Total %Gravel	Total %Sand	Total %Silt	Total %Clay	d (0.5)	Mean	Mode	Porosity	Cumulative Mass	Corrected Depth
	0-1	0.5	0.02	16.55	68.06	15.37	21.10	35.47	44.83	0.701	0.347	0.500
	1-2	1.5	0.05	14.75	68.12	17.08	19.61	31.72	44.07	0.701	1.092	1.571
	2-3	2.5	0.00	13.31	67.44	19.25	18.61	28.79	42.23	0.685	1.905	2.742
	3-4	3.5	0.00	15.18	65.93	18.89	18.32	35.91	42.85	0.643	2.796	4.023
	4-5	4.5	0.06	14.27	66.09	19.59	17.70	35.00	42.37	0.631	3.758	5.408
	5-6	5.5	0.00	14.92	65.90	19.18	18.11	31.97	42.61	0.622	4.747	6.831
	6-7	6.5	0.00	13.47	67.07	19.46	17.46	28.59	41.94	0.602	5.775	8.310
	7-8	7.5	0.00	14.51	66.07	19.42	18.24	32.92	43.68	0.594	6.840	9.842
	8-9	8.5	0.00	15.97	65.79	18.24	20.00	34.84	44.32	0.614	7.889	11.352
	9-10	9.5	0.06	16.83	64.73	18.38	20.06	39.17	44.64	0.615	8.911	12.823
	10-11	10.5	0.02	16.20	65.28	18.50	19.79	34.25	44.58	0.611	9.937	14.300
	11-12	11.5	0.00	20.32	62.63	17.05	23.96	40.58	49.73	0.599	10.984	15.806
	12-13	12.5	0.00	22.17	61.21	16.62	25.75	43.39	52.23	0.596	12.050	17.339
	13-14	13.5	0.03	23.05	60.00	16.92	25.25	43.22	53.98	0.591	13.127	18.889
	14-15	14.5	0.01	22.15	59.87	17.98	24.01	47.03	52.17	0.589	14.214	20.454
	14-15a	15.5	0.00	21.66	59.83	18.52	23.24	42.41	53.05	0.573	15.325	22.052
	15-16	16.5	0.00	20.05	59.37	20.58	20.43	40.57	52.47	0.553	16.483	23.719
	16-17	17.5	0.00	16.59	60.54	22.87	16.33	37.88	45.82	0.561	17.657	25.408
	17-18	18.5	0.00	16.20	61.58	22.22	16.44	34.30	46.37	0.585	18.788	27.036
	18-19	19.5	0.00	16.42	62.42	21.16	17.19	35.74	46.15	0.600	19.869	28.592
	19-20	20.5	0.00	15.13	62.85	22.02	15.61	37.60	43.91	0.609	20.917	30.100
	20-21	21.5	0.00	15.55	62.73	21.72	15.95	33.37	43.11	0.600	21.965	31.608
	21-22	22.5	0.00	15.94	61.97	22.09	15.63	33.18	45.48	0.603	23.021	33.127
	22-23	23.5	0.00	22.21	58.06	19.73	22.54	42.91	55.98	0.543	24.153	34.756
	23-24	24.5	0.00	24.52	57.10	18.39	25.03	47.39	57.08	0.549	25.357	36.489
	24-25	25.5	0.00	15.90	62.64	21.46	17.84	33.74	44.80	0.564	26.532	38.180
	25-26	26.5	0.00	16.03	62.83	21.14	17.38	32.58	46.29	0.598	27.642	39.777
	26-27	27.5	0.00	17.86	62.45	19.69	19.72	38.81	47.01	0.661	28.625	41.191
	27-28	28.5	0.43	15.80	64.26	19.51	18.66	33.98	44.76	0.624	29.573	42.555
	28-29	29.5	0.00	16.34	63.92	19.74	17.52	43.55	41.51	0.650	30.535	43.939
	29-30	30.5	0.00	14.72	65.13	20.14	17.49	34.56	41.27	0.637	31.480	45.300
	30-31	31.5	0.00	13.82	66.36	19.82	17.04	32.32	38.95	0.631	32.450	46.696
	31-32	32.5	0.00	12.36	67.35	20.29	16.04	30.84	37.03	0.630	33.428	48.103
	32-33	33.5	0.00	13.89	65.28	20.82	16.18	33.48	38.50	0.613	34.431	49.547
	33-34	34.5	0.00	14.88	64.96	20.16	17.14	33.40	41.35	0.614	35.456	51.021
	34-35	35.5	0.00	15.21	64.62	20.17	17.09	33.81	41.69	0.612	36.481	52.496
	35-36	36.5	0.00	14.83	64.53	20.64	16.54	36.48	40.35	0.604	37.520	53.992
	36-37	37.5	0.00	15.46	63.89	20.64	16.44	43.18	39.88	0.607	38.566	55.497
	37-38	38.5	0.00	15.47	63.14	21.39	16.30	40.16	42.10	0.596	39.623	57.018
	38-39	39.5	0.00	15.68	62.36	21.97	16.67	36.55	43.87	0.578	40.717	58.592

SBBC2	Interval	Depth	Total %Gravel	Total %Sand	Total %Silt	Total %Clay	d (0.5)	Mean	Mode	Porosity	Cumulative Mass	Corrected Depth
	0-1	0.5	0.03	3.46	59.07	37.45	5.83	23.11	6.71	0.804	0.260	0.519
	1-2	1.5	0.10	3.88	59.56	36.45	5.98	27.40	6.83	0.811	0.770	1.539
	2-3	2.5	0.00	2.27	61.37	36.36	5.93	18.20	6.88	0.772	1.322	2.642
	3-4	3.5	0.00	1.59	60.59	37.82	5.69	13.53	6.69	0.779	1.917	3.831
	4-5	4.5	0.25	2.15	57.85	39.74	5.40	24.23	6.59	0.769	2.516	5.030
	5-6	5.5	0.00	1.45	58.41	40.15	5.34	15.44	6.53	0.768	3.130	6.257
	6-7	6.5	0.08	1.84	60.30	37.77	5.67	16.36	6.60	0.770	3.743	7.481
	7-8	7.5	0.00	2.99	59.51	37.50	5.76	25.69	6.61	0.756	4.372	8.738
	8-9	8.5	0.24	3.19	60.71	35.85	6.01	23.74	6.79	0.749	5.027	10.048
	9-10	9.5	0.00	2.88	59.57	37.55	5.75	23.77	6.56	0.748	5.693	11.380
	10-11	10.5	0.00	1.05	60.40	38.56	5.57	9.50	6.56	0.740	6.373	12.737
	11-12	11.5	0.00	1.56	60.54	37.90	5.66	13.77	6.59	0.738	7.064	14.120
	12-13	12.5	0.00	1.46	59.12	39.43	5.44	13.04	6.44	0.738	7.758	15.506
	13-14	13.5	0.25	1.52	59.18	39.05	5.49	12.99	6.44	0.729	8.463	16.916
	14-15	14.5	0.00	4.02	60.37	35.61	6.12	26.08	6.63	0.733	9.176	18.341
	15-16	15.5	0.43	4.29	59.55	35.73	6.10	27.54	6.56	0.730	9.888	19.764
	16-17	16.5	0.00	2.05	61.05	36.90	5.86	12.90	6.54	0.725	10.611	21.208
	17-18	17.5	0.00	3.44	60.28	36.29	5.98	22.81	6.49	0.724	11.342	22.670
	18-19	18.5	0.07	4.29	59.93	35.71	6.12	26.14	6.57	0.721	12.078	24.140
	19-20	19.5	0.00	4.07	59.06	36.88	5.91	31.80	6.44	0.718	12.821	25.625
	20-21	20.5	0.00	3.89	59.24	36.87	5.90	24.93	6.51	0.721	13.556	27.094
	21-22	21.5	0.00	3.56	58.57	37.87	5.71	25.29	6.35	0.702	14.358	28.697
	22-23	22.5	0.05	0.55	57.45	41.96	5.06	8.48	6.09	0.721	15.034	30.049
	23-24	23.5	0.00	2.02	57.00	40.99	5.22	19.62	6.22	0.719	15.892	31.764
	24-25	24.5	0.00	0.60	57.19	42.22	5.04	8.46	6.28	0.715	16.529	33.037
	25-26	25.5	0.00	0.37	57.30	42.33	5.05	8.31	6.70	0.706	17.416	34.810
	26-27	26.5	0.00	0.40	57.77	41.83	5.13	8.40	6.82	0.706	18.064	36.104
	27-28	27.5	0.00	0.06	56.90	43.04	4.94	7.76	6.75	0.699	18.993	37.962
	28-29	28.5	0.00	0.79	57.92	41.29	5.18	13.66	6.66	0.697	19.645	39.266
	29-30	29.5	0.00	0.79	57.92	41.29	5.27	30.38	6.14	0.690	20.613	41.199
	30-31	30.5	0.00	0.25	58.75	41.01	5.18	8.29	6.22	0.683	21.288	42.549
	31-32	31.5	0.00	0.36	58.10	41.54	5.10	8.29	6.08	0.682	22.279	44.529
	32-33	32.5	0.00	1.71	57.49	40.80	5.22	16.42	6.19	0.684	22.966	45.902
	33-34	33.5	0.00	0.88	57.39	41.73	5.06	12.68	6.04	0.682	23.964	47.897
	34-35	34.5	0.00	0.19	57.06	42.75	4.91	7.76	5.93	0.681	24.649	49.267
	35-36	35.5	0.00	0.09	56.76	43.16	4.86	7.64	5.88	0.683	25.646	51.260
	36-37	36.5	0.00	0.49	55.97	43.54	4.81	7.90	5.92	0.677	26.351	52.667
	37-38	37.5	0.01	0.28	55.04	44.66	4.66	7.45	5.88	0.674	27.352	54.670

SBBC3	Interval	Depth	Total %Gravel	Total %Sand	Total %Silt	Total %Clay	d (0.5)	Mean	Mode	Porosity	Cumulative Mass	Corrected Depth
	0-1	0.5	0.00	2.05	53.78	44.18	4.70	19.37	5.60	0.861	0.184	0.500
	1-2	1.5	0.00	1.30	56.33	42.37	4.91	15.58	5.77	0.825	0.601	1.629
	2-3	2.5	0.00	1.77	56.97	41.27	5.06	16.14	5.85	0.810	1.084	2.939
	3-4	3.5	0.00	0.22	57.11	42.67	4.85	7.40	5.73	0.805	1.593	4.321
	4-5	4.5	0.00	0.10	56.08	43.82	4.72	7.12	5.73	0.799	2.117	5.743
	5-6	5.5	0.23	1.80	56.48	41.49	5.03	19.18	5.82	0.784	2.669	7.240
	6-7	6.5	0.01	0.00	56.81	43.18	4.80	7.11	5.80	0.785	3.240	8.788
	7-8	7.5	0.00	1.65	56.64	41.71	5.00	19.14	5.83	0.779	3.818	10.355
	8-9	8.5	0.05	0.00	54.94	45.00	4.57	6.76	5.69	0.774	4.410	11.962
	9-10	9.5	0.00	0.04	54.99	44.97	4.58	6.85	5.69	0.776	5.005	13.576
	10-11	10.5	0.02	0.45	55.96	43.57	4.76	7.61	5.73	0.767	5.610	15.217
	11-12	11.5	0.00	0.47	54.52	45.01	4.58	7.34	5.60	0.765	6.230	16.899
	12-13	12.5	0.00	2.08	54.68	43.25	4.82	22.25	5.61	0.757	6.864	18.618
	13-14	13.5	0.00	0.47	55.94	43.60	4.77	7.66	5.73	0.746	7.523	20.405
	14-15	14.5	0.11	1.63	57.05	41.21	5.08	13.77	5.84	0.749	8.192	22.221
	15-16	15.5	0.00	0.50	55.97	43.53	4.76	7.58	5.70	0.745	8.864	24.042
	16-17	16.5	0.12	2.27	56.21	41.40	5.07	19.44	5.81	0.738	9.550	25.902
	17-18	17.5	0.00	2.26	55.76	41.98	4.99	22.04	5.76	0.734	10.250	27.802
	18-19	18.5	0.00	0.67	56.18	43.15	4.82	7.97	5.70	0.726	10.965	29.742
	19-20	19.5	0.00	2.14	55.92	41.94	5.00	15.69	5.73	0.725	11.692	31.714
	20-21	20.5	0.00	0.28	54.46	45.27	4.54	7.07	5.57	0.722	12.425	33.703
	21-22	21.5	0.00	1.30	54.02	44.68	4.62	13.22	5.47	0.726	13.158	35.689
	22-23	22.5	0.00	0.68	54.40	44.92	4.59	7.65	5.64	0.744	13.861	37.596
	23-24	23.5	0.00	0.00	57.13	42.87	4.85	7.26	6.00	0.744	14.540	39.437
	24-25	24.5	0.00	0.00	56.83	43.17	4.80	7.15	5.81	0.745	15.216	41.273
	25-26	25.5	0.00	0.00	56.70	43.30	4.78	7.08	5.86	0.750	15.886	43.089
	26-27	26.5	0.00	0.00	55.09	44.91	4.58	6.71	5.72	0.741	16.561	44.920
	27-28	27.5	0.00	0.00	57.19	42.81	4.84	7.14	5.86	0.739	17.250	46.789
	28-29	28.5	0.00	0.00	54.45	45.55	4.51	6.75	5.70	0.737	17.945	48.674
	29-30	29.5	0.00	0.00	54.11	45.89	4.47	6.70	5.67	0.736	18.643	50.568
	30-31	30.5	0.00	0.00	53.60	46.40	4.41	6.56	5.64	0.730	19.351	52.487
	31-32	31.5	0.00	0.00	52.91	47.09	4.33	6.59	5.52	0.725	20.073	54.447
	32-33	32.5	0.00	0.00	52.64	47.36	4.30	6.39	5.55			
	33-34	33.5	0.46	3.39	52.64	43.50	4.77	37.43	5.60	0.710	21.410	58.073
	34-35	34.5	0.58	0.00	53.46	45.96	4.43	6.70	5.58	0.694	22.200	60.216
	35-36	35.5	0.37	0.00	53.47	46.16	4.42	6.66	5.56	0.689	23.018	62.434
	36-37	36.5	0.14	0.00	53.03	46.83	4.35	6.47	5.53	0.701	23.826	64.626

SBBC4	Interval	Depth	Total %Gravel	Total %Sand	Total %Silt	Total %Clay	d (0.5)	Mean	Mode	Porosity	Cumulative Mass	Corrected Depth
	0-1	0.5	0.00	3.36	64.14	32.50	6.94	24.16	8.53	0.862	0.183	0.500
	1-2	1.5	0.00	3.66	70.90	25.45	8.56	17.04	9.77	0.836	0.584	1.593
	2-3	2.5	0.00	3.82	65.26	30.91	7.32	22.18	8.80	0.788	1.083	2.952
	3-4	3.5	0.00	3.99	66.98	29.04	7.73	21.08	9.02	0.772	1.666	4.541
	4-5	4.5	0.00	2.79	66.71	30.50	7.42	15.42	9.08	0.736	2.317	6.315
	5-6	5.5	0.00	2.56	67.67	29.77	7.48	13.76	8.96	0.726	3.029	8.258
	6-7	6.5	0.00	4.39	70.89	24.71	8.74	19.93	9.66	0.761	3.710	10.113
	7-8	7.5	0.00	3.04	67.22	29.75	7.51	16.30	8.96	0.751	4.357	11.878
	8-9	8.5	0.00	3.96	66.75	29.30	7.68	22.50	8.90	0.731	5.044	13.750
	9-10	9.5	0.00	1.20	65.14	33.66	6.73	10.84	8.94	0.754	5.728	15.613
	10-11	10.5	0.00	4.86	66.97	28.17	7.98	25.78	8.96	0.727	6.416	17.489
	11-12	11.5	0.00	1.49	65.79	32.72	6.83	11.24	8.62	0.735	7.129	19.433
	12-13	12.5	0.08	3.28	65.31	31.33	7.19	23.13	8.62	0.723	7.848	21.391
	13-14	13.5	0.00	1.85	65.97	32.18	7.01	11.88	8.76	0.690	8.625	23.510
	14-15	14.5	0.00	5.34	63.66	31.00	7.39	34.55	8.68	0.682	9.456	25.776
	15-16	15.5	5.38	2.76	61.50	30.36	7.09	15.55	8.75	0.696	10.280	28.021
	16-17	16.5	0.77	2.91	64.08	32.25	7.00	17.85	8.67	0.685	11.101	30.259
	17-18	17.5	0.00	3.41	64.56	32.03	7.09	21.74	8.68	0.683	11.938	32.542
	18-19	18.5	0.05	3.12	63.82	33.02	6.84	26.58	8.48	0.668	12.797	34.884
	19-20	19.5	0.00	2.69	64.68	32.63	6.93	16.75	8.61	0.660	13.687	37.310
	20-21	20.5	1.14	3.31	62.87	32.68	6.85	24.74	8.53	0.657	14.593	39.778
	21-22	21.5	0.44	2.42	63.77	33.38	6.71	16.01	8.48	0.637	15.529	42.329
	22-23	22.5	0.01	3.12	63.03	33.85	6.69	22.25	8.54	0.635	16.493	44.956
	23-24	23.5	9.13	2.68	57.14	31.06	6.63	23.21	8.43	0.633	17.463	47.601
	24-25	24.5	0.00	3.44	61.78	34.78	6.58	27.15	8.51	0.627	18.444	50.276

SBBC5	Interval	Depth	Total %Gravel	Total %Sand	Total %Silt	Total %Clay	d (0.5)	Mean	Mode	Porosity	Cumulative Mass	Corrected Depth
	0-1	0.5	0.00	3.69	67.14	29.17	7.90	20.43	9.17	0.832	0.223	0.500
	1-2	1.50	0.00	3.89	66.91	29.20	7.89	26.68	9.21	0.771	0.749	1.679
	2-3	2.50	0.00	2.04	67.96	30.00	7.65	12.80	9.34	0.750	1.383	3.099
	3-4	3.50	0.00	2.58	67.18	30.25	7.63	15.71	9.29	0.740	2.058	4.612
	4-5	4.50	0.00	3.01	67.77	29.22	7.90	16.08	9.33	0.725	2.767	6.200
	5-6	5.50	0.02	2.90	67.08	29.99	7.66	20.07	9.17	0.718	3.504	7.852
	6-7	6.50	0.00	2.13	67.43	30.44	7.45	12.65	8.95	0.718	4.251	9.526
	7-8	7.50	0.00	2.01	67.32	30.68	7.45	12.57	9.06	0.705	5.017	11.241
	8-9	8.50	0.00	1.71	66.91	31.38	7.31	12.21	9.01	0.714	5.787	12.968
	9-10	9.50	0.11	1.65	66.59	31.66	7.20	12.03	8.86	0.708	6.554	14.686
	10-11	10.50	0.00	1.59	67.02	31.39	7.27	12.07	8.94	0.703	7.334	16.435
	11-12	11.50	0.44	1.77	66.52	31.27	7.26	12.20	8.89	0.707	8.116	18.188
	12-13	12.50	0.01	2.36	66.47	31.16	7.34	13.86	8.90	0.684	8.924	19.996
	13-14	13.50	0.00	3.25	65.10	31.65	7.25	24.19	8.80	0.679	9.768	21.888
	14-15	14.50	0.00	3.25	65.10	31.65	6.89	11.07	8.64	0.666	10.635	23.832
	15-16	15.50	0.00	3.38	64.09	32.53	7.08	25.40	8.71	0.655	11.535	25.848
	16-17	16.50	0.00	1.03	65.79	33.19	6.76	10.92	8.41	0.643	12.465	27.933
	17-18	17.50	0.00	1.30	64.66	34.04	6.62	14.34	8.46	0.649	13.402	30.033
	18-19	18.50	0.00	0.80	65.23	33.98	6.61	10.54	8.42	0.646	14.335	32.123
	19-20	19.50	0.00	0.97	65.20	33.83	6.65	10.76	8.44	0.629	15.295	34.274
	20-21	20.50	0.34	1.09	64.28	34.29	6.53	12.73	8.37	0.627	16.281	36.483
	21-22	21.50	0.00	0.63	64.74	34.63	6.47	10.19	8.34	0.624	17.274	38.708
	22-23	22.50	0.00	0.71	64.64	34.65	6.48	10.30	8.37	0.615	18.283	40.968
	23-24	23.50	0.00	0.43	63.54	36.03	6.13	9.43	8.07	0.616	19.301	43.252
	24-25	24.50	0.00	1.37	63.67	34.96	6.50	10.93	8.49	0.617	20.318	45.529
	25-26	25.50	0.00	1.99	64.78	33.23	6.86	15.54	8.75	0.607	21.345	47.832
	26-27	26.50	0.29	1.69	64.77	33.26	6.83	11.86	8.78	0.600	22.395	50.184
	27-28	27.50	0.00	2.31	65.17	32.52	7.05	15.45	8.99	0.607	23.445	52.537

SBBC6	Interval	Depth	Total %Gravel	Total %Sand	Total %Silt	Total %Clay	d (0.5)	Mean	Mode	Porosity	Cumulative Mass	Corrected Depth
	0-1	0.5	0.00	6.97	63.12	29.91	8.23	27.59	8.57	0.813	0.248	0.500
	1-2	1.5	0.00	9.85	62.55	27.61	9.29	38.66	8.64	0.753	0.823	1.661
	2-3	2.5	0.03	7.49	62.88	29.60	8.28	29.06	8.29	0.730	1.507	3.044
	3-4	3.5	0.26	8.43	63.30	28.01	9.07	26.44	8.78	0.704	2.257	4.557
	4-5	4.5	0.11	8.42	62.71	28.75	8.87	35.71	8.82	0.672	3.083	6.226
	5-6	5.5	0.31	8.34	63.76	27.59	9.01	28.39	8.72	0.665	3.962	8.000
	6-7	6.5	0.00	9.12	63.51	27.38	9.23	29.99	8.78	0.681	4.828	9.749
	7-8	7.5	1.20	8.64	62.50	27.66	8.96	30.54	8.63	0.663	5.696	11.503
	8-9	8.5	0.64	8.75	62.97	27.64	9.01	28.68	8.67	0.663	6.589	13.306
	9-10	9.5	0.11	7.33	63.11	29.45	8.51	24.82	8.77	0.648	7.502	15.150
	10-11	10.5	0.18	6.77	62.66	30.39	7.96	27.15	8.49	0.637	8.449	17.062
	11-12	11.5	0.22	6.87	62.58	30.34	7.97	29.56	8.43	0.621	9.433	19.047
	12-13	12.5	0.16	6.09	62.37	31.38	7.58	27.17	8.39	0.611	10.450	21.102
	13-14	13.5	0.26	7.79	62.41	29.53	8.31	28.41	8.62	0.606	11.487	23.197
	14-15	14.5	1.10	5.45	62.83	30.62	7.84	19.80	8.67	0.592	12.550	25.343
	15-16	15.5	0.00	6.70	62.49	30.81	7.90	28.57	8.62	0.588	13.636	27.536
	16-17	16.5	0.00	3.74	64.12	32.14	7.41	14.45	8.64	0.589	14.727	29.738
	17-18	17.5	0.00	6.01	62.63	31.36	7.73	33.28	8.76	0.588	15.819	31.943
	18-19	18.5	0.00	4.91	63.91	31.19	7.81	18.65	9.10	0.584	16.916	34.160
	19-20	19.5	0.00	4.33	64.70	30.97	7.86	15.40	9.18	0.574	18.033	36.414
	20-21	20.5	0.02	4.98	64.18	30.82	7.95	17.29	9.17	0.576	19.159	38.689
	21-22	21.5	0.38	5.89	63.49	30.24	8.14	22.85	9.26	0.575	20.284	40.961
	22-23	22.5	0.00	5.89	63.64	30.46	8.15	18.54	9.12	0.572	21.414	43.242
	23-24	23.5	0.14	5.60	63.87	30.40	8.11	18.50	9.21	0.573	22.546	45.527
	24-25	24.5	0.03	7.35	63.25	29.37	8.56	23.52	9.10	0.570	23.680	47.819
	25-26	25.5	0.18	7.04	63.44	29.35	8.51	20.57	9.01	0.568	24.823	50.125
	26-27	26.5	1.01	7.48	61.90	29.61	8.41	26.54	9.05	0.566	25.971	52.444
	27-28	27.5	0.23	8.71	62.19	28.87	8.99	26.63	9.64	0.553	27.139	54.802
	28-29	28.5	1.52	10.20	60.18	28.10	9.19	34.13	9.42	0.551	28.326	57.199
	29-30	29.5	1.34	8.30	61.24	29.13	8.62	28.03	9.14	0.559	29.505	59.580
	30-31	30.5	0.62	8.79	61.41	29.17	8.64	26.82	9.08	0.562	30.670	61.933
	31-32	31.5	2.37	7.79	59.89	29.95	8.14	26.79	8.86	0.551	31.845	64.306
	32-33	32.5	0.01	9.57	60.95	29.47	8.56	32.89	8.80	0.554	33.030	66.699
	33-34	33.5	4.02	6.59	59.40	30.00	7.78	23.53	8.58	0.557	34.208	69.077
	34-35	34.5	0.00	8.14	61.16	30.70	8.06	23.50	8.61			

SBBC7	Interval	Depth	Total %Gravel	Total %Sand	Total %Silt	Total %Clay	d (0.5)	Mean	Mode	Porosity	Cumulative Mass	Corrected Depth
	0-1	0.5	25.02	7.95	42.63	24.40	7.12	55.28	6.82	0.671	0.436	0.500
	1-2	1.5	53.43	4.14	27.48	14.95	7.07	39.43	6.81	0.469	1.575	1.808
	2-3	2.5	34.31	5.48	37.38	22.83	6.53	43.52	6.65	0.587	2.826	3.244
	3-4	3.5	17.79	9.01	46.49	26.71	7.10	55.11	6.77	0.582	3.927	4.508
	4-5	4.5	7.04	7.08	53.91	31.97	6.61	34.70	6.79	0.582	5.035	5.780
	5-6	5.5	13.13	7.88	49.49	29.49	6.79	43.46	6.82	0.593	6.129	7.036
	6-7	6.5	6.33	5.89	54.06	33.73	6.26	32.06	6.75	0.569	7.239	8.310
	7-8	7.5	9.36	8.91	50.48	31.25	6.71	49.54	6.75	0.572	8.377	9.617
	8-9	8.5	3.34	8.35	55.17	33.14	6.74	38.24	6.87	0.551	9.540	10.951
	9-10	9.5	2.38	8.83	55.15	33.65	6.71	38.01	6.84	0.559	10.719	12.305
	10-11	10.5	4.88	9.51	53.52	32.09	6.93	58.80	6.93	0.563	11.882	13.640
	11-12	11.5	3.62	8.51	55.02	32.85	6.83	42.79	6.82	0.553	13.052	14.984
	12-13	12.5	11.69	7.53	51.20	29.58	7.00	33.17	6.97	0.566	14.219	16.323
	13-14	13.5	5.49	9.32	53.37	31.81	6.97	47.79	6.82	0.552	15.388	17.665
	14-15	14.5	2.32	7.86	56.49	33.33	6.77	30.51	6.82	0.569	16.552	19.002
	15-16	15.5	3.43	6.97	55.31	34.29	6.42	27.87	6.65	0.558	17.708	20.329

SBBC8	Interval	Depth	Total %Gravel	Total %Sand	Total %Silt	Total %Clay	d (0.5)	Mean	Mode	Porosity	Cumulative Mass	Corrected Depth
	0-1	0.5	0.01	4.91	63.49	31.59	7.10	24.36	7.82	0.810	0.252	0.500
	1-2	1.5	0.00	5.62	63.95	30.43	7.36	27.31	7.94	0.773	0.804	1.596
	2-3	2.5	0.00	6.58	62.59	30.83	7.35	38.16	7.99	0.745	1.442	2.861
	3-4	3.5	0.00	5.04	61.89	33.07	6.93	28.99	8.16	0.724	2.145	4.256
	4-5	4.5	0.00	7.19	62.51	30.30	7.59	36.30	8.17	0.710	2.894	5.744
	5-6	5.5	0.00	8.00	62.77	29.24	7.88	44.40	8.18	0.709	3.665	7.272
	6-7	6.5	0.07	7.44	63.89	28.61	8.07	31.81	8.17	0.707	4.440	8.810
	7-8	7.5	0.02	6.39	64.30	29.29	7.83	26.49	8.07	0.707	5.217	10.352
	8-9	8.5	0.36	5.15	65.10	29.39	7.78	33.09	8.19	0.696	6.008	11.922
	9-10	9.5	0.00	6.88	63.71	29.41	7.81	29.34	8.16	0.681	6.834	13.561
	10-11	10.5	0.00	6.66	63.04	30.30	7.63	31.28	8.16	0.679	7.683	15.246
	11-12	11.5	0.16	6.67	63.73	29.43	7.72	30.14	8.15	0.685	8.526	16.920
	12-13	12.5	0.01	5.70	63.00	31.29	7.34	28.87	8.10	0.670	9.382	18.617
	13-14	13.5	0.02	3.55	63.65	31.29	6.92	18.65	8.12	0.669	10.258	20.357
	14-15	14.5	0.00	6.09	62.77	31.14	7.34	32.49	7.99	0.674	11.129	22.085
	15-16	15.5	0.00	4.48	63.93	31.58	7.13	20.78	8.02	0.674	11.994	23.801
	16-17	16.5	0.15	5.74	62.46	31.65	7.23	29.77	7.94	0.675	12.857	25.514
	17-18	17.5	0.00	4.45	63.11	32.44	6.93	24.86	7.84	0.676	13.717	27.221
	18-19	18.5	0.07	3.56	62.84	33.53	6.70	24.66	7.69	0.676	14.576	28.925
	19-20	19.5	0.00	5.90	62.30	31.80	7.21	29.26	7.79	0.671	15.441	30.642
	20-21	20.5	0.00	6.45	61.46	32.09	7.18	33.86	7.69	0.672	16.312	32.371
	21-22	21.5	0.00	4.32	62.04	33.64	6.71	27.38	7.55	0.663	17.194	34.121
	22-23	22.5	0.21	7.20	61.40	31.20	7.41	32.48	7.70	0.674	18.073	35.865
	23-24	23.5	0.52	4.99	61.88	32.61	6.94	19.48	7.61	0.667	18.947	37.599
	24-25	24.5	0.39	5.95	61.24	32.42	7.07	28.17	7.68	0.661	19.837	39.365
	25-26	25.5	0.03	4.49	62.02	33.46	6.80	23.60	7.66	0.650	20.750	41.177
	26-27	26.5	0.22	5.62	61.26	32.91	6.96	36.51	7.75	0.649	21.679	43.020
	27-28	27.5	0.29	5.25	61.48	32.99	6.92	37.03	7.84	0.637	22.625	44.898
	28-29	28.5	0.73	5.23	61.86	32.18	7.12	28.59	8.03	0.623	23.606	46.844
	29-30	29.5	0.68	5.78	61.69	31.85	7.26	30.74	8.15	0.615	24.616	48.849
	30-31	30.5	0.20	6.46	61.55	31.78	7.37	36.88	8.27	0.611	25.642	50.884
	31-32	31.5	0.14	5.33	63.16	31.38	7.37	21.86	8.44	0.613	26.670	52.924
	32-33	32.5	0.14	5.61	62.47	31.78	7.31	34.08	8.39	0.621	27.685	54.939
	33-34	33.5	0.00	6.90	62.29	30.81	7.61	33.41	8.50	0.628	28.681	56.915
	34-35	34.5	1.58	5.11	62.08	31.23	7.33	22.82	8.49	0.636	29.657	58.851
	35-36	35.5	0.05	5.63	62.46	31.87	7.34	28.15	8.44	0.641	30.615	60.752
	36-37	36.5	0.00	6.06	62.39	31.55	7.41	27.65	8.37	0.654	31.548	62.605
	37-38	37.5	0.00	6.00	62.07	31.93	7.33	27.61	8.32	0.653	32.467	64.428
	38-39	38.5	0.00	5.62	62.56	31.83	7.34	24.42	8.40	0.650	33.391	66.261
	39-40	39.5	0.02	5.38	62.46	32.14	7.26	24.94	8.32	0.651	34.318	68.101
	40-41	40.5	1.33	5.92	61.24	31.51	7.35	27.38	8.37	0.631	35.269	69.989
	41-42	41.5	0.26	7.42	61.12	31.20	7.58	36.25	8.40	0.649	36.224	71.883
	42-43	42.5	0.06	7.04	61.33	31.57	7.54	35.37	8.40	0.641	37.164	73.750

SBBC9	Interval	Depth	Total %Gravel	Total %Sand	Total %Silt	Total %Clay	d (0.5)	Mean	Mode	Porosity	Cumulative Mass	Corrected Depth
	0-1	0.5	0.04	3.59	68.47	27.90	8.38	23.76	10.42	0.819	0.240	0.500
	1-2	1.5	0.00	2.31	71.03	26.66	8.53	13.88	10.39	0.767	0.789	1.642
	2-3	2.5	0.00	2.01	70.41	27.59	8.36	13.42	10.62	0.726	1.461	3.038
	3-4	3.5	3.03	2.18	68.31	26.49	8.46	13.72	10.70	0.702	2.219	4.614
	4-5	4.5	0.00	2.46	70.28	27.26	8.50	13.96	10.63	0.694	3.020	6.279
	6-5	5.5	0.00	3.79	68.57	27.64	8.57	27.28	10.48	0.469	4.129	8.585
	5-6	6.5	0.00	4.81	68.21	26.98	8.94	29.40	10.67	0.811	5.082	10.568
	6-7	7.5	0.00	3.40	68.98	27.61	8.62	19.22	10.48	0.662	5.781	12.022
	7-8	8.5	0.00	3.15	67.70	29.16	8.24	21.58	10.29	0.578	6.789	14.117
	8-9	9.5	0.03	2.68	68.01	29.28	8.08	17.73	10.06	0.612	7.863	16.350
	9-10	10.5	0.00	3.73	66.98	29.29	8.06	27.83	9.76	0.744	8.716	18.123
	10-11	11.5	0.02	3.65	66.84	29.49	7.93	27.60	9.55	0.769	9.360	19.463
	11-12	12.5	0.03	3.36	66.91	29.71	7.82	29.49	9.55	0.703	10.059	20.916
	12-13	13.5	0.33	2.28	67.55	29.84	7.71	16.79	9.53	0.590	10.994	22.862
	13-14	14.5	0.24	2.12	67.50	30.14	7.64	15.97	9.52	0.660	11.988	24.927
	14-15	15.5	4.36	3.03	63.61	29.00	7.65	24.91	9.48	0.604	12.963	26.955
	15-16	16.5	2.47	3.07	64.82	29.64	7.65	26.14	9.47	0.666	13.931	28.968
	16-17	17.5	0.26	4.17	65.57	30.00	7.79	32.19	9.47	0.715	14.751	30.674
	17-18	18.5	0.10	2.82	66.36	30.72	7.54	19.56	9.35	0.667	15.570	32.376
	18-19	19.5	0.00	3.55	65.52	30.94	7.50	27.22	9.26	0.701	16.407	34.117
	19-20	20.5	0.00	3.07	65.59	31.34	7.36	26.92	9.17	0.711	17.186	35.737
	20-21	21.5	0.24	3.35	64.88	31.53	7.29	27.23	9.07	0.435	18.317	38.090
	21-22	22.5	0.06	3.27	64.89	31.79	7.25	28.48	9.09	0.672	19.501	40.551
	22-23	23.5	0.00	2.82	65.75	31.43	7.27	24.09	9.08	0.704	20.329	42.272
	23-24	24.5	0.00	2.93	65.34	31.73	7.25	22.86	9.14	0.493	21.393	44.485
	24-25	25.5	0.69	2.68	64.94	31.69	7.18	26.20	9.12	0.569	22.636	47.070
	25-26	26.5	0.23	3.21	65.00	31.56	7.28	28.33	9.18	0.699	23.606	49.088
	26-27	27.5	0.00	3.35	65.06	31.60	7.32	27.36	9.11	0.586	24.554	51.058

SBBC10	Interval	Depth	Total %Gravel	Total %Sand	Total %Silt	Total %Clay	d (0.5)	Mean	Mode	Porosity	Cumulative Mass	Corrected Depth
	0-1	0.5	0.32	13.75	62.72	23.20	12.49	38.85	10.22	0.780	0.291	0.500
	1-2	1.5	1.51	13.81	59.98	24.69	12.58	43.01	12.60	0.743	0.922	1.585
	2-3	2.5	9.16	14.98	57.20	18.66	15.03	45.30	12.49	0.717	1.637	2.815
	3-4	3.5	1.17	15.46	62.00	21.37	14.77	41.01	36.00	0.650	2.477	4.258
	4-5	4.5	0.31	17.49	60.93	21.27	15.72	48.34	37.78	0.628	3.433	5.902
	6-5	5.5	2.76	16.12	60.43	20.69	15.75	42.43	38.38	0.611	4.441	7.635
	5-6	6.5	3.29	17.15	59.33	20.23	16.46	47.14	40.12	0.605	5.479	9.420
	6-7	7.5	1.67	16.51	60.20	21.62	15.51	45.20	37.18	0.575	6.566	11.287
	7-8	8.5	8.85	16.62	54.98	19.54	15.87	50.88	41.70	0.568	7.701	13.239
	8-9	9.5	14.91	14.53	51.72	18.85	15.10	40.04	40.57	0.504	8.931	15.353
	9-10	10.5	7.21	17.49	55.35	19.94	15.74	63.84	37.76	0.537	10.202	17.539
	10-11	11.5	2.97	17.32	57.96	21.75	15.14	49.79	41.03	0.573	11.381	19.566
	11-12	12.5	6.70	16.25	55.87	21.18	14.61	44.78	41.22	0.566	12.521	21.526
	12-13	13.5	5.37	18.29	54.98	21.36	15.33	50.74	45.81	0.549	13.694	23.542
	13-14	14.5	15.24	19.48	46.44	18.84	16.90	67.87	54.59	0.525	14.920	25.651
	14-15	15.5	10.79	19.38	49.65	20.18	16.52	53.84	53.65	0.536	16.165	27.790
	15-16	16.5	11.42	17.68	49.73	21.17	14.99	49.42	48.87	0.430	17.534	30.145
	16-17	17.5	37.75	12.97	35.05	14.23	15.14	60.99	10.57	0.492	18.963	32.600

SBBC11	Interval	Depth	Total %Gravel	Total %Sand	Total %Silt	Total %Clay	d (0.5)	Mean	Mode	Porosity	Cumulative Mass	Corrected Depth
	0-1	0.5	85.43	2.03	8.24	4.30	8.51	65.11	7.16	0.768	0.307	0.500
	1-2	1.5	28.35	6.90	43.80	20.95	8.37	35.82	7.53	0.743	0.954	1.554
	2-3	2.5	37.51	5.46	38.06	18.97	7.96	38.25	7.48	0.728	1.655	2.695
	3-4	3.5	35.57	5.69	39.79	18.95	8.22	37.54	7.59	0.610	2.533	4.124
	4-5	4.5	7.85	9.04	55.96	27.15	8.34	39.24	7.58	0.679	3.474	5.657
	6-5	5.5	35.86	5.53	38.50	20.11	7.87	37.94	7.51	0.621	4.401	7.166
	5-6	6.5	11.53	9.02	52.97	26.48	8.32	42.59	7.62	0.572	5.470	8.907
	6-7	7.5	3.31	9.02	57.98	29.68	8.14	33.78	7.70	0.722	6.407	10.432
	7-8	8.5	6.26	8.58	56.83	28.33	8.29	36.97	7.90	0.539	7.386	12.026
	8-9	9.5	37.11	6.07	38.04	18.78	8.44	34.06	7.91	0.582	8.550	13.922
	9-10	10.5	7.92	8.97	55.40	27.72	8.35	38.98	7.89	0.597	9.638	15.692
	10-11	11.5	3.43	9.29	57.70	29.58	8.22	47.37	7.92	0.458	10.889	17.730
	11-12	12.5	47.22	7.35	30.24	15.19	9.05	67.60	7.93	0.458	12.325	20.069
	12-13	13.5	60.55	5.02	23.04	11.40	8.97	57.41	8.02	0.507	13.697	22.302
	13-14	14.5	23.17	8.76	45.54	22.52	8.84	40.03	8.28	0.437	15.097	24.581
	14-15	15.5	12.64	11.37	51.27	24.73	9.32	44.87	8.52	0.559	16.427	26.747

SBBC12	Interval	Depth	Total %Gravel	Total %Sand	Total %Silt	Total %Clay	d (0.5)	Mean	Mode	Porosity	Cumulative Mass	Corrected Depth
	0-1	0.5	76.90	2.53	12.91	7.66	7.00	54.14	6.69	0.749	0.333	0.500
	1-2	1.5	20.79	7.15	45.29	26.77	6.78	23.99	6.61	0.628	1.158	1.740
	2-3	2.5	6.09	10.14	51.60	32.18	6.78	46.78	6.62	0.558	2.236	3.360
	3-4	3.5	5.30	7.40	53.60	33.71	6.40	41.89	6.70	0.629	3.314	4.979
	4-5	4.5	2.04	9.65	54.36	33.94	6.69	44.92	6.78	0.618	4.313	6.479
	5-6	5.5	6.21	7.21	53.06	33.52	6.39	33.49	6.81	0.611	5.335	8.015
	6-7	6.5	1.70	7.58	55.94	34.78	6.49	36.33	6.99	0.593	6.390	9.600
	7-8	7.5	2.46	7.01	55.73	34.80	6.40	33.09	7.01	0.592	7.470	11.222
	8-9	8.5	4.27	8.19	54.53	33.01	6.75	41.24	7.18	0.579	8.568	12.872
	9-10	9.5	1.20	6.85	57.20	34.75	6.54	31.71	7.22	0.548	9.725	14.610
	10-11	10.5	3.17	7.11	55.99	33.73	6.68	37.48	7.35	0.545	10.926	16.415
	11-12	11.5	5.29	12.28	51.84	30.59	7.62	55.42	7.33	0.554	12.120	18.208
	12-13	12.5	53.38	5.36	25.79	15.47	7.41	43.17	7.27	0.539	13.322	20.013
	13-14	13.5	10.58	10.92	48.01	30.49	7.33	43.98	7.02	0.532	14.552	21.862
	14-15	14.5	21.85	9.69	40.84	27.62	7.00	56.25	6.85	0.546	15.774	23.697
	15-16	15.5	24.80	12.73	37.74	24.74	8.17	77.16	6.96	0.534	16.992	25.528
	16-17	16.5	13.55	22.68	39.08	24.68	11.29	115.86	7.00	0.476	18.304	27.498
	17-18	17.5	4.30	12.00	50.40	33.30	7.34	52.02	6.91	0.533	19.617	29.470
	18-19	18.5	7.09	14.49	47.09	31.32	7.85	67.36	6.93	0.529	20.859	31.336
	19-20	19.5	7.81	10.07	48.83	33.29	6.89	52.24	6.89	0.523	22.115	33.224
	20-21	20.5	9.94	15.42	44.86	29.78	8.20	77.59	7.08	0.511	23.396	35.148
	21-22	21.5	22.59	13.07	38.72	25.62	8.22	70.93	7.01	0.486	24.725	37.145
	22-23	22.5	17.79	13.26	41.37	27.58	7.98	51.72	6.82	0.409	26.189	39.344
	23-24	23.5	17.52	17.40	39.32	25.76	9.30	71.51	7.12	0.500	27.635	41.516
	24-25	24.5	14.70	19.97	40.07	25.26	10.69	90.60	7.40	0.480	28.987	43.548
	25-26	25.5	19.89	16.70	39.85	23.55	10.59	68.74	8.22	0.505	30.333	45.570
	26-27	26.5	16.98	15.95	43.18	23.88	10.76	62.03	8.44	0.498	31.654	47.555
	27-28	27.5	23.72	28.34	31.60	16.34	23.10	161.53	9.75	0.491	32.993	49.567
	28-29	28.5	24.07	14.38	38.44	23.10	9.83	65.09	8.13	0.496	34.336	51.584

SBBC13	Interval	Depth	Total %Gravel	Total %Sand	Total %Silt	Total %Clay	d (0.5)	Mean	Mode	Porosity	Cumulative Mass	Corrected Depth
	0-1	0.5	21.17	8.12	43.75	26.97	6.80	56.47	6.62	0.692	0.409	0.500
	1-2	1.5	1.53	11.39	52.41	34.67	6.84	53.83	6.76	0.622	1.318	1.613
	2-3	2.5	3.19	5.93	57.08	33.80	6.65	18.55	6.99	0.593	2.358	2.886
	3-4	3.5	0.00	7.74	58.73	33.52	7.19	37.32	7.55	0.573	3.464	4.238
	4-5	4.5	0.00	6.75	59.83	33.43	7.33	31.33	7.97	0.563	4.608	5.639
	5-6	5.5	0.00	4.41	61.97	33.62	7.32	19.87	8.58	0.544	5.792	7.087
	6-7	6.5	0.26	3.35	62.22	34.17	7.11	18.19	8.86	0.544	7.001	8.567
	7-8	7.5	0.10	4.05	62.24	33.61	7.31	26.31	9.36	0.541	8.213	10.050
	8-9	8.5	0.00	3.42	61.94	34.64	6.96	26.30	8.84	0.543	9.426	11.535
	9-10	9.5	0.00	4.78	61.44	33.79	7.25	32.33	8.93	0.545	10.635	13.014
	10-11	10.5	0.78	3.64	62.16	33.43	7.26	16.28	9.13	0.546	11.841	14.489
	11-12	11.5	0.00	4.09	62.26	33.65	7.27	24.15	9.14	0.552	13.036	15.951
	12-13	12.5	0.08	2.62	63.19	34.11	7.05	16.30	9.17	0.551	14.224	17.405
	13-14	13.5	0.55	3.98	62.15	33.32	7.27	23.17	9.18	0.556	15.407	18.853
	14-15	14.5	2.72	5.36	59.64	32.28	7.43	28.69	9.09	0.564	16.573	20.280
	15-16	15.5	0.00	6.35	60.98	32.68	7.52	30.38	8.89	0.565	17.726	21.691
	16-17	16.5	0.31	5.03	61.41	33.24	7.29	28.11	8.90	0.564	18.879	23.102
	17-18	17.5	0.18	3.40	63.22	33.21	7.27	19.57	9.21	0.550	20.053	24.538
	18-19	18.5	0.31	3.97	62.64	33.08	7.32	25.07	9.35	0.544	21.253	26.007
	19-20	19.5	0.05	3.50	63.16	33.29	7.31	28.08	9.48	0.538	22.470	27.495
	20-21	20.5	0.00	1.37	64.99	33.64	7.17	12.22	9.81	0.532	23.702	29.003
	21-22	21.5	0.00	1.92	64.80	33.28	7.29	16.48	9.92	0.534	24.940	30.518
	22-23	22.5	0.16	1.25	65.14	33.45	7.19	12.11	9.92	0.540	26.167	32.019
	23-24	23.5	0.00	1.02	65.10	33.88	7.02	11.65	9.65	0.539	27.388	33.513
	24-25	24.5	0.00	0.97	65.19	33.85	6.99	11.52	9.61	0.541	28.606	35.004
	25-26	25.5	0.00	0.83	65.55	33.62	7.05	11.43	9.80	0.542	29.820	36.489
	26-27	26.5	0.14	1.39	64.87	33.60	7.06	14.90	9.62	0.539	31.037	37.979
	27-28	27.5	0.00	1.52	65.20	33.28	7.18	14.92	9.85	0.526	32.277	39.495

SBBC15	Interval	Depth	Total %Gravel	Total %Sand	Total %Silt	Total %Clay	d (0.5)	Mean	Mode	Porosity	Cumulative Mass	Corrected Depth
	0-1	0.5	0.00	3.89	68.04	28.07	8.02	23.43	9.11	0.819	0.239	0.500
	1-2	1.5	0.00	2.30	67.35	30.35	7.54	13.09	9.17	0.808	0.733	1.532
	2-3	2.5	0.11	2.17	67.50	30.22	7.61	12.92	9.44	0.774	1.287	2.688
	3-4	3.5	0.17	3.30	67.08	29.45	7.89	18.52	9.59	0.734	1.938	4.047
	4-5	4.5	0.00	3.45	67.38	29.17	7.90	20.94	9.45	0.724	2.656	5.547
	5-6	5.5	0.00	2.39	66.14	31.46	7.42	16.35	9.43	0.720	3.394	7.087
	6-7	6.5	0.00	2.09	68.05	29.86	7.63	12.84	9.26	0.715	4.143	8.652
	7-8	7.5	0.00	2.01	66.71	31.28	7.40	12.61	9.24	0.707	4.908	10.251
	8-9	8.5	0.00	2.15	65.95	31.90	7.20	15.53	9.01	0.701	5.692	11.888
	9-10	9.5	0.00	3.09	65.70	31.21	7.41	19.49	9.14	0.690	6.500	13.574
	10-11	10.5	0.03	3.09	65.49	31.40	7.25	22.29	8.77	0.684	7.330	15.309
	11-12	11.5	0.03	2.18	65.99	31.80	7.19	15.41	8.98	0.673	8.182	17.088
	12-13	12.5	0.06	2.93	65.93	31.08	7.37	18.58	8.94	0.660	9.066	18.933
	13-14	13.5	0.00	1.58	66.17	32.25	7.10	11.83	8.98	0.652	9.977	20.837
	14-15	14.5	0.00	2.75	64.64	32.60	6.98	22.08	8.71	0.634	10.923	22.813
	15-16	15.5	0.00	1.76	65.38	32.86	6.90	14.73	8.70	0.636	11.890	24.833
	16-17	16.5	0.00	2.82	63.82	33.36	6.82	25.61	8.62	0.625	12.870	26.878
	17-18	17.5	0.00	1.12	65.35	33.53	6.75	10.97	8.68	0.622	13.867	28.960
	18-19	18.5	0.10	2.82	63.06	34.02	6.67	24.65	8.40	0.613	14.880	31.077
	19-20	19.5	0.53	1.41	63.76	34.29	6.54	14.28	8.43	0.617	15.901	33.209
	20-21	20.5	0.00	3.81	62.63	33.56	6.79	30.30	8.35	0.613	16.922	35.340
	21-22	21.5	0.00	1.54	64.55	33.92	6.67	14.19	8.56	0.618	17.941	37.468
	22-23	22.5	0.00	1.75	64.18	34.06	6.64	14.30	8.46	0.621	18.949	39.575
	23-24	23.5	0.00	1.06	64.85	34.09	6.62	10.75	8.57	0.626	19.947	41.659
	24-25	24.5	0.00	2.00	64.43	33.57	6.77	17.97	8.64	0.627	20.938	43.728
	25-26	25.5	0.00	2.48	64.19	33.33	6.84	21.98	8.73	0.620	21.936	45.812
	26-27	26.5	0.00	2.23	64.72	33.05	6.93	19.30	8.86	0.621	22.941	47.912
	27-28	27.5	0.00	2.96	64.23	32.82	7.02	26.15	8.90	0.616	23.953	50.025
	28-29	28.5	0.00	2.14	64.37	33.49	6.87	18.90	8.97	0.608	24.982	52.173
	29-30	29.5	0.00	1.73	65.16	33.10	6.99	15.14	9.22	0.608	26.020	54.342
	30-31	30.5	0.70	2.68	64.62	32.00	7.25	22.01	9.42	0.608	27.059	56.512
	31-32	31.5	0.00	1.40	65.88	32.72	7.06	11.63	9.29	0.604	28.104	58.693
	32-33	32.5	0.00	2.78	64.45	32.77	7.13	24.58	9.34	0.608	29.148	60.874
	33-34	33.5	0.00	3.08	64.12	32.80	7.11	27.83	9.25	0.603	30.193	63.057
	34-35	34.5	0.00	1.57	65.83	32.60	7.13	14.13	9.54	0.609	31.238	65.238
	35-36	35.5	0.00	0.93	66.09	32.98	7.03	11.12	9.58	0.605	32.279	67.413

SBBC16	Interval	Depth	Total %Gravel	Total %Sand	Total %Silt	Total %Clay	d (0.5)	Mean	Mode	Porosity	Cumulative Mass	Corrected Depth
	0-1	0.5	0.00	11.29	59.78	28.93	8.41	44.296	8.56	0.826	0.231	0.500
	1-2	1.5	0.00	9.71	60.03	30.26	8.015	35.123	8.511	0.782	0.751	1.624
	2-3	2.5	0.00	9.64	62.43	27.92	8.447	27.312	8.494	0.761	1.357	2.935
	3-4	3.5	0.00	12.52	58.61	28.87	8.521	44.526	8.349	0.726	2.037	4.407
	4-5	4.5	0.48	13.77	58.22	27.53	8.958	46.067	8.518	0.687	2.816	6.091
	5-6	5.5	5.39	12.45	56.31	25.85	8.94	43.039	8.516	0.675	3.661	7.919
	6-7	6.5	0.99	11.04	59.35	28.61	8.391	39.386	8.472	0.697	4.493	9.719
	7-8	7.5	0.13	11.88	59.05	28.94	8.443	41.848	8.475	0.678	5.321	11.511
	8-9	8.5	1.77	13.70	57.10	27.42	8.888	52.594	8.323	0.613	6.261	13.544
	9-10	9.5	8.83	11.77	52.82	26.59	8.442	56.986	8.243	0.639	7.253	15.689
	10-11	10.5	2.86	11.01	56.64	29.50	8.013	47.77	8.301	0.612	8.245	17.835
	11-12	11.5	0.59	13.29	56.60	29.52	8.307	57.637	8.23	0.701	9.155	19.805
	12-13	12.5	2.69	12.13	55.60	29.58	8.05	67.459	8.275	0.598	10.084	21.815
	13-14	13.5	0.42	8.20	58.74	32.63	7.207	32.428	8.113	0.594	11.155	24.129
	14-15	14.5	0.23	9.51	57.83	32.43	7.283	42.514	7.915	0.596	12.227	26.450
	15-16	15.5	0.00	9.47	58.29	32.24	7.358	38.481	7.977	0.598	13.295	28.760
	16-17	16.5	0.19	8.49	58.87	32.45	7.257	24.133	8.006	0.598	14.360	31.064
	17-18	17.5	3.44	7.86	57.15	31.55	7.195	30.286	8.005	0.599	15.424	33.364
	18-19	18.5	1.28	10.94	56.91	30.86	7.694	46.781	8.127	0.593	16.493	35.678
	19-20	19.5	0.33	8.55	58.74	32.38	7.288	29.322	8.109	0.581	17.587	38.045
	20-21	20.5	1.13	7.76	58.25	32.87	7.144	29.349	8.13	0.576	18.704	40.461
	21-22	21.5	1.09	12.91	55.44	30.56	8.273	59.776	8.457	0.558	19.851	42.941
	22-23	22.5	0.29	16.01	53.84	29.86	8.897	69.422	8.465	0.566	21.011	45.452
	23-24	23.5	1.75	13.28	54.57	30.40	8.32	49.365	8.415	0.567	22.161	47.939
	24-25	24.5	2.30	14.95	54.22	28.53	9.122	55.406	8.619	0.560	23.318	50.441

SBBC17	Interval	Depth	Total %Gravel	Total %Sand	Total %Silt	Total %Clay	d (0.5)	Mean	Mode	Porosity	Cumulative Mass	Corrected Depth
	0-1	0.5	0.00	3.36	64.14	32.50	6.94	24.16	8.53	0.862	0.183	0.500
	1-2	1.5	0.00	3.66	70.90	25.45	8.56	17.04	9.77	0.836	0.584	1.593
	2-3	2.5	0.00	3.82	65.26	30.91	7.32	22.18	8.80	0.788	1.083	2.952
	3-4	3.5	0.00	3.99	66.98	29.04	7.73	21.08	9.02	0.772	1.666	4.541
	4-5	4.5	0.00	2.79	66.71	30.50	7.42	15.42	9.08	0.736	2.317	6.315
	5-6	5.5	0.00	2.56	67.67	29.77	7.48	13.76	8.96	0.726	3.029	8.258
	6-7	6.5	0.00	4.39	70.89	24.71	8.74	19.93	9.66	0.761	3.710	10.113
	7-8	7.5	0.00	3.04	67.22	29.75	7.51	16.30	8.96	0.751	4.357	11.878
	8-9	8.5	0.00	3.96	66.75	29.30	7.68	22.50	8.90	0.731	5.044	13.750
	9-10	9.5	0.00	1.20	65.14	33.66	6.73	10.84	8.94	0.754	5.728	15.613
	10-11	10.5	0.00	4.86	66.97	28.17	7.98	25.78	8.96	0.727	6.416	17.489
	11-12	11.5	0.00	1.49	65.79	32.72	6.83	11.24	8.62	0.735	7.129	19.433
	12-13	12.5	0.08	3.28	65.31	31.33	7.19	23.13	8.62	0.723	7.848	21.391
	13-14	13.5	0.00	1.85	65.97	32.18	7.01	11.88	8.76	0.690	8.625	23.510
	14-15	14.5	0.00	5.34	63.66	31.00	7.39	34.55	8.68	0.682	9.456	25.776
	15-16	15.5	5.38	2.76	61.50	30.36	7.09	15.55	8.75	0.696	10.280	28.021
	16-17	16.5	0.77	2.91	64.08	32.25	7.00	17.85	8.67	0.685	11.101	30.259
	17-18	17.5	0.00	3.41	64.56	32.03	7.09	21.74	8.68	0.683	11.938	32.542
	18-19	18.5	0.05	3.12	63.82	33.02	6.84	26.58	8.48	0.668	12.797	34.884
	19-20	19.5	0.00	2.69	64.68	32.63	6.93	16.75	8.61	0.660	13.687	37.310
	20-21	20.5	1.14	3.31	62.87	32.68	6.85	24.74	8.53	0.657	14.593	39.778
	21-22	21.5	0.44	2.42	63.77	33.38	6.71	16.01	8.48	0.637	15.529	42.329
	22-23	22.5	0.01	3.12	63.03	33.85	6.69	22.25	8.54	0.635	16.493	44.956
	23-24	23.5	9.13	2.68	57.14	31.06	6.63	23.21	8.43	0.633	17.463	47.601
	24-25	24.5	0.00	3.44	61.78	34.78	6.58	27.15	8.51	0.627	18.444	50.276
	25-26	25.5	0.00	1.97	63.62	34.41	6.59	12.32	8.58	0.676	19.368	52.795
	26-27	26.5	0.00	0.99	63.75	35.27	6.42	10.36	8.72	0.628	20.291	55.310
	27-28	27.5	0.00	1.55	63.94	34.52	6.62	13.72	8.93	0.628	21.278	58.001
	28-29	28.5	0.73	2.99	63.79	32.49	7.07	21.64	9.12	0.627	22.266	60.693
	29-30	29.5	0.17	2.22	64.29	33.32	6.94	17.63	9.30	0.627	23.254	63.388
	30-31	30.5	0.35	1.18	65.02	33.45	6.89	11.13	9.41	0.630	24.238	66.069
	31-32	31.5	0.00	1.19	65.54	33.27	6.98	11.22	9.58	0.632	25.215	68.732
	32-33	32.5	0.00	2.23	64.56	33.21	7.04	15.43	9.46	0.631	26.191	71.393
	33-34	33.5	0.25	1.97	65.30	32.47	7.15	15.81	9.58	0.634	27.165	74.047
	34-35	34.5	0.31	3.11	65.10	31.49	7.42	19.40	9.66	0.632	28.138	76.700
	35-36	35.5	0.00	3.11	64.88	32.02	7.34	21.98	9.70	0.632	29.114	79.360
	36-37	36.5	0.59	3.31	64.42	31.68	7.37	22.76	9.70	0.618	30.107	82.066
	37-38	37.5	0.00	1.57	65.69	32.74	7.12	11.66	9.71	0.633	31.098	84.769
	38-39	38.5	0.11	2.69	65.72	31.48	7.42	17.50	9.75	0.642	32.059	87.388
	39-40	39.5	0.00	2.25	65.58	32.17	7.25	14.76	9.73	0.632	33.022	90.013
	40-41	40.5	0.00	1.56	66.45	31.99	7.23	11.80	9.63	0.636	33.992	92.658
	41-42	41.5	0.00	1.81	64.88	33.31	6.94	16.76	9.47	0.636	34.957	95.286

SBBC18	Interval	Depth	Total %Gravel	Total %Sand	Total %Silt	Total %Clay	d (0.5)	Mean	Mode	Porosity	Cumulative Mass	Corrected Depth
	0-1	0.5	1.56	5.12	64.10	29.22	7.98	28.14	8.79	0.829	0.226	0.500
	1-2	1.5	0.00	2.92	65.65	31.43	7.50	13.74	8.93	0.666	0.895	1.979
	2-3	2.5	0.00	3.88	67.54	28.58	8.06	17.13	8.96	0.751	1.668	3.686
	3-4	3.5	0.00	4.65	65.86	29.49	7.87	24.19	8.86	0.826	2.228	4.926
	4-5	4.5	0.00	3.46	66.57	29.98	7.92	14.64	9.23	0.685	2.877	6.359
	5-6	5.5	0.39	4.59	66.06	28.97	8.06	23.22	8.99	0.709	3.680	8.135
	6-7	6.5	1.06	4.43	64.37	30.14	7.64	26.14	8.63	0.694	4.471	9.885
	7-8	7.5	0.00	3.33	65.76	30.91	7.54	17.55	8.74	0.695	5.282	11.676
	8-9	8.5	0.00	3.28	65.78	30.94	7.46	16.72	8.62	0.695	6.091	13.466
	9-10	9.5	0.00	4.38	65.03	30.59	7.67	24.39	8.71	0.679	6.921	15.301
	10-11	10.5	0.02	4.18	64.69	31.11	7.51	26.08	8.62	0.686	7.763	17.163
	11-12	11.5	0.15	4.46	63.87	31.52	7.37	29.99	8.46	0.669	8.618	19.053
	12-13	12.5	0.00	4.14	64.22	31.64	7.31	28.14	8.37	0.660	9.507	21.019
	13-14	13.5	0.13	4.08	63.69	32.10	7.21	27.41	8.38	0.651	10.420	23.037
	14-15	14.5	0.00	3.95	63.40	32.66	7.02	27.98	8.22	0.643	11.356	25.105
	15-16	15.5	0.04	3.24	63.72	33.00	6.93	21.07	8.24	0.641	12.306	27.205
	16-17	16.5	0.94	4.10	61.45	33.51	6.81	30.25	8.19	0.637	13.263	29.322
	17-18	17.5	0.00	3.85	62.34	33.81	6.80	27.75	8.22	0.628	14.238	31.477
	18-19	18.5	0.00	2.70	63.62	33.68	6.78	20.55	8.24	0.621	15.233	33.677
	19-20	19.5	0.71	2.84	62.34	34.10	6.64	21.06	8.13	0.617	16.243	35.910
	20-21	20.5	0.00	1.60	64.59	33.81	6.71	11.51	8.28	0.612	17.265	38.169
	21-22	21.5	0.03	3.61	62.77	33.60	6.81	28.97	8.18	0.604	18.304	40.466
	22-23	22.5	0.00	3.24	62.74	34.01	6.76	24.41	8.35	0.600	19.359	42.798
	23-24	23.5	0.00	4.15	62.78	33.07	7.04	18.91	8.48	0.591	20.431	45.168
	24-25	24.5	0.00	1.79	64.86	33.35	6.90	12.01	8.70	0.595	21.510	47.553
	25-26	25.5	0.00	2.27	65.21	32.51	7.15	16.43	8.95	0.602	22.574	49.907
	26-27	26.5	0.00	3.31	63.93	32.76	7.12	25.03	8.86	0.604	23.626	52.233
	27-28	27.5	0.00	2.53	65.59	31.88	7.31	17.35	9.09	0.599	24.682	54.567
	28-29	28.5	2.69	2.59	63.60	31.12	7.47	29.24	9.07	0.591	25.756	56.940
	29-30	29.5	2.69	2.59	63.60	31.12	7.33	16.92	9.24	0.577	26.859	59.379
	30-31	30.5	0.05	2.17	65.43	32.35	7.23	15.69	9.22	0.578	27.979	61.856
	31-32	31.5	0.04	3.21	65.05	31.69	7.46	25.18	9.28	0.590	29.082	64.294
	32-33	32.5	0.20	4.15	64.10	31.55	7.50	28.75	9.38	0.581	30.181	66.724

SBBC19	Interval	Depth	Total %Gravel	Total %Sand	Total %Silt	Total %Clay	d (0.5)	Mean	Mode	Porosity	Cumulative Mass	Corrected Depth
	0-1	0.5	0.00	2.45	67.40	30.15	7.49	13.05	8.86	0.801	0.264	0.500
	1-2	1.5	0.00	2.84	67.07	30.09	7.53	15.73	8.95	0.808	0.782	1.483
	2-3	2.5	0.00	1.90	65.72	32.38	7.20	12.25	9.41	0.773	1.338	2.535
	3-4	3.5	0.01	4.20	65.73	30.06	7.68	27.23	9.16	0.751	1.967	3.729
	4-5	4.5	0.00	2.85	66.32	30.83	7.51	17.21	9.36	0.736	2.646	5.016
	5-6	5.5	0.00	3.07	67.16	29.77	7.68	18.04	9.29	0.733	3.349	6.348
	6-7	6.5	0.00	3.10	67.58	29.32	7.75	18.99	9.19	0.733	4.056	7.688
	7-8	7.5	0.00	3.79	67.58	28.63	7.92	20.72	9.18	0.720	4.781	9.062
	8-9	8.5	0.00	2.19	66.58	31.24	7.35	12.66	9.08	0.712	5.534	10.489
	9-10	9.5	0.00	1.94	66.14	31.93	6.99	12.33	8.47	0.702	6.310	11.960
	10-11	10.5	1.24	2.78	64.79	31.19	7.26	19.33	9.03	0.688	7.117	13.490
	11-12	11.5	0.00	1.49	66.24	32.27	7.05	11.59	9.00	0.679	7.955	15.078
	12-13	12.5	0.00	2.32	66.26	31.43	7.26	16.48	8.99	0.676	8.809	16.698
	13-14	13.5	0.00	2.10	65.67	32.23	7.03	15.82	8.72	0.671	9.675	18.340
	14-15	14.5	0.00	1.99	65.69	32.33	7.03	14.95	8.82	0.669	10.550	19.997
	15-16	15.5	0.35	2.18	65.52	31.95	7.07	14.84	8.73	0.656	11.444	21.693
	16-17	16.5	0.00	2.84	64.43	32.73	6.95	21.82	8.63	0.652	12.362	23.432
	17-18	17.5	0.84	3.15	63.75	32.26	7.02	25.46	8.58	0.642	13.298	25.206
	18-19	18.5	0.00	1.87	64.65	33.48	6.75	15.62	8.54	0.627	14.266	27.042
	19-20	19.5	0.13	2.41	64.08	33.37	6.78	19.99	8.47	0.629	15.252	28.911
	20-21	20.5	0.31	3.14	62.81	33.74	6.71	26.86	8.35	0.620	16.247	30.797
	21-22	21.5	0.00	2.44	63.86	33.70	6.74	20.11	8.43	0.627	17.244	32.687
	22-23	22.5	0.00	2.33	63.29	34.37	6.57	20.09	8.30	0.617	18.246	34.585
	23-24	23.5	0.00	2.66	62.61	34.72	6.49	25.65	8.17	0.618	19.260	36.506
	24-25	24.5	0.00	1.28	64.64	34.08	6.64	11.01	8.51	0.616	20.275	38.431
	25-26	25.5	0.00	1.76	64.53	33.71	6.76	15.36	8.75	0.617	21.291	40.357
	26-27	26.5	0.00	2.25	64.28	33.47	6.84	18.09	8.82	0.606	22.321	42.310
	27-28	27.5	0.00	2.60	64.22	33.18	6.96	21.15	9.00	0.595	23.380	44.317
	28-29	28.5	0.00	3.53	64.18	32.29	7.20	24.69	9.12	0.603	24.442	46.330
	29-30	29.5	0.25	1.18	64.72	33.85	6.72	10.97	8.96	0.599	25.499	48.333
	30-31	30.5	0.34	1.51	65.06	33.10	6.98	11.65	9.28	0.603	26.555	50.336

SBBC20	Interval	Depth	Total %Gravel	Total %Sand	Total %Silt	Total %Clay	d (0.5)	Mean	Mode	Porosity	Cumulative Mass	Corrected Depth
	0-1	0.5	0.00	9.74	63.19	27.06	8.59	34.12	8.50	0.850	0.199	0.500
	1-2	1.5	0.00	10.91	60.93	28.16	8.84	34.91	8.81	0.753	0.726	1.822
	2-3	2.5	1.72	13.38	58.79	26.11	9.79	40.21	9.42	0.699	1.452	3.644
	3-4	3.5	0.01	13.77	59.44	26.78	9.65	43.60	9.23	0.689	2.262	5.677
	4-5	4.5	1.19	12.21	60.27	26.32	9.65	36.23	9.51	0.684	3.092	7.761
	5-6	5.5	0.00	10.77	60.15	29.07	8.83	36.82	9.35	0.689	3.922	9.845
	6-7	6.5	0.43	12.15	59.92	27.50	9.27	41.41	9.30	0.671	4.770	11.973
	7-8	7.5	4.79	10.34	57.45	27.42	8.62	36.46	8.86	0.672	5.641	14.159
	8-9	8.5	2.48	16.99	54.87	25.65	10.23	59.70	9.26	0.652	6.537	16.407
	9-10	9.5	2.03	8.13	60.13	29.71	8.03	29.88	8.83	0.625	7.494	18.810
	10-11	10.5	0.04	9.44	60.11	30.41	8.08	33.07	8.78	0.616	8.500	21.334
	11-12	11.5	3.78	9.46	57.53	29.24	7.73	33.39	8.86	0.614	9.520	23.895
	12-13	12.5	3.78	9.46	57.53	29.24	8.17	51.13	9.13	0.593	10.570	26.530
	13-14	13.5	5.72	15.29	52.54	26.46	9.51	74.18	9.46	0.573	11.675	29.303
	14-15	14.5	3.12	8.75	58.77	29.36	8.21	33.54	9.23	0.555	12.830	32.203
	15-16	15.5	3.07	12.22	56.60	28.10	8.92	42.67	9.42	0.562	13.999	35.137
	16-17	16.5	1.54	13.22	57.31	27.93	9.12	56.58	9.40	0.548	15.177	38.094
	17-18	17.5	1.73	11.82	57.09	29.35	8.54	50.34	9.31	0.517	16.416	41.204
	18-19	18.5	6.10	18.19	50.94	24.77	10.52	80.60	9.50	0.522	17.690	44.403
	19-20	19.5	12.64	14.31	49.57	23.48	10.06	51.03	9.46	0.474	19.022	47.744
	20-21	20.5	18.20	20.01	41.82	19.97	12.47	90.41	9.39	0.471	20.420	51.254
	21-22	21.5	13.27	23.69	43.30	19.74	14.37	97.42	9.66	0.470	21.823	54.775
	22-23	22.5	9.12	13.43	51.98	25.48	9.57	45.47	9.27	0.462	23.238	58.326
	23-24	23.5	12.88	24.61	42.72	19.79	14.44	93.68	9.56	0.493	24.622	61.801
	24-25	24.5	2.12	25.10	49.41	23.37	12.80	104.36	9.48	0.514	25.937	65.102

SBBC21	Interval	Depth	Total %Gravel	Total %Sand	Total %Silt	Total %Clay	d (0.5)	Mean	Mode	Porosity	Cumulative Mass	Corrected Depth
	0-1	0.5	0.25	4.40	68.67	26.68	8.60	24.82	10.16	0.791	0.277	0.500
	1-2	1.5	0.00	3.04	69.03	27.93	8.26	17.85	10.12	0.763	0.869	1.565
	2-3	2.5	0.00	2.64	69.24	28.12	8.24	17.58	10.30	0.721	1.552	2.798
	3-4	3.5	2.34	3.15	66.42	28.09	8.15	16.91	10.29	0.712	2.304	4.152
	4-5	4.5	0.00	2.00	69.47	28.53	8.06	13.07	10.18	0.699	3.084	5.558
	6-5	5.5	0.11	1.91	68.96	29.01	7.97	12.97	10.10	0.689	3.895	7.020
	5-6	6.5	0.00	2.19	68.96	28.85	8.13	13.47	10.29	0.700	4.705	8.480
	6-7	7.5	0.00	2.83	68.83	28.33	8.22	19.17	10.14	0.685	5.521	9.950
	7-8	8.5	0.00	2.46	68.41	29.13	8.03	16.50	10.00	0.683	6.358	11.459
	8-9	9.5	0.00	2.78	68.24	28.98	8.10	19.84	10.06	0.684	7.196	12.969
	9-10	10.5	0.00	1.91	68.63	29.46	7.94	13.08	9.98	0.673	8.048	14.504
	10-11	11.5	0.00	1.86	68.50	29.64	7.82	12.90	9.77	0.672	8.916	16.069
	11-12	12.5	0.00	1.69	68.11	30.20	7.69	12.59	9.71	0.656	9.807	17.674
	12-13	13.5	0.00	1.58	67.96	30.47	7.55	12.28	9.51	0.655	10.719	19.319
	13-14	14.5	0.00	1.50	66.86	31.64	7.26	14.95	9.32	0.666	11.618	20.939
	14-15	15.5	0.00	1.83	67.24	30.93	7.40	14.39	9.20	0.665	12.504	22.536
	15-16	16.5	0.00	2.61	66.60	30.79	7.46	17.56	9.18	0.666	13.392	24.135
	16-17	17.5	0.07	2.16	66.88	30.89	7.42	15.38	9.20	0.666	14.277	25.731
	17-18	18.5	0.00	1.33	67.29	31.38	7.26	11.73	9.15	0.657	15.175	27.350
	18-19	19.5	0.00	3.05	66.55	30.40	7.54	22.06	9.15	0.663	16.077	28.975
	19-20	20.5	0.14	3.35	66.01	30.51	7.53	22.59	9.19	0.657	16.979	30.600
	20-21	21.5	0.14	3.35	66.01	30.51	7.45	26.87	9.12	0.648	17.900	32.260
	21-22	22.5	0.00	2.81	65.20	31.99	7.17	25.52	9.08	0.651	18.830	33.936
	22-23	23.5	0.00	3.08	65.53	31.39	7.24	25.89	8.86	0.640	19.769	35.629
	23-24	24.5	0.00	3.31	65.09	31.60	7.26	27.34	9.06	0.643	20.719	37.341
	24-25	25.5	0.05	1.49	66.38	32.09	7.04	13.48	8.94	0.629	21.684	39.080
	25-26	26.5	0.05	1.49	66.38	32.09	7.52	53.62	9.02	0.628	22.669	40.855
	26-27	27.5	0.00	1.13	66.54	32.33	6.97	11.14	8.91	0.626	23.658	42.638
	27-28	28.5	0.00	1.16	66.80	32.05	7.03	11.23	8.92	0.629	24.646	44.418
	28-29	29.5	0.00	1.16	66.80	32.05	7.11	23.54	8.91	0.627	25.633	46.196
	29-30	30.5	0.00	0.93	66.36	32.71	6.92	10.90	8.98	0.634	26.612	47.960

SBBC28	Interval	Depth	Total %Gravel	Total %Sand	Total %Silt	Total %Clay	d (0.5)	Mean	Mode	Porosity	Cumulative Mass	Corrected Depth
	0-1	0.5	84.89	6.96	5.00	3.14	28.12	374.84	799.91	0.467	0.706	0.606
	1-2	1.5	11.99	25.30	38.05	24.65	9.69	204.77	6.38	0.434	2.162	1.857
	2-3	2.5	17.39	16.99	39.51	26.12	7.73	135.41	6.38	0.532	3.533	3.034
	3-4	3.5	11.29	24.01	39.49	25.21	9.35	199.25	6.43	0.544	4.758	4.087
	4-5	4.5	7.72	15.08	46.32	30.88	7.01	103.27	6.42	0.538	5.975	5.132
	6-5	5.5	16.34	14.30	42.20	27.17	8.37	189.81	6.49	0.554	7.178	6.165
	5-6	6.5	12.09	20.79	40.57	26.55	7.32	121.65	6.54	0.561	8.350	7.172
	6-7	7.5	23.92	17.81	35.43	22.83	8.46	172.89	6.63	0.543	9.538	8.192
	7-8	8.5	16.14	14.59	42.38	26.89	7.54	112.69	6.67	0.542	10.751	9.234
	8-9	9.5	8.15	33.84	35.71	22.29	13.54	312.95	825.04	0.529	11.982	10.291
	9-10	10.5	14.48	17.15	41.79	26.58	7.97	164.59	6.77	0.524	13.236	11.368
	10-11	11.5	10.57	16.21	45.28	27.94	7.79	138.08	6.79	0.547	14.467	12.425
	11-12	12.5	11.85	10.69	47.83	29.63	6.93	69.70	6.80	0.548	15.666	13.455
	12-13	13.5	8.88	12.65	48.22	30.26	7.11	89.68	6.98	0.555	16.854	14.475
	13-14	14.5	22.32	12.08	40.20	25.40	7.28	107.47	6.84	0.499	18.106	15.551
	14-15	15.5	22.35	18.52	36.28	22.86	8.82	193.66	6.94	0.502	19.429	16.687
	15-16	16.5	20.79	23.59	34.13	21.49	10.43	220.69	6.79	0.499	20.753	17.824
	16-17	17.5	10.39	16.24	45.12	28.25	7.74	140.65	6.80	0.500	22.079	18.963
	17-18	18.5	12.04	19.55	41.95	26.46	8.44	174.93	6.78	0.523	23.374	20.075
	18-19	19.5	7.81	13.22	48.15	30.81	7.04	94.29	6.68	0.529	24.630	21.154
	19-20	20.5	11.64	29.14	36.91	22.31	12.15	232.90	683.88	0.519	25.891	22.237
	20-21	21.5	16.32	16.35	41.13	26.20	7.84	120.39	6.38	0.517	27.167	23.333
	21-22	22.5	13.37	25.62	37.80	23.20	10.66	181.68	590.57	0.513	28.451	24.436
	22-23	23.5	12.21	14.05	45.15	28.58	7.36	98.83	6.73	0.512	29.743	25.545
	23-24	24.5	24.62	22.61	32.61	20.16	10.71	242.92	792.77	0.502	31.048	26.666
	24-25	25.5	8.66	22.77	42.07	26.50	9.03	198.03	6.62	0.526	32.336	27.772
	25-26	26.5	42.74	4.61	31.99	20.66	6.23	52.21	6.51	0.517	33.604	28.861
	26-27	27.5	16.31	5.77	47.28	30.65	6.10	35.94	6.45	0.499	34.909	29.982
	27-28	28.5	19.00	9.62	43.30	28.08	6.71	66.08	6.38	0.504	36.231	31.117
	28-29	29.5	11.02	12.42	46.20	30.36	6.83	83.22	6.37	0.527	37.516	32.221
	29-30	30.5	25.72	6.97	40.68	26.63	6.30	50.40	6.36	0.515	38.785	33.311
	30-31	31.5	11.81	9.40	47.66	31.13	6.48	60.49	6.36	0.523	40.059	34.406
	31-32	32.5	14.44	6.76	47.67	31.12	6.17	46.63	6.51	0.508	41.344	35.509
	32-33	33.5	33.96	5.75	37.24	23.05	6.50	56.53	6.71	0.506	42.651	36.631
	33-34	34.5	12.55	6.34	50.37	30.73	6.42	45.94	6.82	0.520	43.942	37.740
	34-35	35.5	5.90	10.31	51.83	31.97	6.80	63.59	6.72			

SBPTC1_1	Interval	Depth	Total %Gravel	Total %Sand	Total %Silt	Total %Clay	d (0.5)	Mean	Mode	Porosity	Cumulative Mass	Corrected Depth
	0-1	0.5	0.00	4.21	63.42	32.37	7.12	37.20	8.97	0.644	0.472	0.966
	1-2	1.5	0.00							0.632	1.431	2.930
	2-3	2.5	0.00							0.630	2.409	4.933
	3-4	3.5	0.00							0.624	3.398	6.958
	4-5	4.5	0.00							0.622	4.397	9.002
	5-6	5.5	0.00	0.43	63.85	35.72	6.23	9.54	8.36	0.626	5.392	11.041
	6-7	6.5	0.00							0.632	6.376	13.055
	7-8	7.5	0.00							0.632	7.350	15.050
	8-9	8.5	0.00							0.619	8.342	17.080
	9-10	9.5	0.00							0.612	9.359	19.164
	10-11	10.5	0.00	0.07	63.77	36.16	6.17	9.19	8.49	0.603	10.398	21.291
	11-12	11.5	0.00							0.593	11.463	23.471
	12-13	12.5	0.00							0.591	12.545	25.686
	13-14	13.5	0.00							0.587	13.634	27.916
	14-15	14.5	0.00							0.596	14.716	30.132
	15-16	15.5	0.00	0.11	65.69	34.20	6.63	9.77	9.23	0.602	15.779	32.308
	16-17	16.5	0.00							0.602	16.834	34.468
	17-18	17.5	0.00							0.600	17.892	36.634
	18-19	18.5	0.00							0.608	18.942	38.784
	19-20	19.5	0.00							0.602	19.989	40.927
	20-21	20.5	0.00	0.21	65.07	34.72	6.51	9.71	9.00	0.599	21.048	43.096
	21-22	21.5	0.00							0.596	22.115	45.281
	22-23	22.5	0.00							0.596	23.186	47.474
	23-24	23.5	0.00							0.589	24.267	49.686
	24-25	24.5	0.00							0.592	25.352	51.909
	25-26	25.5	0.00	1.14	64.88	33.99	6.71	10.84	8.96	0.601	26.422	54.099
	26-27	26.5	0.00							0.598	27.483	56.273
	27-28	27.5	0.00							0.600	28.545	58.447
	28-29	28.5	0.00							0.596	29.610	60.627
	29-30	29.5	0.00							0.592	30.686	62.830
	30-31	30.5	0.00	1.32	66.05	32.63	7.13	11.64	9.42	0.583	31.779	65.068
	31-32	31.5	0.00							0.583	32.884	67.330
	32-33	32.5	0.00							0.582	33.990	69.595
	33-34	33.5	0.00							0.574	35.108	71.884
	34-35	34.5	0.00							0.556	36.260	74.243
	35-36	35.5	0.00	2.89	67.60	29.51	8.23	14.32	10.29	0.554	37.439	76.657
	36-37	36.5	0.00							0.545	38.634	79.103
	37-38	37.5	0.00							0.547	39.836	81.566
	38-39	38.5	0.00							0.551	41.031	84.012
	39-40	39.5	0.00							0.556	42.214	86.433
	40-41	40.5	0.00	5.60	65.88	28.51	8.87	25.41	10.60	0.552	43.395	88.853
	41-42	41.5	0.00							0.539	44.599	91.318
	42-43	42.5	0.00							0.564	45.788	93.752

SBPTC1_1	Interval	Depth	Total %Gravel	Total %Sand	Total %Silt	Total %Clay	d (0.5)	Mean	Mode	Porosity	Cumulative Mass	Corrected Depth
Continued	43-44	43.5	0.00							0.583	46.919	96.067
	44-45	44.5	0.00							0.589	48.015	98.312
	45-46	45.5	0.00	3.63	68.41	27.96	8.93	20.83	11.50	0.577	49.120	100.575
	46-47	46.5	0.00							0.578	50.240	102.868
	47-48	47.5	0.00							0.567	51.373	105.188
	48-49	48.5	0.00							0.568	52.519	107.535
	49-50	49.5	0.00							0.575	53.654	109.858
	50-51	50.5	0.00	3.88	66.60	29.52	8.31	25.64	10.55	0.586	54.765	112.133
	51-52	51.5	0.00							0.587	55.862	114.378
	52-53	52.5	0.00							0.578	56.968	116.644
	53-54	53.5	0.00							0.553	58.120	119.002
	54-55	54.5	0.00							0.550	59.308	121.435
	55-56	55.5	0.00	2.54	69.20	28.26	8.90	14.74	11.90	0.548	60.503	123.881
	56-57	56.5	0.00							0.559	61.685	126.302
	57-58	57.5	0.00							0.570	62.838	128.663
	58-59	58.5	0.00							0.578	63.967	130.974
	59-60	59.5	0.00							0.580	65.083	133.260
	60-61	60.5	0.00	2.13	69.47	28.40	8.93	14.48	12.59	0.559	66.225	135.596
	61-62	61.5	0.00							0.540	67.419	138.043
	62-63	62.5	0.00							0.538	68.641	140.544
	63-64	63.5	0.00							0.555	69.842	143.003
	64-65	64.5	0.00							0.506	71.086	145.550
	65-66	65.5	0.00	1.66	68.50	29.84	8.20	13.31	10.98	0.547	72.340	148.117
	66-67	66.5	0.00							0.559	73.523	150.540
	67-68	67.5	0.00							0.578	74.666	152.881
	68-69	68.5	0.00							0.571	75.794	155.191
	69-70	69.5	0.00							0.510	77.012	157.683
	70-71	70.5	0.00	2.11	69.05	28.85	8.64	14.31	11.40	0.556	78.249	160.217
	71-72	71.5	0.00							0.551	79.432	162.639
	72-73	72.5	0.00							0.529	80.651	165.135
	73-74	73.5	0.00							0.528	81.901	167.695
	74-75	74.5	0.00							0.536	83.143	170.236
	75-76	75.5	0.00	5.61	68.99	25.40	10.81	32.40	16.03	0.541	84.366	172.742
	76-77	76.5	0.00							0.547	85.575	175.217
	77-78	77.5	0.00							0.531	86.796	177.717
	78-79	78.5	0.00							0.564	87.994	180.171
	79-80	79.5	0.00							0.554	89.163	182.562
	80-81	80.5	0.00	2.94	70.70	26.36	9.91	16.16	14.08	0.546	90.355	185.004
	81-82	81.5	0.00							0.534	91.575	187.502
	82-83	82.5	0.00							0.516	92.834	190.079
	83-84	83.5	0.00							0.506	94.129	192.731
	84-85	84.5	0.00							0.522	95.416	195.366
	85-86	85.5	0.00	3.89	71.20	24.91	11.07	17.88	18.35	0.528	96.674	197.943

SBPTC1_1	Interval	Depth	Total %Gravel	Total %Sand	Total %Silt	Total %Clay	d (0.5)	Mean	Mode	Porosity	Cumulative Mass	Corrected Depth
Continued	86-87	86.5	0.00							0.521	97.935	200.524
	87-88	87.5	0.00							0.513	99.216	203.146
	88-89	88.5	0.00							0.501	100.523	205.824
	89-90	89.5	0.00							0.491	101.860	208.560
	90-91	90.5	0.00	4.34	71.67	23.99	11.65	18.58	18.61	0.515	103.176	211.255
	91-92	91.5	0.00							0.521	104.452	213.869
	92-93	92.5	0.00							0.522	105.720	216.464
	93-94	93.5	0.00							0.521	106.989	219.062
	94-95	94.5	0.00							0.522	108.258	221.660
	95-96	95.5	0.00	4.15	71.51	24.35	11.32	18.15	17.32	0.467	109.598	224.405
	96-97	96.5	0.00							0.528	110.930	227.131
	97-98	97.5	0.00							0.509	112.205	229.743
	98-99	98.5	0.00							0.523	113.488	232.369
	99-100	99.5	0.00							0.543	114.725	234.902
	100-102	101	0.00	8.21	68.26	23.54	12.08	41.05	17.39	0.558	117.106	239.777
	102-104	103	0.00							0.518	119.555	244.791
	104-106	105	0.00	3.33	71.39	25.28	10.70	17.04	16.76	0.526	122.088	249.979
	106-108	107	0.00							0.533	124.581	255.082
	108-110	109	0.00							0.543	127.028	260.093
	110-112	111	0.00	2.58	70.40	27.02	9.76	15.62	14.58	0.540	129.457	265.066
	112-114	113	0.00							0.534	131.911	270.092
	114-116	115	0.00							0.551	134.337	275.058
	116-118	117	0.00	2.42	70.94	26.65	9.66	15.32	13.65	0.567	136.674	279.843
	118-120	119	0.00							0.578	138.938	284.478
	120-122	121	0.00	0.99	68.20	30.81	7.87	12.41	10.97	0.575	141.181	289.072
	122-124	123	0.00							0.565	143.461	293.740
	124-126	125	0.00							0.572	145.748	298.423
	126-128	127	0.00	1.34	68.21	30.45	7.95	12.69	10.94	0.570	148.023	303.080
	128-130	129	0.00							0.582	150.271	307.684
	130-132	131	0.00	0.09	67.94	31.97	7.31	10.71	10.36	0.586	152.477	312.201
	132-134	133	0.00							0.592	154.656	316.662
	134-136	135	0.00	0.00	66.80	33.20	6.89	9.99	9.62	0.584	156.841	321.135
	136-138	137	0.00							0.561	159.106	325.773
	138-140	139	0.00							0.567	161.417	330.504
	140-142	141	0.00	2.28	64.12	33.60	6.71	12.17	8.46	0.582	163.671	335.121
	142-144	143	0.00							0.583	165.882	339.648
	144-146	145	0.00	0.26	65.78	33.96	6.73	10.30	9.07	0.602	168.042	344.070
	146-148	147	0.00							0.600	170.157	348.401
	148-150	149	0.00							0.586	172.314	352.817
	150-152	151	0.00	0.51	65.11	34.38	6.55	9.96	8.81	0.596	174.483	357.257
	152-154	153	0.00							0.599	176.617	361.627
	154-156	155	0.00	0.07	65.23	34.69	6.46	9.51	8.78	0.595	178.753	366.002
	156-158	157	0.00							0.597	180.895	370.386

SBPTC1_1	Interval	Depth	Total %Gravel	Total %Sand	Total %Silt	Total %Clay	d (0.5)	Mean	Mode	Porosity	Cumulative Mass	Corrected Depth
Continued	158-160	159	0.00							0.594	183.037	374.773
	160-162	161	0.00	0.41	62.83	36.76	5.98	9.09	7.96	0.579	185.228	379.259
	162-164	163	0.00	3.03	62.18	34.79	6.43	29.86	8.19	0.575	187.471	383.851
	164-166	165	0.00	0.09	61.58	38.33	5.66	8.40	7.59			

APPENDIX C

Interval	%OC	%N	C/N	Σ_8 (mg/g)	λ_8 (µg/100mg OC)	S/V	C/V	(Ad/Al)v	(Ad/Al)s	3,5Bd/V	P/(V+S)	PON/P
Core	**SBBC1**											
0-1	0.910	0.190	5.588	0.139	1.525	0.401	0.195	0.474	0.332	0.099	0.174	0.156
1-2	0.990	0.150	7.700	0.171	1.728	0.357	0.171	0.408	0.288	0.086	0.168	0.141
2-3	0.890	0.080	12.979	0.201	2.028	0.317	0.147	0.357	0.316	0.072	0.146	0.152
3-4	0.900	0.180	5.833	0.161	1.805	0.435	0.192	0.457	0.327	0.099	0.162	0.165
5-6	0.860	0.190	5.281	0.139	1.616	0.411	0.203	0.477	0.327	0.100	0.182	0.147
6-7	0.890	0.140	7.417	0.160	1.801	0.417	0.188	0.458	0.319	0.097	0.160	0.155
7-8	0.900	0.070	15.000	0.153	1.705	0.425	0.211	0.433	0.317	0.095	0.174	0.156
8-9	0.880	0.080	12.833	0.149	1.698	0.437	0.193	0.440	0.307	0.094	0.179	0.163
9-10	0.930	0.130	8.346	0.129	1.433	0.401	0.189	0.450	0.318	0.095	0.167	0.158
11-12	0.930	0.160	6.781	0.147	1.580	0.395	0.195	0.454	0.313	0.102	0.170	0.151
13-14	0.850	0.140	7.083	0.136	1.602	0.382	0.197	0.449	0.337	0.084	0.160	0.162
14-15	0.900	0.090	11.667	0.139	1.550	0.362	0.167	0.390	0.274	0.071	0.190	0.143
15-16	0.690	0.110	7.318	0.192	2.783	0.418	0.201	0.454	0.291	0.092	0.181	0.141
17-18	0.800	0.130	7.179	0.132	1.649	0.424	0.199	0.463	0.293	0.093	0.185	0.149
18-19	0.880	0.140	7.333	0.140	1.630	0.400	0.197	0.445	0.294	0.089	0.171	0.140
19-20	0.850	0.070	14.167	0.124	1.459	0.399	0.180	0.426	0.311	0.095	0.181	0.143
21-22	0.890	0.060	17.306	0.143	1.611	0.389	0.181	0.470	0.311	0.105	0.195	0.148
23-24	0.720	0.080	10.500	0.135	1.874	0.424	0.195	0.455	0.307	0.089	0.161	0.139
26-27	0.870	0.110	9.227	0.127	1.462	0.348	0.178	0.430	0.310	0.093	0.198	0.138
27-28	0.800	0.130	7.179	0.132	1.656	0.357	0.166	0.420	0.301	0.087	0.188	0.141
29-30	0.850	0.090	11.019	0.121	1.419	0.352	0.179	0.431	0.331	0.090	0.184	0.141
31-32	0.860	0.100	10.033	0.126	1.469	0.380	0.190	0.471	0.314	0.091	0.187	0.132
32-33	0.910	0.120	8.847	0.140	1.540	0.368	0.185	0.445	0.315	0.090	0.180	0.143
34-35	0.870	0.110	9.227	0.156	1.797	0.344	0.164	0.432	0.320	0.080	0.164	0.145
36-37	0.950	0.140	7.917	0.160	1.681	0.350	0.160	0.408	0.303	0.087	0.171	0.133
38-39	0.900	0.150	7.000	0.166	1.806	0.337	0.172	0.424	0.302	0.086	0.161	0.145

Interval	%OC	%N	C/N	Σ_8 (mg/g)	λ_8 (µg/100mg OC)	S/V	C/V	(Ad/Al)v	(Ad/Al)s	3,5Bd/V	P/(V+S)	PON/P
Core	**SBBC3**											
0-1	1.290	0.170	8.853	0.079	0.609	0.214	0.144	0.472	0.361	0.125	0.364	0.088
1-2	1.320	0.250	6.160	0.069	0.523	0.188	0.129	0.453	0.322	0.133	0.349	0.087
3-4	1.360	0.260	6.103	0.084	0.621	0.143	0.126	0.434	0.416	0.123	0.296	0.099
5-6	1.250	0.190	7.675	0.077	0.620	0.141	0.111	0.497	0.415	0.108	0.290	0.090
7-8	1.240	0.140	10.333	0.066	0.529	0.185	0.138	0.520	0.387	0.134	0.348	0.090
10-11	1.210	0.140	10.083	0.069	0.568	0.189	0.130	0.448	0.379	0.137	0.322	0.102
13-14	1.250	0.070	20.833	0.069	0.552	0.175	0.126	0.427	0.379	0.129	0.319	0.082
17-18	1.170	0.040	34.125	0.071	0.611	0.174	0.119	0.421	0.364	0.126	0.289	0.090
21-22	1.240	0.070	20.667	0.077	0.620	0.153	0.113	0.424	0.407	0.119	0.270	0.098
25-26	1.130	0.100	13.183	0.072	0.639	0.159	0.113	0.412	0.348	0.106	0.278	0.104
29-30	1.170	0.080	17.063	0.075	0.668	0.168	0.125	0.456	0.323	0.108	0.243	0.105
33-34	1.340	0.070	22.333	0.072	0.536	0.142	0.118	0.407	0.361	0.103	0.250	0.105
35-36	1.130	0.080	16.479	0.069	0.615	0.146	0.104	0.450	0.412	0.099	0.239	0.110

Interval	%OC	%N	C/N	Σ_8 (mg/g)	λ_8 (µg/100mg OC)	S/V	C/V	(Ad/Al)v	(Ad/Al)s	3,5Bd/V	P/(V+S)	PON/P
Core	**SBBC4**											
1-2	1.630	0.210	9.056	0.093	0.569	0.183	0.164	0.504	0.379	0.091	0.224	0.131
6-7	1.380	0.180	8.944	0.089	0.643	0.163	0.165	0.482	0.372	0.085	0.219	0.155
10-11	1.270	0.170	8.716	0.093	0.730	0.146	0.153	0.444	0.347	0.083	0.201	0.142
13-14	1.280	0.200	7.467	0.086	0.670	0.159	0.174	0.423	0.334	0.080	0.198	0.138
15-16	1.200	0.160	8.750	0.097	0.812	0.143	0.143	0.459	0.338	0.072	0.175	0.153
19-20	1.230	0.180	7.972	0.086	0.695	0.184	0.157	0.459	0.319	0.082	0.178	0.149
22-23	1.180	0.170	8.098	0.079	0.667	0.135	0.149	0.427	0.353	0.078	0.196	0.153

Interval	%OC	%N	C/N	Σ_8 (mg/g)	λ_8 (μg/100mg OC)	S/V	C/V	(Ad/Al)v	(Ad/Al)s	3,5Bd/V	P/(V+S)	PON/P
Core	**SBBC8**											
1-2	1.500	0.220	7.955	0.103	0.684	0.203	0.136	0.460	0.381	0.095	0.200	0.135
6-7	1.500	0.220	7.955	0.081	0.537	0.177	0.146	0.435	0.360	0.095	0.197	0.155
10-11	1.510	0.200	8.808	0.083	0.548	0.186	0.153	0.425	0.338	0.086	0.189	0.158
13-14	1.570	0.210	8.722	0.124	0.790	0.166	0.115	0.402	0.315	0.082	0.192	0.122
14-15	1.430	0.200	8.342	0.128	0.897	0.185	0.117	0.392	0.305	0.084	0.199	0.125
17-18	1.340	0.180	8.685									
20-21	1.340	0.190	8.228	0.127	0.946	0.176	0.119	0.381	0.295	0.079	0.193	0.128
23-24	1.280	0.160	9.333	0.124	0.971	0.223	0.112	0.380	0.276	0.070	0.176	0.150
25-26	1.270	0.190	7.798									
27-28	1.250	0.140	10.417	0.135	1.080	0.165	0.106	0.360	0.284	0.063	0.169	0.140
29-30	1.310	0.160	9.552									
35-36	1.350	0.190	8.289	0.134	0.992	0.128	0.089	0.371	0.293	0.061	0.168	0.182
41-42	1.220	0.160	8.896									

VITA

Name: Christian John Noll, IV
Address: Texas A&M University at Galveston
1001 Texas Clipper Rd Suite 710
Galveston TX 77554
Email: cjn7680@neo.tamu.edu

Education:

Texas A&M University at Galveston, Galveston, Texas — May 2002
B.S. Marine Sciences GPA 3.5

Texas A&M University, College Station, Texas
M.S. Oceanography GPA 4.0 — December 2005

Texas A&M University, College Station, Texas — December 2008
Ph.D. Oceanography GPA 4.0